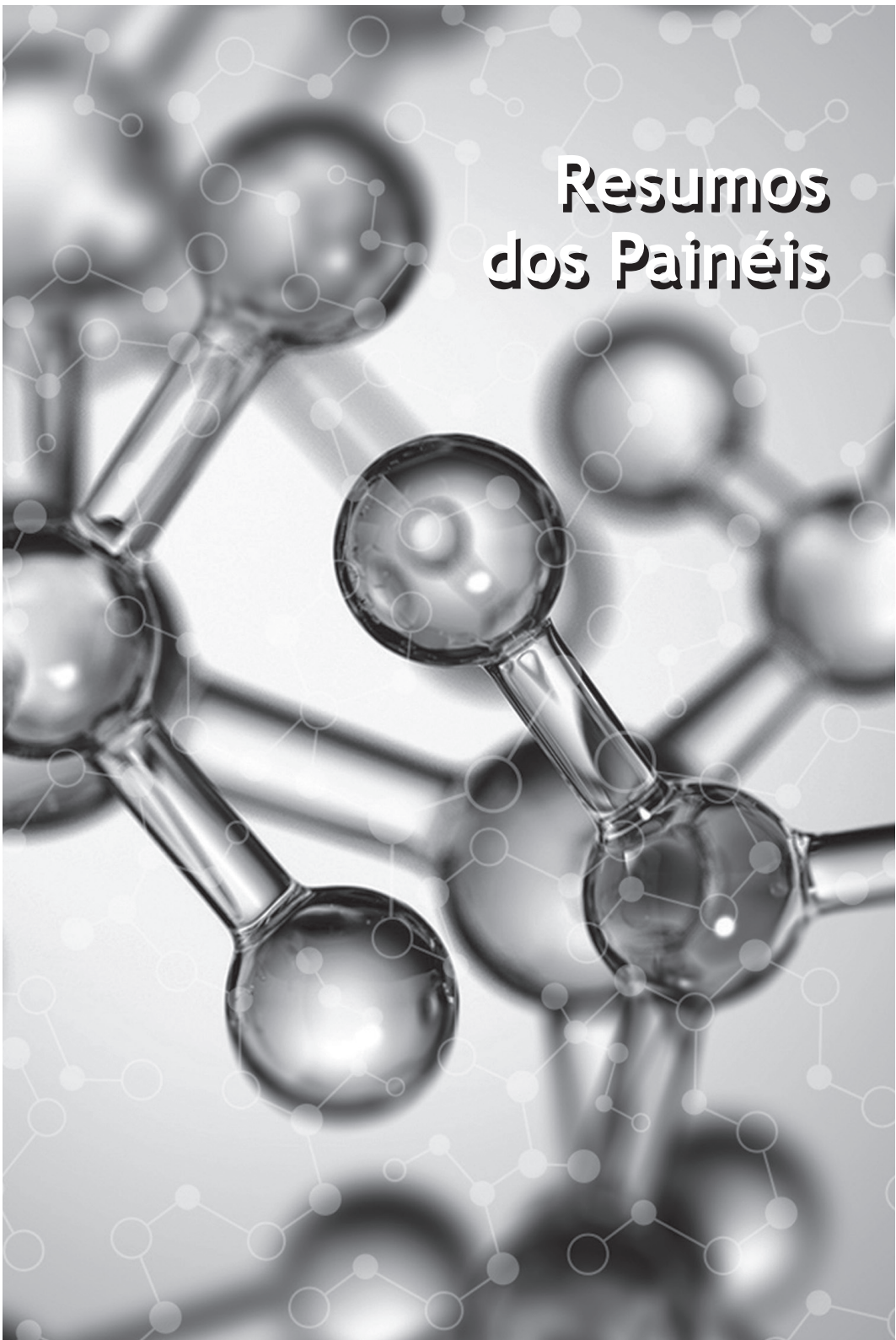




Resumos dos Painéis



Semiempirical ΔH_{bind} calculations for interactions between the RTA and RTB subunits and ricin inhibitors

Acassio Rocha Santos (PG)¹, Elton José Ferreira Chaves (PG)², Gabriel Urquiza de Carvalho (PQ)¹, Gerd Bruno da Rocha (PQ)¹

¹Chemistry Department, Universidade Federal da Paraíba (UFPB), Cidade Universitária, s/n, Castelo Branco, (58051-900), João Pessoa, Paraíba, Brazil

²Biotechnology Department, Universidade Federal da Paraíba (UFPB), Cidade Universitária, s/n, Castelo Branco, (58051-900), João Pessoa, Paraíba, Brazil

Abstract: Industry, governments and the media have become increasingly more interested in the castor bean seeds (*Ricinus communis* L.). This stems from the unusual properties of its byproducts, such as castor oil and ricin. The ricinoleic acid comprises around 90% of all fatty acids extracted from the castor bean plant [1].

Besides the interest in its oil, the co-products generated during its production have garnered wide commercial attention. This is due to the production of around 1.5 million tons per year [1]. Hence, it is in the best interest of the industry to find an economically viable purpose for these co-products. A welcoming alternative regards the use of these co-products as animal food, though it is still not possible due to the presence of ricin, a ribosome-inactivating protein composed by two sub-units (known as RTA and RTB), in which the RTA serves as the catalytic sub-unit [2]. In addition to the problems related to co-products in the production of castor oil, terrorist groups yet utilize the ricin as a chemical weapon [3]. In this manner, the inhibition of the action mechanism within the ricin is of major economic, public and military interest, with the RTA being the target of inhibitors. Recently, fields of study within theoretical and computational chemistry have developed a capital role in the research of biological and/or biochemical systems, which provide with a proper orientation towards the conception of new drugs.

This study has carried out calculations for enthalpy of formation (ΔH_f) and ground state geometries of RTA and RTB subunit, both separately and joined to form complexes containing possible inhibitors, through semiempirical methods such as: RM1, PM6, PM6-DH+ and PM7. Crystallographic structures available at the PDB(ID) of the complexes containing inhibitors (ORB, PT1, EJ5, JP2) and of the RTA and RTB Ricin subunits (2AAI) were used in these studies. We also performed studies with two different inhibitor candidates synthesized by the group (Lv213 and Lv215). The structures were positioned in the active site of RTA through *Molecular Docking* [4]. The objective was to identify mechanisms that would favor ricin inhibition and to verify which semiempirical method would better describe the binding enthalpies (ΔH_{bind}) of the RTA-ligand and RTA-RTB complexes, at least from a qualitative viewpoint.



Semiempirical calculations of ΔH_f for ligands (ORB, PT1, EJ5, JP2, Lv213 and Lv215), RTA-ORB (4228 atoms), RTA-PT1 (4250 atoms), RTA-EJ5 (4234 atoms), RTA-JP2 (4218 atoms), RTA-Lv213 (4245 atoms) and RTA-Lv215 (4238 atoms) complexes were performed using the MOZYME [5] linear scaling technique implemented on the MOPAC program [6]. We carried out these calculations with the crystallographic structures, optimized by each of the mentioned methods. For the ricin structure (2AAI), since the RTB subunit presents glycosylations in its structure, ΔH_f calculations were conducted for the RTA-RTB systems without glycosylations (8212 atoms) and RTA-RTB with glycosylations (8444 atoms). Once the data for the ΔH_f of the ligands, RTA, RTB and the RTA-ligands and RTA-RTB complexes were calculated, one obtains the $\Delta H_{(bind)}$ values for the RTA-RTB systems (without glycosylations), RTA-RTB systems (with glycosylations) and the various RTA-ligands complexes. In all calculations, we considered the effects of the solvent through the implicit COSMO model for proteins solvated in water.

The ΔH_f results on the crystallographic geometry using the PM7 semiempirical method presented the following values for the RTA-ligand complexes: RTA-ORB2 [$\Delta H_{(bind)} = -61.04$ kcal/mol], RTA-1PT [$\Delta H_{(bind)} = -62.04$ kcal/mol], RTA-EJ5 [$\Delta H_{(bind)} = -69.23$ kcal/mol], RTA-JP2 [$\Delta H_{(bind)} = -60.39$ kcal/mol], RTA-Lv213 [$\Delta H_{(bind)} = -32.31$ kcal/mol] and RTA-Lv215 [$\Delta H_{(bind)} = -17.62$ kcal/mol]. All values are consistent with those were experimentally observed for common enzyme-ligand complexes (at least in terms of the value range). Therefore, the data shows that, from an enthalpy viewpoint, the EJ5 ligand presented the lowest $\Delta H_{(bind)}$ when forming a complex with the RTA. On the other hand, the Lv215 ligand was the one presented the highest interaction value. Another interesting point is that the RTA-RTB complex without glycosylations presented an unfavorable interaction enthalpy ($\Delta H_{(bind)} = 80.91$ kJ/mol) for its formation. However, the RTA-RTB complex with glycosylations presented a very pronounced favorable interaction ($\Delta H_{(bind)} = -6568.311$ kJ/mol). Such results suggest the glycosylations play an important role in the formation of the ricin enzyme complex (RTA-RTB).

Key-words: Ricin, semi-empirical methods, enzyme-ligand interaction energy

Support: This work has been supported by CAPES/FAPESQ, CNPq and CAPES (biologia computacional, auxpe1375/2014)

References:

- [1] Severino, L., Auld, D., *et al.* *Agronomy Journal*, **104** (4), 853–880 (2012).
- [2] Endo, Y., Tsurugi, K. The RNA N-glycosidase activity of ricin A-chain. In *Nucleic acids symposium series*, **19**, 139–142 (1987).
- [3] Franz, D., Jaax, N. Ricin toxin. *Medical aspects of chemical and biological warfare*, 631–642 (1997).
- [4] Chaves, H. J. F. *Simulação Molecular de Inibidores da subunidade da ricina, RTA*. 2016. 80f. Dissertação (Mestrado em Biotecnologia) – Departamento de Biotecnologia, Universidade Federal da Paraíba, João Pessoa.2016.
- [5] Stewart, J. P. J. *Int. Journal of Quantum Chemistry*, **58**, 133-146 (1996).
- [6] Stewart, J. P. J. *Journal of Computer-Aided Molecular Design*, **4**, 1-105 (1990).



Title: Theoretical study of the molecular and electronic structures of β -carbolines and MAO substrates using the theory of density functional

Authors: Thayná Borges da Silva (IC), Alberto dos Santos Marques

Address: Universidade Federal do Amazonas, Departamento de Química, Laboratório de Tecnologia com Moléculas Bioativas, LTMB, Departamento de Química.

E-mail: marquesalbertods@gmail.com

A theoretical spectroscopic study of the reversible inhibitory β -carbolines of monoamine oxidase (MAO) and the specific substrates of their enzymes, serotonin and noradrenaline, was carried out using the Functional Density Theory (FDT). The β -carbolines studied were: Harmina (7-methoxy-1-methyl-9H-pyrido [3,4-b] indole); Harmana, 1-Methyl-9H-pyrido [3,4-b] indole; Norharmana, 9H-pyrido [3,4-b] indole; Harmaline, 7-methoxy-1-methyl-4,9-dihydro-3H-pyrido [3,4-b] indole; Harmol, 1-methylethyl-2,9-dihydropyrido [3,4-b] indol-7-ol. Molecular structures were determined by optimizing the geometry of each molecule with the abinitio method and the 6-31G * base function, the $\Delta H_{\text{formation}}$ with semi-empirical methods PM3 and the excitation energies using TFD. The results showed that the calculations produced UV absorption spectra similar to the experimental spectra in both hydrophobic and hydrophilic media. In view of this, predictions were made of the photoactive region, photophysical properties and mode of action of each molecule and it was found that between β -carbolines and the two substrates, besides the structural similarity, there are similarities in the electronic structures. For example, for serotonin, harmana, and harmaline, the lowest fluorescent state S1 are ($\pi \pi^*$) and it was originated from electronic transition between indole N to benzene C. The HOMO and LUMO energies in eV are: (5.08 and 0.96), (5.62 and 0.98) and (5.03 and 0.94) respectively. The possible explanations for the inhibition of MAO, mode of action of β -carbolines and the interaction of these molecules with the biological material are discussed.

Key-words: density functional theory, β -carbolines, serotonin

Support: Fundação de Amparo à Pesquisa do Estado do Amazonas, (FAPEAM) .

References:

- [1] A.D.S. Marques; H. F. Souza, I. C. Costa, W.M. Azevedo, J. of Mol. Struct. 520, 179 (2000).
- [2] A. H. A. Reis, A. S. Marques e Y. Takahata. Scientia Amazonia, 3(1), 41(2014). Revista on-line <http://www.scientia.ufam.edu.br>.
- [3] A. D. S. Marques, C. T. Lin, L. G. Pereira, Y. Takahata, International J. Quantum Chemistry. 110, 2047(2010).
- [4] A.D.S. Marques, C. Zheng, C. T. Lin, J. of Mol. Struct. 753, 13(2005).

Bond metamorphosis between coordinate (dative) and single covalent bonds: BN-ethylamine molecule

Alejandro Lopez-Castillo* and Nelson H. Morgon**

*Departamento de Química, Universidade Federal de São Carlos (UFSCar), 13565-905 São Carlos-SP, Brazil

**Instituto de Química, Universidade Estadual de Campinas (UNICAMP), CP 6154, 13083-970 Campinas-SP, Brazil

Abstract: The BN-ethylamine molecule ($\text{NH}_2\text{BH}_2\text{NH}_3$) [1] was studied in order to show the bond metamorphosis step-by-step between BN single (...H₂B-NH₂) and coordinate (dative) (...H₂B-NH₃) [2-4]. Analyzing the molecular orbitals, charges and bond order along the hydrogen tunneling process ($\text{NH}_3\text{BH}_2\text{NH}_2 \leftrightarrow \text{NH}_2\text{BH}_3\text{NH}_2 \leftrightarrow \text{NH}_2\text{BH}_2\text{NH}_3$), it is possible to follow the bond metamorphosis between single covalent and coordinate (dative) bonds. The bond metamorphosis can also be followed along the hydrogen transfer observing the three main molecular orbitals. The IRC profile and the HOMO are shown in Fig.1. The hydrogen tunneling potential and its two first states are shown in Fig.2.

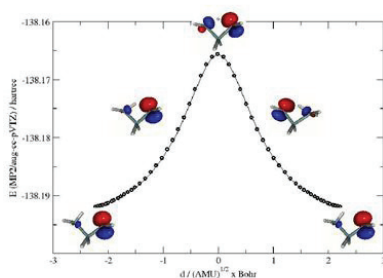


Fig.1

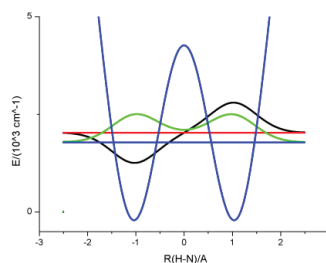


Fig.2

The molecular geometries, the harmonic vibrational analysis, and the IRC calculation were carried out at the MP2/aug-cc-pVDZ level of theory. MP2 and CCSD(T) single point energies were obtained using a larger aug-cc-pVTZ basis set. All calculations were performed with Gaussian09. The potential energy curve to dissociation limit of transferred hydrogen ($\text{H}\dots\text{NH}_2\text{BH}_2\text{NH}_2 \leftrightarrow \text{NH}_3\text{BH}_2\text{NH}_2 \leftrightarrow \text{NH}_2\text{BH}_3\text{NH}_2 \leftrightarrow \text{NH}_2\text{BH}_2\text{NH}_3 \leftrightarrow \text{NH}_2\text{BH}_2\text{NH}_2\dots\text{H}$), obtained by the methods previously described, was considered to solve the Schrödinger equation to find the eigenstates of the tunneling hydrogen process.

The main objective of this work was to illustrate the smooth modification between the two important different kinds of chemical bond. The technical analysis was presented

and the practical result was condensed in three most important MOs, which describe the metamorphosis process. These three MOs are shown in Fig.3 for the minimum of energy, intermediary geometry, and transition state. The charges, bond orders, and bond lengths were considered to study the bond transformation connected to tunneling transfer of hydrogen atom. This work can also contribute to educational issues, for example showing the difference between covalent and dative chemical bonds.

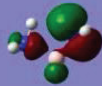
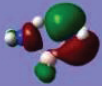
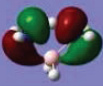

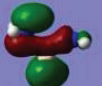
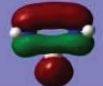
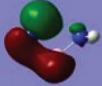


	Energy Minimum	Intermediary Geometry	Transition State
HOMO			
HOMO-2			
HOMO-5			

Fig.3

Key-words: BN coordinate (dative) bond, BN covalente bond, hydrogen tunneling

Support: This work has been supported by Fapesp.

References:

- [1] C. F. Pupim and A. Lopez-Castillo, Boron-Nitrogen Dative Bond (submitted).
- [2] G. Frenking, Nature, 522, 297 (2015).
- [3] G. N. Lewis, J. Am. Chem. Soc., 38, 762 (1916).
- [4] A. Haaland, Angew. Chem. Int. Ed., 28, 992 (1989).

Kinetics of the O + HCN Reaction

Patrícia R. P. Barreto¹, Washington B. Silva², Eberth A. Correa³, Alessandra Albernaz⁴

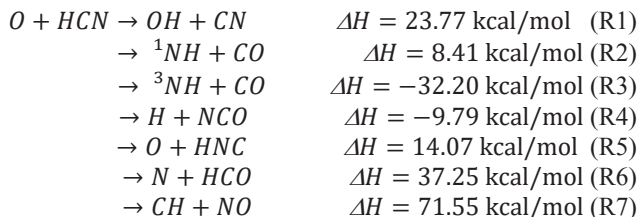
¹Laboratório Associado de Plasma, INPE, CP515, São José dos Campos, SP, CEP 12247-970

²Instituto Federal de Brasília, Campus Ceilândia, Ceilândia, DF, CEP 72220-260

³Universidade de Brasília, Campus do Gama – Engenharias, Brasília, DF, CEP 72444-240

⁴Instituto de Física, Universidade Brasília, CP04455, Brasília, DF, CEP 70919-970

Abstract: The reactions of the decomposition products, such as HCN and O, CH and NO, NH and CO, OH and CN, also play important roles in the combustion of N-containing hydrocarbon fuels [1-5]. Kinetics of these species are therefore of considerable interest in developing improved models for the combustion of fuels containing organically bound nitrogen. The elucidation of chemical mechanisms in flames is difficult, because there are several pathways involving reactants that are equilibrated among themselves. Even if a mechanism predicts the correct dependence on temperature and composition, it may not be unique. The goal of this work is to investigate global features of potential energy surface (PES) for the exit and isomerization channels on both singlet and triplet O + HCN reactions, represented by:



The singlet and triplet PES (see Figure 1) were calculated using the complete basis set model chemistry, CBS-QB3. The vibrational frequencies and geometries for all species involved in the reaction were calculated using B3LYP/6-311G(2d,d,p) level, internal level of CBS-QB3 method. Seven different channels were analyzed and the results from the potential energy surface calculations were used to determine rate constant with Master Equation Solver for Multi-Energy Well Reactions (MESMER) [6] and APUAMA [7] programs. Ab initio transition state theory (TST) based master equation simulations are used to predict the temperature and pressure dependence of the O+HCN reaction rate and product branching. In the singlet state, isocyanic acid, HNCO, has been found to be the most stable isomer (-119.17 kcal/mol) followed by cyanic acid, HOCN (-94.26 kcal/mol), fulminic acid, HCNO (-51.41 kcal/mol), isofulminic acid, HONC (-35.77 kcal/mol), NC(H)O (-33.51 kcal/mol), N(H)CO (-11.97 kcal/mol) and O(H)CN (-6.00 kcal/mol). In the triplet state, the ³HNCO is 9.50 kcal/mol higher than O+HCN (reactants), the branched ³NC(H)O isomer is -33.46 kcal/mol energetically lower than, followed by ³HNCO (-31.71 kcal/mol). The cyclic c-³NC(H)O is by 49.63



kcal/mol less stable than the branched conformation of the $^3\text{NC(H)O}$, followed by $^3\text{HCNO}$ with a relative energy of 48.03 kcal/mol.

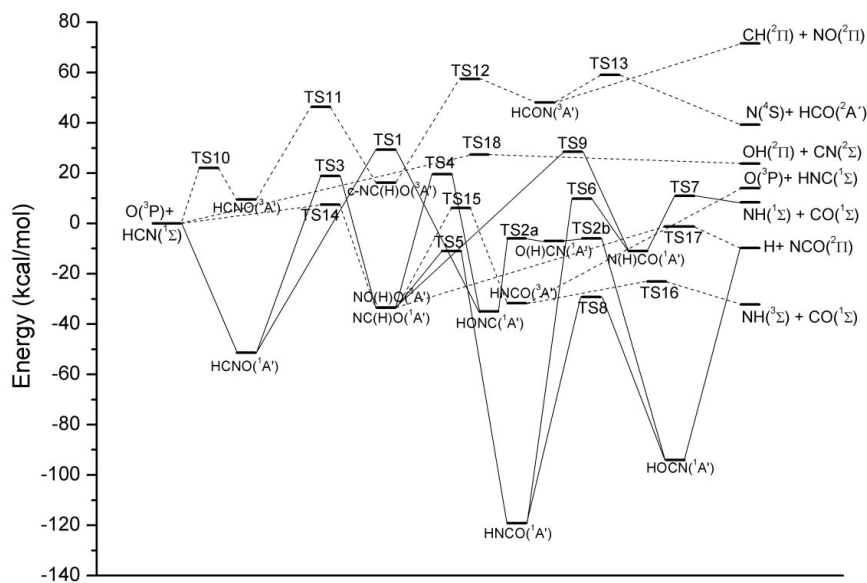


Figure 1. Schematic potential energy diagram for the O + HCN reaction calculated using CBS-QB3 level. Solid lines denote singlet states, while dashed lines denote triplet states.

Key-words: HCN; O+HCN; Transition State Theory; Master Equation; Reaction Rate

Support: This work has been supported by CNPq

References:

- [1] J. A. Miller and C. T. Bowman, *Prog. Energy Combust. Sci.*, 15, 287 (1989).
- [2] B. S. Haynes, D. Iverach, and N. Y. Kirov, "Fifteenth Symposium (International) on Combustion" The Combustion Institute, 1103 (1975).
- [3] B. S. Haynes, *Combust. Flame*, 28, 113 (1977).
- [4] C. Morley, *Combust. Flame*, 27, 189 (1976).
- [5] A. Szekely, Ph.D. thesis, Department of Mechanical Engineering, Stanford University (1984).
- [6] D. R. Glowacki, C.-H. Liang, C. Morley, M. J. Pilling and S. H. Robertson; *J. Phys. Chem. A*, 116, 9545 (2012).
- [7] H. O. Euclides, P. R. P. Barreto, *J. Mol. Model.*, 23, 176 (2017).



Total photoabsorption cross sections with square integrable basis set

Authors: Bruno Nunes Cabral Tenorio, Marco Antonio Chaer do Nascimento,
Alexandre B. Rocha

*UFRJ - Universidade Federal do Rio de Janeiro, Instituto de Química,
Av. Athos da Silveira Ramos, 149, Rio de Janeiro - RJ, 21941-909, Brasil*

Abstract: Photoionization cross-section and dynamic polarizabilities are important properties in areas such as optical refractivity and photoelectron spectra of free and adsorbed species. On the theoretical side, the main difficulty in determining the photoionization cross-section resides in the calculation of continuum wave functions. This can be done by explicit construction¹, which has the disadvantage, among others, of treating bound electrons at Hartree-Fock level. The other possibility is the discretization of the continuum. In the spirit of the second approach, Langhoff² proposed a procedure for constructing the photoionization cross-section from an approximate spectral representation of the dynamic polarizability by moment-theory techniques with L^2 basis functions. The technique is known as Stieltjes imaging. The complex dynamic polarizability contains both the absorptive and dispersive information about the system. Thus, the photoionization cross-section and the dynamic polarizability can be obtained simultaneously, once a representation is found for the complex polarizability. This can be achieved by using a discrete basis set L^2 to represent both the bound and the continuum states of the system.

Alternatively, the complex dynamic polarizability can be constructed by analytic continuation of the approximated representation^{3,4}, by using Padé approximants or continued fractions⁵. Pseudo-spectra, which are used as input for an approximated form of the complex dynamic polarizability can be obtained by a variety of methods of electronic structure. Recently, our group has shown the suitability of using linear response coupled cluster approximation (LR-CC)⁶ based on the Lanczos diagonalization to obtain pseudo-spectra used in analytic continuation. Lanczos algorithm is able to converge a large number of pseudo-states while diagonalization by Davidson algorithm is efficient only for a few low-lying states. In the present work, we try another possibility, i.e., to use time-dependent density functional theory (TDDFT) to generate pseudo-spectra and, consequently, total photoabsorption cross sections in both valence and inner-shell regions.

In Figure 1, we present our recent results obtained with TDDFT for the furan molecule. On the top panel we have the total photoabsorption cross section and on the bottom one we show the oxygen K-shell cross section. As one can observe from the results presented in Figure 1, there is a good agreement among calculated and experimental cross-section. In the symposium we will show that, in general, results obtained from TDDFT are not as accurate as LR-CC, as could be expected, but they are accurate enough to describe the general trends of the photoabsorption spectra. This has encouraged us to extend the method to larger molecules. (CNPq, FAPERJ, CAPES)

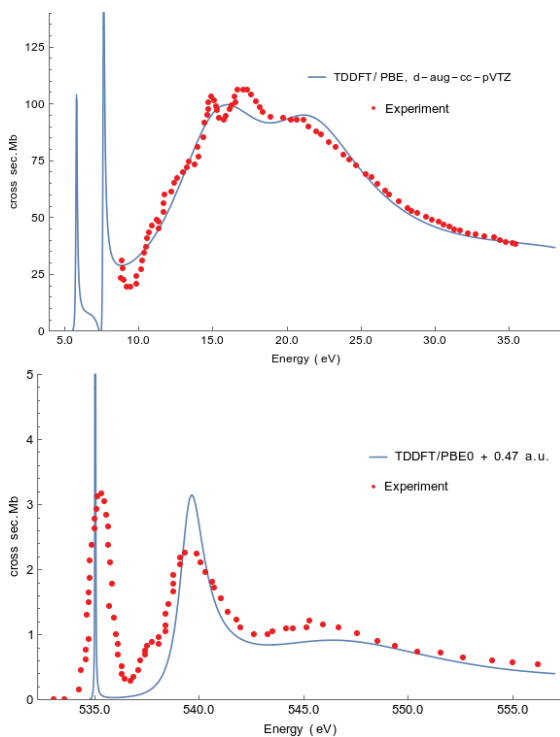


Figure 1: (Top) Furan total photoabsorption cross section obtained with TDDFT where PBE functional has been employed. Experimental values [7]. (Bottom) Oxygen K-shell photoabsorption cross section obtained with TDDFT where PBE0 functional has been used. Experimental values [8].

Key-words: Time-dependent density functional theory, cross-sections, photoabsorption, coupled cluster

References:

- [1] Lucchese, R.R.; McKoy, V. *Phys. Rev. A*, 1980, 21, 112.
- [2] Langhoff, P. W.; Corcoran, C. J. *Chem. Phys.* 1974, 61, 146.
- [3] Broad, J. T.; Reinhardt, W. P. *J. Chem. Phys.* 1974, 60, 2182.
- [4] Nascimento, M. A. C.; Goddard, W. A. *Phys. Rev. A: At., Mol., Opt. Phys.* 1977, 6, 1559.
- [5] Kaufmann, K.; Baumeister, W.; Jungen, M. *J. Phys. B: At., Mol. Opt. Phys.* 1989, 22, 2223.
- [6] Tenorio, B. N. C., Coriani, S., Nascimento, M. A. C., Rocha, A. B., *J. Chem. Theory Comput.* 12, 4440 (2016).
- [7] Rennie, E.E., Johnson, C.A.F, Parker, J.E., Holland, D.M.P. Shaw, D.A., MacDonald, M.A., Hayes, M.A., Shpinkova, L.G., *Chem. Phys.* 1998, 236, 365.
- [8] Newbury, D. C., Ishii, I. Hitchcock, A. P., *Can. J. Chem.*, 1986, 64, 145.



DFT approach of uranyl species originating from acid mine drainage and its interaction with ion exchange resin

Authors: Alexandre Carvalho Bertoli, Hélio Anderson Duarte, Heitor Avelino de Abreu

*Address: Departamento de Química, Universidade Federal de Minas Gerais - UFMG
Av. Pres. Antônio Carlos, 6627 - Pampulha, Belo Horizonte - MG, 31270-901, Brasil
bertolialexandre@yahoo.com.br*

Abstract: Acid drainage, commonly referred to as acid mine drainage (AMD), has become an economic and environmental burden. It is a very ubiquitous problem in areas where there has been a history of coal or hard rock mining. This phenomenon is generally associated with heavy metals as a uranium mine localized in the southeast of Brazil, in the state of Minas Gerais (Poços de Caldas Municipality). The study and identification of uranium complexes from such acid water are imperative not only from the point of view of its economic value but it is important for understanding actinide separation and predicting actinide transport in the environment, particularly with respect to the safety of nuclear waste repositories [1]. The uranyl, UO_2^{2+} , ion has received considerable interest due to its importance for environmental chemistry of radioactive elements and its role as a benchmark system for larger actinides. Many useful insights into structures and intrinsic stabilities of actinide complexes can be gained from quantum-chemical calculations are it through ab initio wave function theory or density functional theory (DFT). As for the latter, hybrid DFT and small-core relativistic effective core potentials (ECPs) or all-electron relativistic treatments have proven fairly robust in describing the thermochemistry of actinides. Therefore, it is a challenge to evaluate the thermodynamic properties of the hydrolyzed UO_2^{2+} species and the interactions with SO_4^{2-} ions and an amino exchanger group, present in ion exchange resins [2]. DFT computations were performed using the Gaussian 09 program package. Full geometry optimizations and frequency computations were performed using the B3LYP hybrid functional; the Stuttgart–Dresden triple-valence basis sets together with the corresponding effective small-core potential (SDD) were used for uranium and the Pople triple-zeta basis sets, 6-311G(d,p), for hydrogen and oxygen. A thermodynamic study aims to provide a theoretical discussion on the complexes, in order to obtain the parameters that determine their chemical properties. The heats of formation values (ΔG) of the complexes were obtained using a thermodynamic cycle. The calculation of relative energy ($\Delta\Delta G_{\text{(aq)}}$) was performed to identify the most stable species. The following structures were calculated UO_2OH^+ , $\text{UO}_2(\text{OH})_2$, $\text{UO}_2(\text{OH})_3^-$, $(\text{UO}_2)_2(\text{OH})^{3+}$, $(\text{UO}_2)_2(\text{OH})_2^{2+}$, $(\text{UO}_2)_3(\text{OH})_4^{2+}$, $(\text{UO}_2)_3(\text{OH})_5^+$ and $(\text{UO}_2)_3(\text{OH})_7^-$, reported previously based on experimental evidences [3]. The formation reaction energies of the different species from the UO_2^{2+} and H_2O were estimated. The relative formation energies follow



the order: UO_2OH^+ (20.99 kcal/mol) > $(\text{UO}_2)_2(\text{OH})^{3+}$ (21.67 kcal/mol) > $(\text{UO}_2)_2(\text{OH})_2^{2+}$ (41.73 kcal/mol) > $(\text{UO}_2)_3(\text{OH})_5^+$ (51.14 kcal/mol) > $\text{UO}_2(\text{OH})_2$ (56.63 kcal/mol) > $(\text{UO}_2)_3(\text{OH})_4^{2+}$ (81.71 kcal/mol) > $\text{UO}_2(\text{OH})_3^-$ (93.23 kcal/mol) > $(\text{UO}_2)_3(\text{OH})_7^-$ (180.20 kcal/mol). The interaction of these species with the SO_4^{2-} and benzyltriethylammonium ion exchange their relative energies will be also presented. Sulfate ions are present in the acid rock drainage that occur in the mining areas of uranium and may affect the chemical speciation of the uranyl in aqueous solution. From experimental data it is observed that the ion exchange resins work well, in a wide range of pH, for the removal of uranium. According to our results, we can suggest the formation of ionic pairs due to a strong electrostatic attraction between the sulphate oxygens coordinated to the UO_2^{2+} ions and the quaternary ammonia of the resin. This mechanism is probably predominant, although not the only one, since these functional groups can participate in covalent, hydrogen bonds and weak Van der Waals forces [4].

Key-words: Uranyl, Hydrolysis, Ionic exchange, Acid drainage.

Support: INCT-ACQUA, GPQIT, FAPEMIG, CNPQ.

References:

- [1] A. C. Q. Ladeira, and C. R. Gonçalves, *J. Hazard. Mater.*, 148, 499 (2007).
- [2] M. Bühl, N. Sieffert, A. Chaumont, and G. Wipff, *Inorg. Chem.*, 50, 299 (2011).
- [3] R. Guillaumont, "Update on the chemical thermodynamics of uranium, neptunium, plutonium, americium and technetium" (2003), OECD Nuclear Energy Agency, Data Bank. Orsay, France.
- [4] M. Wawrzkievicz and Z. Hubicki, "Anion Exchange Resins as Effective Sorbents for Removal of Acid, Reactive, and Direct Dyes from Textile Wastewaters" (2015), *Ion Exchange - Studies and Applications*, Prof. Ayben Kilislioglu (Ed.), InTech.





Painel 009 | PN.009

Aluminum-silicon nanoalloys: search for the most stable structures up to 13 atoms.

Authors: Alexandre C. R. Gomes, Breno R. L. Galvão, Ana Débora P. Silveira

Address: CEFET-MG, Av. Amazonas, 5.253, Nova Suíça, Belo Horizonte, MG, CEP: 30.421-169.

Abstract: Clusters are aggregates of a countable number of particles, where a hetero-atomic cluster is constituted of two or more different species. Metal clusters may be constituted of a single metallic element or of more than one, giving rise to nanoalloys^[1]. The study of hetero-atomic clusters opens a great channel to design new mixed materials, whose physicochemical properties can differ from those of their pure elemental counterparts^[2]. Silicon based clusters possess great interest due to their potential applications in semiconductor and optoelectronic industries and aluminum-silicon compounds possess considerable significance in nanomaterials fields^[2]. However, nowadays, there is a lack of studies of these nanoalloys^[2]. The properties of alloy clusters may be “tunable” by changing the composition of a cluster of a given size, and to find the most stable structures there is a need to study all possible isomers that appear from atom permutations (homotops)^[3,4]. This is a very difficult task, given that the number of local minima increases very fast with cluster size. The goal of this work is to find the most stable structure and composition of aluminum and silicon nanoalloys, using computational calculations. For this purpose, we consider nanoalloys that possess between three and thirteen atoms, and all possible composition of aluminum and silicon. In each case, all possible isomers are considered, permuting the position of all the atoms that constitute each cluster. There are a lot of possible permutations, and these lead to thousands of structures to be analyzed. The initial coordinates are taken from the singly aluminum doped silicon neutral clusters obtained by Tam *et al*^[2], and from these coordinates the structures are optimized using the Møller-Plesset (MP) Perturbation Theory methodology. The MP2 calculations consume a considerable amount of time and in this work, the basis set chosen is the LANL2DZ with an Effective Core Potential (ECP)^[5], which makes the calculations of all homotops faster. In order to generate all homotops, we developed an algorithm that reads the skeleton of the molecule from Cartesian coordinates inserted in a separated file and select the desired spin multiplicity. After performing these simple steps, the program generates a GAMESS input for all possible homotops to be locally optimized. Vibrational frequencies are also calculated for the optimized structures. At the same time, when executed, the program presents the nuclear repulsion energy of each structure and search for similar values. This is useful to compare the generated inputs and verify if they represent the same structure, avoiding a repeated calculation. If the energies differ only in the last decimal places, the program accuses a possible equivalence of the structures. After performing all calculations, the optimized energies are analyzed and the lowest energy minimum is selected, therefore, the most stable structure with that specific composition is determined. Average binding

1 2 1





energies and excess energies of each composition and cluster size are calculated. After performing these calculations, for selected compositions, the homotops will be re-optimized using a more sophisticated method and basis set. This will enable a comparison between the methods, and verify if the most stable structure obtained with the MP2/ECP method is the most stable structure obtained by a more refined method. All electronic structure calculations are carried out using the GAMESS 2016 program package.

Key-words: Nanoclusters; electronic structure; optimization.

Support: This work is supported by Fundação de Amparo à Pesquisa do Estado de Minas Gerais (FAPEMIG), Conselho Nacional de Desenvolvimento Científico e Tecnológico (CNPq) and Centro Federal de Educação Tecnológica de Minas Gerais (CEFET-MG).

References:

- [1] Roy L. Johnston, "Atomic and Molecular Clusters" (2002), Taylor & Francis, London and New York.
- [2] Several authors, quoted by Nguyen Minh Tam, Truong Ba Tai, Vu Thi Ngan, and Minh Tho Nguyen, " Structure, Thermochemical Properties, and Growth Sequence of Aluminum-Doped Silicon Clusters Si_nAl_m ($n = 1 - 11$, $m = 1-2$) and their anions" (2013), The Journal of Physical Chemistry, ACS Publications.
- [3] Mateus A. M. Paiva, Barbara M. T. C. Peluzo, Jadson C. Belchior and Breno R. L. Galvão, "Structure and Stability of neutral Al-Mg nanoclusters up to 55 atoms" (2016), Phys. Chem. Chem. Phys, Royal Society of Chemistry.
- [4] J. Jellinek and E. B. Krissinel, Chem. Phys. Lett., 258,283 (1996).
- [5] LANL2DZ ECP Basis set, available in:
<https://bse.pnl.gov/bse/portal/user/anon/panel/Main/template/courier_content/js_pe/id/11535052407933> Accessed on 21/07/2017.



Azulene and naphthalene polymers

Alexandre Costa (PG) and Alejandro Lopez Castillo (PQ)

*Departamento de Química, Universidade Federal de São Carlos (UFSCar), 13565-905
São Carlos-SP, Brazil*

There is strong interest in the application of polyazulenes and polynaphthalenes as materials have unique electrochemical and nonlinear optical properties that make applications possible in the fabrication of sensors, batteries, and electrochromic and electroluminescence devices [1,2]. Azulene is an aromatic compound isomer of naphthalene, although naphthalene and azulene are structurally similar with the same number of carbon and hydrogen atoms and 10 π -electrons, the properties of the azulene molecule differ from that of its isomer in many respects. The azulene molecule consists of fused five and seven membered rings, exhibits a large dipole moment $\mu=1.08\text{D}$ and an intense blue color, on the contrary, naphthalene molecule consists of two fused six membered rings with zero dipole moment and colorless appearance [3-5]. In the present work, we propose a theoretical study of a small polymer chain up to 10 azulene and naphthalene monomers in C_1 symmetry according to Fig.1.

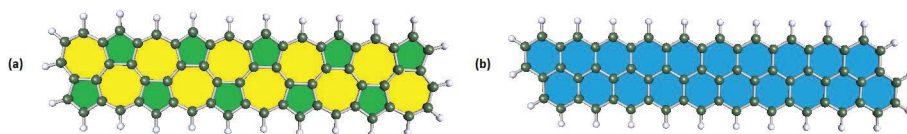


Fig.1 – Polymers: (a) [10]-azulene and (b) [10]-naphthalene

All calculations have been performed with TURBOMOLE software [6]. Calculations on the electronic ground state were carried out by Density Functional Theory (DFT), B3LYP/6-311G**. The [n]-naphthalene polymers are energetically more stable than the [n]-azulene ones. HOMO-LUMO energy gaps decrease as the polymer chain grows as shown in Fig.2.

The peaks of electronic transitions in the visible region (see Fig.3) are attributed to the small HOMO-LUMO energy gap, due to the extension of the π -electron system.

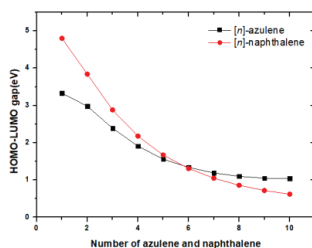


Fig.2 – HOMO-LUMO gap for [n]-azulene and [n]-naphthalene

We observed a shift of the maximum absorption peaks ($\pi \rightarrow \pi^*$ transition), from the visible region to the infrared, increasing polymer chains.

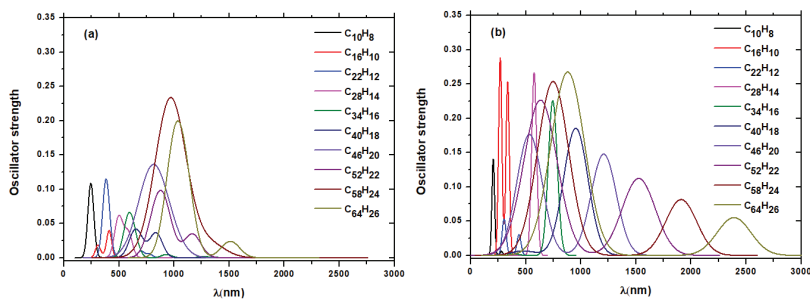


Fig.3 – UV-Vis spectra: (a) [n]-azulene and (b) [n]-naphthalene

Key-words: Density Functional Theory, Polyazulenes, Polynaphthalene

Support: The authors are grateful for the support given from the CAPES.

References:

- [1] M. Porsch, G. Sigl-Seifert and J. Daub, *Adv. Mater.* 9, 635 (1997).
- [2] J.X. Zhang, C. Liu, G.Q. Shi, Y.F. Zhao *J. Polym. Sci. Polym. Phys.* 43, 241 (2005).
- [3] E. Heilbronner, in *Nanbenzenoid Aromatic Compounds*, edited by D. Ginsburg (Interscience, New York, 1959), Chaps. 5 and 6.
- [4] J. Michl and E. W. Thulstrup, *Tetrahedron* 32,205 (1976).
- [5] L. T. Scott and M. A. Kirms, *J. Am. Chem. Soc.* 103, 5875 (1981).
- [6] R. Ahlrichs, M. Bär, M. Häser, H. Horn, and C. Kölmel, *Chem. Phys. Lett.* 162, 165 (1989).



Study of the interaction between resins and albite by MM/QM methods.

Kelly F.Pessôa, Fernanda B. da Silva, Júlio C.G.Correia^a, Alexandre N.M.Carauta^{a,b}

Address: ^aCentro de Tecnologia Mineral – CETEM/MCTI. Rio de Janeiro-RJ. Brasil

^bFundação Técnico-Educacional Souza Marques. Rio de Janeiro-RJ. Brasil

Abstract: The resin process of ornamental stones is crucial in the treatment of this type of stone, because, besides conferring an esthetic beauty, it protects against the action of physical, chemical and biological inclement weather increasing the mineral durability. However, the epoxy resin, which is the most used in this process, it presents toxicity, besides of not being biodegradable, thus creating an important environmental liability and contributes to the interest in finding alternatives in renewable sources[1]. The present work studies, through molecular modeling techniques, the interaction of epoxy resin and two possible active principles of biodegradable resins, cardanol [2] and ricinoleic acid [3], with the mineral albite which is representative of granitic stone, in order to better understand the adsorption process and the energies involved, in order to investigate a renewable alternative to the epoxy resin. A conformational analysis, using mechanical and molecular dynamics techniques, with the COMPASS force field, it was carried out for each of the representative molecules of the resins. The most stable structures obtained were submitted to a geometric optimization with frequency calculation by semi-empirical PM6-DH + [3] methodology, in order to obtain the minimum energy structure and ensure that they were in the ground state. Obtained the minimum structure, geometric optimization calculations with the PM6-DH+ method [4] were performed for successive approximations and in different orientations of each resin in relation to the albite structure constructed from crystallographic data. The maximum distance between the resin and the albite so that the method used admits that there is an interaction was 5Å. Above this value, the optimizations did not evolve into an interaction and the two structures have separated. In all cases, the resins assumed a position very close of the albite indicating the formation of chemical bonds. This seems to indicate that phenomena of chemisorption are expected. The figure 1 shows the results for the adsorption energy of the three systems studied and it indicates that the interaction with ricinoleic acid is the strongest, followed by the epoxy and finally by the resin the cardanol.

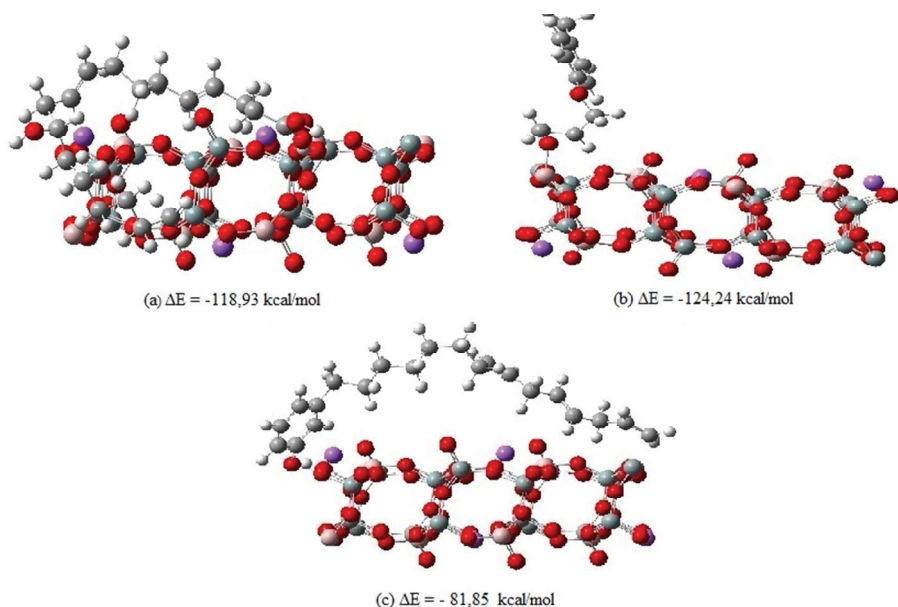


Figure 1 – Resin-Albite structures and respective adsorption energies: (a) Ricinoleic Acid-Albite; (b) Epoxy-Albite; (c) Cardanol-Albite.

Key-words: Ornamental Stones, Resins, Compass force field, PM6-DH+

Support: The authors acknowledge support from CNPq and PCI/CETEM and LABMOL collaborators. The authors thanks Prof. Prof. Peter Seidl by the Accelerlys Inc. package license.

References:

- [1] Silva, B. B. R.; Santana, R. M. C., Forte, M, M. C., International Journal of Adhesion & Adhesives, 2010, 30, pp 559–565.
- [2] Mazzetto, S. E.; Lomonaco, D.; Mele, G., Química Nova, 2009, 32 (3), pp 732-741.
- [3] Dalen, M. B.; Ibrahim, A. Q.; Adamu, H. M., British Journal of Applied Science & Technology 4(18): 2661-2683, 2014
- [4] M. Korth, J. Chem. Theory Comput., 2010, 6 (12), pp 3808–3816.



Anion Recognition by Heterocalixarenes: Understanding the Physical Nature of the Interaction

Authors: Alexandre O. Ortolan,^a Giovanni F. Caramori,^a F. Matthias Bickelhaupt,^{b,c}
Renato L. T. Parreira,^d Alvaro Muñoz-Castro^{e,f} and Tapas Kar^g

Address: ^aDepartamento de Química, Universidade Federal de Santa Catarina, Campus Universitário Trindade, CP 476, Florianópolis, SC, 88040-900, Brazil.

^bDepartment of Theoretical Chemistry and Amsterdam Center for Multiscale Modeling (ACMM), Vrije Universiteit Amsterdam, De Boelelaan 1083, 1081 HV Amsterdam, The Netherlands.

^cInstitute of Molecules and Materials, Radboud University,

Heyendaalseweg 135, 6525 AJ Nijmegen, The Netherlands. ^dNúcleo de Pesquisa em Ciências Exatas e Tecnológicas, Universidade de Franca, Franca, SP, 14404-600, Brazil.

^eLab. de Química Inorgánica y Materiales Moleculares, Universidad Autónoma de Chile, Llano Subercaceaux 2801, San Miguel, Santiago, Chile. ^fDoctorado en Físicoquímica Molecular, Universidad Andres Bello, Av. Republica 275, 8370146 Santiago, Chile.

^gDepartment of Chemistry and Biochemistry, Utah State University, Logan, Utah 84322, United States.

Abstract:

Non-covalent interactions are the main forces involved in the recognition, transport and regulation of virtually all events in biological systems [1]. Although the chemical relevance of anionic molecules is very defined, the chemistry of anion receptors is still a growing area [2]. Host molecules which can interact with anionic species through non-covalent interactions have some advantages due to intrinsic characteristics of the anions, such as size, polarizability and coordination number [3].

Recently, Wang and co-workers [4] prepared a family of heterocalixarenes containing rings of 1,3,5-triazine, bridged by either oxygen or nitrogen atoms. Using the Wang's compound *bis*-chloro-tetraoxacalix[2]arene[2]triazine as a reference model compound, we carefully addressed the nature and the magnitude of the anion- π interactions with the anionic guests Cl^- , Br^- , I^- , BF_4^- , CH_3CO_2^- , H_2PO_4^- , HSO_4^- , NCS^- , NO_3^- , PF_6^- , and SO_4^{2-} [5]. The role of the bridging heteroatoms (N(H)-, O-, and S-) were also studied. The magnitude and the physical nature of the interaction in these host-guest complexes were analyzed through the energy decomposition analysis (EDA) [6], natural bond orbitals (NBO) [7] and the non-covalent index (NCI) [8] as fundamental tools.

The most stable situation in the host-guest systems was observed when the anions are disposed between the triazine rings, leading to different sorts of non-covalent interactions, as well as hydrogen bond formation (Fig. 1a). Anions containing hydrogen atoms also acts as weak hydrogen bond donors to the nitrogen atoms of the triazine units. Non-covalent regions due dispersion interactions are observed between the anions and the triazine unities, specially for the sulfur-bridged heterocalixarene, Fig 1c. The



EDA results reveal stabilizing interactions in all host-guest complexes. The electrostatic interaction plays a fundamental role in oxygen-bridged complexes, whereas the orbital term is the most significant contribution in sulfur- and nitrogen-bridged heterocalixarene complexes. Since in all complexes the Pauli repulsion and the electrostatic term are very similar in magnitude, they cancel each other to a large extent, which suggests that is the orbital interactions the driven forces to the host-guest complex formation.

Two different orbital contributions to the host-guest interaction was found in the NBO analysis: (a) the donation from lone pairs of the anion to the σ^* antibonding orbital of C-H bonds, which is related to the hydrogen bonds and (b) the donation from the anion lone pair to the triazine C-N π^* antibonding orbital, which is the orbital part of the anion- π interaction, Fig. 1b.

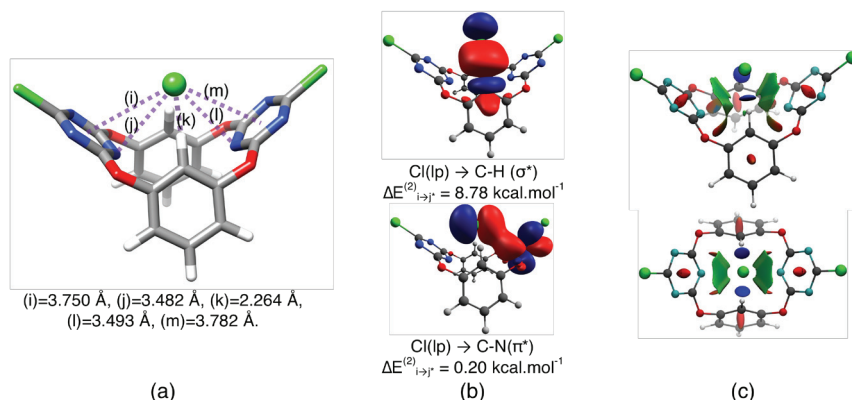


Figure 1: (a) Minima structure with selected geometrical parameters; (b) NBO donor-acceptor interactions with their respective energy; and the (c) Perspective and superior view of NCI analysis for the host-guest complex of oxygen-bridged heterocalixarene with chloride.

Key-words: Anion Recognition. Heterocalixarenes. DFT. EDA. NBO. NCI.

Support: This work has been supported by CNPq, CAPES, NWO and FAPESP.

References:

- [1] A. Frontera, P. Gamez, M. Mascal, T. J. Mooibroek, and J. Reedijk, *Angew. Chemie - Int. Ed.*, 50, 9564 (2011).
- [2] J-M. Lehn, *Supramolecular Chemistry*. (1995) Wiley-VCH, Weinheim, Germany.
- [3] J. W. Steed and J. L. Atwood, *Supramolecular Chemistry*. (2009) Wiley-VCH, Weinheim, Germany
- [4] D. X. Wang and M. X. Wang, *J. Am. Chem. Soc.*, 135, 892 (2013).
- [5] Full article submitted to *Physical Chemistry Chemical Physics (PCCP)* journal.
- [6] F. M. Bickelhaupt and E. J. Baerends, *Rev. Comput. Chem.*, 15, 1 (2000).
- [7] E. D. Glendening, C. R. Landis, and F. Weinhold, *Wiley Interdiscip. Rev. Comput. Mol. Sci.*, 2, 1 (2012).
- [8] E. R. Johnson, S. Keinan, P. Mori-Sánchez, J. Contreras-García, A. J. Cohen, and W. Yang, *J. Am. Chem. Soc.*, 132, 6498 (2010).



Theoretical Studies of CO_2 Capture in Structured and Humid Nanopores

Alexsander Carvalho Vendite

Instituto de Física, USP - Brasil

Abstract: Metal-Organic Frameworks (MOFs) constitute a crystalline material class that has been heavily studied since the last decade and they present structured nanopores [1-5]. MOFs are built coordinating metallic ions with organic multifunctional binders [6]. The combination of organic functional groups with specific inorganic unities allow infinite different arranges to be possible, while presenting unique properties and easy modulation [7]. The ability to identify and capture a variety of gas molecule based on the interaction affinity between a MOF and the gas is highly desirable. That would reduce the financial cost and the time needed to capture undesirable molecules in the atmosphere, like CO_2 , for example. Computational simulations might offer a microscopic perspective about the interactions between the molecules, which is inaccessible with experimental measures.

This work is organized in two steps. At first, simulations considering infinitely long MOFs with CO_2 and Metane gases are compared to previously done simulations. The second part consist of finite MOFs, of different sizes, along with atmosphere gases simulations to identify the effect of humidity in the system. The MOF considered in this work simulations is zinc-methylimidazolate framework-8 (ZIF-8).

The goal of this work is to develop and validate computational methodologies with low processing cost that can identify MOFs with potential to capture CO_2 . Then, the expected results are: (i) develop and validate different force fields for the Monte Carlo computational simulations, using the software DICE [8], to describe the process of absorption and liberation of molecules from the atmosphere in the MOFs; (ii) identify the effects of finite sized MOFs for gas capture; (iii) identify how humidity affect the MOFs and the consequences on gas capture.

Key-words: MOF, Atmosphere, Monte Carlo, Computational Simulation, Carbon Dioxide

Support: This work is being supported by CNPq, CAPES and FAPESP.

References:

- [1] Janiak, C. Dalton Transactions 2003, 2781.
- [2] Kitagawa, S.; Kitaura, R.; Noro, S. Angew. Chem. Int. Ed. Engl. 2004, 43, 2334.
- [3] Mueller, U.; Schubert, M.; Teich, F.; Puetter, H.; Schierle-Arndt, K.; Pastre, J. J. Mat. Chem. 2006, 16, 626.
- [4] Rowsell, J. L. C.; Yaghi, O. M. Microporous and Mesoporous Materials 2004, 73, 3.
- [5] Yaghi, O. M.; O'Keeffe, M.; Ockwig, N. W.; Chae, H. K.; Eddaoudi, M.; Kim, J. Nature 2003, 423, 705.



- [6] Ramanan, A.; Whittingham, M. S. *Cryst. Growth Des.* 2006, 6, 2419.
- [7] Horcajada, P.; Serre, C.; Maurin, G.; Ramsahye, N. A.; Balas, F.; Vallet-Regi, M.; Sebban, M.; Taulelle, F.; Ferey, G. *J. Am. Chem. Soc.* 2008, 130, 6774.
- [8] K. Coutinho, S. Canuto, DICE: Um programa para simulação computacional de líquidos moleculares, utilizando o método Monte Carlo Metropolis e Teoria de Perturbação Termodinâmica para cálculos de energia livre, Universidade de São Paulo, 1997.



Structural and electronic properties of MOF-74

Aline de Oliveira*, Guilherme Ferreira de Lima and Heitor Avelino De Abreu

*Departamento de Química – Universidade Federal de Minas Gerais
Av. Antônio Carlos, 6627 – Pampulha – Belo Horizonte – MG – Brazil, Zip Code 31270-901
alinetgqui@yahoo.com.br

The Metal-Organic Frameworks (MOFs) compose a class of solids with diversified properties, justifying their potential application in different areas, such as gas storage, separation methods, catalysis, sensors, controlled drugs release devices and magnets [1]. The reticular chemistry (methodology that consists on the connection of molecular construction blocks to the formation of predetermined structures) combined with the understanding at molecular level of those solids in their application allow the design of materials with adjusted properties for more efficient technological applications. In this context, computational simulations to obtain structural and electronic information of MOFs are very important.

The MOF-74 is obtained from the combination of divalent metallic cations with the divergent organic ligand 2,5-dihydroxybenzene-1,4-dicarboxylate (DBDC). Its crystalline structure presents a honeycomb topology (Figure 1). A wide diversity of materials can be synthesized based on the topology of MOF-74 [2]. Besides the different divalent metallic cations which can be used to the

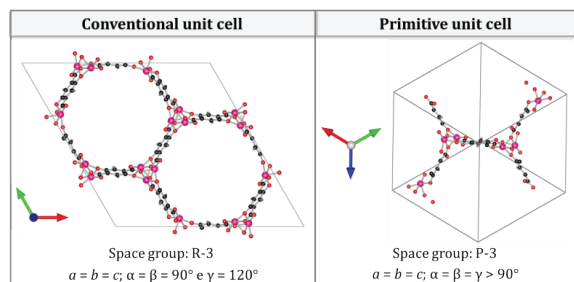


Figure 1. Unit cells of MOF-74. Legend of atoms: oxygen (red), carbon (black), metallic cation (pink), hydrogen (grey).

preparation of these solids, and even the combination of them (in the mixed metals MOFs), organic ligands with larger sizes and with other functional groups can also be employed. After the synthesis of the MOF, it is still possible to make post-synthetic modifications in its structure [3]. All of this justifies the importance to obtain structural and electronic information of the MOF-74, to better understand this solid at molecular level to assist the design of materials with optimized properties.

Computational simulations were performed based on Density Functional Theory (DFT) with plane waves methodology under periodic boundary conditions. The exchange-correlation functionals PBE and PW91 with pseudopotentials of ultrasoft type were used in the Quantum Espresso package [4]. The dispersion was included by the D2 method of Grimme. Cutoff energies of 50 and 500 Ry for plane waves and charge density and potential, respectively, were applied. The Monkhorst-Pack scheme was chosen to the Brillouin-zone integration in the Gamma point, besides Marzari-Vanderbilt 0.02 Ry smearing. The choice of these values for the calculation parameters guarantees a convergence for energy of 1 mRy. The solids Mg-MOF-74, Co-MOF-74 and Mn-MOF-74 were investigated using the primitive unit cell (Figure 1). The spin configuration utilized to simulate the solids constituted by open shell cations (Co(II) and Mn(II)) was the one resulting of an antiferromagnetic coupling among all the ions. Effective Hubbard parameters from 0.0 to 8.0 eV were evaluated to cobalt and manganese atoms, in order to obtain a properly description of the electronic correlation on *d* orbitals.

The levels of theory that best describe both structural (Table 1) and electronic parameters of these materials were PBE-D2/US, PBE-D2+U4+J1/US and PBE-D2+U5.5+J0 for Mg-MOF-74, Co-MOF-74 and Mn-MOF-74, respectively. These levels of theory were used to the detailed investigation of the solids.

Table 1. Lattice parameters for the evaluated MOFs. The percentage errors in relation to the experimental data are in parenthesis.

MOF	Method	$a / \text{\AA}$	$c / \text{\AA}$	Work
Mg-MOF-74	PBE-D2/US	26.039 (0.46)	6.860 (-0.04)	This work
Mg-MOF-74	Neutron Powder Diffraction	25.921	6.863	Queen <i>et al.</i> [5]
Co-MOF-74	PBE-D2+U4+J1/US	26.166 (1.0)	6.836 (0.3)	This work
Co-MOF-74	X-Ray Powder Diffraction	25.906	6.817	Dietzel <i>et al.</i> [6]
Mn-MOF-74	PBE-D2+U5.5+J0/US	26.555 (1.2)	6.975 (-0.9)	This work
Mn-MOF-74	X-Ray Powder Diffraction	26.230	7.035	Zhou <i>et al.</i> [7]

The direct band gaps on the Γ point were 2.10, 1.97 and 2.00 eV for Mg-MOF-74, Co-MOF-74 and Mn-MOF-74, respectively. The experimental value for Co-MOF-74, which was obtained through diffuse reflectance UV-VIS spectroscopy, is 2.02 eV [8], indicating the good description of the material. The analyses of the electronic band structure show that the band gap with the lower energy variation is indirect from Γ to Z point, and occurs between states localized on carbon atoms. There is a significant contribution in the conduction band of states from metallic cations, indicating a possible Lewis acidic activity of these atoms, and a significant contribution in the valence band of states from oxygen atoms, indicating their possible Lewis basic activity.

The methods Electron Localization Function (ELF) and the Quantum Theory of Atoms in Molecules (QTAIM) were applied to the analyses of the electronic density topology obtained to the three solids. These methodologies indicated that the bonds between the metallic cations and the oxygen atoms are predominantly ionic while the other ones are predominantly covalent. Furthermore, through QTAIM analyses were possible to identify non-conventional hydrogen bonds in Mg-MOF-74 and Co-MOF-74, which were not observed to Mn-MOF-74 (Figure 2). This interaction occurs between the oxygen atoms of carboxylate group and the hydrogen atoms bonded to the aromatic ring of the organic ligand. The absence of this interaction in Mn-MOF-74 makes its structure more flexible than the others. The Bader charges to the metallic cations were +1.74, +1.56 and +1.41 a.u. to Mg(II), Mn(II) and Co(Mn), indicating that the increasing order of Lewis acidic strength is $\text{Co(II)} < \text{Mn(II)} < \text{Mg(II)}$. In this way the catalytic activity of these materials, for example, is dependent of the combination of the flexibility of the structure to accommodate the substrates involved in the reaction process (highest to Mn-MOF-74) and of the Lewis acidic strength (highest to Mg(II)).

In conclusion, the levels of theory suitable for computational simulations of Mg-MOF-74, Co-MOF-74 and Mn-MOF-74 were optimized, which provide data in agreement with the experimental ones. Besides that, it was exposed structural and electronic properties of the evaluated MOFs that allow to better understand these solids at molecular level, which can assist the design of new materials and even to recognize processes already described in literature.

Key-words: Metal-Organic Frameworks, MOF-74, DFT, ELF, QTAIM.

Support: This work has been supported by CNPq, CAPES, FAPEMIG and INCT-ACQUA.

References:

- [1] Ramos, A. L. D. *et al. Quim. Nova*, **2014**, 37, 123.
- [2] Deng, H. X. *et al. Science*, **2012**, 336, 1018.
- [3] Larabi, C. *et al. ACS Catal.*, **2012**, 2, 695.
- [4] Paolo, G. *et al. J. of Phys. Condens. Matter*, **2009**, 21, 395502.
- [5] Queen, W. L. *et al. J. Phys. Chem. C*, **2011**, 115, 24915.
- [6] Dietzel, P. D. C. *et al. JACS*, **2008**, 130, 15268.
- [8] Botas, J. A. *et al. Int. J. Hydrogen Energy*, **2011**, 36, 10834.

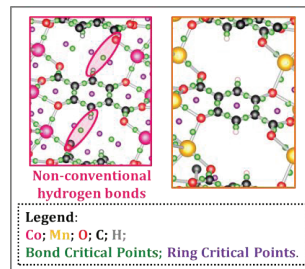


Figure 2. Critical points found to Co-MOF-74 and Mn-MOF-74.

Hydrogen Absorption/Desorption in Palladium and Metal Hydrides

Alyson Celson Medeiros de Oliveira and Antonio Carlos Pavão

Departamento de Química Fundamental, Universidade Federal de Pernambuco, 50740-540 Recife □PE, Brasil

Abstract: Electrical generation from hydrogen, the element with higher energy density per unit mass, requires appropriated materials that can be used in its storage [1]. Palladium, with a high capacity to dissociate, absorb and desorb gaseous hydrogen, has been widely used for hydrogen storage [2], in separation membranes [3] and catalytic hydrogenation [4]. The present DFT calculations on clusters models reveal interesting details of the hydrogen absorption/desorption process in palladium and metal hydrides. The results point to the existence of a pre-absorption state of the hydrogen atom on palladium and indicate that occupation of the tetrahedral site is preferred at low hydrogen concentrations (α -phase), whereas in β -phase the octahedral site is the most stable. Taking the absorption and desorption energies of palladium as reference, we analyzed the properties of the metal hydrides AlH_3 , MgH_2 , $\text{Mg}(\text{BH}_4)_2$, $\text{Mg}(\text{BH}_4)(\text{NH}_2)$ and Li_2NH for hydrogen storage. Among these compounds, MgH_2 most closely resembles the properties of palladium, but the complex hydrides in borohydrides (BH_4^-) and amide (NH_2^-) show better properties both in absorption and desorption. Furthermore we found that Cu and Pd doping of MgH_2 can reduce the desorption energy, improving the hydrogen release.



Keywords: Palladium storage hydrogen; metal hydrides storage hydrogen; DFT calculations;

Support: This work has been supported by Conselho Nacional de Desenvolvimento Científico e Tecnológico (CNPq)

References:

- [1] P. Jena, “Materials for hydrogen storage: Past, present, and future,” *Journal of Physical Chemistry Letters*, vol. 2, no. 3. pp. 206–211, 03-Feb-2011.
- [2] C. Lebouin, Y. Soldo, S. A. Grigoriev, M. Guymont, and P. Millet, “Kinetics of hydrogen sorption by palladium nanoparticles,” *Int. J. Hydrogen Energy*, vol. 38, no. 2, pp. 966–972, 2012.
- [3] W. D. Michalak, J. B. Miller, D. R. Alfonso, and A. J. Gellman, “Uptake, transport, and release of hydrogen from Pd(100),” *Surf. Sci.*, vol. 606, no. 3–4, pp. 146–155, 2012.
- [4] W. Ludwig, A. Savara, R. J. Madix, S. Schauer mann, and H. J. Freund, “Subsurface hydrogen diffusion into Pd Nanoparticles: Role of low-coordinated surface sites and facilitation by carbon,” *J. Phys. Chem. C*, vol. 116, no. 5, pp. 3539–3544, 2012.



Analysis of the interaction of water with TiO₂ nanotubes

Amanda F. Gouveia^a, Mateus M. Ferrer^b, Naiara L. Marana^b, Júlio R. Sambrano^b, Elson Longo^a

^aCDMF - Departamento de Química, Universidade Federal de São Carlos, Brasil

^bGrupo de Modelagem e Simulação Molecular, Universidade Estadual Paulista, Bauru, Brasil.

Abstract: TiO₂ is a multifunctional semiconductor that presents a wide variety of applications in different fields, such as: ceramic, cosmetic, catalyses, etc [1, 2]. At atmospheric pressure, TiO₂ presents three stable polymorphs: rutile, which is thermodynamically favored, anatase and brokita. These polymorphs show different degrees of chemical reactivity and studies have shown that the TiO₂ anatase is more reactive when used for catalysis and photocatalysis studies. The TiO₂ anatase, focus of this study, presents a tetragonal structure formed by clusters [TiO₆]. In this work a study of the TiO₂ nanotubes and the interactions with the water molecule were carried out. The CRYSTAL14 program associated to DFT and to the B3LYP hybrid functional was used. The theoretical results of the nanotubes were correlated with experimental data of the group and those found in the literature.

Key-words: TiO₂ anatase, nanotubes, DFT.

Support: This work has been supported by FAPESP (process n° 2013/26671-9)

References:

- [1] Wang, C.; Hu, Q.; Huang, J.; Wu, L.; Deng, Z.; Liu, Z.; Lui, Z.; Cao, Y., *Applied Surface Science* **2013**, 283, 188-92.
- [2] Chen, B.; Hou, J.; Lu, K., *Langmuir* **2013**, 29, 5911-19.

Segmented all-electron Gaussian basis sets of double and triple zeta qualities for Fr, Ra, and Ac

C.T. Campos^{a,b}, A.Z. de Oliveira^{a*}, I.B. Ferreira^a, F.E. Jorge^{a,c}, L.S.C. Martins^a

^a*Departamento de Física, Universidade Federal do Espírito Santo, Brazil*

^b*Coordenadoria de Ciência e Tecnologia, Instituto Federal do Espírito Santo, Brazil*

^c*Unidade Acadêmica de Física, Universidade Federal de Campina Grande, Brazil*

Keywords: Non-relativistic and relativistic basis sets. Fr, Ra, and Ac elements. B3LYP hybrid functional. Atomic and molecular property calculations.

Support: This work has been supported by CNPq, Capes e Fapes.

Introduction: Segmented all-electron basis sets of valence double and triple zeta qualities plus polarization functions for the elements Fr, Ra, and Ac are generated¹ using non-relativistic and Douglas-Kroll-Hess (DKH) Hamiltonians. The sets are augmented with diffuse functions with the purpose to describe appropriately the electrons far from the nuclei. At the DKH-B3LYP level, first atomic ionization energies and bond lengths, dissociation energies, and polarizabilities of a sample of diatomics are calculated. Comparison with theoretical and experimental data available in the literature is carried out. It is verified that despite the small sizes of the basis sets, they are yet reliable. Here, we will discuss only the first ionization energies.

Methods: The Hartree-Fock (HF) and restricted openshell Møller-Plesset perturbation theory (ROMP2) methods were used to construct the nonrelativistic DZP and TZP basis set. The relativistic set was obtained from the DZP and TZP set by re-optimizing the values of the contraction coefficients using the second-order DKH Hamiltonian. At the end of this process, one obtains: DZP – [9s7p4d1f] for Fr and Ra and [9s6p5d2f] for Ac; TZP – [10s7p5d2f] for Fr and Ra and [10s6p6d3f1g] for Ac. It should be mentioned here that for Ac, it is not possible to optimize any function associated with the 7p orbital.

Results and Discussion: In Table 1 experimental and theoretical ionization energies for Fr, Ra, and Ac are displayed. For comparison, experimental² and other theoretical results³ are also included. In general, the TZP-DKH results are in better accordance with the benchmark theoretical values^{3,4} evaluated with the DK2-CASPT2/ANO procedure (without SO) than the DZP-DKH ones. The differences between the DKH2-B3LYP/TZP-DKH and DK2-CASPT2/ANO results do not exceed 0.131 eV, being the largest one for Ra. Pantazis and Neese⁵ reported a value of 5.18 eV for Ac using the DKH2-B3LYP/[21s13p10d7f] model. The TZPDKH and ANO ionization energies for Fr and Ra agree well with the experimental values², whereas for Ac, they are overestimate about 4.6%. For Ac, a 6d electron is removed in the ionization process, whereas for the other elements it is a 7s one. Considering the Ac element yet, one verified that the SO effects are not large⁴ and that they get worse according to the experimental data². So, the origin

of the problem was attributed to the used electron correlation treatment. The expectancy for Fr and Ra is that the SO corrections be small since in both the cases an electron of s symmetry is ionized. Finally, it should be mentioned here that at the DKH2-B3LYP level of theory, the first ionization energies for Fr (4.154 eV) and for Ra (5.31 eV) calculated in this work with the large contracted ANO basis sets^{3,4} are in good agreement with the TZP-DKH results.

Table 1. First ionization energies (in eV).

	DZP-DKH ^a	TZP-DKH ^a	ANO basis set ^b	Expt. ^c
Fr (² S)	3.869	4.024	3.929	3.942
Ra (¹ S)	5.258	5.241	5.110	5.277
Ac (² D)	5.350	5.231	5.21	5.00

^a Present investigation (DKH2-B3LYP calculations). Basis set generated in this work.

^b DKH2-CASPT2 calculations (without SO)^{2,3}. [12s11p8d5f] and (27s24p18d14f6g3h) basis sets for Fr and Ra and Ac, respectively.

^c Experimental data from Ref. [2] averaged over the J quantum number.

Conclusions: Segmented basis sets (DZP, TZP, DZP-DKH, and TZP-DKH) for Fr, Ra, and Ac are developed to be employed in conjunction with the non-relativistic and DKH Hamiltonians. These sets are compact enough, but still accurate, to be competitive with the ECP valence basis sets. Computationally, they are more efficient than generally contracted basis sets on DFT calculations of large molecules and, according to our knowledge, the smallest all-electron basis set sizes of valence double and triple zeta valence qualities so far presented in the literature. The DKH2-B3LYP/TZP-DKH ionization energies are in excellent agreement with benchmark theoretical values^{3,4}. Except for Ac, which is overestimate, they are close to the experimental data². In summary, along these years we have shown that it is possible to develop all-electron segmented basis sets that have a good balance between accuracy and computational cost on atomic and molecular property calculations. The XZP and XZP-DKH (X = D and T) basis sets for the atoms from H to Lr are available on different formats at <http://qcgv.ufes.br>.

References:

- [1] Campos, C. T., et al, Chem. Phys. Lett 675 (2017) 1.
- [2] C.E. Moore, National Bureau Standards Circular 467, US Government Printing Office, Washington, 1982.
- [3] B.O. Roos, V. Veryazov, P.-O. Widmark, Theor. Chem. Acc. 111 (2004) 345.
- [4] B.O. Roos, R. Lindh, P.-A. Malmqvist, V. Veryazov, P.-O. Widmark, Chem. Phys. Lett. 409 (2005) 295.
- [5] D.A. Pantazis, F. Neese, J. Chem. Theory Comput. 7 (2011) 677.

Theoretical and experimental study of lanthanide ion complexes: Spectroscopy and chemical bond analysis

Amauri F. Silva (G)¹, G. B. V. Lima (PG)¹, Albano N. Carneiro (PG)², Renaldo T. Moura Jr. (PQ)³, Oscar L. Malta (PQ)¹, Wagner M. Faustino (PQ)¹

¹Federal University of Paraíba, Department of Chemistry, João Pessoa-PB, Brazil.

²Federal University of Pernambuco, Department of Fundamental Chemistry, Recife-PE, Brazil.

³Federal University of Paraíba, Department of Chemistry and Physic, Areia-PB, Brazil. email: amauriquimica@gmail.com

Abstract: The theoretical intensity parameters of 4f-4f transitions in lanthanide complexes depend on the chemical environment and the nature of rare-earth ion, where in the absence of inversion center, the two main contributions are the forced electric dipole mechanism (FED) and the dynamics coupling (DC) mechanism [1,2]. The overlap polarizability (α_{op}) and ionic specific valence were recently used [3] to reshape and reinterpret the expressions of these two mechanisms, in which the ligand effective polarizability describes the environment polarizability not accounted into α_{op} . In this work, a set of different complex were analyzed by using the new methodology [3]. The investigated complexes are $[Ln(\beta D)_3(L)_X]$, (where $Ln = Eu^{3+}$, Tb^{3+} and Gd^{3+}) with β -diketones ligands βD (BZAC = benzoylacetate; DBM = dibenzoylmethanate and TTA = 2-thenoyltrifluoroacetate) and ligands L derived from 2-aminopyridine (2AP) and 2-aminoprимidine (2APM), wherein $X = 1$ or 2. These compounds were synthesized, characterized and their quantum efficiency, radiative (A_{rad}) and nonradiative (A_{nrad}) emission coefficients, and intensity parameters Ω_2 and Ω_4 where experimentally obtained from spectroscopic data (Table 1).

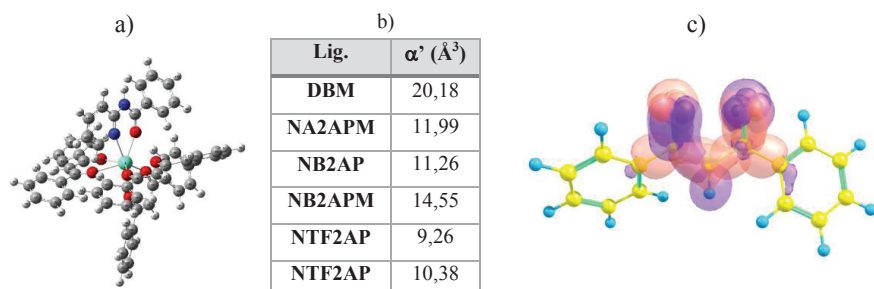


Figure 1. (a) Eu^{3+} complex $[Eu(DBM)_3(NP2AP)]$ (b) Table with the obtained values of the ligand effective polarizabilities; (c) DBM ligand orbitals localized at the coordination region.

It is known that the ligand field breaks the symmetry of the metal Ln, and modifies the electron density around the metal center. Consequently, the energies of the $^5D_0 \rightarrow ^7F_\lambda$ transitions, on the Eu^{3+} ion (for example), also change as a consequence

the nephelauxetic effect [1,2]. This electron density is dependent on the characteristics of the ligand, that is, whether a ligand is a soft or hard Lewis basis or if it has an electron donor or withdrawn substituent. The characterization of the $\text{Ln}^{3+}\text{-L}$ bond situation [2] reveals that chemically more polarizable bonds and environments contribute to increase of the intensity parameters in lanthanide compounds [1-3]. It can be seen in Table 1 that the experimental Ω_2 and Ω_4 values change a lot, when some systematic ligand modifications are imposed. For instance, Ω_2 for $[\text{Eu}(\text{DBM})_3(\text{NTF2AP})]$ is $18.6 \cdot 10^{-20} \text{cm}^{-2}$, while the same parameter for $[\text{Eu}(\text{DBM})_3(\text{NTF2APM})]$ is $37.3 \cdot 10^{-20} \text{cm}^{-2}$, making it clear the importance of the theoretical study.

Table 1. Experimental intensity parameters Ω_λ (in 10^{-20}cm^{-2}), radiative (A_{rad}), nonradiative (A_{nrad}) and total (A_{total}) emission coefficients (in s^{-1}), emitter lifetimes τ (in ms) and quantum efficiency η_{cal} (in %).

Complexes	Ω_2	Ω_4	A_{rad}	A_{nrad}	A_{total}	τ	η_{cal}
$[\text{Eu}(\text{BZAC})_3(\text{H}_2\text{O})_2]$	16.9	2.2	437.7	4825.5	5263.2	0.19	8.3
$[\text{Eu}(\text{BZAC})_3(\text{NA2APM})]$	21.9	2.5	541.5	582.1	1123.6	0.89	48.2
$[\text{Eu}(\text{BZAC})_3(\text{NA2AP})]$	15.7	6.5	464.2	2984.1	3448.4	0.29	13.5
$[\text{Eu}(\text{BTF})_3(\text{H}_2\text{O})_2]$	18.6	1.8	461.1	2170.5	2631.6	0.38	17.5
$[\text{Eu}(\text{BTF})_3(\text{NTF2AP})]$	8.9	6.2	339.9	822.9	1162.8	0.86	29.2
$[\text{Eu}(\text{BTF})_3(\text{NTF2APM})]$	18.4	2.5	466.8	723.7	1190.5	0.84	39.2
$[\text{Eu}(\text{DBM})_3(\text{H}_2\text{O})_2]$	38.0	1.8	883.6	99116.4	100000	0.01	0.9
$[\text{Eu}(\text{DBM})_3(\text{NTF2AP})]$	18.6	2.5	500	6167	6667	0.15	8.0
$[\text{Eu}(\text{DBM})_3(\text{NTF2APM})]$	37.3	2.6	867.4	1513.5	2380.9	0.42	36.4
$[\text{Eu}(\text{TTA})_3((\text{H}_2\text{O})_2)]$	29.3	3.8	700.5	3466.2	4166.7	0.24	16.8
$[\text{Eu}(\text{TTA})_3(\text{NA2AP})_2]$	29.1	2.5	688.7	1485.2	2173.9	0.46	31.7
$[\text{Eu}(\text{TTA})_3(\text{NA2APM})_2]$	32.8	3.9	782.9	1103.9	1886.8	0.53	41.5
$[\text{Eu}(\text{TTA})_3(\text{NTF2AP})]$	13.7	2.4	393.4	1035.2	1428.6	0.70	27.5
$[\text{Eu}(\text{TTA})_3(\text{NTF2APM})_2]$	39.6	1.5	913	754	1667	0.6	55

Initial geometries of the complexes were pre-optimized by Sparkle/PM6 model, and were used as input for the DFT B3LYP/6-31+g(d) optimizations. The ligand effective polarizabilities were calculated using B3LYP/aug-cc-pVDZ methodology, where the α' values were calculated from the LMOs in a region within two bonds from the ligating oxygen atoms (Figure 1c). The Pipek-Mezey and Ruedenberg localization procedures were used. Each ligands geometries in all complexes were used to calculate the α' value, where some of the results are depicted in Figure 1b. It is important to highlight that the biggest calculated α' was obtained for the DBM ligand, which also has some of the biggest Ω_2 values. The recent developed JOYSpectra program has been used for the calculations of force constants, charge factors and theoretical intensity parameters.

Key-words: Spectroscopy; lanthanide ion; polarizability; chemical bond; DFT.

Support: UFPB, CAPES, CENAPAD/SP and LCCQS/UFPB.

References:

- [1] O. L. Malta, H. J. Batista, L. D. Carlos, Chem. Phys., 282, 21 (2002).
- [2] L. D. Carlos, O. L. Malta, R. Q. Albuquerque, Chem. Phys. Lett., 415, 238 (2005).
- [3] R. T. Moura Jr., A. N. Carneiro Neto, R. L. Longo, O. L. Malta, J. Lumin., 170, 420 (2016).

The spherical-harmonics representation for the interaction between H₂O-HX molecules, with X = H, F, Cl and Br atoms.

Ana Claudia P.S. CRUZ^{1*}, Patrícia R. P. BARRETO¹

¹Instituto Nacional de Pesquisas Espaciais (INPE/MCT), Laboratório Associado de Plasma (LAP), São José dos Campos, SP, CEP 12247-970, CP515, Brazil.

*anaclaudia.ps.cruz@gmail.com

Abstract: The explicit representation of the potential energy surfaces (PES) for interactions of H₂O-HX systems, with X representing the atoms H, F, Cl and Br, based on orthogonal vectors, via harmonic expansion functional depending on the distance between the centers of mass of the two molecules and on four angles, assuming that the two molecules are rigid[1-3]. In this way, account for two contributions: an external one depending on the three angle variables which define the mutual orientation of the two molecules and an internal one expressed by the angle which describes the position of the oxygen atom in H₂O with respect to the H₂O -HX system, as can be seen in the figure 1.

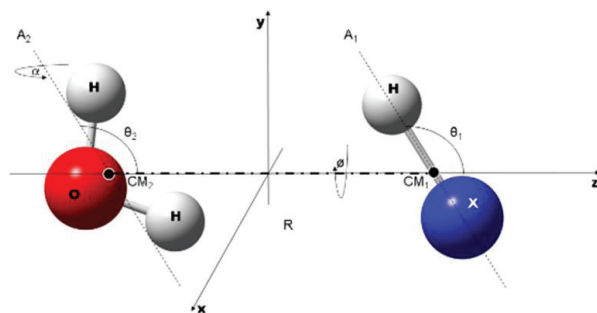


Figure 1. The mutual position of the H₂O and HX molecules is expressed by five coordinates in the Cartesian coordinate framework *xyz*.

The potential energy surface (PES) was generated in the framework of the supermolecular approach, using the counterpoise-corrected interaction energies at the CCSD(T), auc-cc-pVQZ level with the Molpro code. Comparisons with the atoms involved are presented and their features are discussed. The analytical form of the potential energy surfaces, for each of the leading configurations, is constructed by fitting the energies to a fifth degree generalized Rydberg function [4,5] and Improved Lennard Jones [6] respectively into the *ab initio* points, taking the advantage of the parameters also obtained as source of comparisons. The PES was computed for about one hundred points for each of the 27 leading configurations, whose number reduces to 23 because of symmetry properties. In the figure 2, we report the isotropic components of the interaction potential of H₂O -HX system, which can be measured experimentally, allowing the comparison and evaluation of the capacity of the theoretical method used.

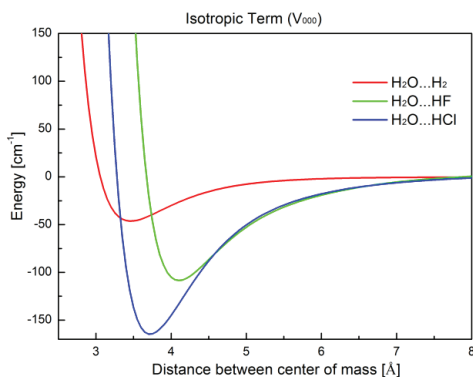


Figure 2. Isotropic Term for the H₂O -HX System, with X = H, F and Cl atoms.

The results for the system reduced the number of degree of freedom, reducing the computational cost simplifying the fitting and representation of the potential energy surface for other applications also to classical and quantum molecular dynamics simulations.

Key-words: Potential Energy Surfaces, van der Waals interactions, Rydberg function, Improved Lennard Jones function, Spherical Harmonics.

Support: This work has been supported by CAPES.

References:

- [1] Aquilanti V., Ascenzi D., Bartolomei M., Cappelletti D., Cavalli S., Vitores M. C., and Pirani F., *J. Am. Chem. Soc.*, 121, 10794, (1999).
- [2] V. Aquilanti, M. Bartolomei, D. Cappelletti, E. Carmona-Novillo and F. Pirani, *Chem. Phys.*, 3, 3891, (2001).
- [3] Barreto P.R.P., *J.Chem.Phys* 113, 15047, (2009).
- [4] Rydberg, R. Z. *Fur Physik.*, v. 73, p. 376, (1931).
- [5] Murrel, J. N.; Carter, S.; Farantos, S. C.; Huxley, P.; Varandas, A. J. C. *Molecular potential energy functions.* John Wiley and Sons,(1984).
- [6] Pirani, F., Brizi, S., Roncaratti, L. F., Casavecchia, P., Cappelletti, D., and Vecchiocattivi, F. *Phys. Chem. Chem. Phys.*, 10(36):5489–503, (2008).



Aluminium-Silicon nanoalloys: structures and stabilities

Authors: Ana Débora Porto Silveira, Alexandre C. R. Gomes, Breno R. L. Galvão

Address: CEFET-MG, Av. Amazonas, 5.253, Nova Suíça, Belo Horizonte, MG, CEP: 30.421-169.

Abstract: Clusters have been a central theme in the development of nanotechnology research, and its study allows the development of properties tunable by size in the nanometric scale.^[1] Agglomerates consisting of two or more metal elements are called nanoalloys, and may also be tuned by composition. These are highly reactive, and can be prepared by means of beam techniques or by matrix isolation.^[1] The metallic nanoalloys that are the object of this work, have as components aluminum and silicon. Al clusters have been extensively studied, both experimentally and theoretically, due to their wide application in the field of catalysis, electronics, among others.^[1,2] Si clusters are of great interest because of two potential applications in the semiconductor and optoelectronic industries. The Al-Si compounds have considerable significance in the nanomaterials areas.^[3] To investigate these alloys theoretically it is necessary first to determine the geometrical configuration of the most stable structures, which is difficult due to the large number of isomers generated by the permutations of Al and Si atoms (called homotops).^[4] The objective of this work is to predict the stability of such clusters, employing previously determined geometries. For this purpose, clusters between three and thirteen atoms with the lowest energies are considered. The structures were optimized using the Möller-Plesset Perturbation Theory (MP). A basis set was used that has an effective core potential (ECP), where the innermost electrons are disregarded (LANL2DZ), culminating in a faster calculation.^[5,6] The results are refined using CCSD and compared to DFT calculations with larger basis sets. The software used for the calculations was the General Atomic and Molecular Electronic Structure System (GAMESS), version 2016^[7] and for visualization wxMacMolPlt was used.^[8] The results obtained are interpreted according to the reactivity and stability of the structures using binding energy, excess energies and the HOMO-LUMO gap. The binding energy (eq.1) gives us the stability of the clusters as a function of composition.^[4]

$$E_b(Al_xSi_y) = E(Al_xSi_y) - xE(Al) - yE(Si) \quad \text{eq.1}$$

According to the binding energy analysis, the larger the amount of silicon atoms in the cluster composition, the more likely they are to become more stable. By means of the excess energy (eq.2), the favorability of the formation of alloy rather than the corresponding pure clusters can be obtained.^[4] A negative value indicates that the formation of the corresponding nanoalloy is favored.

$$E_{exc}(Al_xSi_y) = E_b(Al_xSi_y) - x \frac{E_b(Al_N)}{N} - y \frac{E_b(Si_N)}{N} \quad \text{eq.2}$$

The excess energy analysis indicates that smaller clusters tend to be more stable in the homonuclear form, whereas in cluster with 8, 9 and 11 atoms mixing is favored.



HOMO-LUMO gaps, electron affinity and ionization energies are also relevant to estimate the reactivity of the clusters and will also be calculated.

Key-words: cluster, nanoalloy, Al-Si, bonding energy, excess energy.

Support: This work has been supported by Centro Federal de Educação Tecnológica de Minas Gerais (CEFET-MG), Fundação de Apoio à Pesquisa de Minas Gerais (Fapemig), Programa de Pós-Graduação Multicêntrico em Química de Minas Gerais (PPGMQ-MG), Rede Mineira de Química (RQ-MG) and Conselho Nacional de Desenvolvimento Científico e Tecnológico (CNPq).

References:

- [1] M. Alipour, A. Mohajeri, *J. Phys. Chem. A*, 48, 114 (2010).
- [2] D. J. Henry, A. Varano, I. Yarovsky, *J. Phys. Chem. A*, 40, 112 (2008).
- [3] N. M. Tam, T. B. Tai, V. T. Ngan, M. T. Nguyen, *J. Phys. Chem. C*, 115 (2011).
- [4] M. A. M. Paiva, B. M. T. C. Peluzo, J. C. Belchior, B. R. L. Galvão, *Phys. Chem. Chem. Phys.*, 18 (2016).
- [5] I. N. Levine, “Quantum Chemistry” (2008), Pearson Prentice Hall.
- [6] K. L. Schuchardt, B. T. Didier, T. Elsethagen, L. Sun, V. Gurumoorthi, J. Chase, J. Li, T. L. Windus, *J. Chem. Inf. Model.*, 47, 1045 (2007).
- [7] M. W. Schmidt, K. K. Baldridge, J. A. Boatz, S. T. Elbert, M. S. Gordon, J. H. Jensen, S. Koseki, N. Matsunaga, K. A. Nguyen, S. Su, T. L. Windus, M. Dupuis, J. Montgomery Jr., *J. Comput. Chem.*, 14, 1347 (1993).
- [8] B. M. Bode, M. S. Gordon, *J. of Molecular Graphics and Modelling*, 3, 16 (1998).



Computational Investigation of Ligand Influence on the Insertion of Allene into Cu-B (Boryl) Bond

Ana Paula de Lima Batista, Atualpa A. C. Braga

Departamento de Química Fundamental, Instituto de Química, São Paulo, São Paulo 05508-000, Brazil

Abstract: Borylation of unsaturated compounds catalyzed by transition metal boryl complexes have attracted increasing attention because the reactions yield organoboron derivatives that are used in synthetic processes, especially cross-coupling reactions [1,2]. Recently, Tsuji and co-authors reported, for the first time, the copper catalyzed boraformylation of allenes [1]. In this experimental study, they found that copper complexes bearing different ligands lead to huge discrepancies in the relative yields of β -boryl β,γ -unsaturated aldehydes. A crucial step of the general mechanism of this type of reaction involve the substrate insertion into the Cu-B (boryl) bond, which is usually responsible for the regioselectivity of the reaction [3]. In order to unveil the role of different ligands in the mechanism, the present work uses computational approaches to explore their influence on the insertion of allene into Cu-B (boryl) bond. Figure 1 shows the transition state (TS) associated with this process, in which a N-heterocyclic carbene ligand (NHC) is present. This TS was obtained at the B3LYP-D3/6-31G(d),SDD(Cu) level of theory using Gaussian09. Further DLPNO-CCSD(T) calculations and IBO (Intrinsic Bond Orbitals) analysis will be performed to refine energies and discuss bond interactions, respectively, on this system and others ones with different ligands.

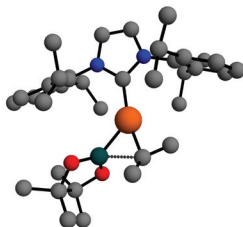


Figure 1. TS associated with the insertion of allene into Cu-B (boryl) bond. The H atoms are omitted for clarity.

Key-words: Boraformylation, Catalysis, DFT and CCSD(T) Calculations.

Support: This work has been supported by FAPESP, grants #2015/01491-3 and #2014/25770-6

References:

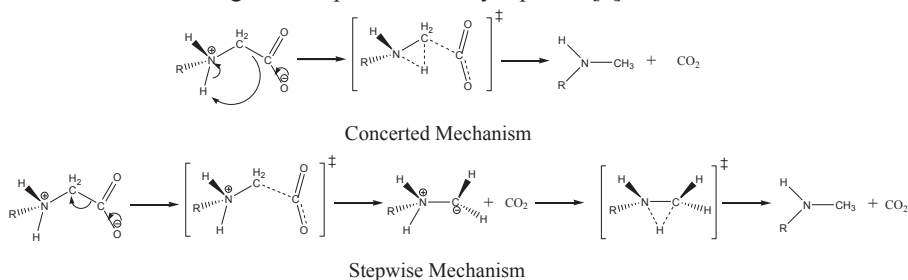
- [1] T. Fujihara, A. Sawada, T. Yamaguchi, Y. Tani, J. Terao, Y. Tsuji, *Angew. Chem. Int. Ed.* 56, 1539 (2017).
- [2] E. C. Neeve, S. J. Geier, I. A. I. Mkhaliid, S. A. Westcott, Todd B. Marder, *Chem. Rev.* 116, 9091 (2016)
- [3] H. Zhao, L. Dang, Todd B. Marder, Z. Lin *J. Am. Chem. Soc.*, 130, 5586 (2008)

On the Degradation Pathway of Glyphosate and Glycine

Anderson José Lopes Catão and Alejandro López-Castillo

*Departamento de Química, Universidade Federal de São Carlos (UFSCar),
São Carlos, SP, 13560-970, Brazil*

Abstract: Glyphosate is a systemic and non-selective herbicide consisting of a glycine and a phosphonomethyl group [1]. The use of glyphosate-based herbicides (GBHs) has increased significantly as to be worthy of attention in the health areas, both environmental and human health [2]. In case of treatment, e.g. water depollution, it is important to know the details of molecular degradation mechanism. Computation models open the possibility of studying such process *in silico*. In processes that occur in liquid phase solvent plays an important rule. One alternative to include solvent effects in quantum chemical calculations is the solvent implicit model. There are several models and they have proved to be very useful to take into account macroscopic effects but they are poor in describing microscopic detail, such as bond-breaking process. Another alternative is to include solvent explicitly, by means of addition of solvent molecules, i.e. microsolvation. We studied the degradation mechanism of glyphosate and glycine, sketched in Scheme 1. All calculations were performed using the GAUSSIAN 09 package [3]. We performed geometry optimizations and intrinsic coordinate reaction (IRC) [4] calculation using aug-cc-pVDZ basis set [5] and M062X [6] functional. Solvent effects were included by means of both microsolvation and the polarizable continuum solvation model IEF-PCM [7]. We found two degradation pathways of glycine and glyphosate. Both routes lead to a decarboxylation of the molecule. In the case of glyphosate the product formed was the aminomethylphosphonic acid (AMPA), which is one of the degradation product already reported [4].



Scheme 1 – Glycine (R = H) and Glyphosate (R = PO₃H₂CH₂) degradation mechanisms: concerted (up) and stepwise (down) mechanisms

The energy barrier is quite similar for both molecule, 3.24 eV and 3.13 in the concerted mechanism for glycine and glyphosate, respectively, and 1.90 eV and 1.36 for glycine and 1.90 eV and 1.09 eV for glyphosate in the two-step mechanism for IEF-PCM. The

concerted mechanism is characterized by a proton transfer, from nitrogen to carbon vicinal atom, accomplish by the breaking of the C—C bond. The stepwise mechanism, which occurs in two steps, begins with decarboxylation followed by the proton transfer. When explicit water molecules are included, mechanism profiles still the same but energy barriers not. Transition states were characterized to each system, with explicit water molecules or not. Water molecules were included in order to preserve the transition state of that obtained with only implicit solvent. Although transition states differ, degradation mechanism is essentially the same. Concerted mechanism seems to be assisted by water molecules, which take a part in the proton transference process. This assistance reduces the energy barrier considerably, as shown in Figure 1. In glycine case energy barrier is reduced by almost half when two water molecules are included.

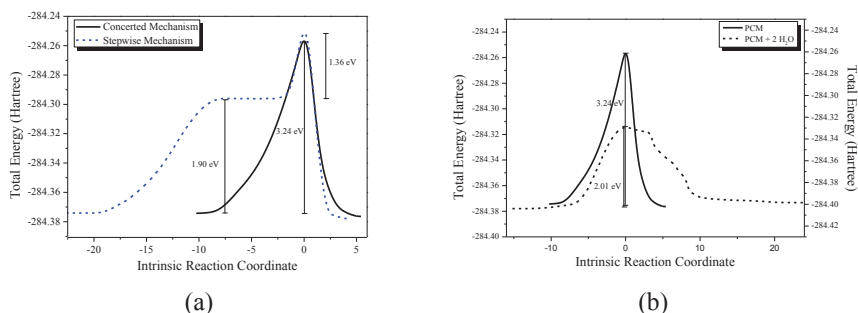


Figure 1 – Glycine IRC pathways: (a) concerted and stepwise mechanisms in implicit solvent model; (b) concerted mechanism with (dashed line – right Y axis) and without (solid line – left Y axis) explicit water molecules (isolated water molecule total energy is -76.41522075 hartree).

In summary, two mechanisms were presented to the degradation of glycine and glyphosate molecule. Although both routes are globally energetic equivalent, the stepwise mechanism needs lower activation energy and might be the most common chemical degradation pathway.

Key-words: Glyphosate, Glycine, Degradation Pathway, Microsolvation

Support: This work has been supported by CAPES

References:

- [1] US patent 3799758, J. E. Franz. **N-phosphonomethyl-glycine phytotoxicant compositions**, issued 1974-03-26, assigned to Monsanto Company.
- [2] Myers et al. **Environ. Health**, 15:19, 2016.
- [3] M. J. Frisch et al. **Gaussian 09**, Revision A.02. Wallingford CT: Gaussian, Inc.; 2009.
- [4] K. Fukui. **Acc. Chem. Res.**, 14, 363-68, 1981.
- [5] R. A. Kendall, T. H. Dunning Jr., and R. J. Harrison. **J. Chem. Phys.**, 96 6796-806, 1992; D. E. Woon and T. H. Dunning Jr. **J. Chem. Phys.**, 98, 1358-71, 1993.
- [6] Y. Zhao, D. G. Truhlar. **Theor. Chem. Acc.**, 120(1-3), 215-241, 2007.
- [7] V. Barone, M. Cossi, J. Tomasi. **J. Chem. Phys.**, 107(8), 3210-3221, 1997.
- [8] J. P. Giesy, S. Dobson, K. R. Solomon. **Rev. Environ. Contam. T.**, 167, 35–120, 2000.

Thermodynamic and Kinetic Study of Germanium Crystal Growth by Computer Simulations

Weverson R. Gomes,^a Edgar D. Zanotto^b and André F. de Moura^a

^a*Department of Chemistry – Federal University of São Carlos*

^b*Department of Materials Engineering – Federal University of São Carlos*

Abstract: Monocrystalline germanium (Ge) is a key material in the fields of semiconductors, infrared optics and high-frequency electronics. In its crystalline form Ge has a diamond structure, whereas in the amorphous state it forms a random and distorted tetrahedral network. The experimental evaluation of its crystallization kinetics in the supercooled liquid is complicated by the fact that it occurs very fast within the interior of a dense liquid [1] and the critical nucleus size is usually too small to be detected. Therefore, the computational study of the molecular origins and microscopic mechanism of homogeneous crystal nucleation can provide relevant molecular insight on this system [2] and can also be useful to other materials. In this work we have carried out standard molecular dynamics simulations using the Tersoff potential [3] for Ge (~4,000 atoms). The crystalline phase was characterized by a tetrahedral order parameter (q) [4], whose values for a unique atom range between -3 and 1 ($q=1$ in a perfect tetrahedral arrangement and $q=-3$ for a linear configuration). Individual Ge atoms were considered to be in the crystalline state whenever $q>0.92$. Spherical crystalline nuclei were created into an amorphous Ge matrix in order to find the critical size of the crystalline nucleus (*Figure 1, left*) in a few temperatures at very deep undercooling conditions. The simulations allowed the calculation of free energy terms related to the formation of a crystalline nucleus with radius r in an amorphous matrix (*Figure 1, right*), to be used latter in the classical nucleation theory (CNT) calculations. Both results are consistent with a critical size of the Ge nucleus at 2000 K of ca. 22 Å (*Figure 1*). The crystallization of Ge is pictured on *Figure 2*, where all atoms in red represent those in tetrahedral configuration ($q> 0.92$). The initial structure had a seed crystal of diameter equal 24 Å (*Figure 2, left*), and after 5000 ps nearly all atoms evolved into a crystalline structure (*Figure 2, right*). The measurement of the crystal growth velocity is being carried out using a tenfold larger system in the SDumont supercomputer, in order to minimize finite-size effects which have been detected in the simulations with these smaller models.

Key-words: molecular dynamics simulations, crystal growth, germanium, entropy, order parameter

Support: The authors are indebted to FAPESP for the financial support (2012/15147-4, 2013/07296-2). AFM thanks MEC/PET for a fellowship. The authors acknowledge the National Laboratory for Scientific Computing (LNCC/MCTI, Brazil) for providing HPC resources of the SDumont supercomputer, which have contributed to the research results reported within this communication. URL: <http://sdumont.lncc.br>

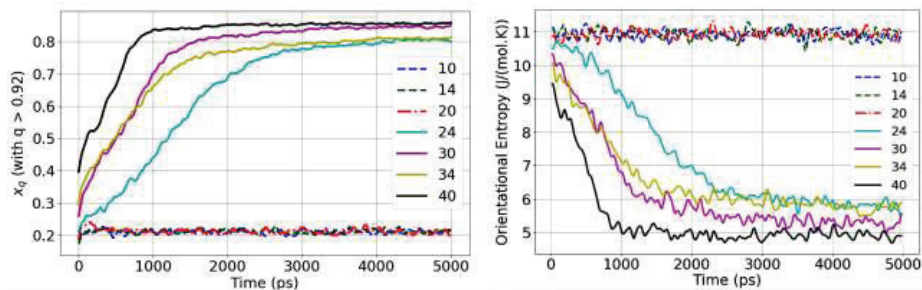


Figure 1: Fraction of Ge atoms with tetrahedral order parameter larger than 0.92 (left) and orientational entropy at 2000 K (right). Different colors stand for the size of the seed used for nucleating the crystal growth (diameters in Å).

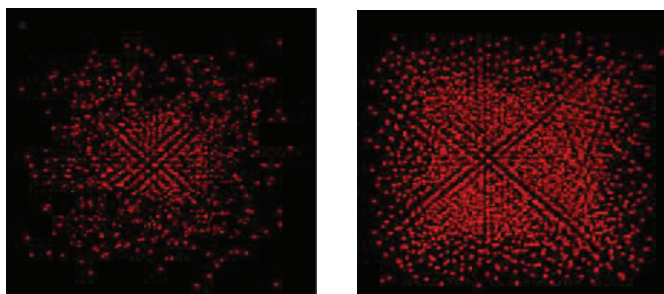


Figure 2: Atoms with $q > 0.92$ at the beginning of the simulation (left) and after 5 ns (right). Atoms with $q < 0.92$ are not shown for clarity (seed diameter of 24 Å, $T = 2000$ K).

References:

- [1] SOSSO, G. C. et al. Crystal Nucleation in Liquids: Open Questions and Future Challenges in Molecular Dynamics Simulations. *Chem. Rev.*, 2016, n. 12, p. 7078–7116, 2016.
- [2] ZANOTTO, E. D.; MAURO, J. C. The glassy state of matter: Its definition and ultimate fate. *Journal of Non-Crystalline Solids*, 490-495, 2017.
- [3] CHAU, P. L.; HARDWICK, A. J. A New Order Parameter for Tetrahedral Configurations. *Mol. Phys.* 1998, 93, 511–518.





Painel 025 | PN.025

Title: Electron-Molecule Collision Calculations Based On The First Born Approximation and EOM-CCSD

Authors: André P. Oliveira, Alexandre B. Rocha, Ginette Jalbert

Address: IQ-UFRJ, Ilha do Fundão, Rio de Janeiro, RJ

Abstract: There is a long history of important developments in quantum theory supported exclusively on scattering experiments. Concerning particularly the subfield of electron collision, there are still important topics such as atmospheric chemistry and the growing relevance of electron energy loss spectroscopy to name just a few[1].

The Born approximation is as old as quantum mechanics itself, and it is still the fundamental tool for collisions within fast electrons. While keeping the energy of the bound states as a lower limit, the Born approximation is the prevalent theoretical treatment for electron-molecule collisions [2]. Therefore, the main issue to be attacked is the dependence on the molecular wave functions. The method is very sensitive to the quality of the wave functions and the theoretical apparatus of highly correlated methods are of fundamental importance.

The problem of electron scattering by molecule has not profited decades of developments of quantum chemistry methods, which is evidenced by the absence of calculations of properties related to scattering problems in modern quantum chemistry computational packages. This led us to work on methods for practical computation of scattering amplitudes based on high quality wave functions. Very successful applications were found by using density matrices obtained from equation of motion – coupled cluster singles and doubles(EOM-CCSD)[3] and configuration interaction(CI). The convenience of using an Octave [4] scripts has an immediate trade off on computer time, although for an average ten minute computation we were able to obtain good accuracy. These results are presented here for a series of small molecules used as benchmark. Results include some scattering experiments never simulated before with quantitative accuracy.

Key-words: Scattering, Collision, EOM-CCSD, Born Approximation

Support: CNPq

References:

- [1] Brydson, R. "Electron Energy Loss Spectroscopy" (2001) A. Köhler (editor) , Royal Microscopical Society MICROSCOPIC HANDBOOKS Volume 48, BIOS Scientific Publishers Ltd, Oxford, UK
- [2] M. Inokuti, Rev. Mod. Phys. 43, 3 (1971). 297-347.
- [3] J. F. Stanton and R. J. Bartlett, J. Chem. Phys., 98 (1993) 7029-39.



Polymorphism of Lipid A bilayers in presence of Al^{3+} at different ionic concentrations of NaCl and $AlCl_3$

Andresa Messias (IC), Frederico Pontes (PQ), Thereza A. Soares (PQ)

¹*Department of Fundamental Chemistry, Federal University of Pernambuco, Cidade Universitária, Recife - PE, 50740-540*

Abstract: Lipid A is the endotoxically active region of the lipopolysaccharide (LPS) molecule composing the outer membrane of Gram-negative bacteria. Lipid A is a highly potent stimulator of the innate and adaptive immune system of mammals. In the last decades, monophosphorilated Lipid A combined with aluminum salts have been commonly used as vaccines adjuvants since it induces similar cytokine profiles as LPS but it is at least 100-fold less toxic [1]. Previous experimental studies have shown a correlation between the chemical structure and aggregation phase of Lipid A and its biological activity [2]. It is also known that different cations can induce transitions from lamellar to non-lamellar arrangement of Lipid A bilayers [3]. Therefore, we have investigated the influence of aluminum cations on Lipid A aggregation phase using atomistic molecular dynamics simulations. We have performed simulations of mono- and diphosphorilated Lipid A bilayers from *E. coli* in presence of Al^{3+} at different salt regimes: (a) 0 mM where Al^{3+} was added only to neutralize the system total charge. (b) 150 mM NaCl and (c) 150 mM $AlCl_3$. All molecular dynamics simulations were carried out in a *NpT* ensemble, semi-isotropic scheme (1 bar) and temperature of 300K using the GROMACS 4.5.6 program [4]. We have used an extension of GROMOS 53A6 force field for Lipid A [2] and in-house developed tools to analyze curved membrane surfaces [5]. The Lipid A bilayer at 0mM salt concentration kept a lamellar arrangement, with the presence of curvature in the surface of the diphosphorilated Lipid A bilayer. Systems containing $AlCl_3$ suffer a structural transition from lamellar to non-lamellar arrangement. Similar behavior was observed for Lipid A bilayers neutralized with Al^{3+} and in presence of NaCl. Furthermore, it is observed the full replacement of aluminum by sodium cations on phosphate binding groups of Lipid A. Lipid A bilayers show selective affinity to cations, which influence directly the final aggregation phase of these systems. We are currently investigating the effect of a broader range of concentrations and multisalt solutions on the aggregation and dynamics of Lipid A bilayers.

Key-words: Hofmeister effects, Order parameters, Radial distribution function, Cation and membrane hydration

Support: This work has been supported by FACEPE, CENAPAD-UFC, BioMol Project/CAPES, STINT, CNPq



References:

- [1] MacLeod, M. K.; McKee, A.S.; David, A.; Wang, J.; Mason, R.; Kappler, J.W.; Marrack, P., Proc. Natl. Acad. Sci. USA 108: 7914–7919 (2011).
- [2] Brandenburg, K. J., Biophys.,64, 1215-1231 (1993).
- [3] Pontes, F.J.S.; Rusu, V.H.; Soares, T.A.; Lins, R.D., J. Chem. Theory Comput. 8, 3830–3838 (2012).
- [4] Kabsch, W.; Sander, C., Biopolymers. 22, 2577 (1983).
- [5] Santos, D.E.S.; Pontes, F.J.S.; Coutinho, K.; Linds, R.D.; Soares, T.A, in preparation (2017)



Substituent effect on $^1J_{\text{CH}}$ in benzaldehyde derivatives

A. Nepel, R. V. Viesser, C. F. Tormena
Institute of Chemistry/University of Campinas, Brazil

Abstract: NMR spin–spin coupling constants (SSCCs) can lead to insights about the electronic structure of molecules when experimental NMR data are combined with quantum mechanical calculations [1]. This is possible because theoretically, the SSCCs can be decoded in different components of the SSCCs mechanism, which allows the identification of “steric” or “hyperconjugative” origin [2]. In this work, the $^1J_{\text{CH}}$ of the formyl group for the substituted benzaldehydes with distinct electronic character in *ortho*, *meta*, and *para* positions were evaluated (Table 1). J -coupling constants and their decompositions were calculated using the method described by Autschbach [3] with the CPL module of ADF package using PBE0 functional and jcp1 basis set. Experimental and theoretical results indicated that there is a significant increase on the SSCC when substituents are in *ortho* position, except for hydroxy and methyl groups, compared to benzaldehyde. To understand the origin of this increase, the theoretical SSCCs of these compounds were decomposed into NLMOs contributions that are calculated in Lewis and non-Lewis terms. For halogenates and methoxy substituents, *anti*-conformers are more populated (> 86%) than *syn*-conformers. So, in these cases, the observed SSCCs can be described by the *anti*-conformers and the $^1J_{\text{CH}}$ couplings increased for these conformers. The decomposition analysis showed that this increase on $^1J_{\text{CH}}$ occurs in the Lewis (L) term of the formyl $\sigma_{\text{C-H}}$ NLMO contribution, suggesting that steric effects are more pronounced than conjugative one. This proposal is supported by two observations: the first one is an increase of s characters on the carbon of formyl C-H bond (about 1%) and on LP_2 for the *ortho* substituent (< 0.2%), indicating an electronic rearrangement to “accommodate/stabilize” electronic density into internal orbitals, and the second one is an increase on $\text{H}_f\text{-C}_f\text{-C}_b$ bond angle, in response of the steric interaction between the formyl C-H bond orbital and the substituent’s lone pairs. The *syn*-conformers showed no significant change on $^1J_{\text{CH}}$ compared to benzaldehyde, but the L and NL components of the C-H formyl NLMO contribution showed important variations that are compensated because these terms have opposed signals. These results can be explained by changes in electronic interaction of $\sigma_{\text{C-H}}$ and $\sigma^*_{\text{C}_b\text{-C}_X}$ (C_b is the benzyl carbon bonded to the formyl group and X is the *ortho* substituent) that contribute positively for NL term and, in response, negatively for L term. When benzaldehydes have two *ortho*-substituents, the increase on $^1J_{\text{CH}}$ can be interpreted by steric effects on *anti*-conformers contributions for the total SSCC and a balance of steric and delocalization effects on *syn*-conformers. For example, in *o,o*-difluorobenzaldehyde there are no significant delocalization contributions in response of fluorine substituents so, steric effects explain the total $^1J_{\text{CH}}$. However, for *o,o*-dichlorobenzaldehyde delocalization contributions (NL term) are as important as steric (L term).

Table 1: Experimental, theoretical $^1J_{CH}$ and its decomposition contributions changes compared to benzaldehyde for benzaldehyde derivatives and conformers population.

Compound	pop.	$^1J_{CH}$	$\Delta\sigma_{C-H^L}$	$\Delta\sigma_{C-H^{NL}}$	pop.	$^1J_{CH}$	$\Delta\sigma_{C-H^L}$	$\Delta\sigma_{C-H^{NL}}$	Δ^1J_{CH}	Δ^1J_{CH}
	<i>syn</i>	<i>syn</i>	<i>syn</i>	<i>syn</i>	<i>anti</i>	<i>anti</i>	<i>anti</i>	<i>anti</i>	teor.	exp.
benzaldehyde	-	-	0	0	-	-	0	0	0	0
<i>o</i> -fluorob.	13.5	178.9	-2.5	5.4	86.5	186.2	10.3	-1.8	9.2	8.2
<i>o</i> -chlorob.	5.8	179.6	-10.6	13.7	94.2	188.7	13.8	-3.6	12.4	8.8
<i>o</i> -bromob.	5.3	180.1	-15.7	19.0	94.7	188.5	12.7	-2.5	12.3	7.1
<i>o</i> -iodob.	7.6	180.7	-14.5	17.9	92.4	186.8	7.9	1.3	10.5	7.1
<i>o</i> -methoxyb.	4.2	175.0	-18.6	17.7	95.8	185.7	5.3	2.7	9.5	6.6
<i>o</i> -hydroxyb.	93.9	176.9	-7.4	7.4	6.1	185.8	6.1	1.9	1.6	2.4
<i>o</i> -methylb.	70.2	174.4	-0.6	1.2	29.8	175.8	-15.8	16.5	-1.0	-1.1
<i>o</i> -nitrob.	2.8	187.2	-5.5	15.3	97.2	203.1	23.4	-1.8	26.8	18.3
<i>o,o</i> -difluorob.	-	-	10.6	1.1	-	-	10.6	1.1	14.1	12.8
<i>o,o</i> -dichlorob.	-	-	-4.4	12.8	-	-	-4.4	12.8	10.5	13.7
<i>o</i> -chloro, <i>o</i> -fluorob.	39.1	190.9	-1.9	14.1	60.9	191.4	12.6	0.3	15.4	13.4
<i>o</i> -bromo, <i>o</i> -fluorob.	44.6	190.9	-7.2	19.3	55.4	191.3	13.1	-0.3	15.3	13.3
<i>o</i> -fluoro, <i>o</i> -iodob.	48.1	191.3	-10.5	22.7	51.9	188.8	10.2	0.7	14.2	12.1
<i>m</i> -fluorob.	55.7	178.3	-	-	44.3	178.6	-	-	2.6	2.5
<i>m</i> -chlorob.	51.8	178.6	-	-	48.2	179.4	-	-	3.2	2.6
<i>m</i> -bromob.	51.9	178.7	-	-	48.1	179.2	-	-	3.1	1.4
<i>m</i> -iodob.	49.2	178.4	-	-	50.8	179.2	-	-	3.0	-
<i>m</i> -methoxyb.	44.4	177.1	-	-	55.6	177.0	-	-	1.2	0.6
<i>m</i> -hydroxyb.	69.1	177.3	-	-	30.9	176.4	-	-	1.2	1.0
<i>m</i> -methylb.	52.6	175.7	-	-	47.4	175.7	-	-	-0.1	-0.5
<i>m</i> -nitrob.	41.3	180.4	-	-	58.7	182.6	-	-	5.9	5.1
<i>m,m</i> -difluorob.	-	-	-	-	-	-	-	-	5.3	5.1
<i>p</i> -fluorob.	-	-	-	-	-	-	-	-	0.7	0.6
<i>p</i> -chlorob.	-	-	-	-	-	-	-	-	1.7	1.3
<i>p</i> -bromob.	-	-	-	-	-	-	-	-	1.6	1.4
<i>p</i> -iodob.	-	-	-	-	-	-	-	-	1.7	1.4
<i>p</i> -methoxyb.	-	-	-	-	-	-	-	-	-2.1	-1.9
<i>p</i> -hydroxyb.	-	-	-	-	-	-	-	-	-1.1	-1.6
<i>p</i> -methylb.	-	-	-	-	-	-	-	-	-0.9	-1.1
<i>p</i> -nitrob.	-	-	-	-	-	-	-	-	5.7	4.8

Key-words: benzaldehydes, $^1J_{CH}$, SSCC decomposition.

Support: This work has been supported by CAPES, CNPQ, FAPESP.

References:

- [1] C. F. Tormena, Prog. Nucl. Mag. Res. Spectrosc., 96, 73 (2016).
- [2] S. J. Wilkens, et al., J. Am. Chem. Soc., 123, 12026 (2001).
- [3] J. Autschbach, J. Chem. Phys., 127, 124106 (2007).

A critical review of some underlying concepts involving both Arrhenius equation and the transition state theory

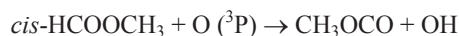
Authors: A. C. Amaro de Faria Jr^{1,3}, E. F. V. de Carvalho², O. Roberto-Neto³

¹*Departamento de Engenharia Mecânica, Universidade Tecnológica Federal do Paraná, 85053-525, Guarapuava, Paraná*

²*Departamento de Física, Universidade Federal do Maranhão, São Luís, 65085-580, Maranhão*

³*Divisão de Aerotermodinâmica e Hipersônica, Instituto de Estudos Avançados, São José dos Campos, 12228-001, São Paulo*

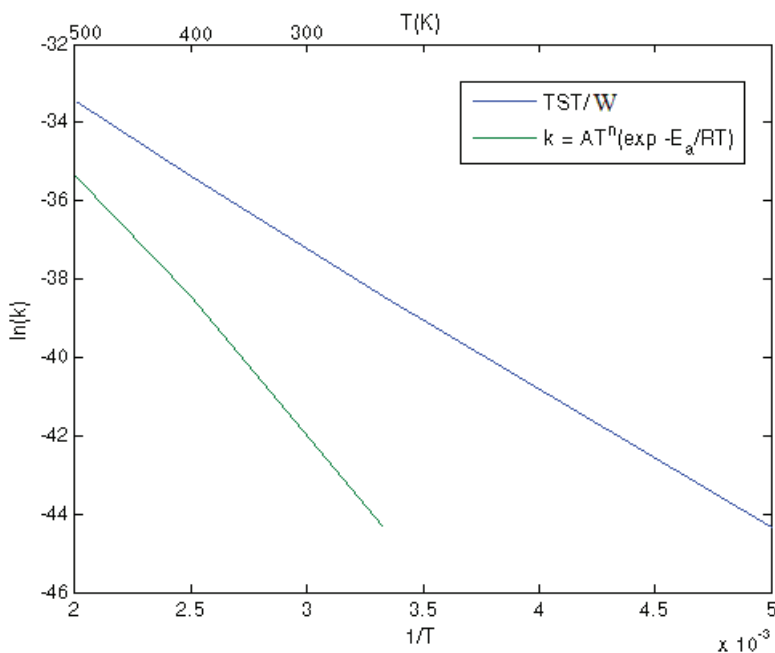
Abstract: In this review, we highlight some parameters and fundamental concepts which are usually not fully discussed concerned to the Arrhenius Law and the transition state(TST) [1]. Most of papers and textbooks consider as a rule of thumb the pre-exponential A and the activation energy E_A as independent of the temperature in the classical Arrhenius equation. However, theoretical and experimentally a non-Arrhenius behavior should be the rule rather than an exception. Measurements of rate coefficients over wide temperature range confirm this effect. The transition state theory is based on a logarithm expression derivative of the classical Arrhenius and represents a culmination of an unified model of four keystones of chemical physics, i.e. quantum mechanical potential energy surface, kinetic theory, thermodynamics, and statistical-mechanics. This theory has an unquestionable success in a variety of applications in the predictions of rate constants and support the interpretation of experiments. However there are some drawbacks of the basic concepts of this model which should be highlighted. One important fact are the structures and the potential force field of the stationary states which are calculated out of the equilibrium geometry and used as input in the calculations of partition functions of the variational transition state theory. Also, the possibility of choice of Cartesian or Curvilinear internal coordinates, for the definition of the framework of reactants, transition state and products show a variance of values of certain complex properties as the coefficients of rate constants. Anharmonic effects on the modes with low values in flexible molecules is another important factor which should be considered in calculations of partition functions specially in the range of medium to high temperatures [1]. Thus, anharmonicity and the multi-structural character of flexible molecules are essential concepts not usually mentioned in the literature but which are essential in the affordable model of kinetics and thermochemistry. One of the starting examples we compare the deviation from the Arrhenius law on the model of the transition state theory (TST) for the elementary reaction [2],



whose rate of reaction is calculated by the adjustment given by the relation

$$k = AT^n \exp(-E_a/RT) \quad (1)$$

where A , n and R are constants E_a is the activation energy and T is the temperature as in the Arrhenius Law, and by the simple model of TST/W rate constants based on the Wigner-unidimensional tunneling corrections. Clearly we can check the deviation between the two methods in the plot below for the Arrhenius Law. We also compare the conventional linear Arrhenius law and TST results with the model of deformed transition TST [3] model which gives some heuristic insights on the critical chemical dynamics parameters controlling the reactivity.



Key-words: Arrhenius law; Transition state theory; Chemical kinetics

Acknowledgements: FAPEMA, CNPq

References:

- [1] A. Fernández-Ramos, J. A. Miller, S. J. Klippenstein, D. G. Truhlar, Chem. Rev. 2006, 106, 4518.
- [2] Horiuti, J. B., Chem Soc Jpn 1938,13,210.
- [3] V. H. Carvalho-Silva, V. Aquilante, H. C. B de Oliveira, K. C. Mundim, J. Comput. Chem. 2017, 38, 178.

Adsorbents for Carbon Capture: A Quantum-chemical Investigation of the Adsorption of CO₂ and N₂ on Pure-silica Chabazite

Antonio Claudio Pinheiro Barbosa^{1,2}, Pierre Mothé Esteves¹ and Marco Antonio Chaer Nascimento^{1,*}

1) Instituto de Química, Universidade Federal do Rio de Janeiro, Brazil

2) Departamento de Química, Instituto Militar de Engenharia, Brazil

Abstract: Carbon capture and storage (CCS) is an important option in the portfolio of mitigation measures for stabilizing the atmospheric concentration of carbon dioxide. Briefly, it consists in capturing CO₂ from large stationary sources, transporting it through pipelines and safely storing it into underground geological formations [1]. The current capture technology is based on amine scrubbing [2], and it has some drawbacks such as a significant energy requirement to regenerate the solvent and environmental impacts due to solvent emissions. Adsorption-based separation processes with microporous solids are expected to reduce the costs and the environmental impact of CCS [3]. Pure-silica zeolites with narrow pores combine hydrophobicity, thermal stability and favorable kinetic effects for CO₂/N₂ separation [4], thus being promising adsorbents for capturing CO₂ from flue gases. In particular, pure-silica chabazite (Si-CHA) separates CO₂ from N₂ in the presence of water, with good selectivity, a much higher CO₂ adsorption capacity than the benchmark zeolite 13X, and without the need for vacuum desorption [5].

The adsorption of CO₂ and N₂ on Si-CHA has been studied at the molecular level with Density Functional Theory in the finite cluster/supermolecule approach. Electronic structure calculations were carried out with GAMESS package [6] at the PBE0-D2/6-311G(d,p) level. Si-CHA has been represented by a cluster (Z) of composition Si₃₆H₃₆O₅₄ consisting on a full ellipsoidal cavity, which has been carefully constructed and validated. Geometry optimizations were performed without any symmetry constraints, and the exact Hessian matrix has been evaluated for each stationary point. Molar enthalpies of adsorption of CO₂ and N₂ on Si-CHA have been calculated for the first time at a quantum chemical level, by taking Boltzmann averages of the energies of all relevant minima on the potential energy surfaces of the (CO₂ · Z) and (N₂ · Z) systems (Tables 1 and 2), including zero-point (ΔZPE) and thermal (ΔE^{Te}) corrections. Vibrational frequency shifts for both adsorbates ($\Delta \nu_3 \text{ e } \Delta \nu$) have also been calculated for the first time.

The calculated molar enthalpies of adsorption of CO₂ and N₂ on Si-CHA (-22.1 kJ/mol and -14.0 kJ/mol, respectively) deviate from the experimental values [7,8] less than 0.5 kJ/mol. Additionally, the experimental structural information available in the case of CO₂ [9] could be correctly reproduced and even better interpreted. Finally, site-specific information for the case of N₂, which are not yet available from experiment,



could be anticipated. Once more, Quantum Chemistry has proven to be a valuable tool in bridging the gap between experimental techniques, thus leading to a molecular-level understanding of the adsorption phenomena under investigation [10].

Work is in progress to extend this study to other pure-silica zeolites, with special attention to the small pore ones. We consider such a long-term contribution to be an important step towards the development of a new generation of adsorbents, designed at the molecular level, for capturing CO₂ from flue gases by adsorptive separation processes.

Table 1: Results for (CO₂ · Z) at 301 K^a

min	ΔE^{el}	ΔZPE	ΔE^{Te}	$-RT$	ΔH^b	$\Delta \nu^c$
1	-38.7	6.3	11.9	-2.5	-23.1	-5.7
2	-39.0	8.3	11.2	-2.5	-21.9	-7.5
3	-39.4	8.8	11.3	-2.5	-21.8	-7.8
4	-36.5	6.7	10.8	-2.5	-21.4	-5.1
5	-36.6	6.9	11.1	-2.5	-21.1	-6.8

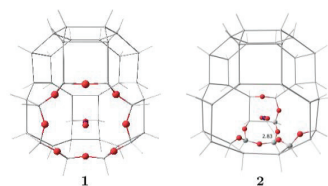
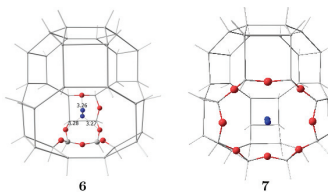


Table 2: Results for (N₂ · Z) at 298.15 K^a

min	ΔE^{el}	ΔZPE	ΔE^{Te}	$-RT$	ΔH^b	$\Delta \nu$
6	-21.7	3.1	6.6	-2.5	-14.5	3.5
7	-23.6	4.6	7.4	-2.5	-14.0	3.8
8	-22.1	3.7	7.0	-2.5	-13.9	2.3
9	-22.2	4.2	7.1	-2.5	-13.4	3.2



a) Energy in kJ/mol, wavenumber in cm⁻¹.

Key-words: Carbon capture, adsorption, zeolite, chabazite, DFT.

Support: This work has been supported by FAPERJ, CNPq and INOMAT.

References:

- [1] IPCC. IPCC Special Report on Carbon Dioxide Capture and Storage; Cambridge and New York, 2005.
- [2] G. T. Rochelle, *Science* 325, 1652 (2009).
- [3] J. Wang, L. Huang, R. Yang, Z. Zhang, J. Wu, Y. Gao, Q. Wang, D. O'Hare, and Z. Zhong, *Energy Environ. Sci.* 7, 3478 (2014).
- [4] O. Cheung and N. Hedin, *RSC Adv.* 4, 14480 (2014).
- [5] M. Miyamoto, Y. Fujioka, and K. Yogo, *J. Mater. Chem.* 22, 20186 (2012).
- [6] M. Schmidt, K. Baldrige, J. Boatz, S. Elbert, M. Gordon, J. Jensen, S. Koseki, N. Matsunaga, K. Nguyen, S. Su, T. Windus, M. Dupuis, and J. Montgomery, *J. Comput. Chem.* 14, 1347 (1993).
- [7] H. Fang, P. Kamakoti, J. Zang, S. Cundy, C. Paur, P. I. Ravikovitch, and D. S. Sholl, *J. Phys. Chem. C* 116, 10692 (2012).
- [8] T. D. Pham, R. Xiong, S. I. Sandler, and R. F. Lobo, *Microporous Mesoporous Mater.* 185, 157 (2014).
- [9] T. D. Pham, M. R. Hudson, C. M. Brown, and R. F. Lobo, *ChemSusChem* 7, 3031 (2014).
- [10] A. C. P. Barbosa, P. M. Esteves, and M. A. C. Nascimento, *J. Phys. Chem. C* Just Accepted Manuscript, DOI: 10.1021/acs.jpcc.7b06611.



Mesoionic Heterocyclics: Theoretical Study of the Structural Stability of Oxazoles (C_3H_3NO-R) and Thiazole (C_3H_3NS-R), with $R = O$ and S

Antonio J. Silva Filho*¹, Elizete Ventura², Silmar A. do Monte³, Otávio L. Santana⁴
*Departamento de Química, Universidade Federal da Paraíba, João Pessoa, Paraíba
CEP 58051-970, Brasil*

Abstract: Mesoionics are five or six-membered heterocyclic structures with a wide variety of applications, such as synthesis of other heterocycles, transition metal complexes, biological activity and non-linear optics [1-5]. This class of molecules has as characteristic a high delocalization and charge separation [6,7]. The present work aims to elucidate the structural stability of the heterocyclic azoles (1,3-oxazol-5-one, 1,3-oxazol-5-thione, 1,3-thiazol-5-one and 1,3-thiazol-5-thione) and their derivatives, in the ground state. MP2 and CCSD calculations were performed with aug-cc-pVDZ basis set and *Gaussian 09* program [8], as well as MCSCF using aug'-cc-pVDZ, aug-cc-pVDZ and cc-pVTZ basis set and single point CI/cc-pVTZ with *Columbus-7.0* program [9]. The structural stability of mesoionic compounds was investigated from relaxed scans in the coordinate referring to the ring-opening, with subsequent optimization of the structures and frequency calculations of stationary points (reagent, transition state and product) at MP2, CCSD, MCSCF and MCSCF//CI/cc-pVTZ. The MCSCF//CI/cc-pVTZ results indicate that the rings containing oxygen (1,3-oxazol-5-one and 1,3-oxazol-5-thione) spontaneously open without barrier. However, the structure with an inner S along with an exocyclic O atom (1,3-thiazol-5-one) has a small activation barrier and a small positive reaction energy (closed structure slightly more stable). On the other hand, the structure containing two S atoms (1,3-thiazol-5-thione) at MCSCF/cc-pVTZ level has a negligible energy difference between open and closed systems. Thus, there is a strong indication that these *thiazoles* (rings with sulfur) form acyclic tautomers [10,11]. The MCSCF and CI results showed a significant multiconfigurational character for these structures and their use is justified by the disagreement with the results obtained at MP2 and CCSD (regarding the relative stability between closed and opened structures), this disagreement being greater for MP2 method, especially for structures with an inner O atom.

Key-words: Mesoionics, structural stability, multiconfiguration, MCSCF and CI.

Support: This work has been supported by CAPES and PRPG/UFPB.



References:

- [1] GRIBBLE. G. W. Mesoionic Ring Systems. *The Chemistry of Heterocyclic Compounds: Synthetic Applications of 1,3-Dipolar Cycloaddition Chemistry Toward Heterocycles and Natural Products*. v. 59, cap 10, (2002).
- [2] MORIN. M. S. T. et al. Modular Mesoionics: Understanding and Controlling Regioselectivity in 1, 3-Dipolar Cycloadditions of Münchnone Derivatives. *J. Am. Chem. Soc.*, 135, p.17349–17358 (2013).
- [3] REISSIG. H. U.; ZIMMER. R. Münchnones - New facets after 50 years. *Angewandte Chemie - International Edition.*, v. 53, n. 37, p. 9708–9710 (2014).
- [4] GALUPPO. L. F. et al. Sydnone 1: A Mesoionic Compound with Antitumoral and Haematological Effects In Vivo. *Basic and Clinical Pharmacology and Toxicology.*, v. 119, n. 1, p. 41–50 (2016).
- [5] RODRIGUES. R. F. et al. Antileishmanial activity of 1,3,4-thiadiazolium-2-aminide in mice infected with *Leishmania amazonensis*. *Antimicrobial Agents and Chemotherapy.*, v. 53, n. 2, p. 839–842 (2009).
- [6] ANJOS. I. C.; VASCONCELLOS, M. L A A.; ROCHA, G. B., A DFT and Natural Resonance Theory investigation of the electronic structure of mesoionic compounds. *Theoretical Chemistry Accounts.*, v. 131, n. 12, p.1–9 (2012).
- [7] ANJOS. I. C.; ROCHA. G. B., A topological assessment of the electronic structure of mesoionic compounds. *Journal of Computational Chemistry*. v. 36, n. 25, p. 1907–1918 (2015).
- [8] *Gaussian 09*, Revision D.01, Frisch, M. J. et al. (2009).
- [9] *Columbus-7.0*, disponível em <<https://www.univie.ac.at/columbus/>>. Acesso em 24 Julho (2017).
- [10] OLLIS. C. A; RAMSDEN, W. D., *Adv. Heterocyclic Chem.* 19, 1 (1976).
- [11] KATRITZKY. A. R; BOULTON. A. J., *Advances In Heterocyclic Chemistry*. v.19 (1976).



A theoretical exploration on the $^1[\text{H}, \text{Se}, \text{I}]$ potential energy surface: energetics, structures, IR spectra, and heats of formation

Antonio Ricardo Belinassi and Fernando R. Ornellas

Departamento de Química Fundamental, Instituto de Química, Universidade de São Paulo, Av. Prof. Lineu Prestes, 748, São Paulo, São Paulo, 05508-900, Brazil

Abstract: There has been considerable interest in the spectroscopy and photochemistry of HOX (X = Cl, Br, and I) species since their important role played in the stratospheric ozone balance in polar regions was described [1,2]. It is believed that HOCl, in particular, participates in heterogeneous chemical reactions in polar stratospheric clouds in the conversion of relatively chlorine stable molecules to more reactive species that participate in the catalytic depletion mechanism of the stratospheric ozone [3]. These studies motivated a recent investigation in our group of similar potential energy surfaces for the sulfur series $^1[\text{H}, \text{S}, \text{X}]$, X = Cl, Br and I [4 – 6]. In the case of the HSCl species, for example, it has been shown that in conditions of high concentrations of hydrogen sulfide, as in the vicinity of active volcanic regions, there is a high possibility of formation of the HSCl molecule [7, 8].

As an extension of the previous studies, the group has also recently characterized, at a high level of electronic structure theory, the species contained on the potential energy surface of the selenium series $^1[\text{H}, \text{Se}, \text{X}]$, X = F, Cl, and Br [9 – 11]. Concerning the surface $^1[\text{H}, \text{Se}, \text{I}]$, theoretical/experimental data for the most stable species are still unknown in the literature, although a couple of theoretical calculations on the SeI_2 [12] molecule and an experimental value for the distance SeI in the SeI_3^+ [13] were reported. In this direction, calculations were performed with the highly correlated CCSD(T) [14] method, along with a series of correlation consistent basis set followed by extrapolations to the complete basis set limit. Corrections that arise due to spin-orbit coupling and scalar relativistic effects were also considered in the atomization energy evaluation. Accounting for core-valence correlation into the wave function, and of anharmonic effects on the vibrational frequencies were also explored, making the present results a very reliable source of data. Our results for the structural parameters, IR spectra, as well as the isomerization barrier and determination of the heat of formation of the species involved are the first ones to be reported in the literature. The HSeI species can be seen as normally covalently bonded and more stable by 42.04 kcal



mol^{-1} than the HISE isomer. These two species are separated by a barrier (ΔG^\ddagger) of 52.35 kcal mol^{-1} . For the diatomic molecule SeI, we estimated enthalpies of formation of 36.87 kcal mol^{-1} and 35.16 kcal mol^{-1} at 0 K and 298.15 K; for the most stable isomer, we obtained 18.25 kcal mol^{-1} and 16.72 kcal mol^{-1} , respectively.

With the results of this study, we can now have an overview of the energy, structural properties, and infrared spectrum of the complete triatomic series (HSeX) containing selenium and halogens. We hope that this study can contribute to the understanding of the potential reactions between halogens and chalcogens in different chemical environments and also further motivate the experimental search and characterization of this new molecular species.

Key-words: Chalcogens-halogens, HSeI and HISE, atomization energy, heats of formation, harmonic and fundamental frequencies, CCSD(T), CBS limit.

Acknowledgment: A. R. B. and F. R. O. are thankful to the Conselho Nacional de Desenvolvimento Científico e Tecnológico (CNPq) of Brazil for continuing academic support.

References:

- [1] L. T. Molina, M. J. Molina, *J. Phys. Chem.*, **82**, 2410 (1978).
- [2] Y. Bedjanian, G. Poulet, *Chem. Rev.*, **103**, 4639 (2003).
- [3] P. J. Crutzen, R. Muller, C. Bruhl, T. Peter, *Geophys. Res. Lett.*, **19**, 1113 (1992).
- [4] F. R. Ornellas, *Theor. Chem. Acc.*, **103**, 469 (2000).
- [5] Y. A. Aoto, F. R. Ornellas, *J. Phys. Chem. A*, **111**, 521 (2007).
- [6] W. Hermoso, F. R. Ornellas, *Chem. Phys. Lett.*, **459**, 77 (2008).
- [7] S. M. Resende, F. R. Ornellas, *J. Phys. Chem. A*, **104**, 11934 (2000).
- [8] S. M. Resende, F. R. Ornellas, *Chem. Phys. Lett.*, **318**, 340 (2000).
- [9] W. Hermoso, F. R. Ornellas, *Chem. Phys. Lett.*, **479**, 201 (2009).
- [10] W. Hermoso, F. R. Ornellas, *Chem. Phys. Lett.*, **499**, 213 (2010).
- [11] W. Hermoso, D. B. Morf, F. R. Ornellas, *J. Braz. Chem. Soc.*, **24**, 1049 (2013).
- [12] J. M. Rautiainen, T. Way, G. Schatte, J. Passmore, R. S. Laitinen, R. J. Suontamo, J. Valkonen, *Inorg. Chem.*, **44**, 1904 (2005).
- [13] J. P. Johnson, M. Murchie, J. Passmore, M. Tajik, P. S. White, C. -M. Wong, *Can. J. Chem.*, **65**, 2744 (1987).
- [14] C. Hampel, K. A. Peterson, H. -J. Werner, *Chem. Phys. Lett.*, **190**, 1 (1992).



FFLUX: Adding Dispersion to a Quantum Mechanical Force-Field through Machine Learning and Electronic Correlation

Authors: Arnaldo F. Silva¹, Roy E. Bruns¹, Paul L. A. Popelier²

*Chemistry Institute, University of Campinas, CP 6154, Campinas, SP, Brazil.
13.083-970.*

Manchester Institute of Biotechnology (MIB), the University of Manchester,

131 Princess Street, Manchester, M1 7DN, Great Britain

And School of Chemistry, the University of Manchester, Oxford Road, Manchester,

M13 9PL, Great Britain

Abstract: The state in which force fields are used in molecular dynamics has changed very little over the past 30 years. The most energy-transferable way to describe an atom within a system is through Quantum Chemical Topology[1] (QCT). A force field based on QCT emerges as an attractive alternative to provide atomistic energies for molecular dynamics simulations. We present, for the first time, an innovative method for predicting the dynamic electron correlation (Dispersion) energy of an atom or a bond in a molecule. Our approach uses the machine learning method Kriging (Gaussian process regression with a non-zero mean function) to predict these dynamic electron correlation energy contributions. The true energy values are calculated by partitioning the MP2 two-particle density-matrix via the Interacting Quantum Atoms[2] (IQA) procedure. In principle, we hope to use Dynamic Correlation to add Dispersion energies our *ab initio* force-fields, named **FFLUX**[3]. We show some results:

I) We show the first *ab initio* Lennard-Jones parameter $B=514.6$, obtained through IQA and correlation energies for the water dimer (Fig .1a and b).

II) Also, we Machine learn the electronic correlation of a GLU-ALA helix, predicting the electronic correlation of around 900 geometries, from 190 training points. The predictions of the helix have a maximum absolute error below 5.3 kJ/mol with R-square equal to 0.997 (Fig 1.c).

III) Finally, we can calculate atomic and bond correlation energies for amino acids in explicit solvation. The **O...H** hydrogen bond interactions are negative and the **O...O** and **O...N** are positive, causing a partial cancelation in the correlation energy of the hydrogen bond(Fig 1d).

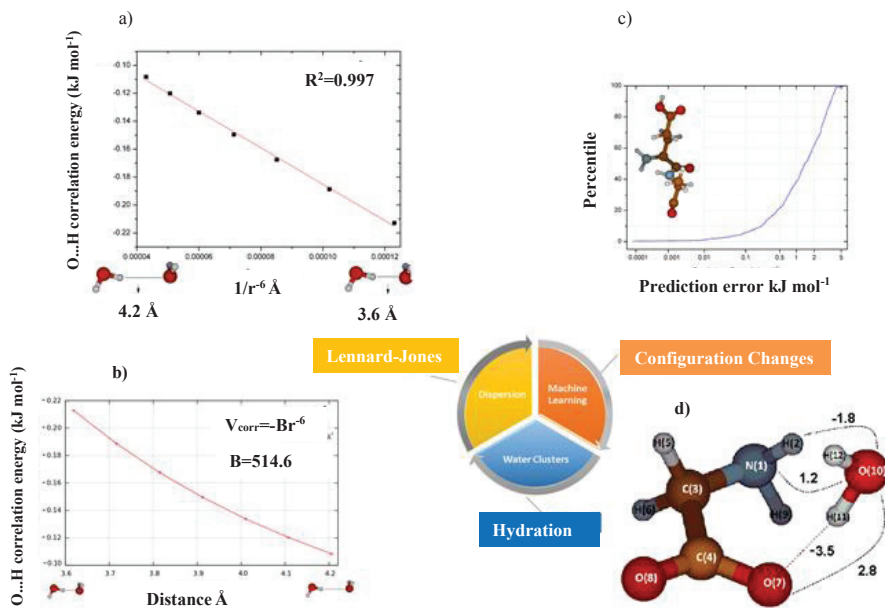


Figure 1. a) The correlation energy (kJ mol⁻¹) of the hydrogen bond (H₂O...H₂O) vs 1/r⁶ distance in Angstroms for the water dimer at the MP4/6-31G++(2d,2p) b) The correlation energy (kJ mol⁻¹) of the hydrogen bond (H₂O...H₂O) vs distance in Angstroms for the water dimer at the MP4/6-31G++(2d,2p) c) The S-curve for the predictions of the total ECE of the alanine-glutamic acid helix derived from kriging.. And d) Optimized geometry of glycine hydrated with one water molecule, with some hydrogen bond correlation values

Key-words: ab initio force-field, peptides, machine learning, dispersion energy

Support: A. F. S. thanks the Brazilian government's FAPESP for the award of postdoctoral position number 2014/21241-9 and 2015/22247-3, We acknowledge the EPSRC for funding through the award of an Established Career Fellowship to P.L.A.P. (grant EP/K005472).

References:

- [1] Popelier, P.L.A. and F.M. Aicken, Atomic Properties of Amino Acids: computed Atom Types as a Guide for future Force Field Design. *ChemPhysChem*, 2003. 4: p. 824-829.
- [2] Blanco, M.A., A. Martín Pendás, and E. Francisco, Interacting quantum atoms: a correlated energy decomposition scheme based on the quantum theory of atoms in molecules. *J.Chem.Theory Comput.*, 2005. 1(6): p. 1096-1109.
- [3] Popelier, P.L.A., *Molecular Simulation by Knowledgeable Quantum Atoms*. *Phys.Scr.*, 2016. 91: p. 033007.

Electronic structure calculations for the study of polyaniline-based chemical sensors

Larissa Oliveira Mandú, Augusto Batagin-Neto

Universidade Estadual Paulista (UNESP), Câmpus Experimental de Itapeva, Brazil

Abstract: Conjugated organic polymers represent an important class of materials for varied technological applications, including in active layers of chemical sensors. In this context, polyaniline (PANI) derivatives have been identified as promising candidates, mainly due to their high chemical stability, good processability, versatility of synthesis/polymerization/doping, as well relatively low cost [1-3]. In this study electronic structure calculations were carried out for varied PANI derivatives in order to identify systems with improved sensory properties. Preliminary reactivity studies were performed to identify possible adsorption centers on the oligomer structures via Condensed-to-atoms Fukui indexes (CAFI) [4] employing a DFT/B3LYP/6-31G approach and Hirshfeld partition charge. Adsorption studies were then carried out for selected derivatives employing five distinct gaseous analytes: H₂, H₂S, H₂O, NH₃ and SO₂ [3]. Structural changes, average bond energies, energy level alignments and theoretical optical absorption spectra of the obtained systems were investigated in order to evaluate the influence of the analytes on the oligomers properties. The obtained results indicate the derivatives PANI-NO₂ and PANI-C₆H₅ as the most promising materials for the development of chemical sensors.

Key-words: chemical sensors, polyaniline derivatives, electronic structure.

Support: This work was supported by CNPq (MCTI/CNPQ/Universal 14/2014 – Proc. 448310/2014-7), FAPESP (Proc. 2016/05954-0) and by the Center for Scientific Computing (NCC/GridUNESP) of Sao Paulo State.

References:

- [1] K. Crowley, M.R. Smyth, A.J. Killard, A. Morrin, *Chem. Pap.* 67, 771 (2012).
- [2] Z. Jin, Y. Su, Y. Duan, *Sensors and Actuators B: Chemical.* 72, 75 (2001).
- [3] I. Fratoddi, I. Venditti, C. Cametti, M.V. Russo, *Sensors and Actuators B: Chemical.* 220, 534–548 (2015).
- [4] E.G. Lewars, “Computational Chemistry: Introduction to the Theory and Applications of Molecular and Quantum Mechanics” (2010), Springer.

Theoretical Study of the Structure and Reactions of Uranium Fluorides

Bárbara M. T. C. Peluzo, Breno R. L. Galvão

Chemistry Department, Centro Federal de Educação Tecnológica de Minas Gerais, Av. Amazonas 5253, Belo Horizonte, Brasil

Abstract:

Uranium is an actinide metal mostly known for its use as fuel at nuclear power plants. Once the amount of fissile isotope (^{235}U) in nature is not enough for a chain reaction, uranium must be enriched in order to achieve roughly 4% of the 235 isotope. Therefore, it is converted into UF_6 , a gaseous compound, which can be used in isotope separation techniques (being centrifugation the most used and laser enrichment a promising one) ¹. Currently UF_6 is made by $\text{UF}_4(\text{s})$ fluorination, a reaction which presents sub-products. An example of related reaction is UF_6 successive reduction by hydrogen, leading to lower uranium fluorides and HF ^{2,3}.

In this work, a DFT study has been performed on 3 uranium fluorides and their reactions in gas phase, covering the most stable equilibrium geometry and spin multiplicities. We used the basis sets TZP-DKH for fluorine and hydrogen and LANL2DZ/ECP for uranium. The DFT functional chosen was the hybrid one PBE0.

Initial optimization calculations lead to two isomers (C_{2v} and D_{2d}) for UF_4 ; C_{4v} symmetry for UF_5 and O_h for UF_6 . After that, it has been investigated possible transition states (TS) for UF_6 formation via reaction between UF_4 and F_2 . It has been employed a Linear Least Motion (LLM) analysis for this TS search, followed by geometry optimizations. Two TS had been obtained, been one of them the structure which connects the minima $\text{UF}_4 + \text{F}_2$ and UF_6 . This reaction mechanism has been studied in detail using Intrinsic Reaction Coordinate (IRC) calculations.

Another reaction studied was UF_6 synthesis via UF_4 and HF , a reaction that occurs in two steps and presents UF_5 as intermediate compound. In the calculations performed, it has been found a TS which consists of a UF_5 (D_{3h}) molecule and a hydrogen atom as a ligand. IRC calculations showed a different product, the complex UF_5H , which had been observed by Eerkens ⁴. Besides this, it has been obtained the infrared spectra of this product, which had not been theoretically or experimentally observed yet.

Vibrational frequency calculations have also been performed for the fluorides and they present good agreement with experimental data available. Finally, we have performed



an investigation on possible isotopic shifts at the vibrational spectra of 6 UF_6 isotopologues, i.e., compounds whose compositions differ by an isotope. As a result, it has been found isotopic shifts for the frequencies ν_3 and ν_4 , which may be used in uranium isotopic separation, since all species presented slightly different frequencies, mainly at ν_3 . Same calculations have been performed for UF_5H and shifts were found at ν_{10} .

Key-words: UF_6 . DFT. potential energy surface. isotopic shift.

Support: This work has been supported by FAPEMIG, CNPq and CEFET-MG.

References:

- [1] S. Cotton, "Lanthanide and actinide chemistry" (2013), John Wiley & Sons, [S.l.].
- [2] WORLD NUCLEAR ASSOCIATION, Uranium enrichment (2016).
- [3] A. L. Myerson, J. J. Chludzinski Jr., "Chemical kinetics of the gas-phase reaction between uranium hexafluoride and hydrogen". The Journal of Physical Chemistry, ACS Publications, 85, 25, 3905 (1981).
- [4] J. W. Eerkens, "Isotope separation process" (1992), Google Patents, US Patent 5, 108, 566.





Painel 038 | PN.038

Computational study of zinc phthalocyanine mobility in a phospholipid bilayer containing cholesterol

Brenda S. D. Frachoni¹, Erick G. França², Carlos A. de Oliveira¹, Eduardo de F. Franca¹

¹Universidade Federal de Uberlândia □ Instituto de Química

²Instituto Federal de Goiás

Abstract:

Computational methods play an important role in the design of new drugs and the prediction of their behavior in biological environment. Many current studies seek to understand how these drugs are capable to interact with biological membranes and also the influence of these molecules into the stability of these biomembranes (1, 2). This work aims to understand the mobility and interaction forces between a hydrophobic drug, zinc phthalocyanine and membrane composed of phospholipids only, also the same drug interacting with a mixture of phospholipids and cholesterol in mass to mass ratio of 5:1. The methodology used was Molecular Dynamics simulations using the GROMACS 5.1.4 computational package with OPLS-AA force field, using NPT ensemble, at 310K and 1 bar with explicit spc water. In order to insert the zinc phthalocyanine into the oplosaa force-field, its RESP charges was obtained by the NWCHEM software (Valiev et al., 2010) after the geometry optimization and energy minimization have been made with 6-31G* basis-sets in ORCA 3.0.3 software (Hočevar et al., 2016). The results showed that freedom of locomotion of drug through the lipid portion of phospholipid bilayer is higher in the presence of cholesterol, this fact is evidenced by higher values of MSD (mean square displacement) found in comparison with the same analysis made for the purely phospholipid bilayer. This interpretation is in agreement with experimental results obtained by our research group in previous studies (Oliveira et al., 2010), in which the drug in question has a higher pharmacological efficiency when encapsulated in phospholipid vesicles containing cholesterol. Recent studies have shown that biomembranes containing cholesterol are more organized and tend to pack the carbon chains of their phospholipids more easily (1). Additional structural analyzes such as the RMSF (root mean square fluctuation) were performed, which displayed that the fluctuation in the position of the atoms of biomolecules of the membrane was smaller in the system in which the cholesterol was present, evidencing a freedom of the carbonic chains when the cholesterol is not part of the vicinity of phospholipids. Faced with such results it is possible to conclude that the greater activity of the drug observed experimentally may be linked to a higher movement liberty that drug possesses through the proposed drug delivery system membrane.

Key-words: zinc phthalocyanine, phospholipid bilayer model, Molecular Dynamics.

Support: This work has been supported by FAPEMIG, CNPq and Rede Mineira de Química (RQ-MG-2014-2016 : RED-00010-14)





References:

- 1 – RÓG, T.; PASENKIEWICZ-GIERULA, M.; VATTULAINEN, I.; KARTTUNEN, M. Ordering effects of cholesterol and its analogues. *Biochimica et Biophysica Acta (BBA)-Biomembranes*, v.1788, n. 1, p. 97-121, 2009.
- 2 – BUNKER, A.; MAGARKAR, A.; VIITALA, T. Rational design of liposomal drug delivery systems, a review: Combined experimental and computational studies of lipid membranes, liposomes and their PEGylation. *Biochimica et Biophysica Acta (BBA)-Biomembranes*, v.1858, n.10, p.2334–2352, 2016.
- 3 – VALIEV, M.; BYLASKA E. J.; GOVIND, N.; KOWALSKI, K.; STRAATSMA, T. P.; VAN DAM, H. J. J.; WANG, D.; NIEPLOCHA, J.; APRA, E.; WINDUS, T. L.; DE JONG, W. A. NWChem: a comprehensive and scalable open-source solution for large scale molecular simulations. *Comput. Phys. Commun.*, v. 181, p. 1477, 2010.
- 4 – HOČEVAR, T.; DEMŠAR, J. Computation of Graphlet Orbits for Nodes and Edges in Sparse Graphs. *Journal of Statistical Software*, v. 71, n. 10, p. 1-24, 2016.
- 5 – OLIVEIRA, C. A.; KOHN, L. K.; ANTÔNIO, M. A.; CARVALHO, J. E.; MOREIRA, M. R.; MACHADO, A. E. H.; PESSINE, F. B. T. Photoinactivation of different human tumor cell lines and sheep red blood cells in vitro by liposome-bound Zn(II) Phthalocyanine: Effects of cholesterol. *Journal of Photochemistry and Photobiology B: Biology*. v. 100, n. 2, p.92-99, 2010.



Theoretical Calculation of pKa Values of Amidines in Aqueous Solution Using an Implicit Solvation Model

Authors: Bruna L. Marcial^{1,2}, Elfi Kraka²

Address: ¹Núcleo de Química, Instituto Federal Goiano, Campus Morrinhos, Morrinhos, GO 75650-000, Brazil

²Computational and Theoretical Chemistry Group (CATCO), Department of Chemistry, Southern Methodist University, Dallas, Texas 75275-0314, USA.

Abstract: Amidines are special nitrogen analogues of the carboxylic acid, containing two N of different functionality. One is formally single bonded like-amino nitrogen (N¹) and the other is a formally double-bonded imino nitrogen (N²), where protonation occurs first. The pKa's of amidines vary from neutral to slightly acidic (pKa ranges from 4.4 to 14) depending on their substitution pattern. Amidines are present in numerous bio-related compounds and can be found important medicinal and biochemical agents [1]. Since there are no theoretical studies on the reliability of computational methods in the prediction of the pKa's of amidines. A benchmark of different computational methods against experimentally determined pKa values available in the literature is necessary to validate a reliable protocol, which could be used to make accurate predictions for complex systems containing an amidine group.

The pKa is one of the most important properties of drug compounds, since it is directly connected to their chemical and biological activity. Although, the calculation of pKa has received considerable attention and many different approaches were developed, accurate prediction of the pKa (with 1 unit) is still a challenging task. In this work, we have calculated the pKa values of a set of 16 amidines. From these set, 12 amidines had their values compared against experimental values, and the other 4 were possible candidates to be tested as enedynes warhead for the development of a new pH sensitive cancer drug [2]. Calculations in aqueous medium were carried out with the density-based solvation model (SMD)[3] and three hybrid exchange-correlation functionals (B3LYP, M06-2X and MN15) with two basis sets (6-31+G(d,p) and 6-311++G(d,p)). The effect of including explicit water molecules on the calculated pKa's was assessed by having up to one water molecule at the protonated site.

The inclusion of one explicit water forming a hydrogen bonding with the imino N was found to reduce the error by about 1 pKa unit, whereas the addition of another water molecule did not improve the pKa values. Among the DFTs tested B3LYP is the least reliable with errors larger than 2 pKa units. The most reliable method is M06-2X combined with 6-31+G(d,p) basis set and one explicit water (mean unsigned error MUE = 0.57 ± 0.82). However, MN15 with 6-311++G(d,p) basis set and one explicit water performed similarly well (MUE = 0.85±0.86) as illustrated in Figure 1. On the basis of the molecules studied here, MN15/6-311++G(d,p) and M06-2x/6-31+G(d,p) with one



explicit water can be used to calculate pK_a's directly without the need for statistical adjust or thermodynamic cycles.

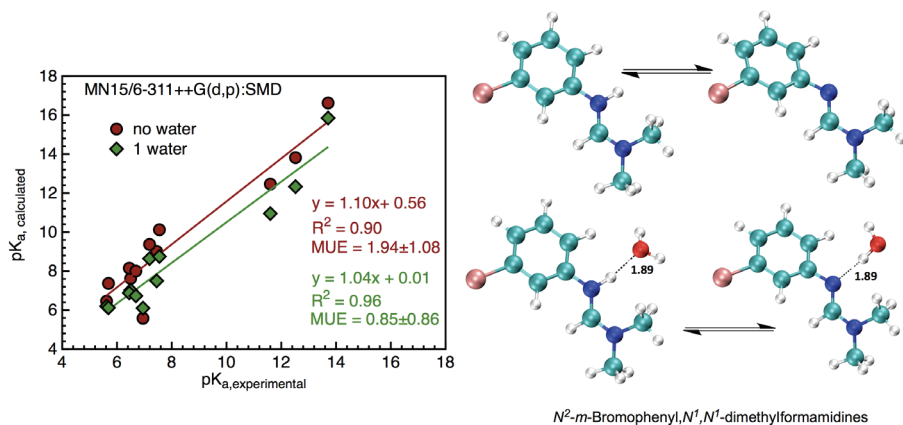


Figure 1. Linear correlation of experimental pK_a's [1] and values calculated by using new DFT functional MN15 with SMD solvation model and the arrangement of one explicit water in the protonated site.

Key-words: Amidine. Acid dissociation. Polarization solvation model.

Support: This work has been supported by NSF-CHE 1464906, SMU, IFGoiano

References:

- [1] Saul Patai, Z. R., Ed. *Amidines and Imidates*; John Wiley & Sons, Ltd., 1991; Vol. 2; pp 1–918.
- [2] Kraka, E.; Cremer, D. *Mol. Sci.* 2014, 4, 285–324.
- [3] Marenich, A. V.; Cramer, C. J.; Truhlar, D. G., *J. Phys. Chem. B* 2009, 113, 6378–6396.



Painel 040 | PN.040

Exploring EPR Parameters of ^{99}Tc Complexes for Designing new MRI Probes: Coordination Environment, Solvent, and Thermal Effects on the Spectroscopic Properties

Bruna T. L. Pereira, Mateus A. Gonçalves, Daiana T. Mancini, and Teodorico C. Ramalho.

Departamento de Química, Universidade Federal de Lavras.

Currently, cancer is one of the most serious health problems. Studies have shown that this disease has increased in last years, including a growing number of deaths. Among the types of cancer, the breast cancer is the most common. Generally this type of cancer is diagnosed in advanced stages, thereby some modern techniques, such as tomography and Magnetic Resonance Imaging (MRI), which allow the diagnosis in early stages, have been used for breast cancer diagnosis. The MRI is a noninvasive technique for diagnosis because it is based on the magnetic properties of the ^1H and ^{17}O nuclei, which are the most abundant elements in the human body [1]. However, with only the natural relaxation of the water molecules in the body, it is often not possible to obtain clear MRI images. Thus, contrast agents (CAs) are used for improving the MRI image resolution. The CAs are paramagnetic compounds able to decrease longitudinal and transverse relaxation times of water molecules in the proximity of their structure, thus facilitating breast cancer diagnosis. Based on this context, it is necessary to understand the relaxation mechanisms of water molecules and the influence of paramagnetic effects on the ^1H and ^{17}O hyperfine coupling constant (A_{iso}) values [2].

In this study, the solvent and thermal effects on spectroscopic parameters of ^{99}Tc complexes coordinated to explicit water molecules were evaluated. Molecular dynamics simulations were performed followed by hyperfine coupling constant calculations (A_{iso}) and the QTAIM method was used to probe hydrogen bonds between the studied complex and water solvent molecules. In order to validate our calculation strategy for ^1H and ^{17}O hyperfine coupling constant values, the complex $[\text{Mn}(\text{H}_2\text{O})_6]^{2+}$ was used.

The results showed a small difference between the explicit and explicit/implicit solvent for A_{iso} calculations on complexes 1 and 2 (figure 1). This small difference between the explicit and explicit/implicit solvent found was expected, which shows that the number of water molecules added during the A_{iso} calculation describes the system well. It can be noted also that thermal effect greatly influence the system. It is important to observe that the Tc coordination environments are different for both complexes, therefore, it is important to know that changes in the coordination environment of Tc complexes can significantly influence the A_{iso} results [3]. The QTAIM methodology is a quantum model considered innovative in studies of chemical bonds but also it is effective in characterizing intramolecular and/or intermolecular interactions. Thus, QTAIM calculations are very important to check the influence of hydrogen bonds in the A_{iso} values. Therefore, QTAIM calculations were performed for evaluating the



interaction between the water molecules and the studied complexes and our results showed a strong interaction between them [4].

Since, it is well-known that the use of gadolinium complexes as MRI contrast agents has generated several problems due to their high toxicity [9]. Our theoretical findings point out that an alternative to this traditional approach is to use technetium complexes as MRI contrast agents, because they present lower toxicity and show good A_{iso} results in solution [4].

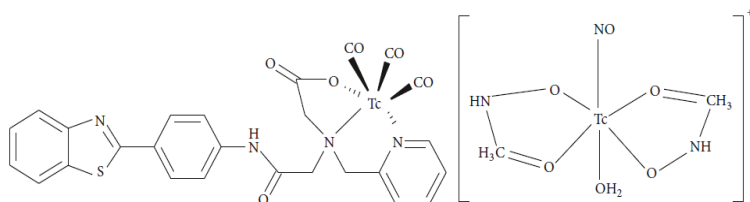


Figure 1: (^{99m}Tc)(CO) $_3$ (NNO) conjugated with 2-(4-aminophenyl)benzothiazole(1); oxotechnetium(V) complex with the ligand N(2(1-Hpyrolmethyl)).

Key-words: ^{99}Tc ; MRI; Contrast Agents; Hyperfine constant.

Support: This work has been supported by FAPEMIG, CNPq and CAPES

References:

- [1] E. R. Galvˆao, L. M. Martins, J. O. Ibiapina, H. M. Andrade, and S. J. Monte, "Breast cancer proteomics: a review for clinicians," *Journal of Cancer Research and Clinical Oncology*, 137, 925, (2011).
- [2] P. Caravan, J. J. Ellison, T. J. McMurry, and R. B. Lauffer, "Gadolinium(III) chelates as MRI contrast agents: structure, dynamics, and applications," *Chemical Reviews*, 99, 2352, (1999).
- [3] R. F.W. Bader, *Atoms in Molecules-A Quantum Theory*, Oxford University Press, Oxford, U.K, (1990).
- [4] Pereira, B. T. L., et al. "Exploring EPR Parameters of ^{99}Tc Complexes for Designing New MRI Probes: Coordination Environment, Solvent, and Thermal Effects on the Spectroscopic Properties" *Journal of Chemistry*, 2017, 8, (2017)



Quasiclassical Trajectory Study of the Kinetics and Dynamics of the $O(^3P) + HBr$ Reaction

Bruno E. S. de Freitas, Antonio G. S. de Oliveira Filho

Departamento de Química, Faculdade de Filosofia Ciências e Letras, Universidade de São Paulo, Ribeirão Preto, SP, Brasil

Abstract: Reactions between atoms and diatomic molecules can be investigated to high degrees of detail and precision using high-level ab initio potential energy surfaces (PES) and the quasiclassical trajectories (QCT) method. [1, 2] In this work, we use a PES constructed using internally contracted multireference configuration interaction with complete basis set extrapolation (icMRCI+Q/CBS) and the QCT method to calculate the rate constant and product energy distribution of the $O(^3P) + HBr$ reaction. [2] The rate constants, in $\text{cm}^3 \text{ molecule}^{-1} \text{ s}^{-1}$ and at 298 K, for the $O + HBr$ reaction is 2.31×10^{-14} for QCT.

Key-words: Quasiclassical trajectory, rate constant, potential energy surfaces

Support: This work has been supported by FAPESP

References:

- [1] D. G. Truhlar, J. T. Muckerman, and R. B. Bernstein, "Reactive Scattering Cross Section: Quasiclassical and Semiclassical Methods" (1979), Plenum Press, New York, USA.
- [2] A. G. S. de Oliveira-Filho, F. R. Ornellas, K. A. Peterson, J. Chem. Phys. 136, 174316 (2012).

Influence of Molecular Dynamics in the Docking of Dialkylphosphorylhydrazones in *Leishmania braziliensis* Hexokinase

Authors: Bruno Henrique de Medeiros Mendes¹, Reinaldo Bellini Gonçalves², Carlos Mauricio R. Sant'Anna¹

Adress: ¹Universidade Federal Rural do Rio de Janeiro, BR-465, Km 7 Seropédica, RJ

²Laboratório de Bioinformática, LNCC, Petrópolis, RJ

Abstract: Leishmaniasis, caused by parasites of the genus *Leishmania*, is one of the so-called neglected diseases. A previous study of our group with a series of dialkylphosphorylhydrazones (DAPH), **4a-4o**, some of which showed leishmanicidal activity both *in vivo* and *in vitro*, indicated hexokinase as a probable target of action of the compounds [1]. Using molecular docking and semi-empirical quantum calculations, we have previously studied the interactions between DAPH and a homology model of *L.*

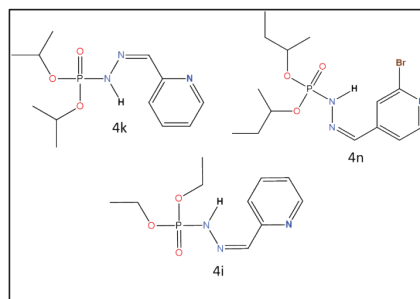


Figure 1: ligands **4i**, **4k** and **4n**.

braziliensis hexokinase (LbHK), in the form of a dimer (chains A and B). The results indicated the ligands **4i**, **4k** and **4n** (figure 1) as the most promising as potential inhibitors of LbHK. The objective of this work is to refine the LbHK model by molecular dynamics (MD) and apply the refined model in molecular docking studies, in order to verify the influence of the use of MD on the quality of the results of these studies. The MD simulations were done through the Gromacs 5.1.2.2 program [2], with the OPLS force field and the tip4p model for water, with a production phase of 50 ns. An alignment of the pre-MD homologous structure with its post-MD structure was performed, resulting in a RMSD value of 9.08 Å, which indicates a substantial conformational change. In order to evaluate if there were significant changes in the catalytic site of the parasite enzyme or emergence of new sites, a blind docking procedure using the ligand **4k**, the best of the three ligands mentioned above, was performed in both structures. In the blind docking procedure, the search space for protein-ligand interaction corresponds to the total surface of the protein, which allows a complete search of possible sites on the surface of the protein. This procedure was made with the SWISSDOCK web server [3]. The protein-ligand conformations given by the docking are grouped in clusters, and cluster 0 is the one that presents the most favorable Gibbs free energy of interaction (ΔG_{int}). The cluster 0 for the pre-MD model is located in the B chain's active site and has a small energy difference ($-2,32 \text{ kcal mol}^{-1}$) when compared to an adjacent site. However, in the post-MD model, the cluster in the adjacent site does not exist, indicating that the active site is the most relevant presenting a $\Delta G_{\text{int}} = -8.78 \text{ kcal mol}^{-1}$ for the cluster's best solution. The blind docking predicted interaction poses of **4k** in the active site in both LbHK conformations, providing favorable interaction energy values for both, being the interaction with the post-MD structure the most favorable. Then, a restricted docking with



the 15 ligands was performed in the post-MD structure, where the search grid was restricted to the region of the active site, in order to compare with the pre-MD docking results. The restricted docking were performed with GOLD 5.4 [4] program (CCDC). The results showed that the **4i**, **4k** and **4n** ligands remained the best among the 15. The absence of one of the poses clusters shows that the results of blind docking were significantly influenced by the MD treatment of the structure obtained by homology modeling, indicating that this treatment of the models must be adopted prior to the docking studies, at least in the case of proteins with high flexibility like LbHK. The next step of this work is to propose changes in the structure of the ligands above mentioned to further improve their activity as inhibitors of the parasite's enzyme.

Key-words: Leishmanicide, hexokinase, dialkylphosphorylhydrazones, Blind docking, Molecular Dynamics.

Support: This work has been supported by CNPq, CAPES, Faperj, INCT-INOVAR.

References:

- [1] Matta, C. B. B., et al., *European Journal of Medicinal Chemistry*, 101, 1; 2015.
- [2] Abraham, M. J., et al., *SoftwareX*, 1–2, 19–25; 2015.
- [3] Grosdidier, A., et al., *Nucleic Acids Research*. 42, W32-W38; 2014.
- [4] Jones ,G., *J. Mol. Biol.*, 267, 727-748; 1997



A DFT Study on the non-covalent interaction control on enantioselective Heck-Matsuda Reactions

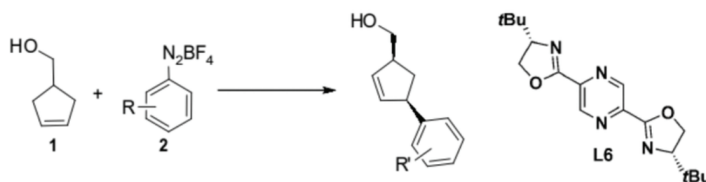
Bruno M. Servilha¹, Robert Paton², Carlos R.D. Correia³, Ataulpa A. C. Braga¹

¹ Instituto de Química – Departamento de Química Fundamental - Universidade de São Paulo, São Paulo, SP, Brazil

² Chemistry Research Laboratory – Oxford University, Mansfield Road, OX1 3TA, Oxford, United Kingdom

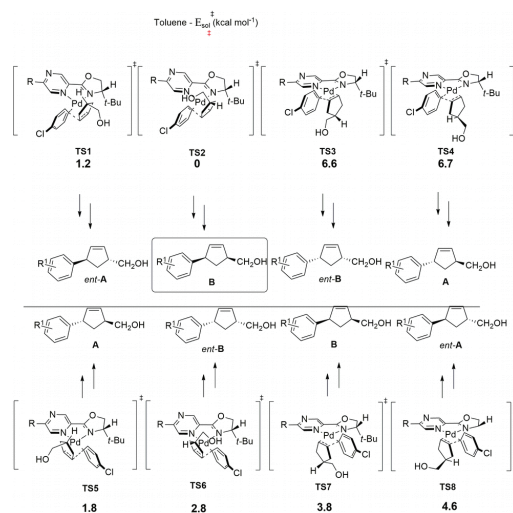
³Instituto de Química – Departamento de Química Orgânica - Universidade de Campinas, Campinas, SP, Brazil

Abstract: Heck-Matsuda reactions are a variant of the well-known Heck-Mizoroki reactions employing aryldiazonium salts as electrophiles.¹ Previously we have shown that a non-covalent interaction between a palladium center and an hydroxyl plays a pivotal role in the high enantioselectivity observed in the desymmetrization of 3-cyclopenten-1-ol.² In this work, we have employed Density Functional Theory (DFT) calculations (M06L-def2SVP(d)//M06L-6-31G(d), SDD(Pd)) on the migratory insertion step of the Heck-Matsuda desymmetrization of the analogous substrate cyclopentylmethanol, which contains an one-carbon tether between the hydroxyl group and the cyclopentane ring, in order to investigate the influence of the hydroxyl group of this substrate on the enantioselectivity of these process (Scheme 1)



Scheme 1: Heck-Matsuda arylation of cyclopentylmethanol with ligand L6

All the eight transition states involved in this reaction were found and their potential energies are reported in Scheme 2. **TS 2**, the lowest energy transition state has the hydroxyl group oriented towards palladium, a C-H π interaction between the pyrazine ring of the ligand and the aryl moiety of **2**, and the tert-butyl group oriented far away from the substrates. Additionally, all the transition states with the *endo* orientation of the hydroxyl group (TS2, TS3, TS5 and TS6) also show a nonclassical C-H-O hydrogen bond between the hydroxyl group and the phenyl ring of the aryldiazonium salt substrate. Non-covalent interaction (NCI) Isosurfaces³ were plotted for TS2 (Figure 1) showing these non-covalent interactions along with steric ones. Benchmark studies on these reactions will be reported in due course in order to correctly these trends in terms of Gibbs Free Energies along with novel experimental results.



Scheme 2: Transition State Energies (kcal.mol⁻¹) for the migratory insertion step
(Single-point energies in toluene (SDD))

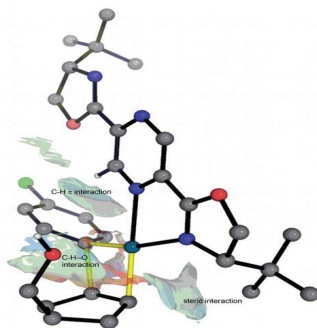


Figure 1: NCI Plot isosurface of TS 2

Key-words: Heck-Matsuda, Non-covalent interactions, DFT

Support: This work has been supported by CAPES and FAPESP (15/01491-3)

References:

- [1] J. G.; Moro, A. V.; Correia, C. R. D. *European J. Org. Chem.* 2011, 2011 (8), 1403–1428.
- [2] De Oliveira Silva, J.; Angnes, R. A.; Menezes Da Silva, V. H.; Servilha, B. M.; Adeel, M.; Braga, A. A. C.; Aponick, A.; Correia, C. R. D. *J. Org. Chem.* 2016, 81 (5), 2010–2018.
- [3] Contreras-García, J.; Johnson, E.R.; Keinan S.; Chaudret, R. ; Piquemal, J-P.; Beratan, D.N.; Yang, W. *J. Chem. Theory. Comput.* 7 (3), 625-632.



Structural and electronic modeling of Cuprum Oxide

Bruno Vilella^a, Mateus M. Ferrer^b, e Júlio R. Sambrano^b

^a*Universidade Estadual Paulista Júlio de Mesquita Filho, Bauru, Engenharia Elétrica,
brunovf96@gmail.com, PIBIC/CNPQ.*

^b*Grupo de Modelagem e Simulação Molecular, Universidade Estadual Paulista,
POSMAT, Bauru, Brasil.*

Abstract:

Recently, the Copper Oxide (Cu_2O) has been used in the fabrication of photovoltaics diodes devices and in the preparation of high sensibility gas sensors. These applications is due to its great characteristics of electrical rectification, photovoltaic performance and the good interaction of the experimental surface of the Cu_2O with gases [1-2]. The Cu_2O has a simple cubic structure (space group Pn-3m) and a band gap about 2.0 eV, a fact the helps to explain its electrical properties [3]. Figure 1 presents the unitcell of the studied Cu_2O .

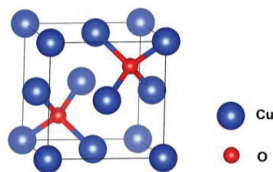


Figure 1: unitcell of the Cu_2O

This work consisted in a quantum computational study applied in the Cu_2O system in order to provide electronic information allowing the explanation of experimental properties. The calculations have been carried out according the DFT method implemented in the CRYSTAL package [4]. Two hybrid functionals, B3LYP e HSE06, and a set of copper Gaussian basis[5–7] were used to define the best theoretical conditions in order to compare with the experimental systems. The oxygen orbitals were described according to the 6-2111d1G basis [8]. All the calculations were performed as open-shell and the initial unitcell parameters were set according the experimental information found in ICSD 52043 card [9].

The gap energy and vibrational frequencies of the optimized structure indicated that the B3LYP functional associated to the base functions provide a better rapprochement when compared with the experimental result. Table 1 depict the structural parameters and the gap energy of the calculations.

Table 1: Structural parameters (a , Å) and band gap energy (E_{gap} , eV) of the Cu_2O .

Functional	E_{gap}	Lattice parameter (a)
B3LYP	2,18	4,26
HSE06	2,12	4,21
Experimental result	2,20	4,27

The best combination functional and basis was used to elaborate a detailed study of density of states and electronic band transitions.

Keywords: Cu_2O , DFT, Theoretical modeling.

Support: This work has been supported by CNPq (46126-4); CAPES (787027/2013, 8881.068492/2014); and FAPESP (2013/07296-2,2016/07476-9)

References:

- [1] Izaki M. et al, J. Phys. D: Appl. Phys., 2007, 40, 3326.
- [2] Zhang J., et al, Chem. Mater., 2006, 18 (4), 867–871.
- [3] Jongh P. E. et al, Chem. Mater., 1999, 11 (12), 3512–3517.
- [4] Dovesi, R. et al, Int. J. Quantum Chem. 2014, 114, 1287.
- [5] Doll, K, et al, Chem. Phys. Lett. 2000, 317, 282-289.
- [6] Ruiz, E. et al, J. Solid State Chem. 2003, 176, 400-411.
- [7] Zhilin, V. M. et al, J. Chem. Phys. 128, Art. N. 034703, 2008.
- [8] Baima, J. et al, J. Phys. Chem. C, **2013**, 117 (24), 12864–12872.
- [9] A. Kirfel, K.D. Eichhorn, Acta Crystallogr. Sect. A 46 (1990) 271–284.

On the description of the orientation state in mesophase pitch-based carbon fibers

Authors: Caio César Ferreira Florindo, Adalberto Bono Maurizio Sacchi Bassi

Address: Department of Physical Chemistry, Institute of Chemistry, University of Campinas-UNICAMP.

Abstract: Due to its high oriented molecular structure and crystalline graphite content, the mesophase pitch is the main precursor of high-performance carbon fibers (HPCFs) with high Young's modulus and great thermal and electrical conductivity [1]. In this work, we propose a mesoscopic continuum approach for mesophase pitch-based carbon fibers, in order to describe how the mesophase regions orientation states can influence the behavior of the pitch in different flows. By using the continuity condition for the orientation distribution function (ODF) of the mesophase pitch, one can obtain a new homogenous non-linear evolution equation for ODF [2]. The finite element method solves the homogeneous non-linear equations. This work shows two-dimensional solutions only, although three-dimensional solutions are straightforward extensions. In the two-dimensional approximation, all mesophase regions are parallel to the shear plane. Thus, the angle between the shear direction and the mesophase region orientation completely specifies its orientation state. In general, the numerical solution for the new homogeneous non-linear equations proposed in the work shows orientation angle values strictly close to those experimentally obtained by Hamada *et al.* [3], indicating the accuracy of the approximation. All calculations were performed by the Mathematica software (version 11.1).

Key-words: Carbon fibers, Fluid dynamics, Orientation distribution, Mesoscopic continuum thermodynamics

Support: This work has been supported by São Paulo Research Foundation, FAPESP (Grant 2016/08563-2).

References:

- [1] D. Edie, M. Dunham, Melt spinning pitch-based carbon fibers, *Carbon* 27, 5 (1989).
- [2] C. C. F. Florindo, C. Papenfuss, A. B. M. S. Bassi, Mesoscopic continuum thermodynamics for mixtures of particles with orientation, *J. Math. Chem.* DOI: 10.1007/s10910-017-0778-0, 2017. ISSN: 0259-9791.
- [3] T. Hamada, M. Furuyama, Y. Sajiki, T. Tomioka, M. Endo, Preferred orientation of pitch precursor fibers, *J. Mater. Res.* 5, 06 (1990).

Aflatoxin B₁: An Inactivation Proposal.

Oliveira, C.C.S.D.¹ ; Soares Neto, L.A.²

^{1,2}Universidade Federal Rural de Pernambuco - UFRPE. Rua Dom Manoel de

Medeiros, s/n, Dois Irmãos - CEP: 52171-900 - Recife/PE.

Abstract: The effects of the high toxicity of most mycotoxins produced by *Aspergillus flavus* compared with the Aflatoxin B₁ (AFB₁) are negligible, thus depicting an alarming picture and reference potential for chemical study of a possible structural modification that establishes inactivation of toxicity and carcinogenic properties performed by AFB₁. Therefore, we seek in this work a proposal for a chemical reaction to modify the toxicity of AFB₁. Our study was based on the addition of acetyl radical due to Michael mechanism. In this perspective we conducted a study of quantum chemistry methods in the calculation of molecular parameters that indicate the feasibility of the proposed in humans and other animals.

Key-words: Aflatoxin B₁, *A.flavus*, quantum chemistry

Support: Universidade Federal Rural de Pernambuco (UFRPE)

Introduction:

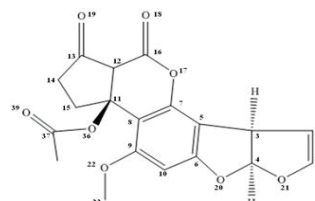
The fungi of the gender *Aspergillus* produce a varied number of toxins, however, a toxicity and carcinogenic power for AFB₁ that is about in 500 times greater in relation to others, being known as one of the natural product most carcinogenic¹. In its molecular structure AFB₁ has a lactone ring that is fundamental for its chemical properties². Our intention is to demonstrate the possible reaction of AFB₁ with acetic acid through the mechanism proposed (Michael Addition), mainly blocking the carcinogenic effect of AFB₁.

Methodology:

From the structures of the four possible isomers of AFB₁, we performed molecular mechanics (AMBER) and semi-empirical calculations AM1 and PM3 to reproduce the values obtained by Nicolás-vázquez et al. (2010)². Once obtained the structures and the respective heat of formation, we start from the lower energy isomer to construct the possible structures resulting from a Michael addition of AFB₁ with acetic acid as in Figure 1. The structures obtained were also optimized with molecular mechanics (MM-AMBER) and Semi-Empirical

(AM1 and PM3). To study the electronic structure of the compound, resulting from the addition of AFB₁ to acetic acid, we performed calculations using the Density Functional Theory (DFT) using the B3LYP Functional and 6-31 * G basis. In this work we made use of HyperChem 7.5 licensed to UFRPE.

Figura 1: AFB₁-Acetyl compound.

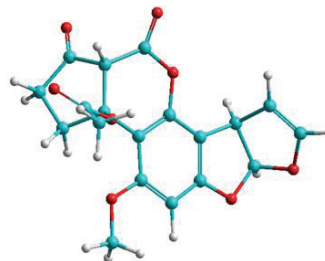


Results Obtained:

First we reproduced the structures of the isomers of AFB₁ with the same values of ΔH_f for the four isomers with the semi-empirical method AM1 as obtained by Nicolás-vázquez et al. (2010)². From the more stable structure, with the inclusion of the acetyl radical on the carbon atom 11 (Fig. 1) and the hydrogen atom on the carbon atom 12 considering all the possibilities as a consequence of the inclusion that can occur in cis and trans with respect to the principal plane of the molecule. Four structures are possible, that have been optimized with MM-AMBER, AM1 and PM3. One of the isomers (Fig. 2) showed the lowest ΔH_f (-251,79 Kcal / mol) with PM3 Method, making it the most stable of the possible structures. With the same PM3, the ΔH_f for the most stable isomer of AFB₁ is -157.61 Kcal / mol. To complete our analysis, we obtain with PM3, the ΔH_f equal to -100.63 Kcal / mol for acetic acid. The sum of the heat of formation of the reactants (AFB₁ + Ac. Acet.) Gives -258.24 Kcal / mol. The product - reagent difference is around only 6.45 Kcal / mol. Considering that the molar mass of AFB₁ is 312 gr, this means that 1 mg of this compound would need only 0.02 calories, the amount of heat that could be supplied if we mixed the contaminated cereal with AFB₁ with a solution of acetic acid heated in Around 40 to 50 C. The amounts of aflatoxins found in contaminated products are of the order of micrograms, therefore, we would need much less heat for the reaction to happen. With the most probable AFB₁-Acetyl structure, we performed DFT calculations. The analysis of the results indicates that the inclusion of acetyl groups significantly

alter the electronic structure in the lactone ring region when compared to AFB₁.

Fig. 2: More stable AFB₁-Acetyl.



Conclusion:

Our results indicated the possibility of the reaction between AFB₁ and acetic acid through a Michael addition in heated medium with the temperature around 40-50 °C. The calculations indicate that the electronic structure of the lactone ring of AFB₁ is significantly altered, indicating change in the chemical behavior of AFB₁. The inclusion of the acetyl group makes the AFB₁ chain more ramified, which will prevent interaction with guanine in the DNA, avoiding its harmful effect on the DNA structure and possibly its carcinogenic effect¹. This work continues with an achievement of the experimental stage in the attempt to verify what was indicated by calculations.

References:

- [1] KENSLER, Thomas W et al. Aflatoxin: Journal Oxford: TOXICOLOGICAL SCIENCES. Pittsburgh, p. 28-48. 29 set. 2010.
- [2] NICOLÁS-VÁZQUEZ, I., et al. Arch Environ Contain Toxicol, [s.l.].

Painel 047 | PN.047

Structure-Activity Relationship of Tacrine and Analogous Against Alzheimer's disease

Machado I.V.¹, Camargo, L.T. F. M.¹ and Camargo A. J.²

1. Instituto Federal de Educação, Ciência e Tecnologia de Goiás, campus Anápolis, Av. Pedro Ludovico, S/N - Residencial Reny Cury, 75131-457, Anápolis - GO, Brazil

2. Unidade de Ciências Exatas e Tecnológicas, Universidade Estadual de Goiás, Campus Henrique Santillo, BR 153, km 98, 75001-970 Anápolis-GO, Brazil

Abstract: Alzheimer's disease is a chronic neurodegenerative disease responsible for almost 70% of all case of dementia. Its cause is not yet completely understood, but 70% of the risk is believed to be genetic with many genes involved. Each year, thousands of new cases are reported around the world and this number is estimated to be three times higher in 2050[1]. Currently, there are some medicines that can control the Alzheimer's disease symptoms but its healing is not yet available[2]. Discovery new drugs that can better control the evolution of that disease is a very active research field in chemistry [3]. Here, we report a structure activity relationship study of a set of tacrine compounds and their analogues with activity against Alzheimer's disease [3]. Density functional theory with the exchange-correlation functional B3LYP[4] and the basis set 6-31G(d) were used to calculate the molecular descriptors. The principal component analysis technique [5] was employed to discriminate the compounds in active (1 a 8, 11 e 13) and inactive groups (9,10 e 12). The results show that five descriptors are required for complete discrimination of the compounds (Figure 1): HOMO and LUMO energies, angle between atoms 1, 6 and 16 (Figure 2), atomic partial charge on atom 4(Figure 2) and dipole moment. These findings can be used in the modeling of new tacrine analogues that have enhanced activities against Alzheimer's disease.

Key-words: Alzheimer, Tacrine and analogues, DFT, PCA.



Figure 1 PC1_PC2 score plot

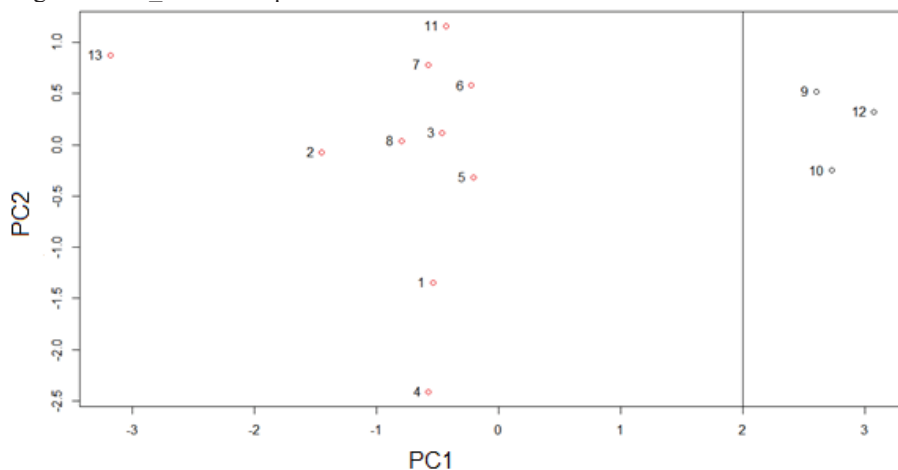
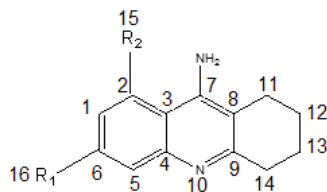


Figure 2 Molecular structure basic numbered for labelling atoms



References:

- [1] Alzheimers Association, A. 2015 Alzheimer's disease facts and figures. **Alzheimer's and Dementia**, v. 11, n. 3, p. 459–509, 2015.
- [2] Castilho, M.S.; C. Guido, R. V.; et al. Classical and Hologram QSAR Studies on a Series of Tacrine Derivatives as Butyrylcholinesterase Inhibitors. **Letters in Drug Design & Discovery**, v. 4, n. 2, p. 106–113, 2007.
- [3] Bautista-Aguilera, O.M.; Esteban, G.; et al. Design, synthesis, pharmacological evaluation, QSAR analysis, molecular modeling and ADMET of novel donepezil-indolyl hybrids as multipotent cholinesterase/monoamine oxidase inhibitors for the potential treatment of Alzheimer's disease. **European Journal of Medicinal Chemistry**, v. 75, p. 82–95, 2014.
- [4] Kohn, W.; Becke, A.D.; et al. Density Functional Theory of Electronic Structure. **The Journal of Physical Chemistry**, v. 100, n. 31, p. 12974–12980, 1996.
- [5] Jolliffe, I.T. Principal Component Analysis. **Book**, v. 2, p. 37–52, 1986.



DFT models for first step of the Chemoselective Hydrogenation of Substituted Aldehydes Using Silver Nanoparticles as Catalyst

Camila Iserhardt,^(a) Felipe S. S. Schneider,^(b) Giovanni F. Caramori^(b) and Maximiliano Segala^(a)

(a) *Departamento de Físico-Química, Instituto de Química, Universidade Federal do Rio Grande do Sul (UFRGS), Av. Bento Gonçalves 9500, Zip Code 91501-970, Porto Alegre, Brazil. maximiliano.segala@ufrgs.br.*

(b) *Departamento de Química, Universidade Federal de Santa Catarina (UFSC), Campus Universitário Trindade - PO Box 476, Zip Code: 88040-900 Florianópolis, Brazil.*

Piet van Leeuwen recently published [1,2] studies about Au nanoparticles stabilized by secondary phosphine oxides (SPOs) and its use as catalyst for the hydrogenation of substituted aldehydes. Silver compounds have desirable physical properties, good relative abundance and low cost; however, there are only a few studies describing its properties. Bigioni et al. published [3] the crystallographic results to $M_4^+[Ag_{44}(p-MBA)_{30}]^{4-}$ (where M_4^+ = alkali counterions and p-MBA = p-mercaptobenzoic acid), which has a very stable Ag_{32} core. Similarly, Bakr et al. published [4] a reversible size control of Silver nanoparticles via ligand-exchange, in which, they observed the metal-ligand binding energy has huge importance in the size of the nanoparticle.

This work aims to understand the interaction of Silver nanoparticles with SPOs starting from complexes of this metal to describe the nature of the interactions between them and describe also the heterolytic cleavage process of hydrogen with complexes of this metal (from step 1 to step 2 in Figure 1). It was done by theoretical studies of the first step of the mechanism proposed by van Leeuwen to the hydrogenation of substituted aldehydes [1] [2] using Ag instead of Au as the metal in nanoparticle. Two models were studied: i) Ag_1 -SPOs complexes; ii) Ag_{32} -SPOs nanoparticles. The geometries both complexes and nanoparticles, except the Ag_{32} core, were full optimized using the Orca package was made in our previous work [5] to chalcogenate-protected gold nanoclusters.

In model (i), two approximations were tested. The H_2 going towards O (step 3) and the H_2 going towards Ag (step 4) where the last one is more stable by 2.3 kcal/mol. The reaction paths from these initial approximations (steps 3 and 4) to products (step 2) produced two transition states (steps 32_TS and 42_TS) where the first one is about 17.2 kcal/mol more stable than the last one. All ground states (steps from 1 to 4) have no imaginary frequencies or have only a few of them below 20 cm^{-1} . The transition state 32_TS has one imaginary frequency at 1210.17 cm^{-1} and the 42_TS has one in 605.83 cm^{-1} . As the product is (step 2), we believe there is a reaction path from 42_TS to 32_TS as showed in Figure 2. From our results we concluded that the reaction starts with the H_2 going towards Ag (step 4), following by steps 42_TS, 32_TS and reach the product (step 2).

In order to evaluate how far is model (i) from model (ii) we compare the Ag_1 -(SPO)₂ with the Ag_{32} -(SPO)₂ (Figure 3). The geometries are quite similar, except for the

bond Ag-P which is longer in $\text{Ag}_{32}\text{-(SPO)}_2$, in this way, model (i) seems to be good enough to model the nanoparticle reaction path.

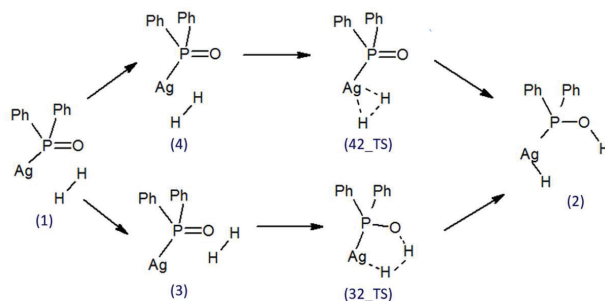


Figure 1. Models steps of the H_2 approximation of the nanoparticle. Steps (1), (2), (3) and (4) are ground states and steps (32_TS) and (42_TS) are transition states.

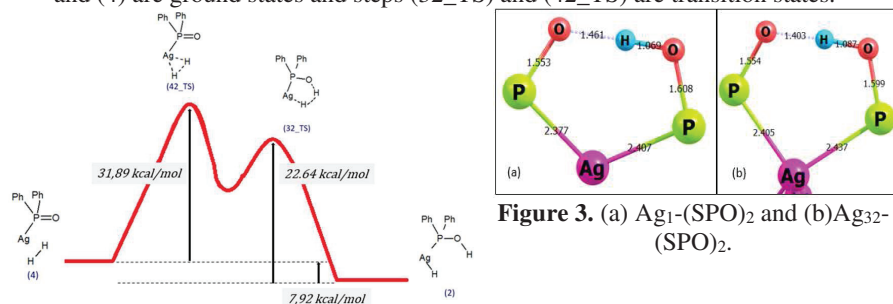


Figure 3. (a) $\text{Ag}_1\text{-(SPO)}_2$ and (b) $\text{Ag}_{32}\text{-(SPO)}_2$.

Figure 2. Reaction path proposed to the first step.

Key-words: SPO, nanoparticles, hydrogenization, silver.

Support: This work has been supported by Brazilian National Council for Scientific and Technological Development (CNPq). We thank the computational services provided by Centro Nacional de Supercomputação (CESUP/UFRGS).

References:

- [1] I. Cano, M. A. Huertos, A. M. Chapman, G. Buntkowsky, T. Gutmann, P. B. Groszewicz, P. W. N. M. van Leeuwen, *J. Am. Chem. Soc.*, 137, 7718 (2015). [2] I. Cano, A. M. Chapman, A. Urakawa, P. W. N. M. van Leeuwen, *J. Am. Chem. Soc.*, 136, 2520 (2014). [3] A. Desireddy, *Nature.*, 501, 399 (2013). [4] M. S. Bootharaju, V. M. Burlakov, T. M. D. Besong, C. P. Joshi, L. G. AbdulHalim, D. M. Black, R. L. Whetten, A. Goriely, O. M. Bakr, *Chem. Mater.*, 27, 4289 (2015). [5] M. Segala, F. S. S. Schneider, G. F. Caramori, R. L. T. Parreira, *Chem. Phys. Chem.*, 17, 3102 (2016).

Nugget Hydrocarbons C_nH_n with Six Four-membered Rings and their growth as 3D-Scaffolds

Camila M. B. Machado^{1*} (PG), Diogo B. Henriques² (PG), Sóstenes L. Lins² (PQ),
Alfredo M. Simas¹ (PQ)

¹*Departamento de Química Fundamental, Universidade Federal de Pernambuco,
Recife, Pernambuco, Brazil.*

²*Centro de Informática, Universidade Federal de Pernambuco,
Recife, Pernambuco, Brazil.*

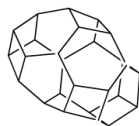
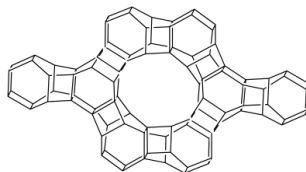
Abstract: Polyhedral hydrocarbons of general formula C_nH_n constitute an important class of compounds, that can be either platonic hydrocarbons, prismanes, form cages, etc. Interest in these compounds arise from their distinct physical properties, chemical reactivities and possible applications in energy storage materials[1,2], in biology, in pharmacology, etc. A special class of polyhedral hydrocarbons, we call nuggets, is comprised of those containing only four- and six- membered rings[3]. It can be easily demonstrated from Euler's polyhedron formula that all such polyhedra must contain exactly six four-membered rings, for an arbitrary number of six-membered rings, with one sole exception: there are no such polyhedra with only one six-membered ring. In this work, we examined all 17 nuggets starting from cubane, with no six-membered rings, up to the one with 28 carbon atoms and 10 six-membered rings. Of these 17, only cubane (C_8H_8), we call Nugget8, has been synthesized in 1964 [4]. A few others have been devised theoretically and had some of their properties computed: Nugget12, Nugget20a, and Nugget24a. As far as we know, all others are being introduced for the first time in this work, and have never been considered in chemistry, not even theoretically. Of these, 3 of them are space filling polyhedral voxels: the cube (Nugget8), the hexagonal prism (Nugget12), and the truncated octahedron (Nugget24a). They are called voxels because they can fill the space completely and can be considered a value in a regular grid in 3-dimensional space; their 2D counterpart being pixels in a bitmap. All nuggets can be fused together in several manners, either through their square faces, or through their hexagonal faces, to generate 3D-scaffolds that can grow indefinitely and that can serve as templates to lead to an enormous number of compounds, either regular or amorphous, space-filled, cage-like, etc. Moreover, the three voxels, in principle, point in the direction of three new allotropes of carbon. In this work, we generated all 17 nuggets, which are the only ones that exist up to 28 vertexes, and calculated their thermodynamic properties in order to verify the likelihood of their existence. Our results indicate that only one of the nuggets seems to be unstable to dissociation: Nugget12, the hexagonal prism, which should easily dissociate into two benzenes, for which RM1 indicates the enthalpy of reaction: $C_{12}H_{12} \rightarrow 2C_6H_6$ to be $\Delta_rH = -39\text{kcal}$. This qualitative result has been confirmed by B3LYP/cc-pVDZ which yielded $\Delta_rG = -148\text{kcal}$. This result indicates that the allotrope of carbon constituted by



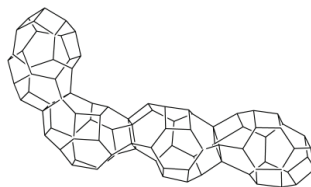
a 2D expansion of six membered rings chemically bound in the third dimension by single bonds would easily dissociate into layers of graphite. The other carbon allotrope made by a 3D expansion of cubes of carbon is stable towards dissociation, but would contain an enormous amount of strained carbon-carbon bonds, so much so that it could constitute a reservoir of energy if ever made. Besides, it would constitute a super dense allotrope of carbon, with a higher density than diamond. The final one, based on Nugget24 would lead to a viable allotrope which has been already found: carbon sodalite [5]. All nuggets had their thermodynamic properties computed by RM1 and B3LYP/cc-pVDZ. Results indicate that, with the exception of Nugget12, all others are found to be stable and likely to exist. Their RM1 average enthalpy of formation per CH bond, is found to range from 6 kcal.mol⁻¹ for Nugget14 to 2,23 kcal.mol⁻¹ for Nugget28c. Furthermore, their structures are found to be nicely rigid, adding to the interest in their eventual discovery, with their RM1 lowest vibrational frequency for Nugget28c with 28 carbon atoms being 144 cm⁻¹, which compares with the one for linear C₂₈H₅₈ of only 2cm⁻¹. Of the 17 nuggets, 3 are chiral. The nuggets can further fuse together through their square or hexagon faces to form the 3D-scaffolds. Disconsidering the cases of cubane and the hexagonal prism, for the other nuggets studied, the enthalpy of reaction for the fusion of squares with the release of a cyclobutane ranges from 47 kcal.mol⁻¹ to -12 kcal.mol⁻¹ and for the fusion of two hexagons with the release of a cyclohexane ranges from 33 kcal.mol⁻¹ to -37 kcal.mol⁻¹. Examples of symmetric and asymmetric 3D-scaffolds made out by fusion of 8 Nugget16s and 4 Nugget26s are shown below.



Nugget 16



Nugget 26



Key-words: Hydrocarbons, prismanes, carbocyclic cage compounds

Support: CNPq, FACEPE, PRONEX.

References:

- [1] L.S. Karpushenkava, G.J. Kabo, A.B. Bazyleva, J. Mol. Struct. THEOCHEM 913 (2009) 43–49.
- [2] J.M. Azpiroz, R. Islas, D. Moreno, A. Ferna, P.K. Chattaraj, G. Mart, J.M. Ugalde, G. Merino, (2014).
- [3] S. Lins, Gems, Computers and Attractors for 3-Manifolds, 1995.
- [4] P. Eaton, T. Cole, J. Am. Chem. Soc. 86 (1964) 962–964.
- [5] A. Pokropivny, S. Volz, Phys. Status Solidi Basic Res. 249 (2012) 1704–1708.



Estudo DFT da organização estrutural de hidratos formados pelos gases, H₂S, CH₄, N₂, CO₂, C₂H₆ e C₃H₈

Camila Rocha de A. Neves^a, Daniel Garcez S. Quattrociochi^b, Victor Hugo M. da Silva^a, Leonardo M. da Costa^b, José Walkimar de M. Carneiro^b

^a Escola de Engenharia Universidade Federal Fluminense, Niterói, RJ, Brazil,

^b Programa de Pós-graduação em Química, Universidade Federal Fluminense, Niterói, RJ, Brazil

Hidratos, ou clatratos, são sólidos cristalinos formados por macro arranjos de moléculas de água associadas por ligações de hidrogênio. Possuem cavidades que podem enclausurar moléculas de gases de pequena massa molecular, estabilizando a estrutura dos hidratos [1]. São comumente formados em poços de produção de petróleo ou gás em águas profundas devido à baixa temperatura e alta pressão. Causam obstrução de dutos e válvulas, danos nos equipamentos e estagnação da produção para manutenção e reparos, reduzindo a produtividade [2].

O objetivo desse trabalho é estudar a estabilidade de hidratos formados por arranjos de 20 moléculas de H₂O com as seguintes moléculas encapsuladas: CH₄, CO₂, H₂S, N₂, C₂H₆ e C₃H₈, a partir de parâmetros termodinâmicos.

Otimizações de geometria e cálculos de energia foram realizados com o método B97D/6-31+G(d), com o modelo de solvatação CPCM para simulação do meio aquoso e ajuste do erro de sobreposição de base. Foram avaliadas as entalpias e energias livres de Gibbs de encapsulamento dos gases em equações análogas à da Figura 1.

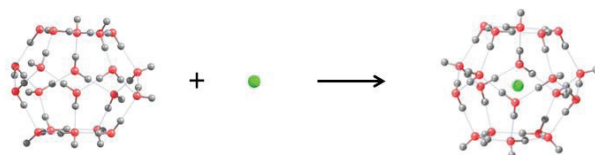


Figura 1- Reação genérica de encapsulamento da molécula convidada pelo arranjo com 20 moléculas de água, resultando na formação do hidrato.

A Figura 2 mostra as estruturas otimizadas dos hidratos encapsulando as moléculas dos gases. Nota-se que os arranjos das gaiolas de água modificam-se pouco após o encapsulamento da molécula convidada, com uma leve expansão no tamanho da gaiola, sendo esta expansão maior para o propano e menor para CH₄, N₂ e H₂S. A Tabela 1 mostra os resultados dos cálculos de variação de entalpia e de energia livre de Gibbs para a formação dos hidratos.

12 a 17/Nov, 2017, Águas de Lindóia/SP, Brasil

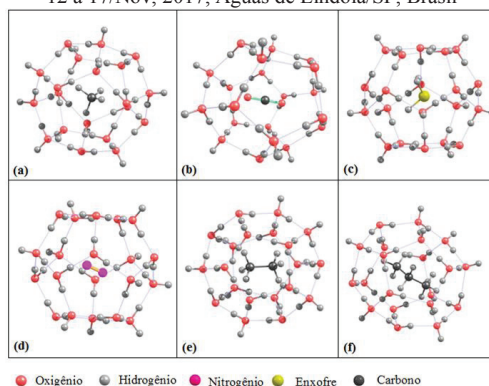


Figura 2- Estruturas dos Hidratos com as moléculas de (a) CH₄, (b) CO₂, (c) H₂S, (d) N₂, (e) C₂H₆ e (f) C₃H₈ encapsuladas.

Tabela 1 – Entalpia (ΔH), energia livre de Gibbs (ΔG^{298}) e 5°C (ΔG^{278}) em 78,95 atm de encapsulamento das moléculas gasosas convidadas, em kcal.mol⁻¹.

Gás	ΔH	ΔG^{298}	ΔG^{278}
CH ₄	-2,66	6,86	2,16
N ₂	-0,76	7,64	2,10
H ₂ S	0,35	10,86	5,04
CO ₂	2,11	11,20	4,40
C ₂ H ₆	1,17	12,96	6,69
C ₃ H ₈	13,34	25,68	17,98

A análise da Tabela 1 nos mostra que embora algumas reações sejam exotérmicas, todas possuem ΔG^{298} positivo. Entretanto, inclusão de efeitos de temperatura (baixa temperatura) e pressão (alta pressão) prevalentes nas condições experimentais de formação dos hidratos, reduz os valores de ΔG , tornando o processo de formação dos hidratos mais favorável. Observa-se que os gases com estruturas mais esféricas (CH₄, N₂ e H₂S) possuem variações de entalpia e energia livre de Gibbs mais negativas do que as moléculas com estruturas mais lineares (CO₂, C₂H₆ e C₃H₈).

Key-words: hidratos, pequenos gases, energia livre de Gibbs de encapsulamento, DFT.

Support: This work has been supported by CNPq, FAPERJ, PROPPi UFF

References:

- [1] Ningru Sun *et al*, J. Phys. Chem. A 121, 2620 (2017).
 [2] P. D. Dholabhai *et al*, Ind. Eng. Chem. Res. 35, 819 (1996).

DFT investigation of Montmorillonite edge surfaces stability and their acid-basic properties in Biodiesel production context

Carla G. Fonseca^{a*}, Viviane S. Vaiss^a, Fernando Wypych^b, Renata Diniz^c, Alexandre A.

Leitão^a

^a*Departamento de Química, Universidade Federal de Juiz de Fora, Juiz de Fora, MG, 36036-330, Brazil.*

^b*Departamento de Química, Universidade Federal do Paraná, P.O. Box 19032, 81531-980 Curitiba, PR, Brazil.*

^c*Departamento de Química, Universidade Federal de Minas Gerais, Belo Horizonte, MG CEP-31270-901, Brazil.*

**carla.grijo@ice.ufjf.br*

Abstract: Renewable energies make up the industrial sector with the greatest growth in the world. The synthesis of biodiesel from renewable biological sources, including animal fats and vegetable oils, has received considerable attention due to its environmental advantages and sustainable production in comparison with fossil fuels [1]. In general, biodiesel is produced by transesterification of vegetable oils or animal fats or by esterification of fatty acids with short chain alcohols, in homogeneous or heterogeneous catalytic conditions. Heterogeneous catalysis based on clays such as Montmorillonite (Mt) have received considerable attention due to their environmental compatibility, low cost, selectivity, thermal stability and recyclability [2].

Montmorillonite is classified as a 2:1 cationic exchanger phyllosilicate family and their acid properties can be enhanced by acid activation, these include: the edges of the crystals are opened and Al^{3+} and M^{2+} cations of the octahedral sheet are leached from the structure, causing an increase in both surface area and pore diameter. The acid-activated Mt proved to be reusable, besides presenting structural improvements and maintenance of catalytic activity. It show to be a promising catalyst for the production of fatty acid esters by esterification of different fatty materials [2,3].

Crystallographic planes that contribute predominantly to Mt edge surfaces are (010) and (110) and they are the catalytically active plans in these applications. In the present work, a comprehensive DFT study on the stability of Mt edge structures is introduced. The aim is to carry out a survey over a range of Mt edge geometry variations for (010) and (110) planes, estimate the Gibbs free energy of the surface formation in order to distinguish the most probable edge structures. To assess the reactivity of these sites, we examined the acid-basic properties by adsorbing a probe molecule CO on the Mt acid-activated surfaces. The changes in the electronic and acid-



basic properties were also investigated by density of states calculations and projected density of states. Solid-State Nuclear Magnetic Resonance analyzes of ^{29}Si and ^{27}Al were performed with the neat and acid-activated Mt. To better understand the reaction mechanism, the theoretical study of the aspects of the esterification reaction catalyzed by Mt edge surfaces were also done.

The quantum mechanical calculations were performed using the codes available in Quantum ESPRESSO (QE) package [4]. Electronic structure calculations were based on density functional theory (DFT) implemented with periodic boundary conditions using plane wave functions as basis set. The electronic correlation and exchange terms were employed using GGA with the PBE functional. The NMR calculations was performed by means of gauge including projector augmented wave (GIPAW) method.

In the presence of water, the stabilization of the lateral facets is achieved through chemisorption of H_2O molecules. Surface Gibbs free energy, ΔG_{surf} , as a function of the water coverage of the (010) and (110) facets are 0.55 and 0.70 kcal mol $^{-1}$ Å $^{-2}$ respectively. Thus, the (010) surface was found to be the most dominant face for Mt. The acid-activated Mt surfaces were simulated and the reactivity of the Al_V sites was checked by means of the CO adsorption. CO is a common Lewis basic probe molecule used to describe the Lewis acidity. The data confirm that the sites of the face (110) are slightly more acid than the sites of the face (010), the adsorption energies were -5.9 kcal/mol and -4.9 kcal/mol, respectively. The density of states (DOS) shows that the gap found for the Mt bulk is greater than the gap of both edge acid-activated surfaces, 4.9 compared to 4.6 and 4.3 regarding to (010) and (110), respectively. The edge (110) is slightly more acid. The projected density of states (pDOS), shows that the H^+ sites present in the hydroxyl groups linked to Si atoms (HO-Si sites) on the surface and the protons present in the hydroxyl groups (HO- Al^V sites), are more acidic than the surface Al_V sites for both acid-activated surfaces. Probably these are the sites responsible for the catalytic activity of the acid-activated Mt. By means of NMR simulation of ^{27}Al and ^{29}Si it was possible to characterize both the Al^{IV} and Al^V sites on the edge surfaces in accordance with the propositions made in literature. The attribution of affected Si environments by the site Al^{IV} was also be discussed. Based on the adsorption energies, we can infer that the esterification mechanism begins with the adsorption of acetic acid, better stabilization of the molecule by both surfaces compared to methanol. The formation of alkoxide has also been verified and does not occur on the surfaces.

Key-words: Montmorillonite, Clay minerals, Edge surfaces, *Ab initio* calculations, Biodiesel, Heterogeneous catalysis.

Support: This work has been supported by CAPES, CNPq, FAPEMIG, Brazilian agencies and the enterprise Petrobras S/A (CENPES). We also acknowledge the CENAPAD-SP computational center.

References:

- [1] L. C. Meher, D. V. Sagar, S. N. Naik, *Renew Sust Energ Rev.*, 10, 248, (2006).
- [2] L. Zatta, L. P. Ramos, F. Wypych, *App Clay Sci.*, 80-81, 231, (2013).
- [3] T. Wang, T. Liu, D. Wu, M. Li, J. Chen, S. Teng, *J. Hazard Mater.*, 173, 335, (2010).
- [4] P. Giannozzi, S. Baroni, N., *et al.*, *J. Phys. Condens. Matter.*, 21, 395502, (2009).



Amino acid polymorphisms in the fibronectin-binding repeats affect the fibronectin bond strength

Authors: Carlos Cruz¹, Roberto Lins¹, Isabelle Viana¹, Nadia Casillas² and Steven²

Lower

Address: 1-Oswaldo Cruz Foundation; 2-Ohio State University

Abstract: The envelope of *Staphylococcus aureus* contains cell wall proteins like fibronectin binding protein A (FnBPA) that bind to host ligands (e.g., fibronectin; Fn) present in the extracellular matrix of tissue or coatings on implants. Molecular simulations was used to investigate interactions between Fn and eight, 20-mer peptide variants synthesized to mimic fibronectin-binding repeat 9 (FnBR-9) of FnBPA from *S. aureus*, with particularly interested in double “mutations” at residues equivalent to positions 782 and 786 in FnBPA. Simulations reveal that the bond strength depends on whether a peptide dissociates through the lowest-energy pathway or is forced to unbind along a determined pathway. Additionally, data show anomalous unbinding behavior for H782Q+K786I compared to the wild- and H782Q+K786N-polymorphs, suggesting structural unfolding of Fn domains distant from the binding site. Together, these data demonstrate that cooperative amino acid substitutions in FnBR-9 may affect adhesion by altering bond strength at the site of binding, and may also influence cell invasion reactions by causing the extension of more distant regions within Fn, particularly under the influence of an external stress [1]. This provides a mechanistic explanation for clinical, endovascular infections caused by *S. aureus* that have nonsynonymous single nucleotide polymorphisms in the region of *fnbA* that codes for FnBRs in FnBPA.

Key-words: Bacterial Adhesion; *Staphylococcus Aureus*; Fibronectin; Metadynamics

Support: BIOMOL, CAPES and CNPQ

References:

- [1] Polymorphisms in fibronectin binding protein A of *Staphylococcus aureus* are associated with infection of cardiovascular devices. *Journal of Biological Chemistry*. Nadia N. Casillas-Ituarte, Carlos H. B. Cruz, Roberto Lins, Alex C. DiBartola, Jessica Howard, Xiaowen Liang, Magnus Hook, Isabelle F. T. Viana, M. Roxana Sierra-Hernandez and Steven K. Lower. 11, 2017.

Theoretical investigation of the metallic bismuth growth on the semiconductor surfaces by electron irradiation

Carlos E. Silva¹, Juan Andrés², Elson Longo³, Edison Z. da Silva¹, Miguel A. San-Miguel¹.

¹Universidade Estadual de Campinas, Campinas – SP, Brazil. ²Universitat Jaume I, Castelló, Spain. ³Universidade Federal de São Carlos, São Carlos – SP, Brazil.

In the search for new photocatalytic nanoparticles, the presence of localized surface plasmon resonance (LSPR) is the major desirable characteristic [1]. In this sense, the nanostructured bismuth and moieties as Bi/Bi-containing-semiconductor (Bi/BCS) are promisor candidates for applications in photocatalysis [1]. Recently, Longo *et al* have shown the nucleation and growth of silver nanoparticles supported on semiconductors surfaces by electron beam irradiation [2]. This method of metallic nanoparticles synthesis has also been applied to BiOX (X = Cl, Br and F) materials in which an epitaxial Bi growth has been observed. In this work, we aim to describe, at atomistic level, the mechanisms associated to these phenomena. For this propose, simulations of these materials by first principles quantum chemistry calculations were carried out.

The interaction between the electron beam and the bulk of the semiconductors was modeled by the charge injection in a $2x2x1$ P4/nmm supercell with charge per cell ratio varying from 0.00 to $15e^-$. DFT calculations were performed with PBE functional using PAW pseudopotentials. A $11x11x7$ Monkhorst-Pack grid was used to sample the Brillouin zone and a value of 520 eV was imposed as energy cut-off. All the calculations were performed with the VASP code [3]. These materials show sheets of X-Bi-O-Bi-X bilayers stacked along the c axis (Figure 1). The preliminary results reveal a stretch in the [001] direction when the e^- /cell rates increase. This fact is accomplished of an enlargement of the interlayer distances. Concomitantly, the X and Bi atoms tend to migrate through the interlayer region. Bader atomic charges and DOS analysis suggest a charge density transference between the Bi and the halogen atoms.

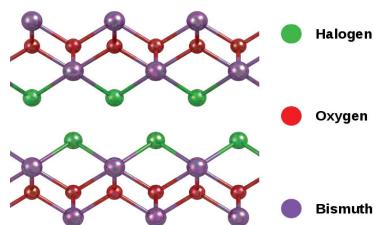


Figure 1. The bilayered arrangement present in the structure of the BiOX (X=Br, Cl and F). View along the [010] direction.



The efficiency of these materials in photocatalysis is hardly influenced by the shape, size, defects and exposed facets [4]. BiOX (Br, Cl and F) compounds present interesting photocatalytic activity in which the exposed facet controlling plays an important role [5]. Stoichiometric (010), (110), (011), (111) and (001) surfaces were evaluated considering slabs with 40 BiOX units, in which the thickness is large enough to reach the convergence at about 1 meV. However, the chemical composition of the exposed (001) surface remains as a controversial issue due to their different possible terminations (O, Bi or X). Our computations have shown that the (001) surface rich in halide ions is the most stable followed by the (010) surface. Nevertheless, the energy of the (001)-X is much lower than the computed for the (010). Therefore, using the Gibbs-Wulff theorem [6], DFT calculations predict a flat shape for the crystals for these compounds which is in good agreement with the experimental observations, where the crystals occur as plates or sheets with the {001} facets predominantly exposed [6].

Key-words: BiOX, Surfaces, Crystal morphology, DFT

Support: This work has been supported by CNPQ and FAPESP

References:

- [1] W. Hou, S. B. Cronin, *Adv. Funct. Mater.*, 23, 1612 (2013).
- [2] J. Andrés, L. Gracia, P. Gonzales-Navarrete, E. Longo *et al*, *Sci. Rep.*, 4, 1 (2014).
- [3] G. Kresse and D. Joubert, *Phys. Rev.*, 59, 1758 (1999).
- [4] J. Li, N. Wu, *Catal. Sci. Technol.*, 5, 1360 (2015).
- [5] H. Zhang, L. Liu, Z. Zhou, *RSC. Adv.*, 2, 9224 (2012).
- [6] S. Wu, Y. Jiang, L. Hu, J. Sun, P. Wan, L. Sun, *Nanoscale*, 8, 12282 (2016).



Imidazolium/Imidazolate $\pi^+ - \pi^-$ stacked ions pair simulations in chloroform

Chiara Valsecchi, Jessé G. Neumann, Hubert K. Stassen

Grupo de Química Teórica, Instituto de Química, Universidade Federal do Rio Grande do Sul, Av. Bento Gonçalves 9500, 91540-180 Porto Alegre - RS, Brazil

Abstract:

Bulk ionic liquids (ILs) have been widely studied by experimental and computational methodologies, due to their enormous variety of potential applications [1, 2, 3]. The imidazolium (Im) group and its derivatives have been of large interest, among the large spectrum of organic cations that might compose/form ILs, also for the possibility of tailoring the ILs thermodynamic and physical properties by alkyl substitutions at different locations [2, 4]. The supermolecular structure of neat ImILs, and consequently their properties, are directly linked to the three-dimensional arrangement of cations and anions. The interplay of the three intermolecular forces, electrostatics, dispersive, and hydrogen bonding, controls the organization of the ImIL in the gas and the liquid phases [4, 5, 6, 7]. More recently, it became of interest to understand cation-anion contact ion pairs when the IL is dissolved in other solvents [8, 9] and to characterize the structure and intermolecular interactions in these intimate ion pairs. The structure of contact ion pairs containing the imidazolate anion and a variety of six methyl substituted 1,3-dimethyl-imidazolium cations in chloroform solution were studied by molecular dynamic simulations in the present work. These ionic liquids were studied under the condition of infinite dilution, that means, only one ion pair. This study focused on determining the importance and the effect of different methylations at the cation's imidazolium ring. The novelty of the work also consists in the fact of having an organic molecule, the imidazolate, as counter-ion, instead of the common chloride or hexafluoroborate. The formation of a stable contact pair in chloroform along the entire simulation period was demonstrated by radial and spatial distribution functions (Figure 1). The cations are localized preferentially above or below the anion's plane ring, reflecting contributions of $\pi^+ - \pi^-$ stacking interaction between the two aromatic planar ions. The most acidic hydrogen at position C2 of the imidazolium cation exhibits the strongest structural correlations with the imidazolate anion, at distances within the range of hydrogen bonding. The structural correlations was in general weakened by methylations at all the cation's ring positions. The difference in the free energy of association for the methylation at the cation's C2 has been determined in the order of 13 kJ/mol from potential of mean-force calculations, favoring the ion pair containing the protonated C2 atom.

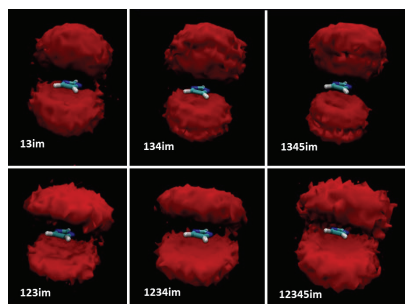


Figure 1. SDFs of the six different functionalized cations studied around the imidazolite anion (at the center, view from the C4 and C5 side). Upper row: cations with hydrogen at C2 of the imidazolium ring; lower row: the corresponding cations with a methyl group at C2. The SDFs depict the same isodensity surface for all the pairs.

Key-words: Imidazolium Ionic Liquid, Contact Pair, Methyl group substitution [Click here to enter text.](#)

Support: This work has been supported by CNPq and CAPES

References:

- [1] P. Wasserscheid, *Nature*, 439, 797 (2006).
- [2] A.A. Pádua, M.F. Costa Gomes, J.N. Canongia Lopes, *Acc. Chem. Res.* 40, 1087–1096 (2007).
- [3] M. Smiglak, J.M. Pringle, X. Lu, L. Han, S. Zhang, H. Gao, D.R. Mac-Farlane, R.D. Rogers, *Chem. Commun.* 50, 9228–9250 (2014).
- [4] R.M. Lynden-Bell, M.G. Del Po' polo, T.G. Youngs, J. Kohanoff, C.G. Hanke, J.B. Harper, C.C. Pinilla, *Acc. Chem. Res.* 40, 1138–1145 (2007).
- [5] J. Dupont, *J. Braz. Chem. Soc.*, 15, 341–350 (2004).
- [6] M.N. Garaga, M. Nayeri, A. Martinelli, *J. Mol. Liq.*, 210, 169–177 (2015).
- [7] R. Hayes, G.G. Warr, R. Atkin, *Chem. Rev.*, 115, 6357–6426 (2015).
- [8] K. Fumino, P. Stange, V. Fossog, R. Hempelmann, R. Ludwig, *Angew. Chem. Int. Ed.*, 52, 12439–12442 (2013).
- [9] M. Zanatta, A.L. Girard, N.M. Simon, G. Ebeling, H.K. Stassen, P.R. Livotto, F.P. dos Santos, J. Dupont, *Angew. Chem. Int. Ed.*, 53, 12817–12821 (2014).



Polarization of Methylene Blue in aqueous solutions: impact over the Hydrogen Bonds

Cleiton Maciel^{1,2}, Maurício Domingues Coutinho-Neto²

¹*Instituto Federal de São Paulo, Rua Primeiro de Maio, 500, CEP 08571-050, Itaquaquecetuba, Brazil.*

²*Centro de Ciências Naturais e Humanas, Universidade Federal do ABC, Avenida dos Estados, 5001, CEP 09210-580, Santo André, Brazil.*

Abstract: Photodynamic Therapy (PDT) is a well known treatment for neoplastic diseases that requires a combined action of a photosensitizer (PS), light-sensitive chemical compound, and a light source. When irradiated, a photosensitizer can be promoted to excited states and induce the formation of reactive oxygen species (ROS) such as singlet oxygen ($^1\text{O}_2$) [1]. ROS has a cytotoxic action over neighboring biomolecules of PS fostering cell death [2]. It's well established that the ROS generation is strongly affected by aggregation of PS, a common phenomena that occurs in homogeneous media and membranes, decreasing the efficacy of PDT treatment. Dimer and higher aggregates formation have been widely discussed in literature, but a molecular picture of this mechanism is still missing. In this work, we studied the dimer formation of a well-known phenothiazine dye, the Methylene Blue (MB) because of its high quantum yield, very low dark toxicity and other desirable properties for PS. We performed Molecular Dynamics (MD) simulations combined with Density Functional Theory (DFT) to understand the formation of hydrogen bonds (HB) between solute-solvent and its impact over the thermodynamic stability of dimer configuration. Since MB is a cationic dye, solvent effects can induce a charge polarization in this solute, affecting hydrogen bond formation. We developed a protocol to estimate converged average solute-solvent potential and to obtain the polarized charge distribution of MB in solution. Cubic cells were modeled with 4000 SPC water molecules in a NPT ensemble using GROMOS 53a6 force field. Running-lengths of 20 ns in MD simulations were adopted to extract representative configurations inputs to study polarization and its effects over the hydrogen bond formation by means of DFT calculations. Solvent induced polarization produces a negative charge localization in central ring N atom which results in stronger hydrogen bonds with solvent molecules. We extended the geometric criteria of HB formation and analyzed the angular distribution of Donor – H – Acceptor from 0 to 180° obtained from MD. One hundred selected configurations were analyzed considering a weight chosen according to the number of times that a specific configuration is accessed in the sampling. In polarized MB, the set of configurations sampled presented to a pattern similar to that of the whole simulation, a bimodal angular distribution with two well defined peaks around 9.5 and 108.5 degrees. Second peak is not expected in conventional hydrogen bond formation, but it represents a strong electrostatic character of this type of bond. Molecular dynamics calculations were performed using GROMACS 4.5 package. All the DFT calculations were done using the Orca 3.0.3 code. The functional B3LYP and def2-PVTZ basis set were used throughout.



Key-words: Methylene Blue, Molecular Dynamics, Density Functional Theory, Polarization, Hydrogen Bond.

Support: This work has been supported by FAPESP, CAPES and UFABC.

References:

[1] Kamat, et al. *The Journal of Physical Chemistry*, 85, 814-818, (1981).

[2] Dougherty, et al. *Journal of the National Cancer Institute*, 90, 889-905, (1998).



Accurate pK_a Determination of Alcohols with BMK And G3(MP2)/B3-CEP

Cleuton de Souza Silva^a and Rogério Custodio^b

^a Instituto de Ciências Exatas e Tecnologia, Universidade Federal do Amazonas, Campus de Itacoatiara, 69100-021 Itacoatiara, Amazonas, Brazil; ^b Instituto de Química, Universidade Estadual de Campinas, Barão Geraldo, P.O. Box 6154, 13083-970 Campinas, São Paulo, Brazil

Abstract: There is much interest in the development of reliable quantum chemical methods for the prediction of thermochemical data. In the last few years, extensive research has been conducted to determine the pK_a value of molecules in a solution. Different theoretical alternatives have been adopted to incorporate the solvation effect for that property. This work presents some theoretical calculations of pK_a for Alcohols by applying SMD (Solvation Model - Density) [1] at the G3(MP2)/B3-CEP [2], and BMK [3] levels of theory. The calculations were carried out with BMK functional with cc-pvtz basis set for the compounds in gas phase and in the presence of the solvent with three waters. The G3(MP2)/B3-CEP theory was also used to estimate the same property in identical conditions. Table 1 shows the results with BMK/cc-pvtz, and G3(MP2)/B3-CEP for calculated and experimental pK_a values. Comparing both theories shows that BMK/cc-pvtz achieved the worst results when compared with the experimental data. The G3(MP2)/B3-CEP theory presented the best pK_a values for the compounds studied. The four results present an absolute error lower than 0.55 units of pK_a . Only the $(CH_3)_2-CH-O$ provided a large deviation of 0.88.

Table 1. Calculated and measured pK_a values for some Alcohols with three waters.

Substance	BMK	G3(MP2)/B3-CEP	Exp.
CH ₃ CH ₂ OH	14.42	15.72	15.90
CH ₃ CH ₂ CH ₂ OH	13.38	16.52	16.10
(CH ₃) ₂ -CH-O	15.89	17.98	17.10
(CH ₃) ₃ -C-OH	18.65	15.45	16.00

Key-words: G3(MP2)/B3-CEP, Alcohols and BMK.

Support: This work has been supported by FAPESP, CNPq, FAEPEX-UNICAMP, CENAPAD-UFC and FAPEAM.

References:

- [1] A. V. Marenich, C. J. Cramer, and Donald G. Truhlar, *J. Phys. Chem. B*, 113, 6378 (2009).
- [2] C. M. R. Rocha, D. H. Pereira, N. H. Morgon, R. Custodio, *J. Chem. Phys.* 139, 184108 (2013).
- [3] A. D. Boese and J. M. L. Martin, *J. Chem. Phys.*, 121, 3405 (2004).

Excited-State Proton Transfer Can Tune the Color of Protein Fluorescent Markers

Daiana T. Mancini*, Tamiris M. Assis, Teodorico C. Ramalho, Kakali Sen, Mario Barbatti, Walter Thiel

**Department of Chemistry, Federal University of Lavras, 37200-000 Lavras, Brazil.*

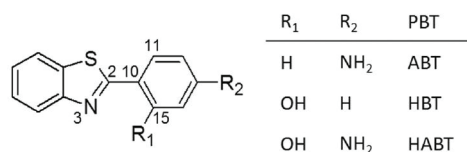
daianateixeira60@yahoo.com.br

Abstract: Phenylbenzothiazole (PBT) compounds exhibit antitumor properties and are highly selective in vitro and in vivo. Their antitumor action relies on the docking to tyrosine kinase (TKs), [1,2] enzymes that are usually over-expressed in several types of carcinomas. [3] A number of PBT compounds and complexes [4] strongly interact with the active site of kinases. The original PBT lead compound [2-(4'-aminophenyl)benzothiazole (ABT)] (Scheme 1) exhibits nanomolar activity against certain human breast cancer cell lines in vitro. [1] With regard to the goals of this work, it is particularly interesting that diverse (hydroxyphenyl)benzothiazole (HBT) compounds also have potent antitumor activity in human breast and colon cancer cell lines. In the physical chemistry community, the HBT isomer 2-(2'-hydroxyphenyl)benzothiazole is well known for its strong Stokes shift caused by excited-state intramolecular proton transfer (ESIPT) [5,6]. HBT undergoes ESIPT in the gas phase and in aprotic solution (Figure 1). Upon photoexcitation, the first singlet excited state (S1) of the enol form is populated. Then, a keto tautomer is formed by ultrafast proton transfer in the S1 state. [19] Because ESIPT is much faster (30–50 fs) than radiative decay (~106 fs), any observed fluorescence is normally due to the keto tautomer. However, depending on the environment, ESIPT in HBT can be partially or completely inhibited, which will increase the fluorescence quantum yield of the enol species. [6,7] ESIPT can also be followed by other relaxation processes affecting fluorescence intensities: intersystem crossing (ISC) with formation of the keto tautomer in the triplet ground state (T1) or isomerization of the cis- to the trans-keto form, which will proceed through a S1/S0 crossing region and may thus lead to internal conversion (IC). [6] This scenario opens the possibility of creating two-color fluorescent markers. Aiming at combining the tumor selectivity of ABT and the ESPT properties of HBT, we chose to study HABT, which differs from ABT by a hydroxyl group at the R1 position (Scheme 1). Our hypothesis is that the proportions and intensities of violet and green emissions from HABT depend on the protein active site conformation, which modulates the rates of ESIPT, ISC, and IC. Thus, changes in the fluorescence spectrum of HABT bound to TK could be the basis for a new method to detect mutations in cancer cells, usually associated to development of drug resistance. We show by quantum mechanical/molecular mechanical (QM/MM) simulations that phenylbenzothiazoles undergoing an excited-state proton transfer (ESPT) can be used to probe protein binding



sites. For 2-(2'-hydroxy-4'-aminophenyl)benzothiazole (HABT) bound to a tyrosine kinase, the absolute and relative intensities of the fluorescence bands arising from the enol and keto forms are found to be strongly dependent on the active site conformation. The emission properties are tuned by hydrogen-bonding interactions of HABT with the neighboring amino acid T766 and with active-site water. The use of ESPT tuners opens the possibility of creating two-color fluorescent markers for protein binding sites, with potential applications in the detection of mutations in cancer cell lines.

Key-words: Phenylbenzothiazole; fluorescence; QM/MM



Scheme 1. ABT, HBT, and HABT

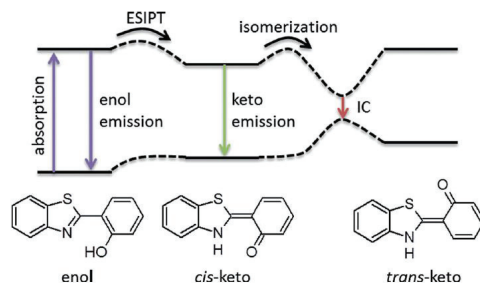


Figure 1. Schematic photophysics of HBT.

Support: This work has been supported by the German agency DAAD and the Brazilian agencies FAPEMIG, CAPES, and CNPq

References:

- [1] S. Tzanopoulou, *et al.* J. Med. Chem. 53, 4633 (2010).
- [2] J. W. Hicks, H. F. VanBrocklin, A. A. Wilson, S. Houle, N. Vasdev, *Molecules* 15, 8260 (2010).
- [3] H. Daub, K. Specht, A. Ullrich, *Nat. Rev. Drug Discovery* 3, 1001 (2004).
- [4] D. T. Mancini, E. F. Souza, M. S. Caetano, T. C. Ramalho, *Magn. Reson. Chem.* 52, 129 (2014).
- [5] J. Zhao, S. Ji, Y. Chen, H. Guo, P. Yang, *Phys. Chem. Chem. Phys.* 14, 8803 (2012).
- [6] M. Barbatti, A. J. A. Aquino, H. Lischka, C. Schrieffer, S. Lochbrunner, E. Riedle, *Phys. Chem. Chem. Phys.* 11, 1406 (2009).
- [7] Y. H. Kim, *et al.*, *Photochem. Photobiol. Sci.* 9, 722 (2010).



MODELING NMR PARAMETERS OF OXIMES IN WATER AND IONIC LIQUIDS – IMPLICATIONS OF SOLVATION SHELL STRUCTURE

Faria, J. A.¹, Polisel, D. A.¹, Mancini, D.T.¹, Costa, L. T.², da Cunha, E. F. F.¹, Ramalho, T. C.¹

¹Department of Chemistry, Federal University of Lavras, University Campus, PO Box 3037, CEP 37200-000, Lavras/MG, Brazil. ²Department of Chemistry, Fluminense Federal University, Miguel de Frias's Street, 9, Icaraí, CEP 24220-900, Niterói/RJ, Brazil

Abstract: Organophosphorus compounds (OP) has been widely used as pesticides and as warfare nerve agents. They act by phosphorylating the hydroxyl group of the Ser 203 residue of the Acetylcholinesterase (AChE) active site, inhibiting its catalytic activity, causing the cholinergic Syndrome [1]. Currently, the OP poisoning treatment consists in the use of reactivators, for example oximes, a class of compounds that is able to reactivate the inhibited enzyme [2]. Typically, expensive techniques are employed for the detection of OPs, such as GC and HPLC, but new techniques have been developed for this purpose using sensors, biosensors and electrolytes [3]. Currently, the use of ionic liquids (IL) as reactional medium for these sensors is little explored, but very promising [4]. In this sense, modern spectroscopic techniques, such as NMR Spectroscopy seems to be adequate for the characterization of this system [5]. In line with that, this work aims to investigate the solvent and thermal effects on NMR parameters of oximes in two different solvents, water and 1-Butyl-3-methylimidazolium tetrafluoroborate (BMIM-BF₄). By using the OPLS force field in the GROMACS 4.6.510 program, 10 ns of classical molecular dynamics simulations were performed for the oxime 3-fluoro-4-[(hydroxyimino)methyl]-1-methyl-pyridinium (3-Fluoro-4-PAM) (Figure 1) in water and ionic liquid.

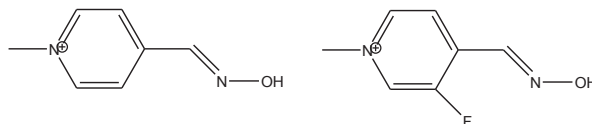


Figure 1 Structures of 4-PAM and 3-Fluoro-4-PAM, respectively.

Ab Initio MD simulations were also performed at the B3LYP/6-31G level at 310K. For NMR calculations, the GIAO method was employed for both dynamics and static systems. Molecular docking calculations between studied oximes and the AChE enzyme, PDB code 5HFA, were performed with the Molegro Virtual Docker software. Finally, theoretical calculations with 4-PAM (Figure 1) were employed to compare with experimental data and to validate the theoretical strategy.

From our theoretical findings, it was possible to notice that the ¹³C chemical shift values are good agreement with experimental data [6] for the level of approximation δ^{310K} [(H₂O//B3LYP/H₂O)], as shown in Table 1.

DFT study of the interaction between neutral ligands and metal cations ($M = Ca^{2+}, Mg^{2+}, Li^+, Ni^{2+}, Pb^{2+}$): Taking an insight into the interaction strength

Daniel G. S. Quattrociochi^a(PG), Glaucio B. Ferreira^a(PQ), Leonardo M. Costa^b(PQ) and José Walkimar de M. Carneiro^a (PQ)

^aUniversidade Federal Fluminense, Outeiro de São João Batista, s/n, 24020-141 Niterói - RJ, Brazil, ^bPrograma de Pós-Graduação em Ciência e Tecnologia Ambiental, Centro Universitário Estadual da Zona Oeste -UEZO, Campo Grande, Rio de Janeiro - RJ, Brasil.

The interaction between organic functional groups and metal cations is largely present in proteins and play an essential role in several biological activities [1]. Alkaline and alkaline earth metal cations have fundamental role in the human body. Some metals when ingested have high toxicity and can cause several diseases. For example, nickel and lead divalent cations are present in wastewater and are toxic species to human body. Therefore, the comprehension of the qualitative and quantitative interactions between the several functional groups and the cations is of fundamental relevance. Our group has been studying a set of systems dealing with the interactions between alkaline, alkaline earth and transition metal cations with a set of functional groups, with the goal to rationalize the intensity and type of forces that control the interactions [2-8].

The B3LYP functional with a variety of basis set has been employed to quantify the interaction energy of several neutral ligands with aquacomplexes $[M(H_2O)_n]$. The several terms that contribute to the stability of the complexes have been evaluated with the energy decomposition analysis (EDA) method. Correlation with empirical parameters for the functional groups has helped rationalize the main electronic features of the functional groups that modulate the interaction. The following metal cations have been studied: Li^+ , Mg^{2+} , Ca^{2+} , Ni^{2+} , Pb^{2+} . The following functional groups were tested: phosphoryl, amide, carboxylic acid, ammonia, imine, thiocyanic acid, nitrile, amine, ammonia, thiocarbonyl, thioether, thioalcohol and phosphine. The interaction energy was quantified in terms of substitution of one water molecule in a water complex for a ligand.

Our results indicate that ligands that bind by oxygen atom have interaction energies more negative than other compounds. The interaction with alkaline and alkaline earth cations has a major electrostatic character and are favored by higher charge on the ligand atom and short distances between the metal and the ligand, typical of ionic bond. Electronic and steric effects were quantified and the most relevant contributions to the interaction energy were identified. Additionally, the influence of substituent groups on the intensity of the metal-ligand binding was also analysed. In general, electron donor groups stabilize the complexes.

This same methodology was applied for Ca^{2+} cation with dicarbonyl ligands, with each ligand substituting two water molecules. In addition to the electronic and geometric parameters previously used to rationalize the metal-ligand interaction, a new parameter called the chelating angle (the angle between the ligand atoms and the metal center) was



used, in which high values represent a gain for the stability of the formed complex. In this case the number of molecules in the product is greater than the number of molecules in the reagent so the entropic term ($-\Delta S$) becomes relevant and contributes to the spontaneity of the reaction. The methodology was also employed for other metal cations like Pb^{2+} and Ni^{2+} . In these cases both electrostatic and covalent components are important to the metal-ligand interaction. The absolute softness of the free ligands was correlated with the covalent contribution.

Key-words: Metal-ligand interaction, DFT, Energy Decomposition Analysis

Support: This work has been supported by FAPERJ, CAPES and CNPQ

References:

- [1] P.G. Daniele, C. Foti, A. Gianguzza, E. Prenesti, S. Sammartano, *Coord Chem Rev*, 252, 1093 (2008).
- [2] a) L. M. da Costa, J. W. de M. Carneiro, G. A. Romeiro, L. W. C. Paes, *J Mol Model*, 17, 243 (2011); b) L. M. da Costa, J. W. de M. Carneiro, G. A. Romeiro, L. W. C. Paes, *J Mol Model*, 17, 2061 (2011); c) L. M. da Costa, J. W. de M. Carneiro, L. W. C. Paes G. A. Romeiro, *J Mol struct (THEOCHEM)* 911, 46 (2009).
- [3] L. M. da Costa, L. W. C. Paes, J. W. de M. Carneiro, *J Braz Chem Soc* 23, 648 (2012).
- [4] D. G. S. Quattrociochi, G. B. Ferreira, L. M. da Costa, J. W. de M. Carneiro, *Comp and Theoretical Chem* 1075, 104 (2016).
- [5] D. G. S. Quattrociochi, M. V. M. Meuser, G. B. Ferreira, L. M. da Costa, J. W. de M. Carneiro, *J Mol Model* 23, 60 (2017).
- [6] M. V. M. Meuser, D. G. S. Quattrociochi, L. M. da Costa, G. B. Ferreira, J. W. de M. Carneiro, *Polyhedron* 102, 193 (2015).
- [7] D. G. S. Quattrociochi, J. W. de M. Carneiro, G. B. Ferreira, R. N. Damasceno, L. M. da Costa, *Chem Select* 2, 4617 (2017).



Investigaç o te rica do complexo de monocarboxilato de praseod mio (III)

Daniel Mungo Brasil¹, Cl udio Teodoro de Carvalho², Leandro Moreira de Campos Pinto¹

¹*Instituto de Qu mica, Universidade Federal de Mato Grosso do Sul (UFMS), 79.074-460, Campo Grande, MS, Brasil*

²*Faculdade de Ci ncias Exatas e Tecnologia, Universidade Federal da Grande Dourados (UFGD), 79.804-970, Dourados, MS, Brasil*

Os lantan deos comp em uma s rie de elementos qu micos que v o do lant nio ($Z = 57$) ao lut cio ($Z = 71$). Nestes elementos os orbitais f passam a ser preenchidos no estado fundamental. Apesar de os orbitais $4f$ serem os orbitais de val ncia destes elementos, eles s o orbitais muito internos e, como consequ ncia, s o blindados do ambiente qu mico, conferindo aos lantan deos propriedades espectrosc picas  nicas [1]. As transi es eletr nicas dos lantan deos s o do tipo $f \rightarrow f$, embora esse tipo de transi o seja considerado proibido pela regra de sele o de paridade de Laporte.

O estudo de materiais compostos por  ons dos lantan deos   de fundamental import ncia devido   ampla variedade de aplica es em diversas  reas industriais, onde os dispositivos dependem de uma certa composi o estrutural e estabilidade t rmica para a emiss o de luz em regi es espec ficas. Al m disso, estes materiais apresentam propriedades  ticas muito  teis: lasers, fibras  ticas, an lise de imagens m dica, entre outras. [2-4].

Devido a estas caracter sticas  nicas apresentas por compostos de lantan deos, a investiga o te rica de suas propriedades se torna muito interessante, em que diversos par metros podem ser calculados por simula o computacional para auxiliar na compreens o das transi es eletr nicas.

Neste estudo foram realizados c culos baseados na teoria do funcional da densidade (DFT) para um complexo monocarboxilato de praseod mio (III). Foi empregado o funcional B3LYP [5, 6] e as bases SDD para o praseod mio e 6-31G* para o C, O e H. Todos os c culos foram realizados utilizando o programa Gaussian 09 [7]. As energias de excita o vertical foram calculadas atrav s da teoria do funcional da densidade dependente do tempo (TD-DFT). Os diagramas dos orbitais moleculares foram produzidos usando o programa Avogadro (vers o 1.2.0) [8].

A partir dos resultados obtidos   poss vel analisar a contribui o dos orbitais moleculares na fronteira HOMO/LUMO respons veis pela transfer ncia eletr nica.   observado que as transi es HOMO-1 \rightarrow LUMO (53%) e HOMO-2 \rightarrow LUMO (60%) caracterizam a transfer ncia eletr nica do ligante para o metal.

Devido a estas caracter sticas  nicas apresentas por compostos de lantan deos, a investiga o te rica de suas propriedades se torna muito interessante, em que diversos par metros podem ser calculados por simula o computacional para auxiliar na



compreensão das transições eletrônicas.

Neste estudo foram realizados cálculos baseados na teoria do funcional da densidade (DFT) para um complexo monocarboxilato de praseodímio (III). Foi empregado o funcional B3LYP [5, 6] e as bases SDD para o praseodímio e 6-31G* para o C, O e H. Todos os cálculos foram realizados utilizando o programa Gaussian 09 [7]. As energias de excitação vertical foram calculadas através da teoria do funcional da densidade dependente do tempo (TD-DFT). Os diagramas dos orbitais moleculares foram produzidos usando o programa Avogadro (versão 1.2.0) [8].

A partir dos resultados obtidos é possível analisar a contribuição dos orbitais moleculares na fronteira HOMO/LUMO responsáveis pela transferência eletrônica. É observado que as transições HOMO-1 \rightarrow LUMO (53%) e HOMO-2 \rightarrow LUMO (60%) caracterizam a transferência eletrônica do ligante para o metal.

Key-words: praseodímio; ligante monocarboxilato; TD-DFT

Support: Os autores agradecem ao CENAPAD-SP (Centro Nacional de Processamento de Alto Desempenho em São Paulo) pelo tempo computacional concedido. DMB agradece à CAPES pela bolsa.

References:

- [1] Atwood, D. A. *The Rare Earth Elements: Fundamentals and Applications*; John Wiley & Sons, Ltd: Hoboken, 2012; p 624.
- [2] *Lanthanoid Series Elements—Advances in Research and Application*, 2012 Edition: A ScholarlyEditions™ eBook. ISBN 978-1-464-99233-9, Atlanta, Georgia.
- [3] Absorption spectra of the 4f electron transitions of the praseodymium complex with 1-cyclopyl-6-fluoro-1,4-dihydro-7-(4-ethyl-1-piperazinyl)-4-oxo-3-quinoline carboxylic acid hydrochloride and its analytical application. *Sciences Analytical*, volume 17, 2001, 1091-1094.
- [4] H A Zamani, M R Ganjali, P Norouzi, S Meghdadi. Application of Novel Praseodymium (III) PVC-Membrane Electrode for Determination of Pr(III) Ions in Soil and Sediment Samples. *Journal Analytical letters*, 2008;41:902-916.
- [5] C. Lee, W. Yang, R. G. Parr, *Phys. Rev. B* 37 (1988) 785.
- [6] A. D. Becke, *J. Chem. Phys.* 98 (1993) 5648.
- [7] M J Frisch, et al., *Gaussian 09, Revision D.01*, Gaussian, Inc.; 2013.
- [8] M D Hanwell, D E Curtis, D C Lonie, T Vandermeersch, E Zurek, G R Hutchison. *J. Cheminform.* 2012;4:17.



Theoretical Investigation of the Emission Spectra and Stokes Shift of Modified Nucleobases in Gas Phase, 1,4-dioxane and Water

Danillo Valverde¹, Adalberto V. S. Araújo², Antonio C. Borin², Sylvio Canuto¹

¹*Instituto de Física, Universidade de São Paulo, 05508-090 São Paulo, SP, Brazil*

²*Instituto de Química, Universidade de São Paulo, São Paulo, SP, Brazil*

Very interesting compounds, obtained from simple chemical modifications on the natural canonical nucleobases, have received considerable attention from theoretical and experimental chemists. Fluorescent nucleosides are among these new compounds, deserving special attention due to potential applications in biophysical analyses and for fabricating effective discovery assays [1]. Recently a second generation of a new class of fluorescent ribonucleoside alphabet was synthesized, employing isothiazole[4,3-d]pyrimidine as a template [2]. These emissive species are isomorphous nucleoside surrogates, with strong resemblance to their native counterparts (isomorphism). Due to these properties, they can replace their canonical counterparts on the genetic code, imposing a minimal change in the native structural and functional properties. That is, they are very good fluorescent probes.

The emission spectra of the emissive nucleobases presented above were investigated in gas phase and solution, employing the Sequential QM/MM methodology [3] and multiconfigurational methods. Solvent effects were included by combining the Sequential QM/MM methodology [3] with an average electrostatic embedding (ASEC) [4] and the Free Energy Gradient method (FEG) [5], called ASEC-FEG method [6]. This methodology has been applied successfully for describing the electronic (ground and excited states) properties of several molecules in solution [7]. For the sake of comparison, the conventional PCM model was employed.

Emission spectra, from the lowest-lying $^1(\pi\pi)^*$ state (bright state) were investigated in two solvents: 1,4-dioxane and water. In gas phase, the geometry of first bright state were optimized at the Multi-State CASPT2 level. However, in solution the geometries were optimized at the CASSCF level to reduce computational costs. The active space comprises the full set of π , π^* orbitals. For consistency with previous work concerning the absorption spectra, emission energies were computed with the single-state CASPT2 method, enlarging the full set of π , π^* orbitals with three n-orbitals (CAS(18,13)). The n-orbital associated to the sulfur atom was kept inactive because its occupation number was always close to two. All CASPT2 calculations were done with no IPEA shift correction and applying an imaginary level shift of 0.2 Hartree.

The main differences between the optimized geometries of the ground and low-lying $^1(\pi\pi)^*$ states are related to the bond lengths and the pyramidalization of the amino group. Emission spectra and Stokes shift were better described when the MS-CASPT2



optimized geometry was adopted, in contrast to the results obtained with the optimized CASSCF structures.

Two approaches were used to describe qualitative the $^1(\pi\pi^*)$ states lifetimes in solution. First, lifetimes were supposed to be long, which allows the achievement of an electrostatic equilibrium between solute and solvent (equilibrium approach). In the second approach (non-equilibrium approach), the lifetimes are considered to be short and the electrostatic equilibrium is not reached. Our results indicate that ^2C does not reach electrostatic equilibrium with the two solvent. The ^2G in water is also better described using the non-equilibrium solvation. Following these assumptions, a better understanding of the photophysics in solution were obtained, with theoretical emission spectra and Stokes shifts in agreement with experimental results. On the other hand, the PCM model does not describe well the emission spectra and the Stokes shift.

Deactivation pathways from the FC to the minimum in the low-lying $^1(\pi\pi^*)$ states were computed with the MEP (minimum energy path) method in gas phase. Furthermore, conical intersections between the ground and the bright states were computed, and linear interpolations in internal coordinates were employed to connect the relevant structures. The computed pathways for the ^2A , ^2G and ^2I molecules are similar to the 2-aminopurine [8], exhibiting a high barrier between the minimum and the conical intersection, which explain the fluorescent property. As to the ^2C molecule, the conical intersection is inaccessible because it is located in a high energetic region. Solvent effects were considered solvating each point on the pathways.

Support: Acknowledgements: grants 2017/02612-4 (DV) from FAPESP, 153104/2015-5 (AVSA) and 303352/2013-3 (ACB) from CNPq.

References:

- [1] R. W. Sinkeldam, N. J. Greco, Y. Tor *Chem. Rev.* **110**, 2579 (2010); M. Kimoto, I. Hirao *Expert Rev. Mol. Diagn.* **11** 321 (2011).
- [2] A. R. Rovira, A. Fin, Y. Tor *J. Am. Chem. Soc.* **237**, 14602 (2015).
- [3] K. Coutinho, R. Rivelino, H. C. Georg, S. Canuto, in *Solvation Effects on Molecules and Biomolecules. Computational Methods and Applications*, S. Canuto (Editor) pp. 159-189, Springer, (2008).
- [4] K. Coutinho, H. C. Georg, T. L. Fonseca, V. Ludwig, S. Canuto *Phys. Lett.* **437**, 148 (2007).
- [5] N. Okuyama-Yoshida, M. Nagaoka, T. Yamabe *Int. J. Quantum Chem.* **70**, 95 (1998).
- [6] H. C. Georg, S. Canuto. *J. Phys. Chem. B* **116**, 11247 (2012); L. R. Franco, I. R. Brandão, T. L. Fonseca, H. C. Georg *J. Chem. Phys.* **145** 19430 (2016).
- [7] I. R. Brandão, L. R. Franco, T. L. Fonseca, M. A. Castro, H. C. Georg *J. Chem. Phys.* **146**, 224505 (2017); C. Bistafa, H. C. Georg, S. Canuto *Comp. Theor. Chem.* **1040**, 312 (2014).
- [8] V. Ludwig, Marcos S. Amaral, Z. M. Costa, Antonio C. Borin, S. Canuto, L. Serrano-Andrés *Chem. Phys. Lett.* **463**, 201 (2008).



One-electron bonds from the quantum interference perspective

David Wilian Oliveira de Sousa, Marco Antonio Chaer Nascimento

Instituto de Química - Universidade Federal do Rio de Janeiro. Avenida Athos da Silveira Ramos, 149, Cidade Universitária, CT Bloco A sala 412. Rio de Janeiro, RJ.

CEP 21.941-909

Abstract: The valence bond-like picture of the chemical bond is deeply rooted into the qualitative general chemistry framework and electron-pair covalent bonds are often considered as the “standard” chemical bond. Conversely, odd-electron and multicenter bonds are seen as anomalous, unrepresentative, or just different types of bonds. In this work, the powerful Interference Energy Analysis (IEA) approach provided by the Generalized Product Function Energy Partitioning method (GPF-EP)[1] was extended to treat two-center one-electron bonds, by means of the Spin Coupled Valence Bond wave function for N electrons in M orbitals, SCVB(N,M) [2]. The bond in several sets of analogous molecules (H_2^+/H_2), (Li_2^+/Li_2), (Na_2^+/Na_2), ($LiNa^+/LiNa$), (K_2^+/K_2), (LiH^+ /LiH), (Cu_2^+/Cu_2), ($H_3C^+CH_3^+/H_3CCH_3/H_3C^+BH_3$), ($H_2C^+CH_2^+/H_2CCH_2/H_2CBH_2/H_2BBH_2^-$), as well as for $[(H_3P)_3Cu^+BH_3]$, were analyzed by the GPF-EP method. The components of the energy accounting for the formation of the bond were evaluated and the results for the analogous cases of the one-electron and the conventional two-electron bonds were compared.

The result of the GPF-EP analysis clearly shows that one-electron bonds have the same mechanism of formation as the regular covalent bonds. In other words, the same phenomenon, quantum interference, rules the stabilization of systems containing such bonds. In all cases studied, the chemical bond occurs because of the concentration of density in the bond region, and the drop in interference kinetic energy. By comparing the cases of one-electron bonds with two-electron bonds in correspondent molecules, calculations have shown that the largest differences in energy are due to quasi-classical factors, mostly the reference electron-electron potential. The case of the alkali metal dimers is different, because of the high polarizability of the atoms involved in bonding. Normally, one-electron bonds have lower bond dissociation energies (BDEs) than the correspondent two-electron bonds. This fact, however, has no relation with bond order – one-electron bonds are not “half-bonds”. Since the interference is the dominant factor for the formation of the bond and interference depends basically on the orbital overlaps, if the orbitals involved in bonding are similar in both cases, the difference has to come from the quasi-classical part. Even the case of the alkali metal dimers, whose cations have higher BDEs than the neutral molecules, can be explained by quasi-classical factors. In conclusion, there is no distinction between one- and two-electron bonds from the conceptual point of view, since they both result from the same phenomenon. This work opens perspectives for the study of other bonding systems, like three-electron two-center bonds and, in general, multicenter bonds.



Key-words: Chemical bonding theory, GPF-EP, GVB, SCVB, one-electron bond.

Support: This work has been supported by the Brazilian agencies FAPERJ, CNPq and CAPES.

References:

- [1] T.M. Cardozo and M.A.C. Nascimento, “Energy partitioning for generalized product functions: The interference contribution to the energy of generalized valence bond and spin coupled wave functions,” *J. Chem. Phys.* 130, 1 (2009).
- [2] P.B. Karadakov, D.L. Cooper, B.J. Duke, and J. Li, “Spin-Coupled Theory for ‘N Electrons in M Orbitals’ Active Spaces,” *J. Phys. Chem. A* 116, 7238 (2012).



Identification of flavonoid with potential for inhibitor Enoyl-ACP Reductase in *Plasmodium falciparum* by hierarquical virtual screening

Dayse Silva^{1,2}, Diego Costa², Hugo Brandão², Manoelito Santos¹

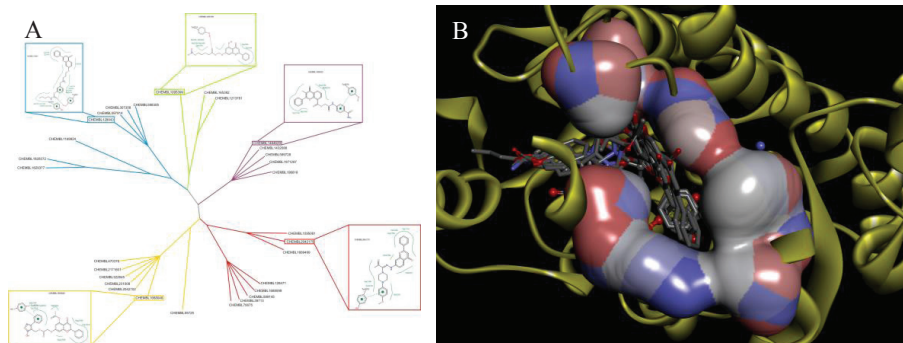
¹ Laboratório de Modelagem Molecular, Universidade Estadual de Feira de Santana.

² Laboratório de Bioprospecção Vegetal, Universidade Estadual de Feira de Santana.
dayse.aasilva@hotmail.com

Abstract: Malaria is a parasitic infection and is considered a serious global public health problem [1]. *Plasmodium falciparum* provides easy adaptability by mutation, causing resistance to antimalarials [2]. This study aimed to search antimalarial potential showed by some flavonoids to inhibit promising target, enoyl-ACP reductase (PfENR), present in limiting step in the biosynthesis of fatty acids type II (FAS II) of *P. falciparum* [2-3]. A flavonoid library obtained in ChEMBL (n = 4008) was filtered through physic-chemical similarity using the Euclidean distance. Inhibitors described in the literature were used as reference molecules. The 3057 selected molecules were submitted to molecular docking using DOCK 6.5. The analysis of the docking parameters was performed by analysis of RMSD value and ROC analysis. The results showed RMSD = 0.54 Å and AUC = 0.86, indicating good performance of the docking method. The top 30 ranked molecules of docking were selected for analysis by self-organizing maps using AuPosSOM program with the objective of cluster molecules according to intermolecular interactions. The 5 higher leaves were selected based on the proximity of the branches of Newick's tree. Thus, a representative molecule of each leaf was selected, in order to illustrate the interaction pattern within these leaves (Figure 1A). The intermolecular interactions analyzed corroborate with that described in the literature. This is because studies show hydrogen interactions, electrostatic and hydrophobic between the catalytic site inhibitor and the PfENR [4-5]. The detailed analysis of intermolecular interactions of the five molecules representing each leaf and PfENR enzyme showed that there are an essential interactions pattern favoring the ligand - receptor complex stability, and consequently result in better binding energy values. It was possible to identify the hydrophobic pocket that performs flavonoid moiety interactions with the core (Figure 1B). This analysis shows the importance of flavonoid moiety for inhibiting PfENR, confirming the choice of this metabolite class to study and development of new antimalarial candidates. Furthermore, it is possible to infer the importance of a candidate molecule inhibitor of the enzyme aromatic PfENR, that have regions that allow electrostatic interactions with the NAD501 and Tyr277 or Tyr267 or regions that allow the hydrogen interaction with these residues, especially Tyr277. Thus, it can be proposed that a successful PfENR inhibitor needs to interact with the Tyr277, and thus occupy the space of interaction with the natural substrate in order to block its role in catalysis. This approach allowed the selection of flavonoids

with potential affinity against PfENR. In addition, it was possible to recognize which intermolecular interactions contribute to the molecular recognition process.

Figure 1. **A-** The 5 leaves selected of the Newick tree and the representative molecule of each leaf. **B-** Region of hydrophobic interactions of PfENR with the flavonoid nucleus of the top five molecules.



Key-words: Malaria • Flavonoids • Virtual screening • PfENR

Support: This work has been supported by CNPq and UEFS

References:

- [1] OMS. World malaria report, 2-243, (2015).
- [2] D. Tasdemir; G. Lack; R. Brun; P. Ruedi; L. Scapozza; R. Perozzo. *J. Med. Chem.*, *49*, 3345-3353 (2006).
- [3] F. Ntie-Kang; P.A. Onguène; L.L. Lifongo; J.C. Ndom; W. Sippl; L.M. Mbaze. *Malaria Journal*, *13*, (2014).
- [4] M.J. Stewart; S. Parikh; G. Xiao; P.J. Tonge; C. Kisker. *J. Mol. Biol.*, *290*, 859-865 (1999).
- [5] K. Maity; S.P. Bhargav; B. Sankaran; N. Surolia; A. Surolia; K. Suguna. *Life*, *62*, 467-476 (2010).

SuAVE: a computational tool for the assessment of curved surfaces

Authors: Denys E. S. Santos¹, Frederico J. S. Pontes¹, Kaline Coutinho², Roberto D. Lins³, Thereza A. Soares¹

¹*Department of Fundamental Chemistry. Federal University of Pernambuco. Cidade Universitária, Recife - PE, 50740-540.*

²*Physics Institute, University of São Paulo. Cidade Universitária, São Paulo, SP – 05508-090.*

³*Oswaldo Cruz Foundation. Cidade Universitária, Recife - PE, 52171-011.*

Abstract: Data analysis is an inevitable and necessary step for engineering predictive models for a studied system. The success of the model depends directly on how precise, and preferably, efficient are the analyses in measuring properties of interest. The program SuAVE (Surface Assessment Via grid Evaluation) is a Fortran-based program developed to analyze geometrical properties of surfaces taking into account the structural morphology of the systems. To do so, this ensemble of numerical routines relies on a surface fitting process established over the basis of differential and computational geometry and numerical calculus¹ (Figure 1).

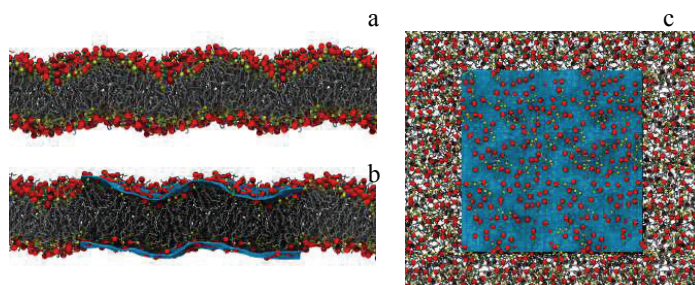


Figure 1. Representation of the generation and fitting of grid along the surface of a bilayer of Lipid A. Lateral (a, b) and top (c) views of the membrane surface. Grid surface is represented in blue, phosphorous and oxygen from phosphate groups are represented in red and yellow respectively, and acyl chains in gray.

The program has been developed to handle any organic, inorganic, or biological system containing a surface or an interface, presenting or not curvature and displaying a wide range of morphologies. It can take as input trajectory files from molecular dynamics (MD) and Monte Carlos simulations as well as any other numerical methodology once an input file in PDB format is provided. The program can efficiently calculate the area and volume per molecule composing an interface, membrane thickness, surface topology maps, density profiles, curvature order parameters and Gaussian curvatures. The accuracy of the numerical methodology implemented in SuAVE to assess the above-mentioned geometrical properties of curved surfaces has been validated via the analysis of four different Lipid A chemotypes² and compared with conventional



methodologies which does not take into account the membrane curvature. The different Lipid A chemotype bilayers displays distinct morphologies, namely gel, lamellar and ripple-shaped phases as shown by MD simulations. MD simulations were carried out for 100 ns after equilibration of the bilayers using GROMOS 53A6 force field³ at the NpT ensemble. The average deviation of the SuAVE fitted points in relation to the system surface was 0,11 nm with a grid refinement of 50X50 points applied to each analysis. The comparison of the area per lipid head-group can exemplify the two most important conclusions in the systematic evaluation of SuAVE efficiency. For bilayers with a lamellar planar shape, the values calculated with SuAVE are in excellent agreement with the same analysis performed with conventional methodologies. However, when comparing the results for bilayers in the ripple phase, conventional analysis underestimates the area per lipid molecule in about 19% because they neglect membrane curvature. Likewise, density profiles for the ripple phase bilayers are rather distinct when the membrane curvature is taken into account or not in the calculations while they are identical for lamellar phase bilayers. The density profiles calculated with SuAVE for the former systems show that even if not planar they conserve a lamellar structure. On the other hands, density profiles obtained via the use of conventional analysis imply the presence of water within the membrane which clearly leads to the equivocal interpretation of the data. Further, the SuAVE code calculates the curvature order parameter which provides a quantitative estimate of how curved is a given surface on average. By using the surface curvature angles with respect to the normal axis to the system, it is possible to demonstrate that for gel and lamellar systems about of 90% of the surface exhibits a surface curvature angle below 30° while for ripple shaped membranes it can increase up to a value of 60°. Through all these examples SuAVE has demonstrated capabilities for evaluating structural properties for different systems taking into account their constitutional geometry, not observed in conventional numerical analysis, displaying a potential for contributing in the evaluation of a wider range of organic, inorganic or biological systems.

Key-words: Membrane Curvature, Voronoi Tesselation, Helfrich Equation, Lamellar Phase, Ripple Phase, Structural Transitions

Support: This work has been supported by CNPq, BioMol, CAPES.

References:

- [1] M. de Berg, O. Cheong, M. van Kreveld, M. Overmars. Computational Geometry. Algorithms and Applications. Third edition, Springer, 2008.
- [2] D. E. S. Santos, L. Pol-Fachin, R D. Lins, T. A. Soares. Polymyxin Binding to the Bacterial Outer Membrane Reveals Cation Displacement and Increasing Membrane Curvature in Susceptible but not in Resistant LPS Chemotypes. Journal of Chemical Information and Modeling. (accepted)
- [3] C. Oostenbrink, A. Villa, A. E. Mark, W. F. Van Gunsteren. A biomolecular force field based on the free enthalpy of hydration and solvation: the GROMOS force-field parameter sets 53A5 and 53A6. Journal of Computational Chemistry. v. 25(13), p. 1656-1676, 2004.



Conformational Analysis of 1,2-Dichloroethane in Implicit Solvent (SMD) through Solvation Thermodynamics

Diego J. Raposo, Ricardo L. Longo

Universidade Federal de Pernambuco, Departamento de Química Fundamental, Recife, PE, Brazil (email: sherlockmang@yahoo.com.br)

Abstract: Solvation Thermodynamics is a theory that properly defines the concept of solvation from statistical thermodynamics and provides insights into how to calculate, interpret, and obtain experimentally solvation thermodynamic quantities (Gibbs energy, entropy, enthalpy, etc.) [1]. Although it allows us to study the effects of the population of different conformers on the Gibbs solvation energy of the flexible molecule and the equilibrium constants of conversion between the conformers in different fluid phases, so far this level of information within the solvation thermodynamics domain has not been obtained by computational methods. The molecule 1,2-dichloroethane (1,2-DCE) is a prototype for studying conformational equilibrium in gas and in solution by different computational techniques and theoretical approaches [2]. It is well known that the relative abundance of the two major conformers of 1,2-DCE, *gauche* (*g*) and *anti* (*a*), characterized by the dihedral angle between chlorine atoms of the molecule, changes in different phases. In pure gas, the *anti* conformer is more abundant (79 %) compared to *gauche* [3], whereas in polar solutions there is a population inversion, and *gauche* is more likely to be found in solution (64.6 % in 1,2-DCE pure liquid, for instance [4]). To test the effectiveness of the solvation thermodynamics in predicting qualitative and quantitatively such population changes, we calculated the so called Conformational Probability Density (CPD) of 1,2-DCE in ideal gas and in water. It quantifies, among other things, the probability of a selected molecule to be within certain dihedral angle (or, more generally, certain volume in conformational space) in a given phase, and also the influence of each conformer on the resulting Gibbs solvation energy, with more abundant conformers have more influence on such energy. We have estimated the CPD function from the internal partition functions of each conformer, restricting the dihedral angle to a given value during the geometry optimization calculated at the MP2/cc-pVTZ level and using solvation energies from SMD implicit solvent model (B3LYP/6-31g(d)). We have found that the population of the *anti* conformer changes from 91% (greater than experimental value) to 52% from the ideal gas 1,2-DCE to 1,2-DCE in water, considering *anti* conformers those with dihedral angle between 120° and 240° [5]. The solvation energies of each conformer ranged from -4.0 to -2.5 kcal/mol, and the total solvation energy was -2.81 kcal/mol, which can be compared with the experimental value of -1.7 kcal/mol [6]. There are two possible *gauche* conformers, with dihedral angles $\sim 70^\circ$ (*g*⁺) and $360^\circ - 70^\circ = 290^\circ$ (*g*⁻), and we calculated the conversion energies from both *gauche* conformers to *anti* (*g*⁺ and *g*⁻ \rightarrow *a*), which is



related to the total population of *gauche* conformers, and the conversion energy of a specific *gauche* conformer to *anti* (g^+ or $g^- \rightarrow a$), both in ideal gas and in implicit solvent model of solution. Therefore, the conversion energy of g^+ and $g^- \rightarrow a$ process (the conversion of both *gauche* conformers is accounted) is 6.10 kcal/mol in gas and 5.44 kcal/mol in solution, and the conversion energy of g^+ or $g^- \rightarrow a$ process (referring to the conversion of one specific *gauche* conformer to *anti*) is -1.79 kcal/mol in gas and -0.47 kcal/mol in solution. The experiments shows that g^+ or $g^- \rightarrow a$ is -1.20 kcal/mol in ideal gas [7], and -0.57 kcal/mol in aqueous solution [8], which compare reasonably well with the calculated values. The relationship between the equilibrium constants of conversion amongst the conformers and the CPD of 1,2-DCE in each phase allows us to estimate equilibrium constants (and conversion energies) even in cases when conformers have the same structure, and therefore with the same Gibbs solvation energy, and to determine the relative population and the conformational equilibrium through probabilistic reasoning. We notice the SMD implicit solvent gives a preference to the *anti* conformer and a larger stability than experimentally verified in gas phase, which increases its population over the *gauche* conformer, even in aqueous solution, were it is expected be less abundant. The decrease in population from gas to polar solvent due to dipole-dipole interactions with water is, however, verified in our results. The importance of this work resides in the first application of the solvation thermodynamics formalism to conformational equilibrium by using well known computational tools, which might be fundamental to deeper understanding of some reactions in solution, such as antiperiplanar eliminations and electrocyclic reactions, from both thermodynamics and kinetics (transition state theory) perspectives. We also verified the consistency of the mathematical formalism of such theory in the predictions of some molecular aspects that drives the solvation process, but the reliability of the computational technique or model used can lead to predictions that need improvement. Other forms of calculating the Gibbs energy of solvation (Monte Carlo simulations, analytical approximations, numerical integrations) to each conformer can lead to more satisfactory results and we are pursuing these approaches.

Key-words: Solvation Thermodynamics, conformer distributions, implicit solvent

Support: This work has been supported by CAPES, CNPq, FACEPE, PRONEX.

References:

- [1] A. Ben-Naim, "Solvation Thermodynamics" (1987), Springer Science+Business Media, New York, USA.
- [2] J. A. Gomez, A. K. Tucker, T. D. Shepherd, W. H. Thompson, J. Phys. Chem. B, 109, 17479 (2005).
- [3] C. Reichardt, T. Welton, "Solvents and Solvent Effects in Organic Chemistry" (2011), Wiley-VCH, Weinheim, Germany.
- [4] K. Tanabe, Spectrochim. Acta, 28A, 407 (1972).
- [5] W. L. Jorgensen, J. Am. Chem. Soc., 103, 677, (1981).
- [6] There are several forms of obtain, from experimental data, such quantity. We used Henry constant of 1,2-DCE at 25 °C of $0.14 \text{ kPa m}^3 \text{ mol}^{-1}$.
- [7] M. W. Wong, M. J. Frisch, K. B., Wiberg, J. Am. Chem. Soc., 113, 4776 (1991).
- [8] M. Kato, I. Abe, Y. Taniguchi, J. Chem. Phys., 110, 11982 (1999).



Conformational Analysis and pK_a Calculations of Glycine in Aqueous Solution

Diego Nascimento de Jesus, Neubi Francisco Xavier Junior, Cristiane Martins Cardoso,
Clarissa Oliveira da Silva, Glauco Favilla Bauerfeldt

Departamento de Química □ Universidade Federal Rural do Rio de Janeiro

Abstract: Glycine is the simplest and perhaps the most important amino acid in general metabolism. Moreover, studies of the behavior of biomolecules in the interstellar medium (ISM) point out that glycine is found in solid phase, covered by icy mantle. The presence of water molecules seems to be essential for its survival [1]. In water solutions, glycine behaves as a zwitterionic specie and can be found in different protonation degrees: H_2Gly^+ ($\text{HO}_2\text{CCH}_2\text{NH}_3^+$), in low pH values; HGly ($^-\text{O}_2\text{CCH}_2\text{NH}_3^+$), in intermediate pH values and Gly^- ($^-\text{O}_2\text{CCH}_2\text{NH}_2$), in high pH values. The transitions from H_2Gly^+ to HGly and HGly to Gly^- occur at pH values equal to the corresponding pK_a values: pK_{a,1} = 2.35 and pK_{a,2} = 9.78 [2]. Although the zwitterion is the most abundant specie in physiological pH, the tautomerization is also possible and the HGly specie is better described as an equilibrium between the zwitterion ($^-\text{O}_2\text{CCH}_2\text{NH}_3^+$) and the neutral ($\text{HO}_2\text{CCH}_2\text{NH}_2$) forms [3]. Despite all the evidences and experimental knowledge about glycine and its related specie in aqueous solutions, a structural model considering all the possible geometries in condensed phase is still missing. This work aims to the description of the several stationary points related to the different species of glycine and to the selection of the lowest energy geometries. Such structural model is here validated through pK_a calculations and these geometries will finally be used to compose a model for the icy mantle and the possible surface reactions leading to the destruction of glycine in the ISM. In order to achieve the microscopic description of glycine's aqueous solution, theoretical calculations have been performed at the B3LYP level, adopting the 6-311++G(2d,2p) basis set. The presence of the solvent has been simulated through CPCM calculations, with Pauling atomic radii for building up the molecular cavity and explicitly including the solute cavitation energy and solute-solvent dispersion and repulsion interaction energies in the total energies. The choices for the CPCM method and Pauling radii have been done from previous test runs. As an isolated system, eight conformers are located for the neutral glycine. In aqueous solutions, the same number of the corresponding conformers is found, although the minimum energy conformer in solution is different from the lowest energy geometry in gas phase. An additional water molecule has been included as a microsolvation model for the neutral HGly form ($\text{HGly}(\text{ne})\cdot\text{H}_2\text{O}$). For the zwitterion, only one conformer has been found and similarly, the inclusion of an addition water molecule allowed the microsolvation description of the zwitterionic specie ($\text{HGly}(\text{zw})\cdot\text{H}_2\text{O}$). The standard Gibbs free energy difference for the tautomerization reaction, $\text{HGly}(\text{ne})\cdot\text{H}_2\text{O} \rightarrow \text{HGly}(\text{zw})\cdot\text{H}_2\text{O}$, at the CPCM/B3LYP/6-311++G(2d,2p) level, is $-6.84 \text{ kcal mol}^{-1}$, in good agreement with the



experimental value ($-7.27 \text{ kcal mol}^{-1}$). Only one conformer has also been found for Gly⁻, whereas three conformers have been located for the H₂Gly⁺ specie and a microsolvated model for both has also been set by inclusion of an additional water molecule, forming the Gly⁻.H₂O and H₂Gly⁺.H₂O specie. The whole set of stationary points has been used for the calculation of the pK_a values, which have been determined based on two reference reactions: H₂Gly⁺.H₂O + MA → MAH⁺ + HGly(zw).H₂O (R1) and HGly(zw).H₂O + A⁻ → Gly⁻.H₂O + HA (R2), where MA = methylamine, MAH⁺ = methylamonium cation, A⁻ = acetate anion and HA = acetic acid. From the standard Gibbs free energy values for each reference reaction, the pK_a values have been determined: pK_{a,1} = 1.31 and pK_{a,2} = 9.41. The good agreement with the literature values suggest that the set of geometries located for each glycine form in aqueous solution is satisfactory and complete enough to provide a good description of the structure of this amino acid in the water environment.

Key-words: glycine, aqueous solution, tautomerization

Support: This work has been supported by CAPES

References:

- [1] A. Pernet, J. Pilmé, F. Pauzat *et al*, *Astronomy & Astrophysics*, 552, A100 (2013)
- [2] D. Voet, J. G. Voet, "Biochemistry" (2011), John Wiley & Sons, Inc.
- [3] C. Kim, B. Park, H. Lee *et al*, *Organic & Biomolecular Chemistry*, *Org. Biomol. Chem.*, 11, 1407. (2013)



Molecular Signature of Atmospheric Organic Aerosols

Douglas de Souza Gonçalves, Puspitapallab Chaudhuri

Department of Physics, Federal University of Amazonas, 69077-000 Manaus, AM

Aerosols are microscopic solid particles and/or liquid droplets suspended in air or gas. Aerosols can be natural (fog, forest exudates, for example) or artificial produced by anthropogenic activities. The study of aerosol particles has become quite relevant in recent years as they are found to influence, directly or indirectly, the climate, both at local and global scale. Atmospheric aerosols play a crucial role in the earth-atmosphere system affecting the natural cycles of rain and drought, precipitation and cloud formation, intensity of storms among others, which, as a consequence, may alter the nature of the local ecosystem and human health conditions. Depending on the size, they may also put influence on the radiative balance of the earth's atmosphere. Aerosol particles may scatter the solar radiation efficiently altering the atmospheric visibility, while others can absorb solar radiation readily to warm the atmosphere. In the Amazon region the aerosol particles play an important role as they act as cloud condensation nuclei (CCN) controlling the process of formation and lifetime of clouds and, thereby, influencing the local hydrological cycle. Understanding how these particles are formed and alter the atmospheric characteristics is of paramount importance for sustainable development [1,2].

In this work we study the interaction of methanesulfinic acid ($\text{CH}_3\text{SO}_2\text{H}$) and methanesulfonic acid ($\text{CH}_3\text{SO}_3\text{H}$) with atmospheric nucleation precursors such as $\text{H}_2\text{SO}_4/\text{NH}_3$ to see if they participate in the formation of aerosols. Analysis of the hydrogen bond for each structure and the structural, thermodynamics and spectroscopic properties were made. In addition, optical and electrical properties of the clusters were considered to analyze the atmospheric implications of each system. In order to obtain these properties we use Density Functional Theory (DFT) in Gaussian 03 [3] program.

Key-words: Aerosol, Methanesulfinic Acid, Methanesulfonic Acid.

Support: This work has been supported by CNPq and Federal University of Amazonas.

References:

- [1] J. H. Kroll and J. H. Seinfeld. *Química Nova*, 28, 859 (2005).
- [2] Y-P Zhu et al. *The Journal of Physical Chemistry A*, 118, 7959 (2014).
- [3] Frisch et al. *Gaussian 03, Revision C.02*. Gaussian Inc.(2004).

Improved calculations of the sensitivity density between phase shift and potential energy function

Éderson D’M. Costa¹ (PQ), Nelson H. T. Lemes¹ (PQ), João P. Braga² (PQ)

¹ *Universidade Federal de Alfenas, 37130-001, Alfenas/MG, Brazil*

² *Universidade Federal de Minas Gerais, 37270-901, Belo Horizonte/MG, Brazil*

Abstract: Retrieving the potential energy function at the quantum level, based on experimental data of thermophysical properties, such as the quantum second virial coefficient and the quantum viscosity coefficients, requires the sensitivity density of the phase shift with respect to the potential energy function $\delta\eta_l(k)/\delta V(r)$ [1]. The calculation of this quantity, because the large integration limits, necessary to find the asymptotic solution of the Schrödinger radial equation with the correct amplitude, has been performed with the approximate Langer JWKB method [1]. In 2014 [2] we showed how the quantity $\delta\eta_l(k)/\delta V(r)$ could be found by means of a system of coupled differential equations involving the Calogero’s equation. This theory was recently used to recover the potential energy function for ⁴He from quantum viscosity coefficient data from 1 to 5 K [3]. In the present work it is shown how this approach can be reformulated to a new integral representation. The Calogero’s equation in terms of the Ricatti-Bessel functions j_l and y_l for the reduced potential $U(\rho)$ is $\frac{d\eta_l(\rho;k)}{d\rho} = -\frac{U(\rho)}{k} \{j_l(k;\rho) \cos[\eta_l(\rho;k)] - y_l(k;\rho) \sin[\eta_l(\rho;k)]\}^2$. By the derivation of this equation with respect to the potential at a specific r coordinate, that is $\frac{\partial}{\partial V(r)} \frac{d\eta_l(\rho;k)}{d\rho} = \frac{d}{d\rho} \frac{\partial\eta_l(\rho;k)}{\partial V(r)} \equiv \frac{dS_l(\rho;k)}{d\rho}$ one obtains the differential equation, which solved up to the asymptotic limit of $\rho \rightarrow \infty$, provides the sensitivity $S_l(k,r) = (\delta\eta_l(k)/\delta V(r))\Delta\rho$. This equation must be solved coupled to $G(\rho;r) \equiv \partial U(\rho)/\partial V(r)$, which has the value of $2\mu/\hbar^2$ if $\rho = r$ or 0 if $\rho \neq r$. Since $G(\rho;r)$ has finite value only at r , the sensitivity begins to be accumulated only from that point, then we suggest to transform the problem into the initial value problem (PVI) below,

$$\frac{dS_l(\rho;k,r)}{d\rho} = \frac{U(\rho)}{k} \{2j_l(k\rho)y_l(k\rho) \cos[2\eta_l(\rho;k)] + [j_l^2(k\rho) - y_l^2(k\rho)] \sin[2\eta_l(\rho;k)]\} S_l(\rho;k,r) \quad (1)$$

$$S_l^0(r;k) = -\frac{2\mu}{k\hbar^2} \{j_l(kr) \cos[\eta_l(r;k)] - y_l(kr) \sin[\eta_l(r;k)]\}^2 \Delta r. \quad (2)$$

Integration can now be performed from r . The above PVI can still be simplified, given that $\frac{\partial\eta_l(k)}{\partial V(r)} = \frac{\delta\eta_l(k)}{\delta V(r)} \Delta\rho$, the convenient integral representation is obtained,

$$\frac{\delta\eta_l(k)}{\delta V(r)} = S_l^0(r;k) e^{\int_r^\infty f_l(\rho;k) d\rho}, \quad (3)$$

in which,

$$f_l(\rho; k) = \frac{U(\rho)}{k} \{2j_l(k\rho)y_l(k\rho) \cos[2\eta_l(\rho; k)] + [j_l^2(k\rho) - y_l^2(k\rho)] \sin[2\eta_l(\rho; k)]\}, \quad (4)$$

and $\Delta r = 1$ in $S_l^0(r; k)$. In equation (3) the integrand depends only on $\eta_l(\rho; k)$, therefore, solving the Calogero's equation only once, for a given k and l , can be find the sensitivity density $\delta\eta_l(k)/\delta V(r)$ for several coordinates, unlike the previous method [2], in which the Calogero's equation should be solved several times coupled, and in ranges where the sensitivity was not accumulated. Figure 1 (a) shows $\delta\eta_l(k)/\delta V(r)$ calculated by equation (3) and with the Langer JWKB approximation using the potential of the reference [4] for the helium system. The radial wave function $u_l(r; k)$, calculated by the relation $\delta\eta_l(k)/\delta V(r) = - (2\mu/\hbar^2)u_l^2(r; k)$, is also presented (Figure 1 (b)).

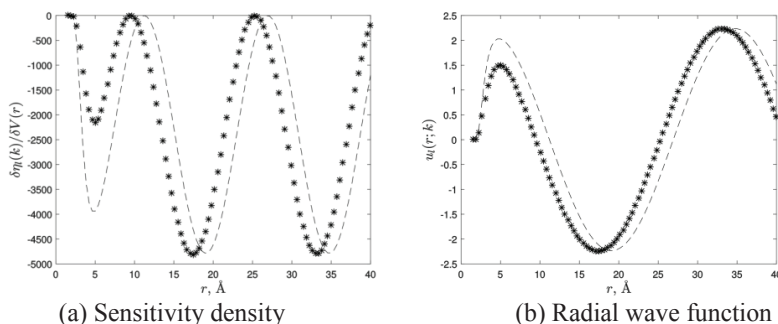


Figure 1: Numeric results at $l = 0$ and $k = 0.2 \text{\AA}^{-1}$: obtained from equation (3) (dashed line); obtained in the Langer JWKB approximation (stars).

Figure 1 (a) highlights the error when using the Langer JWKB approximation, occurring a deviation at the position of the minima and at its intensities. The largest deviation occurs near 5\AA , region of interest for the inversion of potential energy function. The presented method (Equation 3) is precise and simple for computational implementation, which can be used to recover the potential energy function in sensitivity analysis approach, from thermophysical properties within the quantum treatment.

Key-words: Calogero's equation, phase shift, sensitivity analysis approach, sensitivity density, potential energy function.

Support: This work has been supported by CAPES.

References:

- [1] R. Guzman, H. Rabitz, J. Chem. Phys., 86, 1395 (1987).
- [2] N. H. T. Lemes, J. P. Braga, M. O. Alves, É. D'M. Costa, J. Mol. Model., 20, 2317 (2014).
- [3] É. D'M. Costa, N. H. T. Lemes, J. P. Braga, Physica A, 487, 32 (2017)
- [4] A. J. C. Varandas, J. Phys. Chem. A, 114, 8505 (2010).

Can molecular hydrogen reduce cytotoxic hydroxyl radical reactivity in aqueous environment? Combined *ab-initio* molecular dynamics and electronic structure investigation.

Eduardo Campos Vaz^{1*}, Nayara Dantas Coutinho², Vincenzo Aquilanti³, Valter Henrique Carvalho-Silva⁴

^{1,4}*Grupo de Química Teórica e Estrutural de Anápolis, Ciências Exatas e Tecnológicas. Universidade Estadual de Goiás, CP 459, 75001-970 Anápolis, GO Brazil.*

²*Instituto de Química, Universidade de Brasília, Caixa Postal 4478, 70904-970 Brasília, Brazil*

³*Dipartimento di Chimica, Biologia e Biotecnologie, Università di Perugia, Via Elce di Sotto 8, 06123, Perugia, Italy.*

Abstract: The reaction between H₂ and OH molecules is demonstrating to be of great importance in medical and biological environments, this surprises researchers because of the non-complexity of the molecules involved in this reaction. The molecule of H₂ is the smallest gas molecule composed of two protons and two electrons, being very stable and reacting only with the oxide radical ion (O⁻) [1]. There are several documentations regarding H₂, especially in its antioxidant performance. There have been studies of selectivity of H₂ molecule in which cell cultures were induced to an acute oxidative stress and H₂ molecule selectively reduced the more cytotoxic reactive oxygenated species, the hydroxyl radical [1,2,3]. Through researches we could observe that the amount of water in the system was of total influence in the reaction, so the larger the quantity of water, the greater the reactivity [1]. In this project, we performed calculations of Car-Parrinello Molecular Dynamics (CPMD) [4], with several conditions of quantity of OH and H₂ molecules, in vacuum and aqueous solution, in order to map the reaction, however, through the dynamics it was not possible to observe any reaction. We would use the results obtained by dynamics to calculate the reaction rate constant using post-HF and *d*-TST (Deformed Transition State Theory) calculations, but since we did not obtain results, we used a different system from that used in the dynamics. We performed calculations using method MP2-FULL/6-311+G (3df, 2pd) and observed at first something contrary to that reported in researches: with the presence of a water molecule the rate constant decreased, however with the presence of two water molecules we observed an increase of this rate. We observed the rates using the Arrhenius plot. Therefore, we expect that with the addition of more water molecules, this reactivity will continue to increase proportionally. We are performing calculations with other methods to evaluate and



compare the obtained results and to have an average of the system reactional behavior. We hope that with the knowledge of the reaction rates and the reaction behavior of the molecules we can optimize the medical and biological application.

Key-words: Car-Parrinello, antioxidant, *d*-TST.

Support: This work has been supported by CAPES and UEG. Eduardo Vaz would also like to thank PrP/UEG for the assistance.

References:

- [1] K. Ohno, M. Ito, M. Ichihara, and M. Ito, "Molecular hydrogen as an emerging therapeutic medical gas for neurodegenerative and other diseases," *Oxid. Med. Cell. Longev.*, vol. 2012, 2012.
- [2] K. Hayashida, M. Sano, I. Ohsawa, K. Shinmura, K. Tamaki, K. Kimura, J. Endo, T. Katayama, A. Kawamura, S. Kohsaka, S. Makino, S. Ohta, S. Ogawa, and K. Fukuda, "Inhalation of hydrogen gas reduces infarct size in the rat model of myocardial ischemia-reperfusion injury," *Biochem. Biophys. Res. Commun.*, vol. 373, no. 1, pp. 30–35, 2008.
- [3] I. Ohsawa, M. Ishikawa, K. Takahashi, M. Watanabe, K. Nishimaki, K. Yamagata, K. Katsura, Y. Katayama, S. Asoh, and S. Ohta, "Hydrogen acts as a therapeutic antioxidant by selectively reducing cytotoxic oxygen radicals.," *Nat. Med.*, vol. 13, no. 6, pp. 688–94, 2007.
- [4] R. Car and M. Parrinello, "Unified Approach for Molecular Dynamics and Density-Functional Theory," *Phys. Rev. Lett.*, vol. 55, no. 22, pp. 2471–2474, 1985.



NMR spectra interpretation of diastereomeric MacMillan imidazolidinones by DFT calculation of indirect spin-spin coupling constants

Eduardo da Conceição ^a, Victor Augusto Viana Ferreira ^b, Antonio Jorge Ribeiro da Silva, Fernanda Gadini Finelli, Mauro Barbosa de Amorim

^a eduardodcon@gmail.com, ^b victor.augusto7@yahoo.com.br

The indirect spin-spin coupling constants (SSCC) along with chemical shifts are the most important parameters given by nuclear magnetic resonance (NMR) spectroscopy [1,2]. The SSCCs are very sensitive to any variation in molecular geometric structure [3]. DFT based calculations are an efficient approach in the description of indirect SSCCs for various molecular structures in organic chemistry [2,4].

In this work we report the use of SSCC DFT calculations as an auxiliary tool for the interpretation of NMR spectra used in determining the relative configuration of diastereomeric imidazolidinones (1 and 2, figure 1) (MacMillan imidazolidinones) [5,6] synthesized by one of us (FGF). These diastereomers (*cis*, 1, and *trans*, 2) presented different spin coupling patterns that were difficult to assign based only on the experimental spectra obtained. One of them showed a signal with a doublet of triplet pattern while the other showed a doublet of triplets of doublets pattern.

With this objective, each one of the pair of configurations constructed for *cis* (1a,b) and *trans* (2a,b) isomers (figure 1) by inversion of the configurations of the N1 atom were submitted to a systematic conformational search at the B3LYP/6-31G(d,p) level of theory using the Gaussian '09 package. Each of the resulting potential energy minima found on the resulting potential energy surface were resubmitted to geometry optimizations, at the same level of theory, and characterized as energy minima by vibrational analysis. The coupling constants were then calculated for each of the individual conformers at the B3LYP/6-31G(d,p) level of theory and the final value of the coupling constant were obtained as weighted averages based on the Boltzmann distribution of its Gibbs free energies. These final absolute values of the

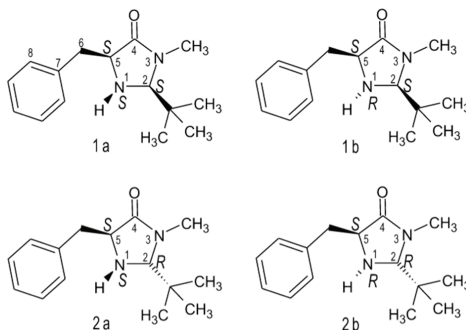


Figure 1 - (+)-2-tert-butyl-3-methyl-5-benzyl-4-imidazolidinone. Diastereomers 1a and 1b (*cis* isomers *cis*); 2a and 2b (*trans* isomers).



coupling constants were then compared with the values obtained experimentally. All the calculations were performed in the gas phase.

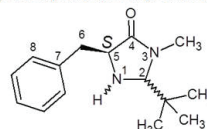
Three conformers were found for each of the diastereomers 1a and 1b and four conformers for each of the diastereomers 2a and 2b. The contributions of each conformer according to the Boltzmann distribution are shown in table 1. The final values of coupling constants are shown in table 2.

Our results show that, although it is not considered a totally reliable and robust level of theory, the popular and widely used hybrid functional B3LYP with the rather small basis set 6-31G(d,p) has led to calculated values of the SSCCs for the imidazolidinone derivatives in very close agreement with the values obtained by experiment, showing that its use, coupled with an adequate conformational analysis, may be very useful for the interpretation of NMR spectra. Being a rather economical level of theory, its use allows the extension of this protocol to larger molecular systems. The use of range-separated functionals, which is capable of capturing both short-range and long-range interactions as WB97X-D, as well as greater basis sets, mainly, but not exclusively, in the conformational analysis stage, is being carried out and its results will be reported as soon as they are finished.

Table 1. Contributions of each conformer of (–)-2-*tert*-butyl-3-methyl-5-benzyl-4-imidazolidinone according to the Boltzmann distribution.

Diastereomer	Dihedral 1 (final) C4-C5-C6-C7	Dihedral 2 (final) C5-C6-C7-C8	Relative energy of the conformers (kcal/mol)	Boltzmann distribution (%)
1a (1 <i>S</i> , 2 <i>S</i> , 5 <i>S</i>)	92,8	117,1	3,04	0,46
	163,1	32,4	2,21	1,85
	-67,4	80,3	1,01	13,94
1b (1 <i>R</i> , 2 <i>S</i> , 5 <i>S</i>)	174,6	-91,6	0,00	76,47
	-63,1	-96,1	1,66	4,62
	95,4	-61,2	1,99	2,67
2a (1 <i>S</i> , 2 <i>R</i> , 5 <i>S</i>)	164,3	-149,9	1,46	4,21
	-178,0	100,1	0,84	11,91
	-67,9	-98,9	0,00	49,43
	93,2	114,7	2,14	1,34
2b (1 <i>R</i> , 2 <i>R</i> , 5 <i>S</i>)	176,2	-92,7	0,30	29,98
	-61,0	-88,4	1,78	2,45
	96,9	125,0	3,42	0,15
	95,6	-63,8	2,69	0,53

Table 2. Final value of the coupling constant weighted by the contributions of the conformers of the (–)-2-*tert*-butyl-3-methyl-5-benzyl-4-imidazolidinone.



Coupling	J_{BREMUM} Calculated (Hz)		J Experimental (Hz)	
	Diastereomers 1a/1b (2 <i>R</i>)	Diastereomers 2a/2b (2 <i>S</i>)	(2 <i>R</i>)	(2 <i>S</i>)
$^1J_{\text{CSH5}}$	147,45	144,09	142,5	-140
$^2J_{\text{CSH6ab}}$	-2,19	-2,14	-	-
$^3J_{\text{CSH2}}$	1,98	-0,70	1,73	-

Key-words: DFT, NMR, Indirect spin-spin coupling constant, imidazolidinone.

Support: This work has been supported by CAPES.

References:

- [1] J. San Fabián, J. M. García de la Vega, E. San Fabián, *J. Chem. Theory Comput.* 10, 4938-4949, (2014).
- [2] Helgaker, T. et al. *Prog. in NMR Spec.*, 53, 249-268 (2008).
- [3] Smith, L. J. *J. Mol. Biol.*, 255, 494-506 (1996).
- [4] Rittner, R. et al. *Chem. Phys. Let.*, 454, 129-132 (2008).
- [5] MacMillan, D. W. C. et al. *J. Am. Chem. Soc.*, 122, 4243 (2000).
- [6] MacMillan, D. W. C. et al. *J. Am. Chem. Soc.*, 122, 9874 (2000).



Potential energy surface and kinetics of reaction between CO₂ and Iron

Eduardo Dias Vicentini, Ana Paula de Lima Batista, Antonio G. S. de Oliveira Filho

Departamento de Química, Faculdade de Filosofia, Ciências e Letras de Ribeirão Preto, Av. Bandeirantes, 3900 – CEP 14040-901 – Bairro Monte Alegre – Ribeirão Preto – SP - Brasil

Abstract: Since the industrial revolution, atmospheric carbon dioxide concentration has increased from 278 ppm to 400 ppm [1]. This rise is related to climate changes and it represents a challenge because of the importance of fossil fuels to the global economy [2]. To use CO₂ in a chemical reaction and to transform it into valuable products, such as chemicals and fuels, one must overcome its thermodynamic stability. Therefore, the search for transition metal-based catalysts is of major importance to chemistry [2]. Ideally, such catalysts should be cheap and made from abundant elements, in order to have a potential impact on CO₂ capture and transformation.

This study aims to determine the potential energy surface (PES) for the reaction between atomic iron and carbon dioxide. The PES is constructed using a functional form based on the many body expansion given in the equation 1. Two-, three-, and four-body interactions are calculated, respectively, using the MRCI-F12, CCSD(T)-F12 and MP2-F12 levels of theory.

$$V(\mathbf{R}) = \sum_a V_a^{(1)} + \sum_{ab} V_{ab}^{(2)} + \sum_{abc} V_{abc}^{(3)} + V_{abcd}^{(4)} \quad (1)$$

Key-words: Potential energy surface, reduction of carbon dioxide, MRCI, CCSD(T).

Support: This work has been supported by CAPES and FAPESP.

References:

[1] D. Archer, *Clim. Change* 138, 1 (2016).

[2] Sakakura, Toshiyasu, Jun-Chul Choi, and Hiroyuki Yasuda, *Chem. Rev* 107.6 (2007): 2365-2387.

Stability, structure, and electronic properties of the pyrite/arsenopyrite solid-solid interface- A DFT study

Egon C. Santos, Maicon P. Lourenço, Lars G. M. Pettersson, Hélio Anderson Duarte
 egoncs@gmail.com

Abstract: Galvanic effects play an important role in the oxidation mechanism of sulfide minerals. Pyrite is the most common sulfide mineral in the Earth, and in the presence of arsenopyrite its oxidation is delayed and the oxidation rate of arsenopyrite is increased, releasing As(III) and As(V) species in the medium.^[1] These arsenic ions are an environment hazards and become health problem in the mining. Here we report a DFT/plane waves study of the pyrite/arsenopyrite galvanic cell (see **Figure 1**). To build the interface models we tested the commensurability of the pyrite (100) surface (the pyrite surface with the highest occurrence in the nature) with the twelve arsenopyrite most favorable surfaces reported in the literature.^[2] Among these surfaces the most stable interfaces were built, and their structure, stability, and electronic properties were evaluated.

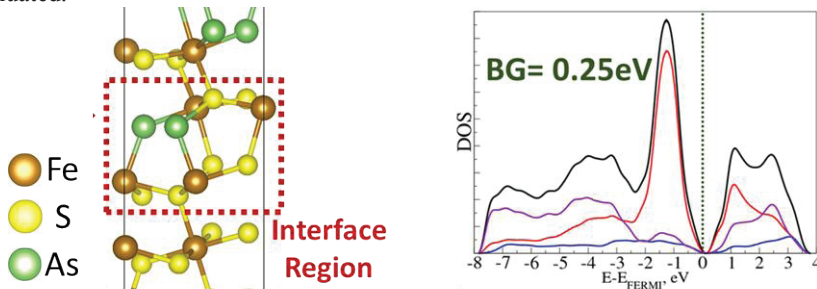


Figure 1- (left) Atomistic model focusing in its interface contact, and (right) the PDOS obtained for one of the most stable interfaces.

The interface bond distances between the interfaces have values largely in accordance with those observed for the two separate phases, but with small deviations in the interface region. As pyrite and arsenopyrite have different bond distances and lattice parameters, it is not possible to perfectly match the phases, and distorted octahedral sites are formed in the interfacial region. This structural observation agrees with the word of adhesion, W_{ad} , and the formation energy, E_{form} , analysis, **Table 1**. The adhesion at the pyrite/arsenopyrite interfaces ($\sim 1.6 \text{ J.m}^{-2}$) is less favorable than the self-adhesion for pyrite/pyrite (4.1 J.m^{-2}) or arsenopyrite/arsenopyrite ($\sim 4.0 \text{ J.m}^{-2}$). Consequently, the interfacial areas tends to be minimized,^[3] and possibly its formation occurs due to kinetic effects in the formation of the two minerals when they are associated. We also evaluated the formation energies for the interfaces and isolated



phases, and it was found that the formation energies for pyrite and arsenopyrite are at least 0.3 eV/(formula unit) more favored than the pyrite/arsenopyrite interface. The non-miscibility and adhesion are in agreement with what is observed in natural samples, where only small nanodomains of about 20 nm² in size is currently found.^[4]

Table 1- Work of adhesion and the formation energy analysis for the most stable interfaces. W_{pyrite} and $W_{\text{arsenopyrite}}$ are, respectively, the work of self-adhesion for pyrite and arsenopyrite pure phases.

Interface	W_{pyrite} , J/m ²	$W_{\text{arsenopyrite}}$, J/m ²	W_{ad} , J/m ²	E_{form} , eV/(formula unit)
FeS ₂ (100)/FeAsS(001)	4.12	3.84	1.63	-2.497
FeS ₂ (100)/FeAsS(100)-As	4.12	4.16	1.47	-2.533
FeS ₂ (100)/FeAsS(100)-S	4.12	4.00	1.70	-2.441

The Projected Density of States (PDOS) calculations, see **Figure 1**, for the interfaces showed that the band gap (BG) values were around 0.6 eV lower than the values found for the pure pyrite (0.9 eV) or arsenopyrite (0.82 eV).^[2] Since sulfide minerals are semiconductors materials that can participate in electrochemical reactions, the decrease in the BG thus facilitates electron transport at the pyrite/arsenopyrite interface contributing to the process of oxidation of these minerals and explaining the galvanic effect in the oxidation process of (arseno)pyrite.

The present study underlines the importance of galvanic effects to understand the oxidation mechanism of arsenopyrite in the presence of pyrite.^[5] Next, we will study the conductivity of the pyrite/arsenopyrite interface comparing to the oxidation of the pyrite and arsenopyrite isolated phases.

Key-words: Sulfide Minerals, Pyrite, Arsenopyrite, Interfaces, DFT.

Support: To the agencies: “Fundação de Amparo à Pesquisa do Estado de Minas Gerais” (FAPEMIG), “Conselho Nacional para o Desenvolvimento Científico e Tecnológico” (CNPq) and “Coordenação de Aperfeiçoamento de Pessoal de Ensino Médio” (CAPES). To the “Universidade Federal de Minas Gerais” (UFMG).

References:

- [1] G. Urbano, et al., J. Phys. Chem. C 112, 10453 (2008).
- [2] J. C. M. Silva, et al., RSC Adv. 5, 2013 (2014).
- [3] L. Martin, et al., J. Mater. Chem. 22, 22063 (2012).
- [4] M. Reich, U. Becker, Chemical Geology. 225, 278 (2006).
- [5] E. C. Santos, L. G. M. Pettersson, M. P. Lourenço, H. A. Duarte, J. Phys. Chem. C **In Press**. DOI: 10.1021/acs.jpcc.7b02642.



Theoretical Investigation of the Ozonolysis Mechanism of Monoterpenes: Reaction Path and Rate Coefficients

Elaine Cesar do Carmo Assumpção de Souza^a, Glauco Favilla Bauerfeldt^b,

Graciela Arbilla de Klachquin^a

^a*Departamento de Físico-Química, Instituto de Química, UFRJ*, ^b*Departamento de Química, UFRRJ*

The atmospheric chemistry of biogenic non-methane hydrocarbons has received special attention, since the emissions of volatile organic compounds (VOCs) from vegetation are the major source of reactive species in the atmosphere and the estimated worldwide emissions range from 825 to 1150 Tg carbon per year. In this group of biogenic volatile compounds, the monoterpenes alpha-phellandrene, beta-phellandrene and terpinolene are included [1]. The unsaturated terpenes are oxidized in the troposphere by either OH (daylight), NO₃ (nighttime) and O₃ (daylight and nighttime). Ozonolysis plays important role in atmospheric chemistry, being a chemical process of strong contribution to the removal of such compounds from troposphere [2]. Furthermore, the ozonolysis reaction also contributes to the formation of OH radicals [3]. Thus, it is important to understand the ozonolysis mechanisms of monoterpenes in the troposphere. The ozonolysis reaction is described by the reversible formation of a pre-barrier complex followed by the ozone addition and molozonide formation, as previously suggested [4]. The aim of this work is to evaluate the ozonolysis reaction of the monoterpenes alpha-phellandrene, beta-phellandrene and terpinolene, based on the Criegee mechanism, through calculations of accurate kinetic parameters by theoretical methods. Stationary points (pre-barrier complexes, saddle points and products) have been located adopting the B3LYP, BHandHLYP and M06-2X functionals, with the aug-cc-pVDZ and aug-cc-pVTZ basis sets. Reaction paths have also been calculated at the same theoretical level. All the theoretical calculations (geometry optimization, vibrational frequencies, reaction path and scans) have been performed using the Gaussian 09 program [5]. The rate coefficients have been calculated at the canonical variational transition state theory level, using the kvct program [6]. Both upward and downward ozone addition paths have been considered. As each monoterpene shows two unsaturated bonds, four pre-barrier complexes and four saddle points have been located for each monoterpene at each theoretical level. The B3LYP functional showed the worst performance, being unable to locate some saddle points for alpha-phellandrene and terpinolene. At the BHandHLYP/aug-cc-pVTZ level, pre-barrier complexes are stabilized by 0.83 – 1.32 kcal mol⁻¹ and saddle points are located in the range from 1.17 to 4.90 kcal mol⁻¹, above the isolated reactants. At the M06-2X/aug-cc-pVTZ level, pre-barrier complexes are stabilized by 3.54 – 5.43 kcal mol⁻¹ and saddle points are located in the range from 0.23 to 4.22 kcal mol⁻¹, under the isolated reactants. M06-2X/aug-cc-pVTZ level have predicted that pre-barrier complexes are located at lower energy values and also higher



central barrier heights. As a global result, rate coefficients obtained from the molecular data obtained at the M06-2X level are higher than those obtained from BHandHLYP molecular properties. The results show and suggest that pre-barrier complexes are important to the kinetics of the global reactions. M06-2X room temperature rate coefficients have been found in reasonable agreement with experimental data (rate coefficients, at 298 K, for the ozonolysis of alpha-phellandrene, beta-phellandrene and terpinolene are: 2.04×10^{-14} , 1.21×10^{-15} and 3.75×10^{-14} $\text{cm}^3 \text{ molecule}^{-1} \text{ s}^{-1}$, respectively, and the corresponding experimental values [7-8] are: 2.97×10^{-15} , 4.77×10^{-17} and 1.88×10^{-15} $\text{cm}^3 \text{ molecule}^{-1} \text{ s}^{-1}$). Both BHandHLYP/aug-cc-pVDZ and M06-2X/aug-cc-pVDZ levels could reasonably describe the ozonolysis of these terpenes, but only M06-2X/aug-cc-pVTZ level could describe the ozonolysis and provide rate coefficients values in good agreement with the experimental values. The $k_{\text{predicted}}/k_{\text{experimental}}$ ratio at M06-2X/aug-cc-pVDZ level of alpha-phellandrene, beta-phellandrene and terpinolene are: 10, 148 and 18. At M06-2X/aug-cc-pVTZ level, the $k_{\text{predicted}}/k_{\text{experimental}}$ ratio of alpha-phellandrene, beta-phellandrene and terpinolene are: 7, 25 and 20. The results show that $k_{\text{predicted}}/k_{\text{experimental}}$ ratio are less sensitive to the relative energy of the pre-barrier complexes than to the location of the saddle point: by raising the relative energies of the saddle points in 1 kcal mol⁻¹, the $k_{\text{predicted}}/k_{\text{experimental}}$ ratio is improved and the rate coefficients achieve excellent agreement with experimental values. Therefore, based on the Criegee mechanism, it can be concluded that the ozonolysis of monoterpenes is better described at M06-2X/aug-cc-pVTZ level and the $k_{\text{predicted}}/k_{\text{experimental}}$ ration is mostly affected by the location of the saddle point, in comparison to the stabilization energy of the pre-barrier intermediates.

Key-words: alpha-phellandrene, beta-phellandrene, terpinolene, ozonolysis, rate coefficients.

Support: This work has been supported by CNPq.

References:

- [1] A. Guenter, C.N Hewitt, D. Erickson, R. Fall, C. Geron, T. Graedel, P. Harley, L. Klinger, M. Lerdau, W.A McKay, T. Pierce, B. Scholes, R. Steinbrecher, R. Tallamraju, J. Taylor, P. Zimmerman. *Journal of Geophysical Research*, 100 (1995), pp. 8873-8892.
- [2] R. Atkinson, *Atmos. Environ.*, 34 (2000), 2063-2101.
- [3] Carlo, P. D.; Brune, W. H.; Martinez, M. *Science*, 2004, 304, 722-725.
- [4] R. C. de M. Oliveira and G. F. Bauerfeldt, *J. Phys. Chem. A*, 119 (2015), 2802-2812.
- [5] M. J. Frisch et al. *Gaussian 09, Revision E.01*, Gaussian, Inc., Wallingford CT, 2009.
- [6] R. C. M. Oliveira, G.F. Bauerfeldt, *Int. J. Quantum Chem.* **112** (2012), 3132-3140.
- [7] Y. Shu, R. Atkinson, *Int J. Chem. Kinet.*, **26** (1994), 1193.
- [8] B. Shorees, R. Atkinson, R. Arey, *Int J. Chem. Kinet.*, **23** (1991), 897.



Bistability and oscillation raised by recombination between dimers

Authors: Elder Taciano Romão da Silva, Fernando de Magalhães Coutinho Vieira

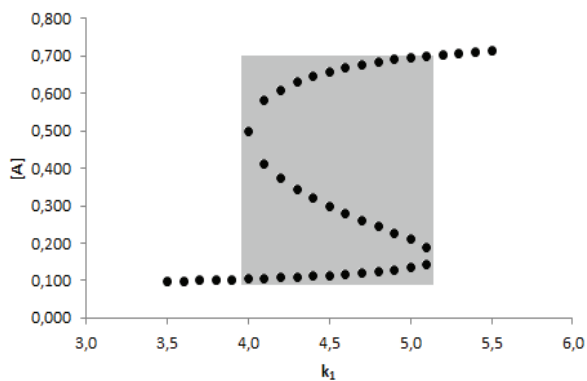
Address: Universidade de Brasília - UnB, Campus Universitário Darcy Ribeiro, Brasília - DF, 70910-900, Brasil

Abstract: Multistability is a phenomenon that describes a condition that a system has two or more steady states. The study of multistability is crucial to the understanding of the cell functions. Such a behavior is present in cell cycles, cell differentiation and apoptosis [1]. Chemical oscillations are rhythmic, temporal or spatial changes in the concentration of each specie in a reaction. Oscillations occurring in biochemical systems are important events for the maintenance of life. Some known examples are the glycolytic oscillations and calcium oscillations [2]. A bistable dynamic is possible during the formation of a trimer. In a hypothetical situation a B homodimer consists of two subunits called A . A second dimer D , a heterodimer, is composed by subunits A and C . By recombining the dimers an E trimer is formed as described in the following equations:



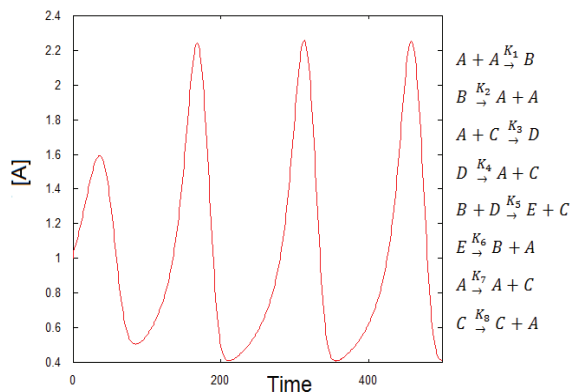
Using the Stoichiometric Network Analysis (SNA) method, a systematic approach to this hypothetical mechanism dynamics was calculated [3] The analysis begins with the determination of a set of velocity vectors from steady states in the reactions. Such set forms an array called "extreme currents" and physically has the value of a subsystem. To study instabilities in the extreme currents is equivalent to observing them in the original system. For this set, the Clarke extreme currents ensure the existence of a saddle knot bifurcation, however, the system still does not present multistability. With an adjustment in the kinetic constants it is possible to generate a sigmoidal curve graph where each point is a stable or unstable steady state.

Figure 1. Bifurcation analysis by kinetic constant k_1 and the concentration of A in arbitrary units (a.u.). The dark area shows in which region there are multiple stationary states.



Here the bistability is caused only by the recombination of dimers with no need for autocatalysis reaction, positive or negative feedback. The same system can be modified by adding a cross-regulation component to obtain an oscillatory dynamics.

Figure 2. Oscillations as a function of time by concentration of species A in a.u.



Key-words: Multistability, oscillations, dimers

Support: This work has been supported by Conselho Nacional de Desenvolvimento Científico e Tecnológico - CNPq and Universidade de Brasília - UnB

References:

- [1] T. Wilhelm, *Bmc Syst Biol*, 3, 90 (2009).
- [2] W. Mazala Junior, U. Schuchardt, M. Paoli, *Química Nova*, 1, 9 (1978).
- [3] B. L. Clarke, *Cell Biophysics*, 12, 237 (1988).



Molecular Wires Formed from Polypyrroles and β -Cyclodextrins: A Theoretical Investigation.

Eliziane S. Santos (PG), Luciana Guimarães (PQ), Clebio S. Nascimento Jr. (PQ)

LQTC: Laboratório de Química Teórica e Computacional - Departamento de Ciências Naturais, Universidade Federal de São João del-Rei (UFSJ), Campus Dom Bosco, São João del-Rei, MG.

eliziane2silva@yahoo.com.br

Abstract: A theoretical investigation using semi-empirical and DFT calculations was performed in order to obtain structural and electronic properties for native and derivatives polypyrroles (PPys). The band gap energies for PPys before and after the formation of β -Cyclodextrin-based molecular wires were estimated at the B3LYP/6-31G(d,p)//PM3 level of theory. For the isolated PPys, the results showed that after the replacement of PPy by the OCH₃ and NO₂ push-pull groups, it presented a significant decrease in the band gap value, which implies a supposed improvement in the polymer conductivity. Moreover, considering the β -Cyclodextrin-based molecular wires, after the introduction of the same OCH₃ and NO₂ push-pull group, it was observed a small decrease in band gap value in comparison to the isolated OCH₃-PPy-NO₂ specie, thus maintaining the polymer conductivity.

Key-words: Polypyrroles, band gap energy, molecular wires.

The fundamental requirement for processing and application of any conjugated polymer (PC) as molecular electronic device is its solubility. Polypyrrole (PPy) belongs to the class of PC, however, one of the main issues concerning the use of PPy as conductive material is due to its poor water solubility [1]. In this context, an alternative and viable strategy to improve the water solubility of PCs is the formation of inclusion complexes with cyclodextrins (CDs), also called CD-based molecular wires (MWs) [2]. In this context, the main goal of this work was to evaluate the molecular structure and electronic properties of native and derivatives PPys as well as a possible MW formed by cross-linked dimeric β -cyclodextrin (β -CD). The central idea was to analyze the encapsulation effect on the structural and electric properties of the PPys guest molecules. The PPys derivatives were substituted at the both ends by electron donors and withdrawers groups (*push-pull groups*) such as: NH₂, OCH₃, OH, SO₃H, NO₂, CF₃. The calculation methodology used was the sequential via B3LYP/6-31G(d,p)//PM3 level of theory which has been successfully used for CD inclusion compounds in our group [3]. As known, the ability of PCs to conduct electricity is fundamentally related to the energy difference between the HOMO / LUMO frontiers orbitals, which is known as band gap energy (Eg). Thus, initially an Eg analysis of native and derivatives PPys with four monomeric units (PPys)₄ was carried out and the results are shown in Table 1. It is



clear to notice that the (PPy)₄ substituted by the OCH₃ and NO₂ push-pull group shows de lowest Eg value. Afterwards, the OCH₃-(PPy)₄-NO₂ were added to the β-CD dimeric tube in the TT orientation with 3 cross-linking, which was chosen based on our previous work [4], in order to evaluate a supposed increase or decrease in conductivity after the formation of a MW. As can be seen in Table 1, after the inclusion process, the OCH₃-(PPy)₄-NO₂ molecular wire presented a slight decreasing in Eg in comparison to the OCH₃-(PPy)₄-NO₂ isolated polymer, which supposedly implies that the formation of a MW could maintain the conductive properties of the polymer now trapped inside the β-CD dimeric tube. In Figure 1, the optimized structure of OCH₃-(PPy)₄-NO₂ molecular wire is shown. Therefore, in the present work we have shown in molecular level that the use of PPys in the form of encapsulating conducting material, which is an interesting alternative to improve the solubility of organic polymers, can be very useful and should be considered in further experimental investigations.

Table 1 – Band gap energies (Eg) for isolated PPys and for a β-CD-based molecular wire calculated at the B3LYP/6-31G(d,p)//PM3.

Specie	Eg (eV)
(PPy) ₄ (native)	3,48
(PPy) ₄ - push-pull (NH ₂ -SO ₃ H)	3,21
(PPy) ₄ - push-pull (OCH ₃ -NO ₂)	2,55
(PPy) ₄ - push-pull (OH - CF ₃)	3,30
Molecular Wire - (PPy) ₄ - push-pull (OCH ₃ -NO ₂)	2,49

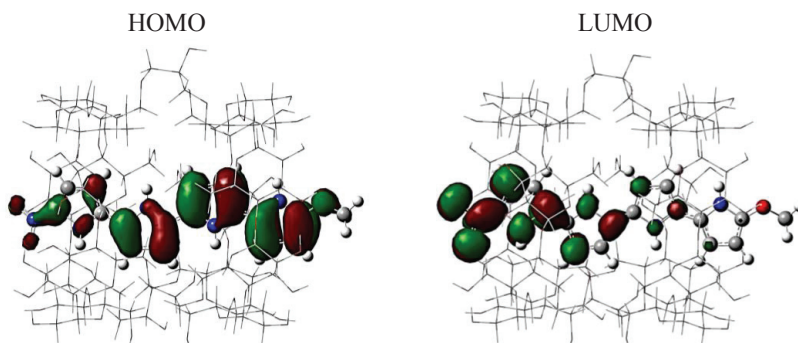


Figure 1 – Optimized geometry for OCH₃-(PPy)₄-NO₂ molecular wire along with HOMO/LUMO orbitals for (PPy)₄.

Support: The authors thank CAPES, FAPEMIG and CNPq for the financial support.

References:

- [1] M. Lu *et al.*, *J. Appl. Polym. Sci.* **135** (2005) 3.
- [2] R. V. Belosludov *et al.*, *Thin Solid Films* **438** (2003) 80.
- [3] C. S. Nascimento Jr. *et al.*, *J. Incl. Phenom. Macroc. Chem.* **59** (2007) 265; C. S. Nascimento Jr. *et al.*, *J. Am. Chem. Soc.*, **130** (2008) 8426.
- [4] V.S. Reis *et al.*, *Chem. Phys. Lett.* **677** (2017) 13.



Automated Fast Computational Screening of Solvents for Extraction of Organic Chemicals from Aqueous Solution Using SMD Solvation Free Energies

Ellen V. Dalessandro, Josefredo R. Pliego Jr.

*Departamento de Ciências Naturais, Universidade Federal de São João del-Rei,
36301-160 São João del-Rei-MG, Brazil*

Abstract: Extraction of organic chemicals is a usual problem in chemistry. However, identification of the best solvent for extraction is not obvious and is usually based on try and error approach. With the development of continuum solvation models like SMD, which is parametrized for a wide set of solvents, it is possible to make a screening of different solvents for extraction. In this work, this idea was applied for finding the best solvent for extraction of chemicals derived from biomass decomposition. Biomass is one of the most promising alternatives for petroleum substitution due to its abundance, low cost and environmentally harmless. Three potential compounds from biomass were listed for fuel and chemical production: furfural, 5-hydroxymethylfurfural and levulinic acid. The acid catalyzed hydrolysis of xylan and glycan components of the wood form C₅ and C₆ sugars, so xylose and glucose (or fructose) are transformed into furfural, 5-hydroxymethylfurfural (HMF) and levulinic acid via acid-catalyzed dehydration. Nevertheless, in the acid medium, undesirable products may appear during the process. Thus, the use of solvent extraction has been advocated as a more effective process. In this work, we are looking for an adequate solvent, which should have low miscibility with water and lead to a high partition coefficient for each compound. We used the SMD method, which has parameters for 179 solvents. We have written the “SNAPY”, a code in Python programming language to automate the process of building the input files, running the GAMESS program and reading the solvation free energy values from the output. In the selection of solvents for simultaneous extraction of furfural, HMF and levulinic acid, we have done an analysis to suggest solvents with the highest partition coefficients (aqueous/organic solvent) for all the solutes. In addition, the solvents must have low miscibility with water, boiling point below 162 °C (furfural boiling point) and, preferentially, low toxicity. Thus, the manual analysis of the results has led us to suggest that C₆ and C₇ ketones are the most adequate solvents.¹

Key-words: partition coefficient, green chemistry, solvation model, free energy of transfer

Support: This work was supported by CNPq and FAPEMIG.

References:

- [1] Dalessandro, E. V.; Pliego Jr. J. R., *Fast Screening of Solvents for Simultaneous Extraction of Furfural, 5-Hydroxymethylfurfural and Levulinic acid from Aqueous Solution Using SMD Solvation Free Energies. J. Brazil. Chem. Soc.* **2017**, (in press)

Multivariate Analysis and Fuzzy Analysis of Acetylcholinesterase Inhibitors: Correlating Inhibition Mechanism and Ligands Properties with Pharmacophoric Profile

Érica C. M. Nascimento,^a Laura Cleofás-Sanchez,^b
Mónica Oliva,^a Joao B. L. Martins,^c Juan Andrés^a

^aDepartment of Physical Chemistry and Analytical, Universitat Jaume I, 12071 Castelló, Spain

^bNational Institute of Genomic Medicine Genómica, Ciudad de México, D.F, México.

^cChemistry Institute, University of Brasília, 70910-000, Brasília-DF.

Abstract: Alzheimer's disease (AD) is the most common kind of dementia. This neurodegenerative disease is characterized by the drastic reduction of the neurotransmitters (NTs) acetylcholine (ACh), serotonin and dopamine in the synapses. The use of the acetylcholinesterase (AChE) inhibitors (AChEIs) is the main strategy used in the treatment of Alzheimer's disease [1]. During the molecular recognition of ACh by AChE, some important interactions are observed between the ligand and the active site of the enzyme. The quaternary nitrogen atom of the AChE substrate forms a strong electrostatic interaction with the carboxyl group of the Asp72 residue ($3.67 \pm 0.13 \text{ \AA}$) [2]. In addition, strong hydrogen bond interactions are observed between the oxygen atom of the ester group of ACh and the residues Gly118, Ala201 and Tyr130 [2,3]. In this way, the intramolecular distance between the nitrogen and the oxygen atoms in a molecule which will be recognized by AChE should be at least similar as the ACh molecule ($3.5 - 6.5 \text{ \AA}$), Figure 1.

In order to elucidate the correlation between the principal properties of 42 molecules and their inhibitory activity against AChE, quantum theoretical studies associated with principal component analysis [4], clusters analysis [5], classification and missing values methods [6] were carried out.

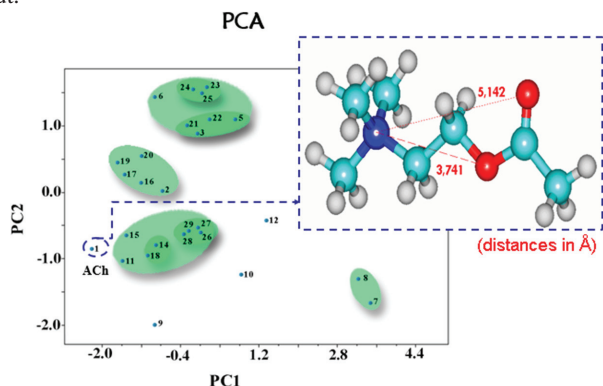


Figure 1. PC1 vs. PC1 and ACh [d(O=N)] and [d(O-N)] distances.



We investigated exhaustively 26 determinant properties that correlate these 42 molecules and their performance in the central nervous system. Among these, 25 AChEIs, 10 monoamine oxidase inhibitors (MAOIs) and the 7 NTs involved in the development of dementias as AD, Parkinson's disease and depression.

Due the diversity of the molecular structure of some ligands, the properties: distance of nearest N and O atoms [d(O-N)] atoms, and the distance of nearest N and O atom of the carbonyl group [d(O=N)] are discarded, i.e., the absence of oxygen and/or nitrogen atom in the molecule is observed in 32 of the 42 inhibitors studied.

The PCA method is not possible to be performed using as variable a set of values with some missed data. For this reason, we performed the PCA analysis without consider the properties d(O-N) and d(O=N) distances. On the other hand, considering the importance of the properties d(O-N) and d(O=N) distances in the molecular recognition of the AChE, and in attempt to mark the load of these two properties in this biochemical process we took on board potent pattern recognition and data mining tools to treating all data set including the missed data.

In order to enrich and validate PCA results, clustering studies were performed with pattern recognition algorithms. Also, missing values problem was treated to avoid missing data may to affect the clustering analyses. In this way, missing values were obtained with K-Nearest Neighbor Imputation and K-Means Imputation methods.

PCA studies revealed that properties as molar mass, number of chiral carbon atom, energy of the molecular orbital LUMO, molecular volume, molecular size, polarizability and number of aromatic rings are the most relevant properties in the study of AChE inhibitors. The missing data values, i.e., the distance of the nitrogen atom and the oxygen atoms in the molecules, are important variable in the study of recognition pattern and correlation in our data set. Hierarchical clustering method was the best predictor with cross-validation coefficient equal to 0.931.

Key-words: Acetylcholinesterase, Inhibitors, PCA, Fuzzy Analysis, Recognition Pattern, Missing Values Methods.

Support: This work has been supported by Generalitat Valenciana (Prometeo II/2014/02) and Ministerio de Economía y Competitividad of Spain (project CTQ2015-65207-P).

References:

- [1] H. Sugimoto, H. Ogura, Y. Arai, Y. Iimura, Y. Yamanishi, *Jpn. J. Pharmacol.*, 89, 7 (2002).
- [2] É. C. M Nascimento, M. Oliva, K. Świderek, J. B. L. Martins, J. Andrés, *J. Chem. Inf. Model.*, 57, 958, (2017).
- [3] G. L. Patrick, "Medicinal Chemistry" (2005), Oxford, New York.
- [4] I. T. Jolliffe, "Principal Component Analysis" (2002), Springer New York, New York.
- [5] D. Li, J. Deogun, W. Spaulding, B. Shuart, *Rough Sets and Current Trends in Computing* (2004), Springer Berlin Heidelberg, Berlin.
- [6] G. E. A. P. A. Batista, M. C. Monard, *Applied Artificial Intelligence*, 17, 519, (2003).



Computational Study of Enzymatic Lignin β -O-4 cleavage

Erica T. Prates^{*#‡}, Gregg T. Beckham[‡], Michael F. Crowley[‡], Munir S. Skaf[#]

[#] *University of Campinas, Campinas SP, Brazil*; [‡] *National Renewable Energy Laboratory, Golden CO, United States*

Abstract: The first challenge in production of lignocellulosic biofuel is to disrupt the complex polymeric matrix of lignin that surrounds cellulose and hemicellulose chains in plant cell walls. Typically, thermo-mechano-chemical pretreatments of biomass are used to break lignin barrier, but developing alternative strategies is of major interest today to avoid the release of toxic compounds and valorize lignin as feedstock. Enzymatic degradation of lignin represents a promising approach to selectively valorize lignin derivatives to the production of fuel, chemicals and materials. In this work, we studied two enzymes that act on the early and last stages in the lignin β -aryl ether cleavage pathway from *Sphingobium sp* SYK-6 [1,2]. Using docking, molecular dynamics, QM/MM simulations and QM calculations, we shed light on the key interactions for substrate binding and came up with strong suggestions for the mechanism of action of these enzymes, named LigF and LigG. Further studies can make use of these results to identify other lignin degrading enzymes in other organisms, as well as to optimize these biocatalysts for future application in biorefineries.

Key-words: quantum mechanics / molecular mechanics, quantum mechanics, ligninase, bioethanol

Support: This work has been supported by FAPESP (Proc. 2016/04775-5). Computer time was provided by Extreme Science and Engineering Discovery Environment (XSEDE) and by the National Renewable Energy Laboratory.

References:

- [1] D. L. Gall, H. Kim, F. Lu, T. J. Donohue, D. R. Noguera, J. Ralph, *J. Bio. Chem.*, 289, 8656 (2014).
- [2] E. Masai, A. Ichimura, Y. Sato, K. Miyauchi, Y. Katayama, M. Fukuda, *J. Bact.*, 185, 1768 (2003).

Computational and experimental study of cholesterol influence on the activity of liposomal zinc phthalocyanine

Erick G. França¹, Roberto R. Faria², Carlos A. de Oliveira², Eduardo de F. Franca²

¹*Instituto Federal de Goiás*

²*Universidade Federal de Uberlândia*

Abstract: Treatment of diseases in modern civilization using new models of drugs delivery systems instead of classical interventions has been considered an important research line for infection and tumors treatment. In this context, a drug delivery system is capable to increase the delivery effectiveness of hydrophobic drugs into cells and tissues in several treatments [1]. Among these examples we can mention the liposomes, which are nanometric vesicles structured in bilayers of phospholipids organized surrounding aqueous compartments [2]. In this work, liposomes containing phospholipids and cholesterol were used to deliver a hydrophobic phototoxic drug, zinc phthalocyanine (ZnPC), to sheep red blood cells experimentally and the phospholipid bilayer sheet of proposed liposomal systems was simulated in a computational study. The computational methodology used was Molecular Dynamics simulations using the GROMACS 5.1.4 computational package with OPLS-AA force field, using NPT ensemble, at 310K and 1 bar with explicit spc water. The molecules geometry and charges were parameterized using ORCA 3.0.3 and NWCHEM 5.1. It was performed computational simulations of lipid membranes containing zinc phthalocyanine and added or not with cholesterol, to obtain membrane density values, disposition of drug in systems and density maps of the lipid bilayers. In the experimental tests, the use of an appropriated delivery system was capable to promote the photoinactivation of red blood cells. Furthermore, liposomes containing cholesterol in mass to mass ratio of 5:1 was more effective in drug delivery than liposomes without cholesterol [3]. The molecular dynamics indicates that interaction between ZnPC and cholesterol may change the spatial disposition of these species in vesicle affecting directly the drug effectiveness. Computational simulations of systems, with or without cholesterol, containing DPPC/ZnPC showed to be effective in predicting the behavior of the drug in the phospholipid bilayer, indicating its greater mobility in cholesterol-containing systems, as well as the formation of rafts and the occurrence of a pronounced interaction between ZnPC and cholesterol molecules in its surroundings, which can potentiate the photodynamic activity of the drug.

Key-words: Liposome, photoinactivation, cholesterol



Support: This work has been supported by FAPEMIG and Rede Mineira de Química (RQ-MG: RED-00010-14)

References:

- [1] E. Paszko, C. Ehrhardt, M. Senge, Photodiagnosis and Photodynamic Ther., 8, 14 (2011).
- [2] A. Akbarzadeh, R. Rezaei-sadabady, S. Davaran, Nanoscale research letters, 8, 1, (2013).
- [3] C. A. Oliveira, L. K. Kohn, M. Antonio, J E Carvalho; Journal of Photochemistry and Photobiology. 100, 92 (2010).



A structural study of Ni/NiO interface materials by Rietveld Refinement and DFT calculations

Authors: Ericson H. N. S. Thaines¹, Carlos S. Ferreira², Raimundo R. Passos², Leandro A. Pocrifka², Renato G. Freitas¹

Address: ¹LCM, Department of Chemistry, Federal University of Mato Grosso, 78060-900 Cuiabá, MT, Brazil.

²GEMATA - LEEN, Department of Chemistry, Federal University of Amazonas - UFAM - CEP 69077-000, Manaus-AM, Brazil

³Program of Natural Sciences, Federal University of Pará West - UFOPA - CEP 68035-110, Santarém-PA, Brazil

Abstract: Electrochemical capacitors (ECs) are devices that combine both the specific energy of the batteries and the specific power of the conventional capacitors characteristics [1]. This feature allows electrochemical capacitors to be present in the industries of renewable energy, digital cameras, mobile phones and electric vehicles [2]. The mixed transition-metal oxides are emerging as promising electrode materials for ECs, due their high electrochemical activities owing to the complex chemical compositions and their synergetic effects contribute to the exceptionally high specific capacity/capacitance [3].

The interface materials were obtained by calcination of a polymeric resin prepared by Pechini method. The X-ray diffraction (XRD) patterns were obtained using a SHIMATZU XRD-6000 model which provides Cu K_{α} radiation ($\lambda=1.544\text{\AA}$). To obtain the microstructural data of the Ni, NiO and Ni/NiO materials, a Rietveld refinement (see figure 1) [4] was performed using the General Structure Analysis System (GSAS) program [5] suite with the EXPGUI interface [6].

All theoretical calculations were performed using the Ni and NiO crystallographic information file (CIF – ICSD 260169 and 9866, respectively). Calculations were performed using density function theory (DFT) [7,8] with the plane wave-pseudopotential framework, as implemented in the Quantum-ESPRESSO (QE) [9] package, with in the generalized gradient approximation (GGA). Electronic interactions were described by Perdew-Burke-Ernzerhof (PBE) exchange-correlation functional [10] with ultrasoft pseudopotential. We performed the electronic energy minimization with a tolerance of 10^{-6} Ry estimated scf accuracy, using a plane wave kinetic energy cutoff of 175 Ry and 700 for the charge densities. The Brillouin-zone (BZ) sampling is carried out with a $8 \times 8 \times 8$ Monkhorst - Pack k-points grid. The strain effects were calculated applying a strain compressive and tensile, consequently varying the volume of unit cell. The equilibrium volume parameters and bulk modulus were obtained by fitting energy vs volume curve to the Murnaghan, Birch-Murnaghan, Poirier-Tarantola and Vinet equation of state – EOS (see figure 2). The stress tensor were obtained after full relaxations of all internal atomic coordinates by means of the conjugate gradient (CG) technique.

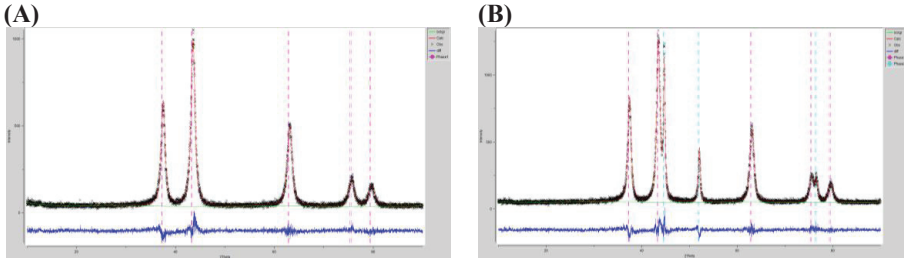


Figure 1 – Adjust by Rietveld method between the experimental and calculated X-ray diffraction patterns for the (A) NiO and (B) NiO/Ni.

The Fig. 1 show that the results obtained by the Rietveld refinement method were in good agreement with the observed XRD patterns. The Fig. 2 show relation between energy versus volume curve with fitting of EOS. The value of the bulk modulus obtained from of EOS were in good agreement with the eq. Murnaghan for Ni of 253.52 GPa with experimental value of 229 GPa and for NiO of 278.77 GPa with experimental value of 205 GPa.

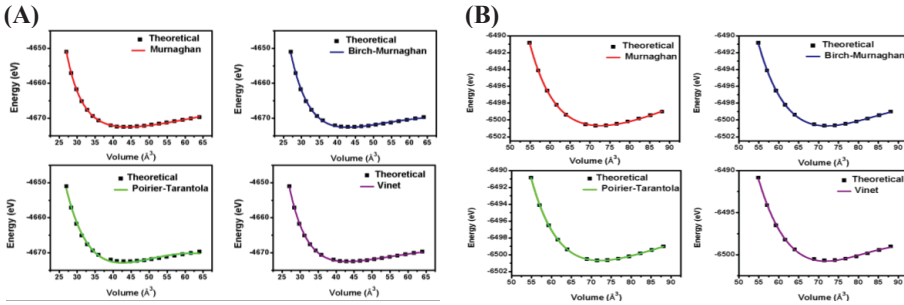


Figure 2- The energy as a function of the volume with fitting of EOS for the (A) Ni and (B) NiO

Key-words: Ni/NiO interface, Rietveld refinement, DFT.

Support: This work has been supported FAPEMAT (214599/2015) for financial support and CENAPAD/SP for providing computational time.

References:

- [1] S. K. Chang et al, *Curr. Appl. Phys.*, 2012, 12, 1421-1428.
- [2] B. E. Conway *Electrochemical Supercapacitors*. Kluwer-Plenum Pub. Co, 1 Ed. New York, 1999
- [3] C. Yuan et al, *Angew. Chem. Int. Ed.* 2014, 53, 1488–1504.
- [4] H.M. Rietveld, *J. Appl. Crystallogr.*, 1969, 2, 65.
- [5] A.C. Larson, R.B. von Dreele, *Lab. Rep. LAUR.*, 2004, 86, 1.
- [6] B.H. Toby, *J. Appl. Crystallogr.*, 2001 34, 210.
- [7] P. Hohenberg and W. Kohn, *Phys. Rev.*, 1964, 136, B864–B871.
- [8] W. Kohn and L.J. Sham, *Phys. Rev.*, 1965, 140, A1133–A1138.
- [9] G. Paolo et al, *J. Phys.: Condens. Matter*, 2009, 21, 395-502.
- [10] J. P. Perdew, K. Burke and M. Ernzerhof, *Phys. Rev. Lett.*, 1996, 77, 3865.

Theoretical Study of the Xenon NMR Chemical Shift in Supercritical Condition: many-body, electron-correlation and relativistic effects

Evanildo G. Lacerda Jr. ^{a,b}, Stephan P. A. Sauer ^a,

Kaline Coutinho ^b, Sylvio Canuto ^b

^a Department of Chemistry, University of Copenhagen,
Universitetsparken 5, DK-2100 Copenhagen, Denmark

^b Instituto de Física da Universidade de São Paulo,
CP 66318, 05314-970 São Paulo, SP, Brazil

Abstract: Xenon in a supercritical condition is an important solvent to investigate various chemical systems. Xe is lipophilic and soluble in many substances. With its highly sensitive NMR chemical shift Xenon serves as a probe used to characterize solids, proteins and biomembranes, nanosystems, polymers, clathrates, mixtures, and even to detect radiations of interest in astrophysics [1]. Consequently, gaseous, liquid and supercritical Xe have been the subject of experimental investigation as well as theoretical calculations [2-4].

In this work we study how the NMR chemical shift of the ¹²⁹Xe in a supercritical condition depends on the solvation and on many-body and relativistic effects. Solvation effects are included using a sequential QM/MM methodology. Relativistic analysis is made using 4-component Hartree-Fock calculations (4c-HF) and electron correlation effects are considered using second order Møller-Plesset perturbation theory (MP2). To simplify the calculations of the relativistic and electron correlation effects we decompose the chemical shift in various contributions. Calculations are made at the non-relativistic Hartree-Fock (HF) level as an average over selected configurations generated by Monte Carlo simulation and then the contributions due to electron correlation and relativistic effects are added in a two-body approximation. Our results are in agreement with the experimental data and show that the chemical shifts for Xe are very well described at the HF level, with small contributions from relativistic and electron correlation effects.

Key-words: Supercritical condition, Xenon, QM/MM, NMR magnetic shielding.

Support: This work has been supported by the Science without Borders program and CAPES/Brazil.

References:

[1] Aprile, E. and Doke, T. "Liquid xenon detectors for particle physics and astrophysics". Reviews of Modern Physics, vol. 82, pp. 2053, 2010.



- [2] Fulton, L. “Fluid Structure in Supercritical Xenon by Nuclear Magnetic Resonance Spectroscopy and Small Angle X-ray Scattering”. *Journal of Physical Chemistry*, vol. 98, pp.11846, 1994.
- [3] Yuan, H., Murad, S., Jameson, C.J. and Olson, J.D. “Molecular dynamics simulations of Xe chemical shifts and solubility in n-alkanes”. *Journal of Physical Chemistry C* , vol. 111, pp. 15771, 2007.



Theoretical Study of the Reactivity of C2 - C5 Alkenes Towards Ozone.

Ewerton Ferreira da Silva Souza¹, Elaine Cesar do Carmo Assumpção de Souza²,
Graciela Arbilla², Glauco Favilla Bauerfeldt¹

1: Departamento de Química, Instituto de Ciências Exatas, Universidade Federal Rural do Rio de Janeiro; 2: Departamento de Físico-Química, Instituto de Química, Universidade Federal do Rio de Janeiro

Abstract: Ozonolysis is an important process for the chemical removal of volatile unsaturated organic specie from troposphere. The reaction proceeds via ozone attack to the unsaturated bond forming a molozonide, which rapidly decomposes to carbonyl products. As the first step is highly exothermic, molozonides are formed with excess internal energy and the consecutive step is generally fast, so that the addition step is the rate controlling. This first step, in turn, is better described by a submechanism taking into account the reversible formation of a pre-barrier intermediate, followed by the addition [1]. The search for a theoretical method to accurately describe the ozonolysis reaction is a topic of interest worldwide, with main concern about the description of the kinetics of different unsaturated species towards ozone and the observed trends in their compared reactivity. In this context, this work aims to the study of the ozonolysis reaction path of some alkenes of low molecular weight (C4 and C5). Our goals are the search for the stationary points in the reaction paths and the prediction of the barrier heights from theoretical methods. Density Functional Theory has been used in all calculations, adopting the BHandHLYP, ω B97X and M06-2X functionals and the aug-cc-pVTZ basis set. The selected alkenes were: 1-butene, Z-2-butene, E-2-butene and isobutene (C4) and 3-methyl-1-butene, 2-methyl-2-butene, E-2-pentene and Z-2-pentene (C5). 2,3-dimethyl-2-butene (C6) has also been included in our list. Each optimized geometry has been validated by vibrational frequencies calculations, observing that stationary points corresponding to reagents and intermediates showed only real vibrational frequencies, whereas, for the saddle points, a single imaginary vibrational frequency was expected. BHandHLYP results for the reaction barriers (electronic energy differences between the saddle point and the reactants, corrected by zero point energies) were, for 1-butene, Z-2-butene, E-2-butene and isobutene: 4.91, 3.53, 4.10 and 5.55 kcal mol⁻¹, respectively. For 2-methyl-2-butene and 3-methyl-1-butene, the calculated barriers were 4.30 and 6.17 kcal mol⁻¹, respectively. Including the thermal and entropic contributions, the values for the Gibbs free energy of activation (298 K) were: 15.99, 14.35, 14.97, 16.74, 15.91 and 17.42 kcal mol⁻¹ (1-butene, Z-2-butene, E-2-butene, isobutene, 2-methyl-2-butene and 3-methyl-1-butene, respectively). From these data, and adopting the conventional transition state theory, the rate coefficients at 298 K were calculated, being (in cm³ molecule⁻¹ s⁻¹): 9.60x10⁻¹⁹ (1-butene), 1.51x10⁻¹⁷ (Z-2-butene), 5.37x10⁻¹⁸ (E-2-butene), 2.69x10⁻¹⁹ isobutene,



1.10×10^{-18} (2-methyl-2-butene) and 8.62×10^{-20} (3-methyl-1-butene). These results are smaller than the experimental results by factors ranging from about 10 to 370. The ratios between the rate coefficients for the ozonolysis of each alkene and the rate coefficient for the propene ozonolysis (calculated at the same theory level) are in agreement with the experimental data. It is concluded that although small adjustments in the theoretical model are still necessary to guarantee the accurate prediction of the rate coefficients of the C4 and C5 alkenes, the model suggested from the BHandHLYP data is already enough accurate for the prediction of reactivity trends of the different alkenes towards ozone .

Key-words: Ozonolyses, alkenes, molozonide, rate coefficients

Support: This work has been supported by CNPq and FAPERJ

References:

[1] R. C. de M. Oliveira, G. F. Bauerfeldt, J. Phys. Chem. A, 119, 2802 (2015).



All-electron Gaussian basis sets of double zeta quality for the actinides

L. S. C. Martins, F. E. Jorge, M. L. Franco, and I. B. Ferreira

Departamento de Física, Universidade Federal do Espírito Santo, 29060-900 Vitória, Espírito Santo, Brazil

Unidade Acadêmica de Física, Universidade Federal de Campina Grande, 58429-900 Campina Grande, Brazil

Abstract: For the actinides, two segmented all-electron basis sets of valence double zeta quality plus polarization functions (DZP) are developed. One of them must be used along with the non-relativistic Hamiltonian, whereas the other with the Douglas-Kroll-Hess (DKH) [1,2] one. Adding diffuse functions of s, p, d, f, and g symmetries to the non-relativistic and relativistic sets, augmented basis sets are developed. These functions are essential to describe correctly electrons far away from the nuclei. For some compounds, geometric parameters, atomic charges and valence orbital populations of the actinides, and bond dissociation energies are calculated using the Becke 3-parameter (exchange) [3] and the Lee, Yang, and Parr (correlation) [4] functional in conjunction with the DZP-DKH basis set. For Am and No, the static electric mean dipole polarizabilities are also reported. Comparison with benchmark theoretical [5-10] and experimental [11-14] values found in the literature is carried out. It is verified that the performances of the relativistic compact size basis sets generated in this work are regular, efficient, and reliable. They will be extremely helpful in molecular property calculations that need explicitly to consider the core electrons.

Key-words: Basis Sets; Actinides; DFT; DKH.

Support: This work has been supported by CNPq, CAPES, and FAPES

References:

- [1] M. Douglas and N. M. Kroll, *Ann. Phys.* 82, 89 (1974).
- [2] B. A. Hess, *Phys. Rev. A* 32, 756 (1985).
- [3] A. D. Becke, *J. Chem. Phys.* 98, 5648 (1993)
- [4] C. Lee, W. Yang, and R. G. Parr, *Phys. Rev. B* 37, 785 (1988).
- [5] J. E. Peralta, E. R. Batista, G. E. Scuseria, and R. L. Martin, *J. Chem. Theory Comput.* 1, 612 (2005).
- [6] E. R. Batista, R. L. Martin, and P. J. Hay, *J. Chem. Phys.* 121, 11104 (2004).
- [7] A. Kovács, R. J. M. Konings, D. Szieberth, and B. Krámos, *Struct. Chem.* 25, 991 (2014).
- [8] L. Joubert and P. Maldivi, *J. Phys. Chem. A* 105, 9068 (2001).
- [9] A. Kovács, R. J. M. Konings, Z. Varga, and D. Szieberth, *J. Phys. Chem. A* 117, 11357 (2013).
- [10] V. Vetere, B. O. Roos, P. Maldivi, and C. Adamo, *Chem. Phys. Lett.* 396, 452 (2004).



- [11] V. I. Bazhanov, Y. S. Ezhov, and S. A. Komarov, *J. Struct. Chem.* **31**, 986 (1990).
- [12] V. I. Bazhanov, Y. S. Ezhov, and S. A. Komarov, *Zh. Strukt. Khim.* **31**, 152 (1990).
- [13] D. L. Hildenbrand and K. H. Lau, *J. Chem. Phys.* **94**, 1420 (1991).
- [14] D. L. Hildenbrand and K. H. Lau, *Pure Appl. Chem.* **64**, 87 (1992).



Protocol for Calculating ^{13}C NMR Chemical Shifts of Flexible Organic Molecules

Authors: Fabio Luiz Paranhos Costa,^{*a} Thais Forest Giacomello,^a Rênica Alves de Moraes Rocha,^a Mariana Aparecida de Souza Martins,^a Antonio Maia de Jesus Chaves Neto,^b Gunar Vingre Da Silva Mota^b

Address: ^aDepartament of Chemistry, Federal University of Goiás, REJ Jataí 75801-615, Brasil.

^bNatural Science Faculty, Federal University of Pará, ICEN UFPA Belém 66075-110, Brasil

Abstract: In this work, we present a new scale factor protocol for calculating ^{13}C NMR chemical shifts (GIAO-mPW1PW91/3-21G//mPW1PW91/3-21G) of flexible organic molecules. Considering a set of 22 molecules with different behaviors (27 different chemical shifts), we were able to generate a universal GIAO-HDFT with a basis set consistent with 3-21G basis set and linear scaling factors using a “chemical shift – chemical shift” correlation approach. NMR chemical shifts were computed at the mPW1PW91/3-21G level using the GIAO method and are given relative to that of TMS calculated at the same level of theory. Thus a scale factor equation was generated $\delta_{\text{scale}} = 1.1 \delta_{\text{calc}} - 3.8$, where δ_{calc} and δ_{scal} are the calculated and the linearly scaled values of the ^{13}C chemical shifts, respectively). The robustness of the new protocol and its applicability to practical problems were evaluated by the calculation of the chemical shifts for a natural compound with synthesis, biological and therapeutic interest: (-)-loliolide ((7aR)-6-hydroxy-4,4,7a-trimethyl-6,7-dihydro-5H-1-benzofuran-2-one) (a rigid molecule), figure **1a** [1]. For flexible molecules, a conformational analysis protocol was created. For evaluated the accuracy of this protocol was selected 2',6'-dihydroxy-4',4-dimethoxydihydrochalcone molecule (a very flexible molecule), figure **1b** [2]. Thus, in order to select the most stable conformer of flexible molecules, will be applied Monte Carlo (MC) simulations. So, a randomized conformational search of the 2',6'-dihydroxy-4',4-dimethoxydihydrochalcone molecule using the MC method with a search limit of 200 structures, and employing the Merck molecular force field (MMFF), by means of 10,000 simulations, as implemented in the Spartan'08 software package [3], considering an initial energy cutoff of 10 kcal.mol⁻¹ was performed. In the first step the 43 more significant conformations of 2',6'-dihydroxy-4',4-dimethoxydihydrochalcone molecule, accounting for more than 99.99% of the total Boltzmann population in the first 10 kcal.mol⁻¹, were saved. This was, followed by single-point energy calculations at the PM6 and level of theory. The 31 more significant conformations within the range of 0.0–3.0 kcal.mol⁻¹, were selected to energy minimization calculations carried out at the mPW1PW91/3-21G level of theory. The 13 more significant conformations within the range of 0.0–2.5 kcal.mol⁻¹. Frequency calculations carried out at the mPW1PW91/3-21G level of theory confirmed the



optimized geometries to be local minima and delivered values of free energy at 298 K and 1 atm. In the last step the 7 more significant conformations within the range of 0.0–2.0 kcal.mol⁻¹ were selected. Finally the lowest-energetic conformer was used to obtain the scaled chemical shifts. All HDFT calculations were carried out using Gaussian09 software [4]. In the calculations, no solvents effects were considered.

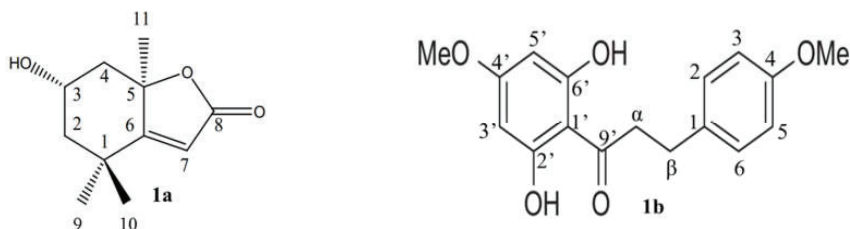


Figure 1. (-)-loliolide (**1a**) and 2',6'-dihydroxy-4',4'-dimethoxydihydrochalcone (**1b**) structures.

In order to achieve widespread application of a scaling factor to GIAO-HDFT ¹³C chemical shifts, it is desirable to combine excellent accuracy of MAD (mean absolute deviation) and RMS (root mean square). The data comparison demonstrated a great agreement between experimental and calculated NMR chemical shifts. For loliolide molecule MAD and RMS before (after), in ppm, application of the scale factor are: 5.71 (1.59) and 9.34 (1.81). For 2',6'-dihydroxy-4',4'-dimethoxydihydrochalcone molecule MAD and RMS before (after) application of the scale factor are: 9.65 (1.30) and 11.02 (1.67). It means that using the equation 1 it was possible to cancel the systematic errors, even using modest basis set. In conclusion, GIAO-mPW1PW91/3-21G//mPW1PW91/3-21G linear regression obtained by using the experimental and the calculated data with the conformational analysis protocol, is a very attractive tool as an alternative to more computationally demanding approaches, which are usually applied in order to achieve ¹³C NMR chemical shift calculations.

Key-words: GIAO-mPW1PW91/3-21G//mPW1PW91/3-21G, flexible molecules, NMR

Support: This work has been supported by Fundação de Amparo à Pesquisa do Estado de Goiás.

References:

- [1] F. L. P. Costa; S. B. O. de Fernandes; C. E. Fingolo; F. Boylan; A. C. F. de Albuquerque; F. M. dos Santos Junior; M. B. de Amorim, *Quantum Matter*, 5, 675 (2016).
- [2] P. K. Agrawal, "Carbon-13 NMR of Flavonoids. Studies in Organic Chemistry, v. 34" (1989), Elsevier, Amsterdam. The Netherlands.
- [3] Spartan'08, Wavefunction Inc., Irvine California, USA, 2010.
- [4] Frisch, A. E.; Frisch, M. J.; Trucks, G.; Gaussian 09 User's Reference, Gaussian Inc., Pittsburgh, USA, 2009.



Molecular dynamics of a highly secreted α -L-arabinofuranosidase (GH62) from *Aspergillus nidulans* grown on sugarcane bagasse

Authors: Fabricio Bracht, Fabiano J. Contesini, Fabio M. Squina, Andre R. L. Damasio, Munir S. Skaf

Address: Universidade Estadual de Campinas, Instituto de Química, Campinas - SP

Arabinases or arabinofuranosidases are the enzymes capable of liberating L-arabinose from polysaccharides, arabino-oligosaccharides or from synthetic substrates, with endo or exo modes of action. An important group of these enzymes corresponds to the α -L-arabinofuranosidases (E.C. 3.2.1.55) that cleave α -(1 \rightarrow 2), α -(1 \rightarrow 3), or α -(1 \rightarrow 5) linked L-arabinofuranosyl residues from non-reducing ends in oligo- and polysaccharides that contain arabinose ¹. In this work, we studied a recently identified GH62 α -L-arabinofuranosidase (AnAbf62A) that was highly secreted when *Aspergillus nidulans* was cultivated on sugarcane bagasse. The crystal structure of the enzyme was solved showing the five-bladed β -propeller fold, which is conserved in family GH62 ^{2,3}. Site-direct mutagenesis produced Y312S and Y312F mutants which showed that Y312 is an important amino acid for binding the substrate as well as for enzymatic activity, and that both mutations are deleterious to catalytic efficiency of the enzyme.

In this computational study, we used molecular dynamics (MD) simulations and the well-tempered adaptive biasing molecular dynamics to address the question of how Y312 affects enzymatic substrate affinity and enzymatic kinetic parameters of the α -L-arabinofuranosidase (AnAbf62, GH62) from *A. nidulans* A773. A comparison of the structure of the AnAbf62wt with other crystal structures of the alpha-L-arabinofuranosidase from *Streptomyces thermoviolaceus* (PDB codes: 4O8O and 4O8P), showed that the loop containing Y312 has two different conformations ⁴. The free energy simulations indicated that the loop containing Y312 can access different conformations separated by moderately low energy barriers. One of these conformations, comprising on a local minimum, is responsible for placing Y312 in the vicinity of the arabinose glycosidic bond, and thus, may be important for catalytic efficiency. This is the first report on the structural investigation of a GH62 from the genus *Aspergillus*.

Key-words: Molecular Dynamics, adaptive biasing molecular dynamics, loop conformation, free energy profile.

Support: This work has been supported by Fundação de Amparo a Pesquisa do Estado de São Paulo (FAPESP)



References:

1. Sturgeon, R. J. *Advances in macromolecular carbohydrate research. Volume 1.* (JAI Press, 1997).
2. Kaur, A. P. *et al.* Functional and structural diversity in GH62 α -L-arabinofuranosidases from the thermophilic fungus *S. cyathidium thermophilum*. *Microb. Biotechnol.* **8**, 419–433 (2015).
3. Siguier, B. *et al.* First structural insights into α -L-arabinofuranosidases from the two GH62 glycoside hydrolase subfamilies. *J. Biol. Chem.* **289**, 5261–73 (2014).
4. Wang, W. *et al.* Elucidation of the molecular basis for arabinoxylan-debranching activity of a thermostable family GH62 α -L-arabinofuranosidase from *Streptomyces thermoviolaceus*. *Appl. Environ. Microbiol.* **80**, 5317–29 (2014).



Constante de acoplamento de longo alcance 4J em cicloexanona e cicloexanotona 2-flúor-substituídas

Fátima M.P. de Rezende(PG), Matheus P. de Freitas(PQ) and Teodorico de C.

Ramalho(PQ)

Universidade Federal de Lavras, Departamento de Química CP 3037, 37200-000, Lavras, MG, Brasil

Abstract: Estudos já realizados para a forma axial e equatorial da 2-bromocicloexanona demonstraram a existência de uma constante de acoplamento de longo alcance $^4J_{H_2,H_6}$ para o conômero equatorial, mas não $^4J_{H_2,H_4}$; como consequência, pode-se inferir que o grupo carbonila desempenha um papel importante no caminho do acoplamento, em decorrência das interações $\sigma_{C_2H_2} \rightarrow \pi^*_{C=O}$ e $\sigma_{C_6H_6} \rightarrow \pi^*_{C=O}$.¹ No presente estudo, cálculos de NBO, em nível B3LYP-aug-cc-pVTZ, e de constantes de acoplamento (SSCCs) foram realizados. Para os cálculos SSCCS, o funcional B3LYP e a função de base EPR-III foi empregada para os átomos de H e F e, para C, S, O, Br, Cl, foi usado o conjunto de bases aug-cc-pVDZ. Os cálculos foram realizados para as cicloexanonas e cicloexanotonas 2-flúor-substituídas (Figura 1) em gás, DMSO e água (modelo PCM). Os resultados indicam interações $\sigma_{C_2H_2} \rightarrow \pi^*_{C=Y}$ e $\sigma_{C_6H_6} \rightarrow \pi^*_{C=Y}$ (Tabela 1) maiores em cerca de 1 kcal mol⁻¹ para a forma equatorial da cicloexanotona em relação à cicloexanona. Por outro lado, $^4J_{H_2,H_6}$ é maior por cerca de 1 Hz para a cicloexanona na forma equatorial (Tabela 2). Isso pode ser explicado pelo FC (contato de Fermi), que contribui para o valor de $^4J_{H_2,H_6}$ (Tabela 3). É importante mencionar que o termo FC é influenciado pela hibridização dos carbonos que participam no caminho do acoplamento (sendo que um menor caráter *s* induz a um decaimento de *J*), bem como pelo comprimento das ligações C-C e C-H. Apesar dos valores de $\sigma_{C_2H_2} \rightarrow \pi^*_{C=Y}$ e $\sigma_{C_6H_6} \rightarrow \pi^*_{C=Y}$ serem maiores para a cicloexanona, essa aparente contradição tem origem no contato de Fermi, que é influenciado pelo caráter *s* e pelo comprimento de ligação.² Os valores para os compostos em fase gasosa, comparando-se com os dados em solvente implícito, permaneceram praticamente constantes, ou seja, não houve diferença significativa

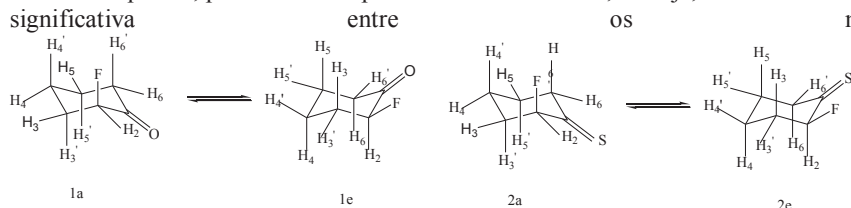


Figura 1 \square 2-flúorcicloexanonas e cicloexanotonas estudadas computacionalmente



Tabela 1: Interações hiperconjugativas (kcal mol^{-1}) relevantes para o estudo de ${}^4J_{\text{H}_2,\text{H}_6}$ em gás, DMSO e água.

Composto	$\sigma_{\text{C}_2\text{H}_2} \rightarrow \pi^*_{\text{C}=\text{Y}}$	$\sigma_{\text{C}_6\text{H}_6} \rightarrow \pi^*_{\text{C}=\text{Y}}$
1 a	-	-
1 e	5,7;5,6;5,6	6,1;6,1;6,1
2 a	-	-
2 e	6,7;6,7;6,7	6,9;6,8;6,9

Tabela 2: Valores de constante de acoplamento ${}^4J_{\text{H}_2,\text{H}_6}$ (Hz) em gás, DMSO e água.

Composto	${}^4J_{\text{H}_2,\text{H}_6}$
1 a	0,5;0,5;0,5
1 e	1,7;1,7;1,7
2 a	0,3;0,3;0,3
2 e	0,8;0,8;0,8

Tabela 3: Valores de FC (Hz) para ${}^4J_{\text{H}_2,\text{H}_6}$ em gás, DMSO e água.

Composto	FC
1 a	1,0;1,0;1,0
1 e	1,2;1,2;1,2
2 a	0,8;0,9;0,9
2 e	0,1;0,1;0,1

Key-words: Acoplamento de longo alcance. Carbonila. Tiocarbonila

Support: FAPEMIG, CNPq and CAPES

References:

- [1] COELHO, J. V.; FREITAS, M. P.; TORMENA, C. F.; RITTNER, R. "On the 4JHH long-range coupling in 2-bromocyclohexanone: conformational insights."(2009), **Magnetic Resonance in Chemistry**, Hoboken.
- [2] RUSAKOV, Y. Y.; KRIVDIN, L. B. "Modern quantum chemical methods for calculating spin-spin coupling constants: theoretical basis and structural applications in chemistry. " (2013), **Russian Chemical Reviews**, England.



Static correlation effects in flavin mediated hydride transfer

Felipe Curtolo^a, Guilherme Menegon Arantes^a

^aInstituto de Química, Universidade de São Paulo.
Av. Prof. Lineu Prestes, 748. São Paulo – SP

Abstract: Many enzymatic reactions use flavin nucleotide cofactors (FAD) as electron acceptors. In cellular respiration, flavoenzymes mediate coupled proton-electron transfer reactions between FAD and succinate/fumarate [1]. Here, we modeled hydride transfer reactions mediated by flavins (Figure) isolated in the gas phase to understand the intrinsic energetics and mechanisms involved and ultimately choose a reliable method to study flavoenzymes reactions.

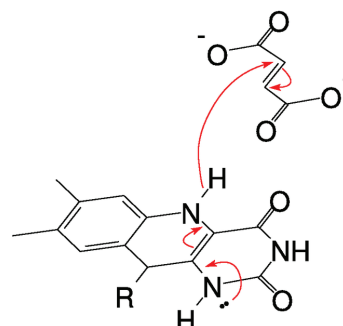


Figure. Flavin hydride transfer reaction

Reaction profiles were determined by density functional theory (DFT) with B3LYP functional and 6-31+G* basis set using the Gaussian 09 program. Relative energies were recalculated with functionals including dispersion corrections, with second-order Møller-Plesset perturbation theory (MP2) using the 6-311+G** basis set and with complete active space self-consistent field method (CASSCF), followed by a perturbative treatment with *n*-electron valence state perturbation theory (NEVPT2) all using the Def2-TZVP basis set in ORCA 3.0.1 package.

Our results show that the distribution of π electrons along flavin's isoalloxazine ring highly contributes to the complexation and orientation of the reactant complex. During flavin reduction, π electrons are rearranged and the isoalloxazine ring bends, losing planarity. As the system approaches the transition state, different electronic states become degenerate and the reaction barriers of hydride transfers are highly affected by static electronic correlation. Although MP2 can recover dynamical correlation and describe well flavin π stacking and dispersion interactions, the reaction barriers of hydride transfer are miscalculated, so multiconfigurational energy profiles have to be used to describe the reactions.

Key-words: multiconfigurational methods, electronic structure, reactivity

Support: This work has been supported by FAPESP and by CNPq.

References: [1] T.M. Iverson, *Biochim. Biophys. Acta*, 1827, 648-57 (2012)

Moving Protons with Pendant Amines in Niobium-Based Electrocatalysts

Authors: Felipe Fantuzzi,^{1,2} Simone Rauegi,² Marco A. C. Nascimento¹

Address: ¹Instituto de Química, Universidade Federal do Rio de Janeiro, Brazil.

²Pacific Northwest National Laboratory, Richland WA, USA.

Abstract: The controlled mobility of protons is a fundamental step in a series of chemical and biological reduction-oxidation processes, such as the reduction of dioxygen to water and the production/oxidation of hydrogen [1,2]. The tailoring of molecular electrocatalysts that effectively forms or cleaves the H-H bond is, therefore, extremely useful for the energy storage problem [3]. Such catalysts, responsible for the electrochemical transformation of abundant substrates into fuels, should be efficient and based on low-cost and abundant metals. In this perspective, Brazil has the largest Niobium (Nb) reserves in the world (98.53%) and exportation as ferroniobium, a type of iron-Nb alloy, is the main commercial destination of the metal [4]. The goal of this work is to aggregate economic and technological value to Nb by developing coordination compounds based on the metal that present electrocatalytic activity for energy-relevant conversions. The intramolecular proton transfer between Nb and positioned pendant amines for the hydrogen oxidation electrocatalyst $[\text{Nb}_2(\text{P}^{\text{Cy}}_2\text{N}^{\text{Bn}}_2\text{H})_2]^{2+}$ ($\text{P}^{\text{Cy}}_2\text{N}^{\text{Bn}}_2 = 1,5\text{-dibenzyl-3,7-dicyclohexyl-1,5-diaza-3,7-diphosphocyclooctane}$, Figure 1) is described herein by Density Functional Theory (DFT) calculations at the B3P86/{Nb(SDD);P,N,C,H(6-31G**)} level. This ligand was successfully applied in early studies for the generation of Ni-based electrocatalysts, in which both experimental and computational results pointed to a metal-mediated intramolecular proton transfer between the nitrogen atoms, and chair-to-boat isomerizations as rate-limiting steps [5]. Important details of the geometrical and energetic properties of Nb-based electrocatalysts are discussed. The authors hope that this study will provide key aspects for the production of a new generation of molecular electrocatalysts based on Niobium.

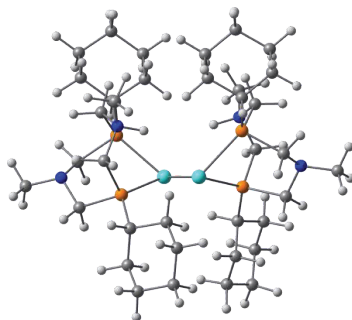


Figure 1. The hydrogen oxidation electrocatalyst $[\text{Nb}_2(\text{P}^{\text{Cy}}_2\text{N}^{\text{Bn}}_2\text{H})_2]^{2+}$.



Key-words: Electrocatalysis, Niobium, Coordination Chemistry, Density Functional Theory, Proton Transfer

Support: This work has been supported by CNPq.

References:

- [1] S. Raugé et al., *Acc. Chem. Res.*, 48, 248 (2015).
- [2] A. Dey, *Inorg. Chem.*, 55, 10831 (2016).
- [3] D. L. DuBois, *Inorg. Chem.*, 53, 3935 (2014).
- [4] A. R. Alves, A. R. Coutinho, *Mater. Res.*, 18, 106 (2015).
- [5] M. O'Hagan, et al., *J. Am. Chem. Soc.*, 133, 14301 (2011).



Determinação do comprimento de espalhamento para colisões H-H, H-D, H-T, D-D, D-T, T-T nos estados eletrônicos ($X^1\Sigma^+$) e ($b^3\Sigma^+$) usando um método variacional

Felipe O. Ventura¹, Marcílio N. Guimarães¹, Frederico V. Prudente¹, Antônio F. C. Arapiraca², Cristina P. Gonçalves³, José R. Mohallem⁴

¹ Instituto de Física, Universidade Federal da Bahia, UFBA, Salvador, BA, Brasil.

² Centro Federal de Educação Tecnológica de Minas Gerais, CEFET-MG, Belo Horizonte, MG, Brasil.

³ Departamento de Ciências Exatas e Tecnológicas, Universidade Estadual do Sudoeste da Bahia, UESB, Vitória da Conquista, BA, Brasil.

⁴ Departamento de Física, ICEX, Universidade Federal de Minas Gerais, UFMG, Belo Horizonte, MG, Brasil.

Palavras-chaves: Átomos ultrafrios. Cálculo eletrônico. Espalhamento quântico.

INTRODUÇÃO

O estudo de átomos ultrafrios tem proporcionado um grande avanço no domínio e controle de átomos, particularmente os alcalinos (família 1A) como Na, K, Rb e Cs, que são facilmente aprisionados e resfriados em armadilhas magneto-ópticas (MOT). Em anos recentes, várias técnicas experimentais e teóricas foram desenvolvidas para o seu estudo e novas descobertas além da condensação de Bose-Einstein (BEC) foram alcançadas (vórtices em BEC, turbulência quântica e topologia em transições de fase).

Com base nisso, abordaremos neste trabalho a colisão elástica fria entre os átomos H-H, H-D, H-T, D-D, D-T e T-T interagindo via os potenciais moleculares ($X^1\Sigma^+$) e ($b^3\Sigma^+$). Determinamos o comprimento de espalhamento (onda-s) para essas colisões atômicas fazendo uso de um

procedimento variacional para cálculos de espalhamento quântico, baseado na teoria da Matriz R e no Método do Elemento Finito (MEF).

METODOLOGIA

Os cálculos de estrutura eletrônica foram realizados no programa GAMESS com a inclusão de uma correção para a massa nuclear [1] e no nível *full-CI/aug-cc-pVQZ* para os estados fundamentais singleto ($X^1\Sigma^+$) e tripleto ($b^3\Sigma^+$). A correção adiabática utilizada se chama Correção de Massa Nuclear Finita (FNMC) [2]. Utilizamos os dados da literatura de L. Wolniewicz e colaboradores [3,4] e adicionamos a FNMC a esses dados, na tentativa de obter uma CEP com boa precisão. Utilizamos a correção counterpoise (CP) para estimar a influência do erro de superposição de bases (BSSE).

As CEP's foram obtidas numa configuração de 200 pontos e distâncias

interatômicas de 0.20 a 20.0 u.a para o ($X^1\Sigma^+$) e 105 pontos e distâncias interatômicas de 1.0 a 20.0 u.a para o ($b^3\Sigma^+$). Fizemos uma interpolação por spline cúbica para conectar o potencial de curto alcance (CEP) a um potencial de longo alcance (van der Waals + troca + correção adiabática).

Para o cálculo de espalhamento, utilizamos um procedimento variacional baseado na teoria da Matriz R e o Método do Elemento Finito (MEF) para expandir a função de onda nuclear em termos de funções de base locais [5]. Calculamos o deslocamento de fase (δ_0) e o comprimento de espalhamento para a onda parcial $l = 0$, usando o potencial com a inclusão da FNMC e também o potencial sem a FNMC (puramente Born-Oppenheimer). A energia cinética relativa adotada nos cálculos foi de $E = 1.10^{-30}$ u.a. Fizemos um estudo da convergência do comprimento de espalhamento em função do $r_{\text{máx}}$ entre os átomos e também em função da ordem dos polinômios (k_i) para duas malhas diferentes, uma com $N_e = 210$ elementos e $k_i = 15$ e outra com $N_e = 420$ elementos e $k_i = 30$. Calculamos o deslocamento de fase (δ_0) para a faixa de energia 10^{-30} - 10^{-9} u.a e obtivemos, usando a teoria do alcance efetivo,

$$k \cot \delta_0 = -\frac{1}{a} + \frac{1}{2}rk^2 + O(k^4)$$

de forma complementar, o comprimento de espalhamento (a) e o alcance efetivo (r) para as colisões H-H, H-D, H-T, D-D, D-T e T-T nos estados ($X^1\Sigma^+$) e ($b^3\Sigma^+$).

RESULTADOS

Figura 1: Curvas de energia potencial do H_2 nos estados ($X^1\Sigma^+$) e ($b^3\Sigma^+$).

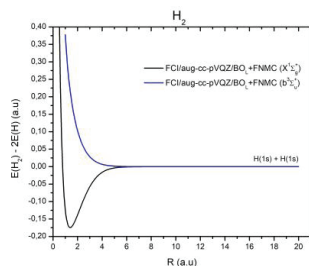


Tabela 1: Comprimento de espalhamento (em bohr) dos sistemas H-H, H-D, H-T, D-D, D-T e T-T nos estados ($X^1\Sigma^+$) e ($b^3\Sigma^+$) para a faixa de energia 10^{-30} - 10^{-9} u.a.

Sistemas	Comprimento de espalhamento			
	($X^1\Sigma^+$)		($b^3\Sigma^+$)	
	BO _{Lit.}	BO _{Lit.} + FNMC	BO _{Lit.}	BO _{Li.} + FNMC
H-H	0,5549	0,2114	1,420	1,417
H-D	11,477	11,119	-0,297	-0,301
H-T	9,4064	9,1903	-1,379	-1,400
D-D	12,693	12,367	-6,350	-6,360
D-T	10,284	10,103	-14,18	-14,20
T-T	23,342	22,316	-64,29	-64,43

AGRADECIMENTOS À CAPES

REFERÊNCIAS

- [1] C. P. Gonçalves, J. R. Mohallem, *J. Comput. Chem.*, **25** 1736-1739 (2004).
- [2] C. P. Gonçalves, J. R. Mohallem, *Theor Chem Acc.* **110**: 367-370 (2003).
- [3] L. Wolniewicz. *J. Chem. Phys.* **99** 1851-1868 (1993).
- [4] M. J. Jamieson, A. Dalgarno and L. Wolniewicz, *Phys. Rev. A*, **61** (2000).
- [5] M. N. Guimarães, F. V. Prudente. *Eur. Phys. J. D*, **64**, 287-296 (2011).

A theoretical investigation on the synthesis of aromatic polyimides

Felipe S. S. Schneider, Thiago Ferreira da Conceição, Giovanni F. Caramori

*Departamento de Química – Universidade Federal de Santa Catarina – Campus
Universitário Trindade – Florianópolis – Santa Catarina – Brazil*

Aromatic polyimides comprise a class of polymers known as “high performance” due to their high T_g (normally above 200 °C) and thermal stability [1,2]. The imide group in this class of polymers is a five- or six-membered ring. The literature reports very distinct synthetic reaction conditions for these two kinds of aromatic polyimides [1] and the reason for these different synthetic conditions is commonly considered to be a higher stability of the six-membered ring anhydride, in comparison to the five-member ones (Figure 1) [3,4]. Nevertheless, no detailed discussion on the reactivity of these monomers is reported in the literature.

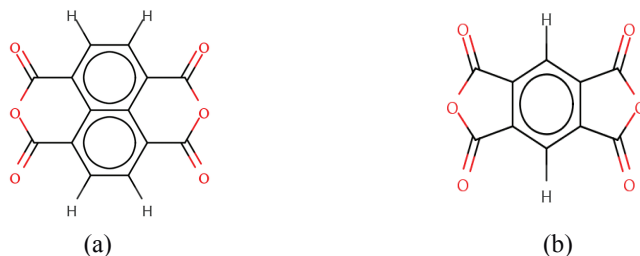


Figure 1: Six- (NTDA, a) and five-membered (PMDA, b) cyclic anhydrides studied.

The present work reports the investigation on the first and most critical step of the synthesis of aromatic polyimides, namely the formation of polyamic acid (Figure 2), by the use of density functional theory (DFT, BP86-D3(BJ)/def2-TZVP/SMD [5–11], using the ORCA package, version 3.0.2 [12]). Two reaction pathways, (a) and (b), between aniline and either naphthalic tetracarboxylic dianhydride (NTDA, Figure 1a) or pyromellitic anhydride (PMDA, Figure 1b) were considered (Figures 2a and 2b). While (a) is a single step process (Figure 2a), (b) passes through an intermediate (Figure 2b). Energies of the reactants, transition states, intermediates and products were calculated and the reactions were compared in regard of kinetic parameters.

It was shown that, although (a) was the fastest pathway found, its reverse reaction is even faster, and (b) might actually occur. In the gas phase, the rate constant of (a) is around five orders of magnitude higher for PMDA when compared to NTDA. Pathway (b) has comparable magnitude for both substrates, but is 10^4 slower than (a).

Solvent plays a major role in this process, as shown by implicit solvation in THF, DMF, DMSO and propylene carbonate (PC). For pathway (a), for instance, PMDA reacts 5.1, 71.6, 407.3 and $6.7 \cdot 10^{12}$ times faster in THF, PC, DMF, and DMSO, respectively, than in vacuum. DMSO shows the largest velocity increase for NTDA as well, but it was found to be only 13 faster than in vacuum in this case. Pathway (b) also depended on solvation, although to a smaller degree than (a).

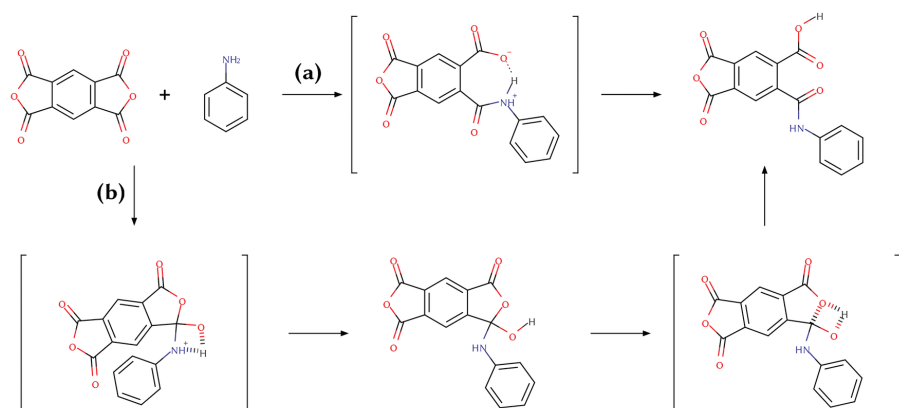


Figure 2: Reaction pathways (a) and (b) employed in this study, here exemplified with PMDA only, for brevity. (a) is a single step process, (b) passes through an intermediate.

We accessed the differences in reactivity between five-membered (PMDA) and six-membered (NTDA) ring anhydrides towards condensation by the use of a homodesmotic reaction (Figure 3), which measured the five-membered ring tension of PMDA to be 3.4 kcal/mol higher than NTDA, in agreement with the prediction of faster reactions promoted by PMDA.

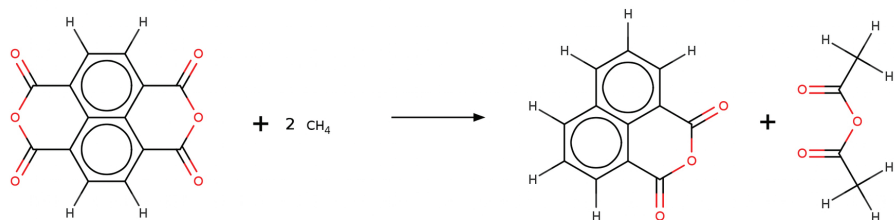


Figure 3: Homodesmotic reaction employed to estimate ring tension, here exemplified with NTDA only, for brevity.

Key-words: polyimides, density functional theory, reaction mechanism.

References:

- [1] D.-J. Liaw *et al*, Prog. Polym. Sci. 37 (2012) 907–974.
- [2] C.E. Sroog, Prog. Polym. Sci. 16 (1991) 561–694.
- [3] H. Niu *et al*, Trans. Nonferrous Met. Soc. China 19 (2009) s587–s593.
- [4] J.P. Gao, Z.Y. Wang, J. Polym. Sci. Part A Polym. Chem. 33 (1995) 1627–1635.
- [5] F. Weigend *et al*, Phys. Chem. Chem. Phys. 7 (2005) 3297.
- [6] S. Grimme, S. Ehrlich, L. Goerigk, J. Comput. Chem. 32 (2011) 1456–1465.
- [7] S. Grimme, J. Antony, S. Ehrlich, H. Krieg, J. Chem. Phys. 132 (2010) 154104.
- [8] A. Schäfer, H. Horn, R. Ahlrichs, J. Chem. Phys. 97 (1992) 2571–2577.
- [9] A.D. Becke, Phys. Rev. A 38 (1988) 3098–3100.
- [10] J.P. Perdew, Phys. Rev. B 33 (1986) 8822–8824.
- [11] A. V. Marenich *et al*, J. Phys. Chem. B 113 (2009) 6378–96.
- [12] F. Neese, Wiley Interdiscip. Rev. Comput. Mol. Sci. 2 (2012) 73–78.

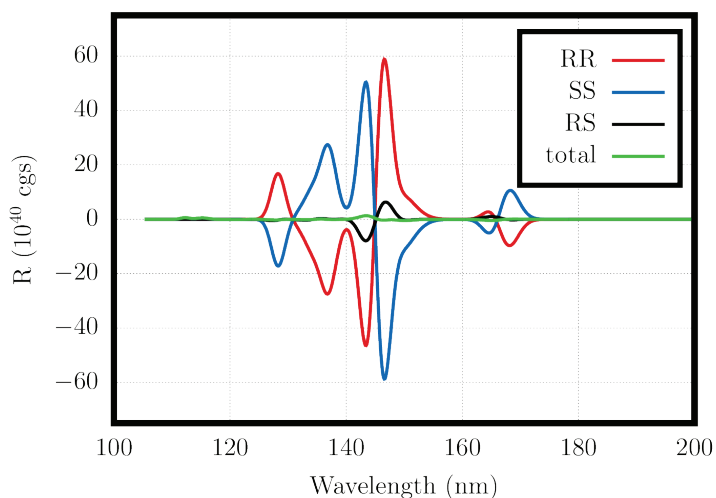


Electronic Circular Dichroism of Gamma-valerolactone dimers extracted from Monte Carlo liquid phase simulation.

Felippe Mariano Colombari (PQ), Luiz Carlos Gomide Freitas (PQ)

Depto. de Química – Centro de Ciências Exatas e Tecnologia – UFSCar

Abstract: Gamma-valerolactone (GVL) is a chiral green solvent which gained high importance in the past decade due to its environmental-friendly properties[1]. The presence of an asymmetric carbon within its structure gives rise to two enantiomers, RGVL and SGVL, leading to different interactions between GVL molecules in the racemic mixture: homochiral interactions (those between equal enantiomers: RR and SS) and heterochiral interactions (those between different enantiomers: RS). From a Monte Carlo NpT ensemble simulation (T = 25 °C, p = 1 atm) the most stable RR, SS and RS dimers from racemic mixture were sampled within a 10k configurations interval and 8000 uncorrelated structures were obtained for each pair. Electronic Circular Dichroism (ECD) calculations were performed for all structures using the semiempirical ZINDO/S hamiltonian. Only single excitations were calculated and the first 20th low excited states were analyzed. The average spectra for RR, SS and RS dimers ensembles and also the total average are shown below:





One observes symmetric curves from RR and SS contributions. The results from RS dimers presents low amplitudes which is consistent with the opposite contributions from each chiral structure. The total average shows a very low amplitude as expected from a racemic mixture.

Key-words: Gamma-valerolactone, Monte Carlo, Dimers, Electronic Circular Dichroism, chirality.

Support: This work has been supported by CNPq, FAPESP and LNCC.

References:

[1] J. M. Tukacs, B. Fridrich, G. Dibó, E. Székely, L. T. Mika. Green Chem. 17, 5189 (2015).



Molecular dynamics and electronic properties of pyridinium-iodide charge-transfer complexes in acetonitrile solution

F. da Silva¹, F. R. Carvalho², N. Hioka² and K. Coutinho¹

¹*Instituto de Física, Universidade de São Paulo, São Paulo, SP, Brasil*

²*Universidade Estadual de Maringá, Maringá, PR, Brasil*

Abstract: The formation of charge-transfer complexes (CTC) is characterized by the appearance of a new absorption band on the electronic spectra, in organic polar solvents like acetonitrile [1,2]. These type of systems have recently received much interest in a broad variety of fields, for example, organic electronics, nonlinear spectroscopy, medical biochemistry, pharmaceutical industry, etc [3,6].

In this work, we have studied theoretically CTC formed by a pyridinium derivative, the $C_3\text{bis}(4\text{CP})^{2+}$, with anions iodide [7]. We have used density functional theory (DFT) and time dependent density functional theory (TDDFT) to calculate electronic properties and the excitation energies. We have found that functional with long-range corrections (CAM-B3LYP and wB97X-D) are essential for an accurate description of the charge-transfer excitations.

A better description of the complex in acetonitrile solution was obtained using classical molecular dynamics, with a fine-tuned OPLS-AA force field. Using this approach, the classical molecular dynamics was able to reproduce results of a first principle Born-Oppenheimer molecular dynamics. No dissociation were observed, i.e., the complexes were formed by the association of two I^- to the $C_3\text{bis}(4\text{CP})^{2+}$. We also have found that only one iodide, however, participates in the charge transfer process, what explain why a stoichiometry of 1:1 was observed in the experiment. The calculated charge-transfer band are in excellent agreement with experiment.

Key-words: CTC, TDDFT, Molecular Dynamics

Support: This work has been supported by CNPq, FAPESP, CAPES, NBioNet and BioMol

References:

- [1] R. S. Mulliken, J. Am. Chem. Soc. 74, 811 (1952).
- [2] C. N. R. Rao and A. S. N. Murthy, in Spectrosc. Inorg. Chem. 1, 107 (1970).
- [3] K. P. Goetz, D. Vermeulen, M. E. Payne, C. Kloc, L. E. McNeil, and O. D. Jurchescu, J. Mater. Chem. C 2, 3065 (2014).
- [4] J. B. Torrance, Acc. Chem. Res. 12, 79 (1979).
- [5] G. J. Meyer, Inorg. Chem. 44, 6852 (2005).
- [6] S. Sadeghi and G. R. Dashti, Anal. Chem. 74, 2591 (2002).
- [7] E. M. Kosower, J. A. Skorcz, J. Am. Chem. Soc. 82, 2195 (1960).
- [8] F. R. Carvalho, N. Hioka. "Caracterização de complexos de transferência de carga entre íons derivados de N,N' -Alquildil-Bis(piridínio Substituídos) com iodeto", Master Dissertation, Universidade Estadual de Maringá, PR, Brasil (2010).

Uso da Expansão de Redlich-Kister e do Modelo SMD para Prever Equilíbrio de Fases em Misturas Binárias

Fernando M. Lisboa e Josefredo R. Pliego Jr.

*Departamento de Ciências Naturais, Universidade Federal de São João del-Rei,
36301-160 São João del-Rei-MG, Brazil*

Equilíbrio de fases é um tópico clássico em química e de grande importância em processos de separação[1,2]. No caso de sistemas líquidos binários, é bem conhecido que a energia livre de mistura pode ser expressa pela expansão de Redlich-Kister:

$$\frac{\Delta G_{mixt}}{n} = x_1 RT \ln x_1 + x_2 RT \ln x_2 + x_1 x_2 (A + B(x_1 - x_2) + \dots) \quad (1)$$

O primeiro e segundo termos do lado direito correspondem à energia livre ideal da mistura. Os parâmetros A e B estão relacionados ao desvio da idealidade, e x_1 e x_2 são as frações molares dos respectivos líquidos. Pode-se mostrar que os parâmetros A e B podem ser expressos pela energia livre de solvatação dos componentes, segundo as equações:

$$A = \frac{1}{2} (\Delta G_{solv}^*(1:2) + \Delta G_{solv}^*(2:1) - \Delta G_{solv}^*(1:1) - \Delta G_{solv}^*(2:2)) \quad (2)$$

$$B = \frac{1}{2} (\Delta G_{solv}^*(2:1) - \Delta G_{solv}^*(2:2)) - \frac{1}{2} (\Delta G_{solv}^*(1:2) - \Delta G_{solv}^*(1:1)) + RT \ln \left(\frac{\rho_1 M_2}{\rho_2 M_1} \right) \quad (3)$$

sendo que 1 e 2 são os dois líquidos, ρ a densidade e M a massa molar. As expressões acima envolvem a solvatação de 1 em 2, de 2 em 1, de 1 em 1 e de 2 em 2. Portanto, inclui informação de como cada componente interage com o outro e consigo mesmo. Essencialmente, esta abordagem utiliza a expansão de Redlich-Kister como uma interpolação para conectar os potenciais químicos de cada componente na fase pura e em diluição infinita. Desta forma, a energia livre de solvatação pode ser obtida por qualquer método que funcione para diluição infinita (e também auto-solvatação). Neste trabalho, utilizamos o modelo SMD, que é um modelo universal, no sentido de que uma vez conhecidas certas propriedades do solvente, este pode ser inserido no modelo. Assim, as equações 1 a 3, juntamente com o modelo de solvatação SMD, foi utilizado para o cálculo da separação de fases de nove misturas líquidas binárias, com um total de 18 pontos de composição de fases. Os resultados teóricos de fração molar do menor componente em cada fase estão apresentados na Figura 1, expresso como -Log da fração molar. Como pode-se observar, há uma boa correlação entre teoria e experimento, com R^2 igual a 0.72, mostrando que o modelo pode ser utilizado para uma rápida previsão semi-quantitativa



de composição das fases. Além disso, a presente abordagem expande nossa primeira investigação sobre o uso do modelo SMD e teoria de soluções regulares para prever separação de fases [3].

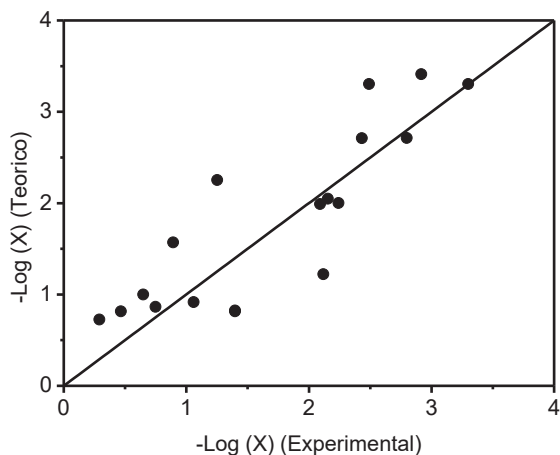


Figura 1. Gráfico do logaritmo na base 10 da fração molar do menor componente em cada fase. Valores teóricos versus experimentais. $R^2 = 0.72$.

Key-words: solvatação, energia livre de mistura, equilíbrio de fases.

Support: This work has been supported by CNPq and FAPEMIG.

References:

- [1] Gmehling, J.; Kolbe, B.; Kleiber, M.; Rarey, J.; Chemical Thermodynamics for Process Simulation; Wiley-VCH: Weinheim, 2012.
- [2] With, G.d.: Liquid-State Physical Chemistry: Fundamentals, Modeling and Applications. Wiley-VCH, 2013.
- [3] Plieho Jr, J. R. *J. Brazil. Chem. Soc.* 2015, **26**, 1737.



Thermodynamic stable diatomic dications: the case of SrO²⁺

Levi Gonçalves dos Santos^a, Klaus Franzreb^b, and Fernando R. Ornellas^{a#}

^a Departamento de Química Fundamental, Instituto de Química, Universidade de São Paulo; Av. Prof. Lineu Perstes, 748, São Paulo, 05508-000, Brazil

^b Chemistry Department, Arizona State University, Tempe, AZ, 551?, USA

Abstract: The perspective that many diatomic dications XY²⁺ should exist as long-lived metastable, or even thermodynamically stable molecules in the gas phase, brings to evidence a class of chemical species with challenging problems to explored both experimentally and theoretically [1]. In the literature, it has been verified qualitatively that if the second ionization potential of X is smaller than the first ionization of Y, leading to the dissociation fragments X²⁺ + Y, then the system is expected to be thermodynamic stable; if it is greater than the first ionization of Y, it has been usually assumed that the channel is associated with a metastable system with the dissociation fragments X⁺ + Y⁺ species. However, it could also lead instead to a purely thermodynamic stable species due to a more delicate energetic balance involving the depth of the potential well and the excitation energies of the two ions.

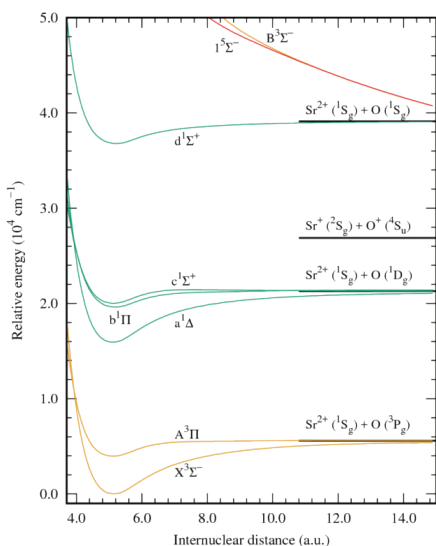


Fig. 1. PEC of the lowest-lying $\Lambda + S$ states of SrO²⁺

In the present work, we constructed potential energy curves, dipole moment, and transition moment functions, and calculated the associated spectroscopic parameters corresponding to the first four dissociation channels of SrO²⁺. Additionally, we also computed the double ionization potential of SrO. In our theoretical approach, we first carried out state-averaged complete active space self-consistent field (SA-CASSCF) calculations [2, 3] followed by the multireference configuration interaction MRCI [4, 5] method, both implemented in Molpro code [6]; the correlation consistent set cc-pV5Z-PP for strontium [8] and cc-pV6Z for oxygen [7] were used as basis functions.



All singlet, triplet, and quintet states investigated are illustrated in Fig. 1, where the four dissociation channels limits are indicated. Correlating with the $\text{Sr}^{2+} + \text{O}$ asymptote, the ground state ($X^3\Sigma^-$) has an equilibrium distance of 5.134 a_0 , and a harmonic vibrational constant of 231.9 cm^{-1} ; the dissociation energy of 5.91 kcal mol^{-1} indicates a much weaker bond than the one in SrO ($X^1\Sigma^+$), 137.93 kcal mol^{-1} , and SrO^+ ($X^2\Sigma^+$), 79.57 kcal mol^{-1} . The repulsive states $^3,5\Sigma^-$, partially shown in the upper right corner, correlate with the third channel in the asymptotic limit; all of the other states are thermodynamic stable. The first excited state, $A^3\Pi$, also correlating with the first channel lies higher by 3 968 cm^{-1} . Still higher in energy, in the approximate range between 16 000 and 20 000 cm^{-1} , we located the three singlet states correlating with the second dissociation channel, namely: $a^1\Delta$ ($R_e = 5.104 a_0$, $T_e = 15\,929 \text{ cm}^{-1}$, $\omega_e = 231.3 \text{ cm}^{-1}$), $b^1\Pi$ ($R_e = 5.189 a_0$, $T_e = 19\,611 \text{ cm}^{-1}$, $\omega_e = 186.6 \text{ cm}^{-1}$), and $c^1\Sigma^+$ ($R_e = 5.134 a_0$, $T_e = 20\,019 \text{ cm}^{-1}$, $\omega_e = 181.0 \text{ cm}^{-1}$). The fourth state, $d^1\Sigma^+$ ($R_e = 5.229 a_0$, $T_e = 36\,778 \text{ cm}^{-1}$, $\omega_e = 186.3 \text{ cm}^{-1}$) is bound by 6.67 kcal mol^{-1} . As an indirect assessment of the quality of the results presented above, we note that our estimates of the energy differences at the asymptotic limit between the atomic fragments is quite concordant with the ones obtained experimentally [9].

This work reports for the first time reliable theoretical data characterizing singlet, triplet and quintet states of the species SrO^{2+} which are expected to be a useful guide to experimentalists to properly identify the states and assign the allowed transitions.

Key-words: spectroscopy, SrO^{2+} , dications, electronic states, CASSCF/MRCI.

Support: Conselho Nacional de Desenvolvimento Científico e Tecnológico (CNPq) of Brazil and the Chemistry Department of Arizona State University, Tempe, AZ (KF).

References:

- [1] S. D. Price, J. D. Fletcher, F. E. Gossan, and M. A. Parkes, *Int. Rev. Phys. Chem.*, **36**, 145 (2017).
- [2] P. J. Knowles and H.-J. Werner, *J. Chem. Phys.* **82**, 5053 (1985).
- [3] H.-J. Werner and P. J. Knowles, *Chem. Phys. Lett.* **115**, 259 (1985).
- [4] P. J. Knowles and H.-J. Werner, *Chem. Phys. Lett.* **145**, 514 (1988).
- [5] H.-J. Werner and P. J. Knowles, *J. Chem. Phys.* **89**, 5083 (1988).
- [6] MOLPRO is a package of *ab initio* programs written by H.-J. Werner, P. J. Knowles, with contributions of A. Almlöf, D. Amos, A. Berning, *et al.*
- [7] H. Li, H. Feng, W. Sun, Y. Zhang, Q. Fan, K. A. Peterson, Y. Xie, and H. F. Schaefer III, *Mol. Phys.* **111**, 2292 (2013).
- [8] A. K. Wilson, T. van Mourik, and T. H. Dunning, *J. Mol. Struct. (Theochem)*, **338**, 339 (1996).
- [9] A. A. Radzig and B. M. Smirnov, *Reference Data on Atoms, Molecules, and Ions*, (Springer-Verlag, Berlin, 1985).



Keggin polyoxometalates: An Electronic structure perspective based on TDDFT

Authors: Fernando Steffler, Guilherme Ferreira de Lima and Hélio Anderson Duarte.

*Address: Departamento de Química – ICEx,
Universidade Federal de Minas Gerais. 31.270-901 – Belo Horizonte – MG*

Polyoxometalates are promising materials for applications in nanoscience and nanotechnology. Their syntheses are simple requiring just a selection of an appropriate solvent and adjustments in the pH of the solution. Keggin Polyoxometalates are the most studied ones with the initial synthesis dating from 1826 by Berzelius [1]. These materials present the general formula $[XM_{12}O_{40}]^n$, with X being the heteroatom (usually P, Si, Ge or As) and M the metal (commonly W, Mo or Nb) with Td symmetry [2] (Figure 1). These structures have a range of applications, spanning metallurgic industries to electrophotocatalysis methods [3]. Recently, the synthesis of polyoxoniobates was made possible giving many possibilities by their high negative charge (-15 or -16). This work aims to compare the electronic spectrum of different Keggin Polyoxometalates calculated by TD-DFT to have insights about the electronic structure of these compounds and their possible application in photocatalysis.

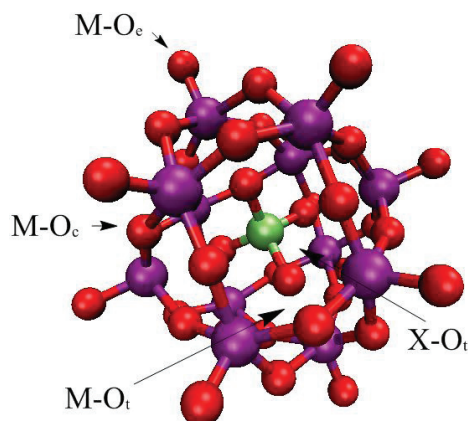


Figure 1: Components of Keggin Heteropolyanion. Where $M-O_e$ it's external metal bonding, $M-O_c$ it's the bonding coordinate in the cage, $M-O_t$ it's metal-oxygen bonding from tetrahedral of secondary element. The purple spheres are mainly metal Green sphere is the secondary element and the red spheres are oxygen atoms.

The geometry optimizations for all Keggin structures were carried out using the Gaussian 09 program, with PBE xc functional, LanL2DZ pseudopotential and cc-PVDZ basis set. To determine the excitation energies in TDDFT we choose 90 states and a xc

functional Cam-B3LYP. The group 6 Keggin polyoxometalates have excitation wavelength around 5 nm lower than experimentally observed (Table 1).

Table 1: Excitation Wavelength and Oscillator Strength (OS) for all Keggin polyoxometalates and comparison with experimental data[4].

Structure	Excitation / nm	OS	Experimental / nm
[AsMo ₁₂ O ₄₀] ³⁻	308.78	0.0617	-
[PMo ₁₂ O ₄₀] ³⁻	309.79	0.0657	309.56
[SiMo ₁₂ O ₄₀] ⁴⁻	309.42	0.0257	303.95
[GeMo ₁₂ O ₄₀] ⁴⁻	309.50	0.0207	303.03
[AsW ₁₂ O ₄₀] ³⁻	268.95	0.1413	-
[PW ₁₂ O ₄₀] ³⁻	256.73	0.1410	265.25
[SiW ₁₂ O ₄₀] ⁴⁻	257.11	0.0993	263.85
[GeW ₁₂ O ₄₀] ⁴⁻	258.26	0.1007	265.95
[AsNb ₁₂ O ₄₀] ¹⁵⁻	387.08	0.0549	-
[GeNb ₁₂ O ₄₀] ¹⁶⁻	334.91	0.0936	-

The polyoxoniobates present different behavior in their electronic spectra, in which Ge[Nb₁₂O₄₀]¹⁶⁻ present a characteristic noise. For As[Nb₁₂O₄₀]¹⁵⁻ three excitation peaks are observed, reinforcing the exotic behavior of this newest class of polyoxometalates. The NBO analysis show that the most basic oxygen atom is the one bonded in the core of Keggin polyoxometalate. This behavior diverge that was predicted, in which the negative charge is expected to be in the external oxygen atoms.

The electronic spectra of group 6 Keggin polyoxometalates shows a good agreement with the experimental data which the peak and spectrum behavior using Cam-B3LYP suited well the excitation. For polyoxoniobates are observed a breaking of one bond metal oxygen core on their structures, the high negative charge, where is concentrated on this oxygen.

Our results help to provide an insight of the uses of the group 6 Keggin polyoxometalates for acid catalysis and polyoxoniobates for basic catalysis. The spectra and electronic density described here gives suggest the sites favorable for the catalysis and which specie are preferable to be formed.

Keywords: Polyoxometalates, Photoelectrochemistry and Time Dependent Density Functional Theory.

Support: This work has been supported by CNPQ, INCT ACQUA, FAPEMIG and Capes.

References:

- [1] J. J. Berzelius, Annual Physic Chemistry, v. 131, n. 908, (1826).
- [2] D. L. Long, R. Tsunashima, L. Cronin, Angewandte Chem. Int. Edit., v. 49, n. 10, p. 1736-1758, (2010).
- [3] F. Steffler, G. F. de Lima, H. A. Duarte, Chem, Phys, Letter, 669, 104–109, (2017).
- [4] K. Nomiya, *et al. Polyhedron*, 6, 519-524, (1987).

Thiophenol: Photoinduced Hydrogen Migration

Authors: Filipe Belarmino, Silmar Monte, Elizete Ventura

Departamento de Química, CCEN, Universidade Federal da Paraíba, João Pessoa, 58059, PB, Brazil

Abstract: Reva *et al* [1] investigated some photoinduced H-transfer isomerization reactions of thiophenol in a solid argon matrix (Figure 1). In this study,

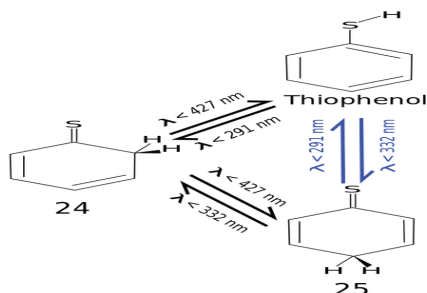


Figure 1: Photoinduced reactions of thiophenol studied in a solid argon matrix [1]. The reactions in blue were not confirmed or discarded in this experiment.

the photogenerated isomers – cyclohexa-2,4-diene-1-thione (**24**) and cyclohexa-2,5-diene-1-thione (**25**) – have never been observed so far. In order to explain the experimental results, our group has performed high level excited-state calculations (CASSCF and MR-CI) to study the reactions thiophenol → **24**, **24** → **25** and thiophenol → **25**. This is the first theoretical study concerning the photochemistry reactions studied by Reva *et al* [1]. The active space CAS consists of twelve electrons distributed among eleven orbitals (Figure 2). Vertical excitation energies of thiophenol

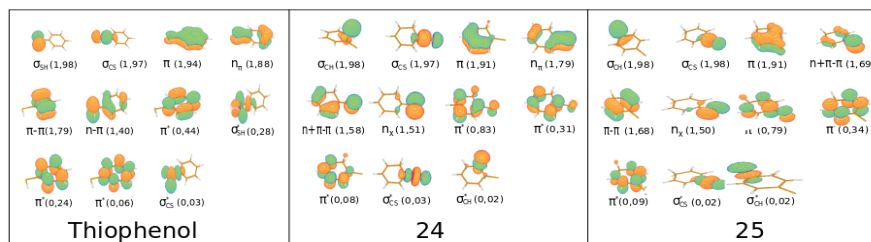


Figure 2: MO diagrams and associated occupation numbers for three lowest excited states of thiophenol, and thiones **24** and **25** at the CAS(12,11) level.



calculated at CASSCF and MR-CISD levels have been compared with the CASPT2 results [2]. The reaction paths were generated by linear interpolation, and the obtained geometries were used to compute the vertical excitation energies at the CASSCF level. So far all calculations were performed with aug-cc-pVDZ basis. The potential energy profiles of thiophenol \rightarrow **24** and **24** \rightarrow **25** are displayed in Figure 3:

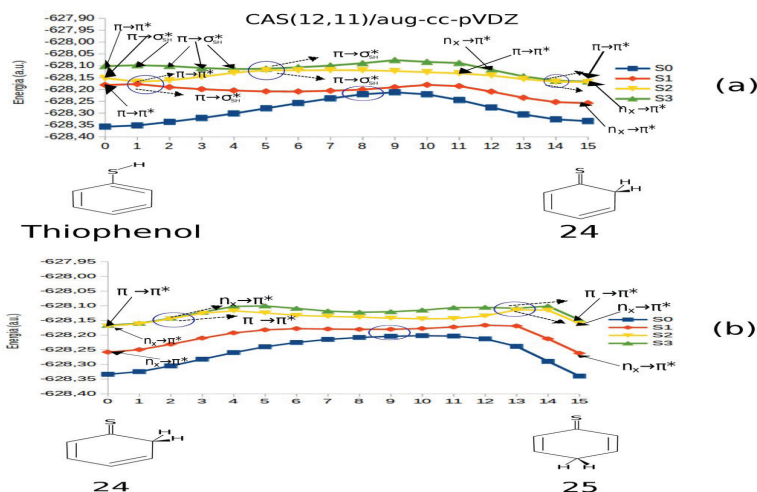


Figure 3: Potential energy profiles of the reactions (a) thiophenol \rightarrow **24** and (b) **24** \rightarrow **25** at CAS(12,11) level using the aug-cc-pVDZ basis.

As it can be seen from Figure 3, several conical intersections (blue circles) are likely to take place. In (a) their occurrence are consistent with formation of **24** from all three studied excited states. The same holds for the reaction **24** \rightarrow **25** (b), although in this case more vibrational energy may be required. The conical intersections between S_0 and S_1 in (a) and (b) suggests either formation of the product or regeneration of the reactants, from the photoreaction starting in S_1 . Preliminary results suggest that the reaction thiophenol \rightarrow **25** actually involves **24** as an intermediate. COLUMBUS program system has been used for most of the calculations.

Key-words: thiophenol, photoinduced H migration, CASSCF, MR-CISD, conical intersection.

Support: This work has been supported by CAPES, CNPQ and UFPB.

References:

[1] I. Reva, M. J. Nowak, L. Lapinski, R. Fausto, *Physical Chemistry Chemical Physics*, 17, 4775, (2015).

[2] M. N. R. Ashfold, G. A. King, D. Murdock, M. G. D. Nix, T. A. A. Oliver, A. G. Sage, *Physical Chemistry Chemical Physics*, 12, 1218, (2010).



Adsorption of Benzoic Acid on Carbonate Surfaces

Authors: Filipe C. D. A. Lima^{1,2}, Raphael S. Alvim¹, Caetano R. Miranda¹

1. Departamento de Física dos Materiais e Mecânica, Instituto de Física, Universidade de São Paulo, São Paulo SP, Brasil. 2. Instituto Federal de Educação, Ciência e Tecnologia de São Paulo (IFSP), campus Matão, SP, Brasil

Abstract: The adsorption of crude oil components through carboxylic acid groups may affect the water wettability of the carbonate reservoirs, usually composed by calcite CaCO_3 or dolomite $\text{CaMg}(\text{CO}_3)_2$ [1,2]. The Benzoic Acids (BA) binding nature and selectivity effects toward either calcite or dolomite are still unclear. We investigate the BA adsorption process on the CaCO_3 and $\text{CaMg}(\text{CO}_3)_2$ surfaces in the more stable plane (10-14), in the framework of the density-functional theory (DFT) [3], using the GGA exchange-correlation functional revised PBE (revPBE) with van der Waals (vdW) correction [4,5]. The adsorption of the BA molecule on *calcium* and *magnesium* sites were systematically analyzed for different conformations, as well dissociation products. The results show that BA can have distinct stable conformations on the carbonate surfaces through the carboxyl group with less influence of the aromatic ring. The molecule tends to be perpendicular with respect to the calcite surface, displaying strong interactions, mainly between the carboxyl group and both calcium and carbonate sites. However, for dolomite, although the perpendicular position is also the more favorable, the most selective interaction is between BA's carbonyl and surface magnesium sites. And it allows the BA's hydroxyl group to be free to interact. Our results also indicate that the BA-dolomite adsorption is influenced by interaction with water molecules. It is shown that the formation of the benzoate on the dolomite is more favored even in the absence of water molecules, increasing the selectivity of BA toward this surface. The obtained adsorption and dissociation landscape provide fundamental insights on the nature of the interaction of oil components and water wettability on carbonates systems with potential impact on oil recovery processes.

Key-words: DFT, Benzoic Acid, Benzoate, Calcite, Dolomite.

Support: This work has been supported by Petrobras, CNPq and Fapesp.

References:

- [1] D. Konopačka-Lyskawa, B. Kościelska, and J. Karczewski, *J. Cryst. Growth* **418**, 25 (2015).
- [2] K. Jarrhian, O. Seiedi, M. Sheykhani, M.V. Sefti, and S. Ayatollahi, *Colloids Surfaces A Physicochem. Eng. Asp.* **410**, 1 (2012).
- [3] W. Kohn and L.J.J. Sham, *Phys. Rev.* **140**, A1133 (1965).
- [4] M. Dion, H. Rydberg, E. Schröder, D.C. Langreth, and B.I. Lundqvist, *Phys. Rev. Lett.* **92**, 246401 (2004).
- [5] G. Román-Pérez and J.M. Soler, *Phys. Rev. Lett.* **103**, 96102 (2009).

Modelos de Nanoestruturas baseadas em Geometrias de Projeções Geométricas do R^7

Autores: Flávio M. B. Oliveira¹, Cristiano C. Bastos² e Antonio C. Pavão¹

¹Universidade Federal de Pernambuco, Departamento de Química Fundamental

²Universidade Federal Rural de Pernambuco, Departamento de Química

Resumo: O carbono tem revelado surpreendentes nanoestruturas que provocaram uma verdadeira busca de novos materiais constituídos por esse átomo. Diferentes geometrias obtidas da matemática combinatória têm sido exploradas na modelagem desses sistemas [1]. Recentemente, projeções do espaço de sete dimensões (R^7) forneceram, através de algoritmos sofisticados, geometrias peculiares e com propriedades bem estabelecidas [2]. O presente trabalho tem como objetivo construir estruturas de carbono baseadas nestas projeções de R^7 . Os modelos construídos foram 8 expansões unidimensionais, 8 bidimensionais e 7 tridimensionais, chegando a sistemas com 564 carbonos. A unidade básica dessa projeção é comparável ao C_{24} [3]. Uma das características fundamentais dessa projeção é que essa estrutura preenche todo o espaço tridimensional euclidiano, algo peculiar em geometria. Através de cálculos AM1 observamos que as estruturas se estabilizam em geometrias com elevada simetria e com distâncias e ângulos de ligação uniformes. Distâncias em torno de valores típicos de três tipos foram observadas: 1,28Å, 1,42Å e 1,54Å. Os valores de energia do HOMO não apresentam variação significativa em comparação com o C_{60} , entretanto para o LUMO há uma diferenciação. Devem por isso, apresentar uma menor capacidade elétron-doadora. Um material formado por essas projeções deverá possuir menor estabilidade comparado ao C_{60} e uma maior maleabilidade, uma vez que a energia de ligação por átomo é menor e tende a diminuir com o aumento da estrutura. Assim, além de um exercício de matemática e química quântica, o estudo dessas estruturas pode conduzir a materiais promissores para aplicações práticas.

Key-words: nanoestruturas, geometria, projeções do R^7 , propriedades eletrônicas

Support: Este trabalho tem apoio do CENAPAD de Campinas e do LQTC/UFPE

References:

- [1] L.C.B. da Silva, C. C. Bastos, F.G. Ribeiro, *Annals of Physics*, 379, 13 (2017).
- [2] S. Lins, *European Journal of Combinatorics*, 9, 291 (1988).
- [3] P. R. C. Kent, M. D. Towler, R. J. Needs, G. Rajagopal, *Physical Review B*, 62(23), 15394 (2000).

Theoretical study on the anomeric, exo-anomeric and reverse anomeric

Francisco Antonio Martins, Matheus Puggina de Freitas

Departament of Chemistry, Federal University of Lavras, 37200, Lavras, MG, Brazil

Abstract: The anomeric effect is well known, but its origin is still controversial, since electrostatic and electron delocalization interactions are invoked to explain the stereochemical preferences of α -substituted tetrahydropyrans. In cases where both endocyclic and exocyclic heteroatoms bearing electron lone pairs take place, the exo-anomeric effect can appear, in addition to the classical anomeric effect. In order to further explore these effects as stabilizing interactions of the conformations of six-membered rings, the present work evaluated a series of heterocyclic compounds substituted at C2 by various groups [F, NH₂, NH(CH₃), OH, OCH₃, N(CH₃)₂]. Calculations were carried out at the ω B97XD-6-311++g(d,p) level, using the Gaussian 09 program. The geometries for the stable conformers were fully optimized in the gas phase and implicit DMSO (using the polarizable continuum model). Subsequently, natural bond orbital (NBO) analysis was also performed; finally, NMR and AIM parameters were calculated in order to assess the interactions responsible for the titled effects. The theoretical calculations allowed to conclude that molecules containing an exocyclic nitrogen show the reverse anomeric effect, while the structures with a fluorine at C-2 and an endocyclic oxygen show the anomeric effect. On the other hand, structures with the fluorine substituent at C-2 and nitrogen as endocyclic atom show the reverse anomeric effect. For molecules containing endocyclic nitrogen and exocyclic oxygen atoms only, the normal anomeric effect takes place. The most important contribution to the effects studied in this work was the classical one. The calculations indicated some structures that induce the reverse anomeric effect.

Key-words: Anomeric effect, exo-anomeric effect, theoretical calculations, Perlin effect

Support: This work has been supported by Federal university of Lavras

References:

- [1] E. Juaristi, G. Cuevas, *Tetrahedron*, V. 48, no. 24, pp. 5019-5087, 1992
- [2] C. L. Perrin, K. B. Armstrong, M. A. Fabian, *J. Am. Chem. Soc.* 1994, 116, 715-722
- [3] U. Salzner, *J. Org. Chem.* 1995, 60, 986-995
- [4] S. Wolfe, B. M. Pinto, V. Varma, R. Y. N. Leung, *Can. J. Chem.* 68, 1990
- [5] J. M. Silla, M. P. Freitas, *RSC. Adv.* 2016, 6, 74598-74603
- [6] J. G. Hernández-Lima, J. E. Barquera-Lozada, G. Cuevas and F. Cortés-Guzmán. *J. Comput. Chem.* 2015, 36, 1573, 1578

The singlet excited states of N-acenes (N=0-5): A CASSCF/CASPT2 study of the L_a and L_b bands

Fernanda Bettanin¹, Luiz F. A. Ferrão¹, Max Pinheiro Jr.¹, Adélia J. A. Aquino², Hans Lischka², Francisco B. C. Machado¹, Dana Nachtigallova³

¹ Departamento de Química, Instituto Tecnológico da Aeronáutica, São José dos Campos, 122228-900, São Paulo, Brazil,

² School of Pharmaceutical Sciences and Technology, Tianjin University, Tianjin, 300072 P.R.China

³ Institute of Organic Chemistry and Biochemistry, Academy of Sciences of the Czech Republic, Flemingovo nám. 2, CZ-16610 Prague 6, Czech Republic

The electronic properties of polyacenes (PACs, Figure 1) are not only a very attractive for material science, but they can also serve as a model system for studying the properties of ground and excited states of extended π systems by means of theoretical methods¹.

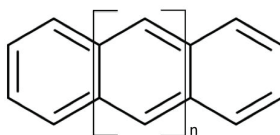


Figure 1. Structure of studied acenes (n=0-5).

In this work¹, MCSCF/CASPT2/6-31G* calculations of the polyacenes from naphthalene (n=0) to heptacene (n=5) the L_a (B_{2u} state) and L_b (B_{3u} state) bands were performed using different schemes to investigate the effect of the active space extension and the freezing of σ orbitals. Considering that acenes has D_{2h} molecular symmetry, the smaller active space consist by the CAS(8,8) which contain one virtual and one occupied orbital of each π symmetry. Larger active spaces were chosen based on the MR-AQCC occupation numbers, been the largest one CAS(14,14). Three freezing scheme were used: DOCC (all σ orbitals freeze); 2s (2s σ orbitals freeze) and 1s (1s σ orbitals freeze). A multi-configurational character of the wavefunction was found for the first excited state (B_{3u}), resulting from a linear combination of HOMO-1 \rightarrow LUMO and HOMO \rightarrow LUMO+1 configurations. For the second excited state (B_{2u}), the wavefunction corresponds almost exclusively to a HOMO \rightarrow LUMO excitation. These investigations show quite different requirements for the two states to be described. In the valence bond formalism, the L_a state is of ionic character; it is sensitive to the



freezing scheme of the σ -orbitals but does not require an extended active space. On the other hand, the covalent L_b state requires a large active space but is not sensitive to the freezing scheme within the σ -space, i.e. to the extent of dynamic correlation. To obtain a balanced description of both states, an active space containing 14 electrons in 14 orbitals and only the 1s orbitals frozen proved to be adequate to provide a balanced description of the L_a and L_b states and very good agreement with experimental absorption energies.

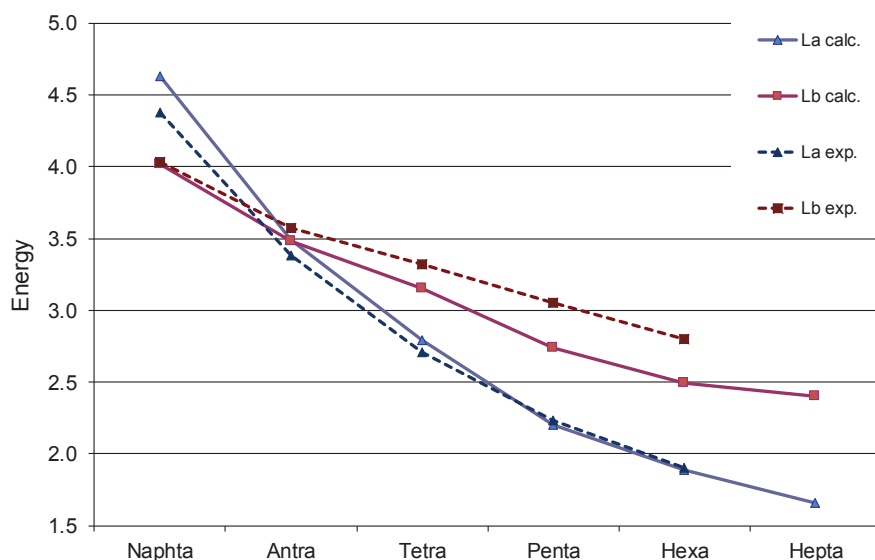


Figure 2. The CASPT2 excitation energies of L_a (1^1B_{2u}) and L_b (1^1B_{3u}) band calculated for the polyacenes series using CAS(14,14)(1s) active space and experimental²

Key-words: Acenes, excited states, absorption spectra, CASPT2.

Support: This work has been supported by CNPq, CAPES, FAPESP.

References:

[1] Bettanin, F.; Ferrão, L. F. A.; Pinheiro, Jr. M.; Aquino, A. J. A.; Lischka, H.; Machado, F. B. C.; Nachtigalova, D., *J. Chem. Theory Comput.* Accepted.

[2] Biermann, D.; Schmidt, W. Diels-Alder. *J. Am. Chem. Soc.* **1980**, *102*, 3163–3173



Structural transition in Lipid A bilayers driven by physical and chemical factors.

Frederico Pontes (PQ)¹, Roberto Lins (PQ)², Thereza A. Soares (PQ)¹

¹*Department of Fundamental Chemistry. Federal University of Pernambuco. Cidade Universitária, Recife - PE, 50740-540.*

²*Oswaldo Cruz Foundation. Cidade Universitária, Recife - PE, 52171-011.*

Abstract: Lipid A constitutes the hydrophobic region of lipopolysaccharides (LPS) molecules, which are the main component of external membrane of Gram-negative bacteria. The Lipid A is the endotoxic factor inducing bacterial toxicity. Chemical modifications of the Lipid A structure promotes changes on its aggregation form and biological properties. In order to understanding the microscopic details involving structure, biological activity and physical properties of these membranes, we have extended the GROMOS 53A6 force field to different Lipid A phenotypes of *P. aeruginosa* [1] and *E. coli* and carried out atomistic molecular dynamics simulations of bilayers at different conditions on the NpT ensemble for 200 ns. The structural dynamics and transition between distinct aggregate forms of Lipid A bilayers were investigated at different temperature conditions (278K, 300K, 328K and 343K), type of cations (Mg^{2+} and Na^+) and structural phenotypes (hexa-, penta- and tetraacilated and mono and diphosphorylated). Structural analyses of the simulated systems were performed with the program SuAVE [2] which takes into account changes in the membrane curvature during transitions between different aggregate states. Properties such as area per lipid, bilayer thickness, deuterium order parameters of acyl chains, curvature degree, coordination number and spatial chemical group density profile were calculated and compared for the simulated systems. The present simulations show that i. Lipid A bilayers undergo a lamellar to non-lamellar arrangement in the presence of monovalent cation independent of the phenotype; ii. Divalent cations stabilize the lamellar arrangement of Lipid A by means of crosslinking phosphate groups in neighbor lipids, whereas monovalent cations are not able to interact in this way as previous reported [3]; iii. Lipid A in non-lamellar structures adopt an average conical shape, while in lamellar one it adopts a conical conformation; iv. Changes in the phase organization shows to be strongly influenced by number and length of acyl chains in the Lipid A structure. Our finds reveal the intrinsic relationship between Lipid A chemical structure, conformation and aggregate arrangement.

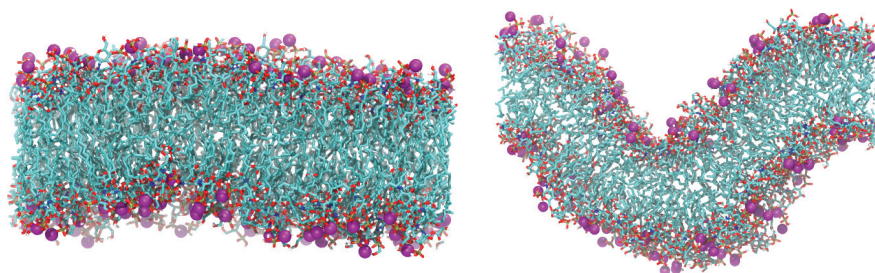


Figure 1: Lamellar (left) and Ripple (right) bilayer arrangement for Lipid A with different phenotypes (hexa- and tetraacylated, respectively). Magnesium cations are represented by purple atoms.

Key-words: Bacterial outer membrane, force field parameters, metal hydration in membrane environments, atomistic computational simulations.

Support: FACEPE, CENAPAD-UFC, BioMol Project/CAPES, STINT (Sweden)

References:

- [1] F. Pontes, V. H. Rusu, T. A. Soares, R. D. Lins, *J. Chem. Theory Comput.*, 8(10), 3830 (2012).
- [2] D. Santos, F. Pontes, K. Coutinho, R. D. Lins, T. A. Soares, in preparation
- [3] A. Nascimento Jr, F. Pontes, R. D. Lins. T. A. Soares. *Chem. Commun.*, 50, 231 (2014).



New genetic algorithm paradigms applied to atomic and molecular clusters studies

Frederico Teixeira Silva^a (PG)

^a *Departamento de Química Fundamental, CCEN, UFPE, 50590-470 □ Recife, PE, Brazil.*

Abstract: New global optimization tools for atomic and molecular clusters studies are constantly been produced [1-4]. It is known that clusters have unique properties, which are difficult to predict using only chemical intuition, so, computational tools can help these studies. Among the current global optimization techniques, genetic algorithms stands out in obtaining the most stable geometry of atomic and molecular clusters. In this work, a study of six specific genetic operators was performed to obtain the most stable geometry of clusters. From these operators, the spherical crossover [4] and cut-and-splice crossover [5] are specific for genetic algorithms. The other four: angular operator, surface angular operator, geometric displacement and twist operator were initially proposed for Basin Hopping technique [1], and, in this work, were implemented in our group's genetic algorithm [2]. In addition, we propose a new paradigm that allows to manage these operators. This paradigm consists in increasing or decreasing the rate of creation of new individuals on the fly. Operators that are generating unstable structures have their creation rate reduced in the next genetic algorithm generation. Likewise, operators who are building structures that approach the global minimum have their creation rate increased. With these operators, nine genetic algorithm arrangements were built, one arrangement for each of the operators alone, and three with management operators' paradigm. As a test of the methods, fifty global optimizations of a Lennard-Jones set containing twenty-six atoms were made for each of the methods. The performance measure was the mean number of optimizations that were required to reach global minimum. Results pointed out twist operator as the best operator. Also, that management operators' paradigm could improve the overall performance of the method.

Key-words: Global optimization, atomic and molecular clusters, genetic algorithm.

Support: This work has been supported by CNPq

References:

- [1] G.G. Rondina, J.L.F. Da Silva. *J. Chem. Inf. Model.* 75, 288, (2013).
- [2] F.T. Silva, B.R.L. Galvão, G.P. Voga, M.X. Silva, D.D.C. Rodrigues, J. C. Belchior, *Chem. Phys. Lett.*, 639, 135, (2015).
- [3] J. Centeno, P. Fuentealba. *Int. J. Quantum Chem.* 111, 1419, (2011).
- [4] Z. Chen, X. Jiang, J. Li, S. Li. *J. Chem. Phys.* 138, 214303, (2013).
- [5] D.M. Deaven, K. M. Ho. *Phys. Rev. Lett.* 53, 2282, (1995).

A DFT Benchmark Study on Ionic Liquids

Gabriel Aguiar de Souza(IC)¹ and Ednilsom Orestes(PQ)^{2*}

¹*Instituto de Ciências Exatas, Universidade Federal Fluminense, Campus do Atarrado, Volta Redonda, Rio de Janeiro, Brazil*

²*Escola de Engenharia Industrial Metalúrgica de Volta Redonda, Universidade Federal Fluminense, Volta Redonda, Rio de Janeiro, Brazil*

Abstract: Ionic Liquids (IL) is a class of substance generally formed by organic cations and inorganic anions which make them liquid at the room temperature. The wide range of possible combinations of cations and anions can result in solvents with many interesting and different properties and applications.[1] Due to its high polarity, low coordination number and almost zero vapor pressure, the IL are able to solvate both organic and inorganic compounds besides being more easily recyclable than common industrial solvents, which highlights its economical and friendly environment characteristics.[2] All these features have brought a lot of attention to IL from both experimental and theoretical point of views.[3] From the theoretical perspective, the majority of the quantum mechanical studies have used Density-Functional Theory (DFT) without, however, a consensus about which functional, and even basis set functions, best describes the microscopic features of IL.[4,5] In this work, the most common ion pair combinations forming IL were investigated with different DFT functionals and basis set functions. The results were compared with a benchmark high-level calculation composed of Coupled-Cluster Method extrapolated to a complete basis set and experiment if possible.[6] The set of selected functionals includes pure and hybrid ones with and without long range dispersion correction, while the basis sets comprise double and triple zeta added with polarization and diffuse functions. The solvent effect was implicitly included in all calculations as well as the counterpoise correction for the basis set superposition error on ionic pairs. The long range corrected functionals with triple zeta basis sets including polarization and diffuse functions show the best agreement with the benchmark high-level calculation indicating they should be the method of choice as starting point calculations of more complex and/or large IL systems and molecular mechanics simulations.

Key-words: ionic liquids, density-functional theory, benchmark.

Support: This work has been supported by FAPERJ.

References:

- [1] J. S. Wilkes, *Green Chemistry*, **4**, 73 (2002).
- [2] M. J. Earle, K. R. Seddon, **72**, 1391 (2000).
- [3] M. García-Mardones, I. Bandrés, M. C. López, I. Gascón, C. Lafuente, *J. Sol. Chem.* **41**, 1836 (2012). I. Zgorodina, Z. L. Seeger, D. L. A. Scarborough, S. Y. S. Tan, *Chem. Rev.*, **117**, 6696 (2017).
- [4] A. A. H. Pádua, *J. Chem. Phys.* **146**, 204501 (2017).
- [5] V. H. Paschoal, L. F. O. Faria, M. C. C. Ribeiro, *Chem. Rev.*, **117**, 7053 (2017).
- [6] D. G. Truhlar, *Chem. Phys. Lett.*, **294**, 45 (1998).

Catalytic mechanism of conversion of ATP to cyclic-AMP catalyzed by the Edema Factor of Anthrax: a QM/MM study

Gabriel E. Jara, Leandro Martinez

Address: Instituto de Química/UNICAMP, Campinas, São Paulo, Brasil; e-mail: leandro@iqm.unicamp.br

Abstract: The Edema Factor (EF) is one of three major toxins involved in the disruption of cellular functions resulting from infection of a host organism by anthrax. EF is an adenylyl cyclases and, as such, catalyzes the production of cyclic-AMP (cAMP) from ATP. In eukaryotes, cAMP is a key signaling molecules, and the infection by EF induces its overproduction, leading to cell death. Other pathogens, such as *Bordetella pertussis*, responsible for Pertussis, or *Yersinia pestis*, which causes bubonic plague, also have similar edema factors [1,2]. On the other hand, mammalian adenylyl cyclases (mAC) catalyzes the same reaction. However, these proteins exhibit little structural homology with the anthrax EF. Several structures of the EF of anthrax were obtained, which allow a qualitative analysis of possible reaction pathways. Nevertheless, these same structures are not conclusive about fundamental aspects of the catalytic mechanism, as the reactive conformation of the ATP, the number and mode of coordination of the ions of the active site, and the amino-acids which are directly involved in the transfer of protons along the reaction. We have performed significant advances on the understanding of the reaction mechanism of EF and mAC.[3] In spite of the advances made at the moment, the causes of the catalytic power of the EF are not fully understood. A complete description of those causes could be obtained by studying EF and mAC mutants, specially, H577A in EF and S1028H in mAC. We present analysis of the mechanism of these two mutant and its free-energy profiles. The results are compared against the previous our previous results obtained for wild-type enzymes. The description of the mechanism of the reaction through the determination of the free energy surfaces determined by each plausible reaction coordinate. The study of the mechanism of the reaction were be performed using quantum mechanics/molecular mechanics simulations (QM/MM). The free energy profiles were calculated using non-equilibrium Quantum Mechanics-Molecular Mechanics/Steered Molecular Dynamics (QM-MM/SMD) simulations, by means of the Jarzynski equality. The QM subsystem is described at the Self-Charge Consistent Density Function Theory Tight-Binding (SCC-DFTB) level and the database that were parametrized to describe phosphate transfer reaction [4].

Besides, the deep analysis of the reaction in solution would add key elements to describe in detail the EF catalytic power. Here, we also present our results of the reaction in solution for identifying the catalytic factors that the enzyme introduces. The reaction has two step, chemical reaction (first step) and the separation of the products (second step). We present results for the two steps of the reaction. Different conditions were tested, e.g. different possible bases that accept the transferring proton. The methodology used in the first step were the similar to that used for mutants (QM/MM), while for the second step, classic molecular dynamics and umbrella sampling were used.

Key-words: QM/MM, Steered Molecular Dynamics, Free-energy profile, Jarzynski, Anthrax Edema Factor.

Support: The authors thank Fapesp (Grants 2010/16947-9, 2011/51348-1, 2013/05475-7, and 2013/22360-9), CNPq (Grant 470374/2013-6) and Faepex (Grant 596/13) for financial support.

References:



- [1] Drum, C. L.; Yan, S.-Z.; Bard, J.; Shen, Y.-Q.; Lu, D.; Soelaiman, S.; Grabarek, Z.; Bohm, A.; Tang, W.-J. *Nature*, 415, 396 (2002).
- [2] Guo, Q.; Shen, Y.; Zhukovskaya, N. L.; Florian, J.; Tang, W.-J. *Journal of Biological Chemistry*, 279, 29427 (2004).
- [3] Jara, G. E.; Martínez, L. *The Journal of Physical Chemistry B*, 120, 6504 (2016).
- [4] Yang, Y.; Yu, H.; York, D.; Elstner, M.; Cui, Q. Description of Phosphate Hydrolysis Reactions with the Self-Consistent-Charge Density-Functional-Tight-Binding (SCC-DFTB) Theory. 1. Parameterization.

